University of Strathclyde

Department of Chemical and Process Engineering

Investigation of Fluid Properties at Non-Ambient Conditions

by

Stewart Charles Vant

Thesis submitted in fulfilment of the requirement for the degree of Doctor of Philosophy

2003

ORIGINAL COPY TIGHTLY BOUND

Contents

	Declaration of Author's Rights	i
	Acknowledgements	ii
	Notation	iii
	Abstract	v
Chapter 1	Introduction	1
Chapter 2	Pressure-Volume-Temperature Measurement	6
	2.1 Background	7
	2.2 Present Method	11
Chapter 3	Viscosity Measurement	40
	3.1 Method	41
	3.2 Detection of Freezing	44
	3.3 Temperature Measurement and Control	48
	3.4 Pressure Measurement and Calibration	50
	3.5 Viscometer Calibration	51
	3.6 Analysis of Uncertainty	57
Chapter 4	Density Correlation and Prediction	62
	4.1 Corresponding States Principle – Previous Work	63
	4.2 Application of Corresponding States for Compressed Liquid Density Prediction	70
	4.3 Establishment of Input Parameters	80
	4.4 Comparison with Data of Rodriguez-Anton et al.	95

Chapter 5	Viscosity Correlation and Prediction	97
	5.1 Empirical Viscosity Prediction	98
	5.2 Semi-Theoretical Viscosity Prediction	101
	5.3 Molecular Theories	103
	5.4 Possible Corrections to Current Theory	124
Chapter 6	Results and Analysis	139
	6.1 Fuels Measured	140
	6.2 Density	140
	6.3 Viscosity	151
Chapter 7	Conclusions	184
	References	191
Appendix A	Viscometer Theory	198
Appendix B	Corresponding States Program Code	206
Appendix C	Code for Estimation of Viscosity by Numerical Solution of Hard Sphere Theory	213
Appendix D	Code for Estimation of Viscosity from Collision Integral Scheme	220

Declaration of Author's Rights

Acknowledgements

Stewart Vant is an Associate of the Postgraduate Training Partnership (PTP) between the National Engineering Laboratory (NEL) and Strathclyde University. The PTP scheme is a joint initiative of the UK's Department of Trade and Industry (DTI) and the Engineering and Physical Sciences Research Council (EPSRC). The PTP scheme is supported by a grant from the DTI. Stewart Vant gratefully acknowledges grant support from both the EPSRC and NEL.

Financial support for the work described in this paper was provided by Delphi Diesel Systems, whose support is gratefully acknowledged. In particular, the author gratefully acknowledges the many useful contributions made by Mr. G. Reid to this work, and Mr. B. C. Hales for sourcing the fuel samples.

The author wishes to thank Dr. N. F. Glen of NEL and Dr. C. J. Schaschke of Strathclyde University for their guidance through their supervision of the project. The author would also like to thank his parents for their continued support throughout this work.

Notation

A	Viscometer coefficient	(mPa.s)
B	Parameter in Tait equation	(MPa)
C	Parameter in Tait equation	
g	Acceleration of gravity	($m.s^{-1}$)
k	Boltzmann constant	($Nm.K^{-1}$)
$\overline{K}_T$	Isothermal secant bulk modulus	(MPa)
L_s	Sinker length	(m)
L_t	Tube length	(m)
m	mass of molecule; mass of sinker (Chapter 3)	(g)
M	Molecular mass	($g.mol^{-1}$)
N_A	Avogadro number	
P	Pressure	(MPa)
Q	Flow rate	(m^3s^{-1})
r_1	Viscometer sinker radius	(m)
r_2	Viscometer tube radius	(m)
R	Universal gas constant	($Nm.mol^{-1}K^{-1}$)
R_0	PRT resistance at 273.16K	(Ω)
$R(T_{90})$	PRT resistance at T_{90}	(Ω)
R_η	Hard sphere theory non-sphericity parameter	
Re	Reynolds number	
t^*	Buoyancy corrected fall time	(s)
T	Temperature	(K)

T_{90}	Temperature measured according to ITS-90	(K)
u_{ave}	average fluid velocity	($m.s^{-1}$)
u_{sinker}	sinker velocity	($m.s^{-1}$)
V_0	Hard sphere close packed volume	(m^3mol^{-1})
V_r	Hard sphere theory reduced volume relative to V_0	
$W(T_{90})$	PRT resistance ratio, $R(T_{90})/R_0$	
$W_r(T_{90})$	Resistance ratio of ideal PRT at T_{90}	
x	Micro-PVT length gauge displacement	(mm)
Z	Compressibility factor	
α	Thermal expansivity	(K^{-1})
β	Compressibility	(Pa^{-1})
η	Coefficient of dynamic viscosity	(mPa.s)
η^*	Reduced viscosity coefficient	
ρ	Density	(kgm^{-3})
σ	Hard sphere diameter	(m)
ν	Kinematic viscosity	(cSt)
ω	Acentric factor	
$\Omega^{(2,2)*}$	Reduced collision integral	

Abstract

A requirement for thermophysical property data of diesel fuels at conditions removed from ambient was identified. A series of measurements of the pressure-volume-temperature relations of diesel fuels was undertaken using a Micro-PVT apparatus at pressures to 300MPa in the temperature range 25 to 75^{0}C. A new calibration procedure for this instrument was devised to enable measurements of high accuracy to be made. Viscosity measurements of diesel fuels over a range of temperature and pressure were made using the National Engineering Laboratory high pressure viscometer to pressures of 460MPa in the temperature range 25 to 100^{0}C.

Corresponding states theory was applied for compressed liquid density prediction. Improvement in density prediction in this region was found through use of iso-octane and heptadecane as reference fluids. Compressibility factors of these were represented by Tait-style equations. An iterative solution technique was developed to allow the corresponding states method to be applied to diesel fuels using limited density measurement and a guess value of boiling point as inputs. Densities predicted from this method agreed well with measurements made using the Micro-PVT apparatus.

Hard sphere theory was applied as a method for viscosity prediction. Despite the complexity of the diesel fuel mixture, reasonable estimates of viscosity were made with limited measurement input at higher temperatures. At lower temperatures, an additional simple empirical correction term was required. A method of viscosity estimation of complex hydrocarbon mixtures based upon composition is presented. Further development of this would require additional measurements and greater characterisation of the fuel.

Chapter 1.

Introduction

1. Introduction

In a review of the current use of diesel engines in passenger cars and the technology applied therein, Pischinger[1.] reached the conclusion that use of diesel engines will be favoured as world-wide use of the car increases and fuel resources become more scarce. This view was reached after considering the comparative emissions and rate of fuel consumption of cars burning diesel and petroleum fuels respectively. Whilst cars with petrol engines generally have higher specific power outputs and produce less noise than comparable diesel engines, the advantage of decreased fuel consumption of the diesel works in its favour. This advantage is also one of the primary reasons why the diesel engine has long been favoured for heavy duty commercial vehicles.

Diesel engine technology is, to a large extent, driven by the demands of legislation and the general public for lower emissions of noise, particulates and gases such as hydrocarbons, CO, CO_2 and oxides of nitrogen. One method which has been successfully applied to meet the stringent requirements governing emissions of all types from diesel engines is the use of a common rail form of fuel injection equipment (FIE). This type of FIE has a single fuel pump which feeds fuel to a manifold (the common rail) from which the fuel is fed to the fuel injectors for each cylinder in the diesel engine. The pressure of fuel in the rail and the timing of the injections of fuel to each cylinder is determined by an electronic control unit (ECU) on the basis of engine speed, load and conditions. Due to the control of fuel delivery determined by the ECU, and the common rail being a store of fuel held at high pressure, a wide range of injection strategies can be employed. Delivery of differing

quantities of fuel throughout the cycle can be beneficial in altering the combustion characteristics for the purpose of reducing noise and other emissions. One example of this is a pilot injection to establish combustion prior to the main injection to provide smoother overall combustion. Examples of the effect that varying the timing of a pilot injection has on emissions and noise are given by Russell et al.[2.] and Yamaki et al.[3.] for light duty and heavy duty engine applications respectively.

Russell et al.[2.] note that use of smaller nozzle holes in the fuel injector has an advantageous effect in the form of the fuel spray produced, which leads to a decrease in the level of emissions. In order to inject the fuel through these small nozzle holes at a fast enough rate, the fuel is supplied to the injector at a high pressure. Jansons et al.[4.] also found a decrease in soot emissions when the injection pressure was increased. Through the combination of high pressure and the flexibility in fuel delivery allowed by the common rail FIE, the injection strategy and timing schedule can be optimised to meet current and future emissions legislation.

Computer simulation is a major method for reducing design cycle time. Use of computer simulation also allows a more complete examination of design parameters and thus contributes to a more robust design. Modelling of fluids is a fundamental component of FIE simulation. This requires thermophysical property data over the extreme range of conditions in the common rail where pressure can be as high as 200MPa. Analysis of leakage is an example where knowledge of the variation of fluid properties is very important. Leakage from FIE is due to the compromise of having clearances tight enough to prevent gross displacement of liquid, but not so tight that the free movement of moving parts is hindered. In order to assess the leakage rate it is necessary to know the viscosity of the fuel, and the

behaviour of this with respect to temperature and pressure. During the leakage process, pressure-volume energy is converted to heat energy. This heat energy increases the fuel temperature and alters the viscosity further thus making the calculation of heat losses coupled with the fluid flow calculation. Therefore accurate knowledge of density and viscosity variation with respect to pressure and temperature is necessary to model both heat loss and the leakage process.

Accurate knowledge of the variation of density and viscosity is also advantageous for metering of the fuel. This is of particular importance when injection rate modulation is employed. Subsidiary injections, for example, pilot injections, will be of a very small volume, and it is therefore necessary to know density variation accurately to inject a correct amount of fuel.

Currently there is a lack of adequate models for predicting density and viscosity data of complex hydrocarbon mixtures at elevated pressure and temperature conditions. This is in no small part due to a lack of measured data to derive such a model from. To go some way towards compensating for the lack of measured data, a program of density and viscosity measurement was undertaken using a Micro-PVT apparatus and the National Engineering Laboratory high pressure viscometer to determine the change of density and viscosity of a number of diesel fuels with respect to temperature and pressure.

The Micro-PVT is a continuous compression method for measurement of pressure – volume – temperature relationships of liquids as described by Belonenko et al.[5.]. A different Micro-PVT apparatus to that used previously[5.] was employed in this work. An alternative calibration procedure was developed for this work to enable accurate measurement of liquid compressions with this apparatus.

A method for liquid density prediction based on the corresponding states principle was developed. Comparisons with measured diesel fuel densities gave good agreement. Analysis of viscosity theory suggested that the hard sphere theory was the most promising technique for the prediction of liquid viscosity over a wide range of conditions. This was tested against the fuel measurements and found to give reasonable prediction despite the complex nature of the diesel fuel mixture.

Although the application of improved physical property data was discussed in detail for common rail diesel FIE only, there is a general requirement for accurate data throughout the process industries. Accurate correlation methods for fluid properties are similarly of particular importance for computer simulations of industrial processes. The simulations use established models for design of processes and equipment, with physical property correlations used to estimate the fluid properties. As process conditions are changed to different temperatures and pressures, the possibility exists that both the design method and input correlation will be outside the ranges which they were originally derived from. The necessity for accurate physical properties can be illustrated by consideration of a design method where viscosity is a significant factor and the process is subject to a large increase in pressure. If the variation of viscosity with respect to pressure was not considered, then at high pressures, where viscosity increases dramatically with respect to pressure, this input to the design will be inaccurate leading to potentially very large errors in the final design. Inaccurate physical properties could be of potentially great consequence as manufacturing techniques, such as the production of printed circuit heat exchangers, allow processing to take place at higher pressures.

Chapter 2.

Pressure–Volume–Temperature Measurement

2. Pressure-Volume-Temperature Measurement

2.1 Background

2.1.1 – Direct Methods

A review of early methods used for measuring volume changes of liquids under pressure is presented by Bridgman[6.]. The earliest measurements were made by enclosing the fluid of interest in a containing bulb with a capillary attached, through which a pressurising fluid such as mercury was also introduced. An external pressure was applied and this transmitted via the pressurising fluid, causing the measured fluid to compress to an extent which may be determined from the displacement of the mercury in the capillary.

Measurement of the extent of compression in the earliest applications of the above method was made in such a way that only one measurement could be made per set-up of the apparatus. This was generally done by leaving a mark, by means of a hair index for example, on the tube containing the pressurising fluid indicating the displacement reached at the maximum pressure applied. A later use of the technique of compressing the fluid sample directly by a hydraulic fluid was applied by Doolittle et al.[7.]. Measurement of volume change in this case was made by measuring the change in distance between two iron cores which bound the fluid sample. The initial position of the iron cores, one of which was fixed, the other floating on top of the mercury pressuring fluid, was determined by moving coils outside the tube until an electric bridge was balanced, indicating centring of the coils. Upon pressurisation the fluid sample was compressed by the mercury, resulting in the floating core changing position and unbalancing the bridge. The bridge was

rebalanced and the new positions of the cores measured, allowing calculation of the displacement of the cores and change of volume of liquid upon compression. Measurement of displacement in this manner allowed many different pressures to be investigated per single set-up of the apparatus. As mercury was used to develop pressure in the fluid sample, friction between moving solid metal parts was eliminated as was leakage of fluid sample. A similar technique was used by Grindley and Lind[8.] to yield PVT properties of water and mercury with sufficient accuracy for the calculation of thermal expansion coefficients and compressibilities accurate to within 1%.

Rather than use a pressure transmitting fluid in direct contact with the fluid of interest, the fluid may be contained in a vessel and compressed by a plunger. This arrangement introduces the problem of leakage past the plunger. Initially attempts at preventing leakage were made by machining a close tolerance between plunger and cylinder. Prior to the plunger entry there would also typically be a stuffing box with viscous liquid to minimise leakage. Despite machining piston and cylinder to as close a tolerance as possible, leakage would still occur due to the cylinder being subject to any temperature rise prior to the piston. Thus the cylinder would expand before the piston resulting in an increased gap between the two components. To overcome this problem of leakage, Bridgman then made his Sylphon device in which the liquid was sealed within a flexible metal bellows.

Measurement of volume change using the plunger method was originally made by noting the change in position of a brass ring attached to the piston or alternatively measuring displacement with a micrometer. Later, displacement measurements were made by electrical means. As the piston was advanced into the

liquid or the bellows were compressed under pressure, a high resistance wire attached to the end of the piston or bellows moved relative to a fixed contact. The change in position of the wire caused by the advance of the piston or compression of the bellows alters the potential difference and provides a precise measure of displacement. A similar apparatus was used by Cutler et al.[9.] for the determination of specific volumes of high molecular weight hydrocarbons to 1000MPa.

A bellows volumometer was also used by Isdale[10.]. The primary difference between this volumometer and Bridgman's sylphon was the method used to measure changes in length of the bellows. Whereas Bridgman's resistance wire was exposed to the high pressure and temperature environment, change in length of the bellows used by Isdale was measured via a detection system which was located outwith the pressure vessel. As the bellows were compressed, a steel rod attached to the top of the bellows moved downwards by an equal length. At the top of this steel rod there was a ferrite tip. The position of the tip was detected by a pair of coils which formed one arm of an AC bridge circuit. The coils were moved by turning an adjusting screw and displacement of the coils was found from micrometer readings taken before and after pressurisation. Displacement of the coils was therefore equal to the displacement of the steel rod and the bellows and this allowed change in volume to be calculated.

Although the measuring apparatus was not directly inside the pressure vessel, a correction was still required for uncertainty in displacement measurement. An uncertainty of ±0.2% was added to the calculated density value because the micrometer was attached to the thermostat bath on a different datum to the bellows inside the pressure vessel. Young[11.], in conjunction with Brawn, modified the

measurement method to eliminate this problem by fixing the micrometer directly to high pressure tubing leading out of the pressure vessel. This same set up was used by Robertson[12.] and also by Glen[13.] who changed the bridge circuit in order that the position of the tip could be located more reliably and accurately. A similar apparatus was designed by Back et al.[14.] with a linear variable differential transformer used to determine rod position. Other sylphon type devices have been used by Figuiere et al.[15.] and Landau and Wurflinger[16.]. In both of these cases the device was used to measure PVT properties in both the liquid and solid phases.

2.1.2 – Indirect Methods

A detailed review of indirect methods for the measurement of pressure volume temperature relationships is presented by Tekac et al.[17.]. One such indirect method is to measure the speed of sound and calculate density by manipulation of the relationship between isentropic compressibility, β_S, and speed of sound, u;

$$\beta_S = \left(\rho u^2\right)^{-1} \tag{2.1}$$

This can be re-arranged to relate density, ρ, at elevated pressure to a known density, ρ_0, at a reference pressure and the same temperature, and thermal expansivity, α_P, and heat capacity, c_P;

$$\rho = \rho_0 + \int_{P_0}^{P} u^{-2} dP + T \int_{P_0}^{P} \frac{\alpha_P^2}{c_P} dP \tag{2.2}$$

This method of density measurement obviously requires measurements of heat capacity at the temperature of interest and a number of density measurements at constant pressure to determine the thermal expansivity of the liquid.

Density can also be related to the frequency of a vibrating element. A vibrating tube apparatus for density measurement is described by Albert and Wood[18]. An instrument employing a wire as the vibrating element is described by de Oliveira[19]. This includes a complete derivation of the equations used to relate the frequency of the vibrating wire to density and also viscosity.

2.2 Present Method

2.2.1 – Micro-PVT Operation

Changes in the volume of a liquid sample upon pressurisation in this study are measured by the Micro-PVT apparatus. More correctly, the Micro-PVT system forces a change in the volume of the liquid and measures the pressure that is developed as a result of this volume change. A stainless steel rod continuously driven into the liquid sample by a stepper motor causes the liquid to compress to an extent determined by the bulk modulus of the liquid. As the stepper motor causes the rod to drive into the cell at a constant rate (mm/s) and assuming the cross sectional area of the cell and rod to be constant throughout the compression, it follows that the volume of the sample decreases at a constant rate with respect to time. Ignoring the effect of material distortion, the curvature of the resultant pressure-volume graph is therefore due to the non-linear development of pressure with respect to time.

Compressions in the Micro-PVT apparatus are performed on a liquid sample which will typically have an approximate volume of 0.7ml at ambient temperature and pressure. A small sample size such as this is advantageous as it allows for the sample to obtain a uniform temperature throughout on a short time scale. The range of temperature operation quoted by the manufacturer is –60 to 150^{0}C but this is

limited in practice to 20 to 80^{0}C through the use of water as the heat transfer medium. A maximum pressure of 500 MPa is quoted by the manufacturer but the sealing was found to fail at high pressures. 300 MPa was chosen as the maximum pressure throughout the trials as sealing could be consistently maintained up to this pressure.

The liquid sample is contained in a high pressure cell by the stainless steel rod at the bottom and the temperature sensor at the top as shown in Figure 2.1. Liquid leakage from the high pressure cell between the rod and the walls of the cell is prevented by an arrangement of o-rings held in place by a copper bushing and a nut which is tightened before the high pressure cell is fitted on to the rest of the rig. A rubber o-ring set into the thermistor body prevents liquid leaking from the top of the cell once the thermistor is secured into the cell by a nut. Friction between the rod and the seals at the bottom of the cell is minimised by having the rod rotate as it is driven into the cell. By changing the speed at which the rod advances into the cell, it is possible to alter the thermodynamic mode of the compression.

Once the temperature is stable in the cell and speed of rotation and maximum pressure have been set into the operating software, the cycle of compression to the maximum pressure followed by depressurisation to atmospheric is started. A complete cycle to 250MPa and back to 0.1MPa will typically take between 2-3 hours for an isothermal compression depending on the compressibility of the fluid being tested. Such a cycle will give between 1,200 and 1,800 data points of volume, pressure and temperature to describe the volumetric behaviour of the fluid being tested.

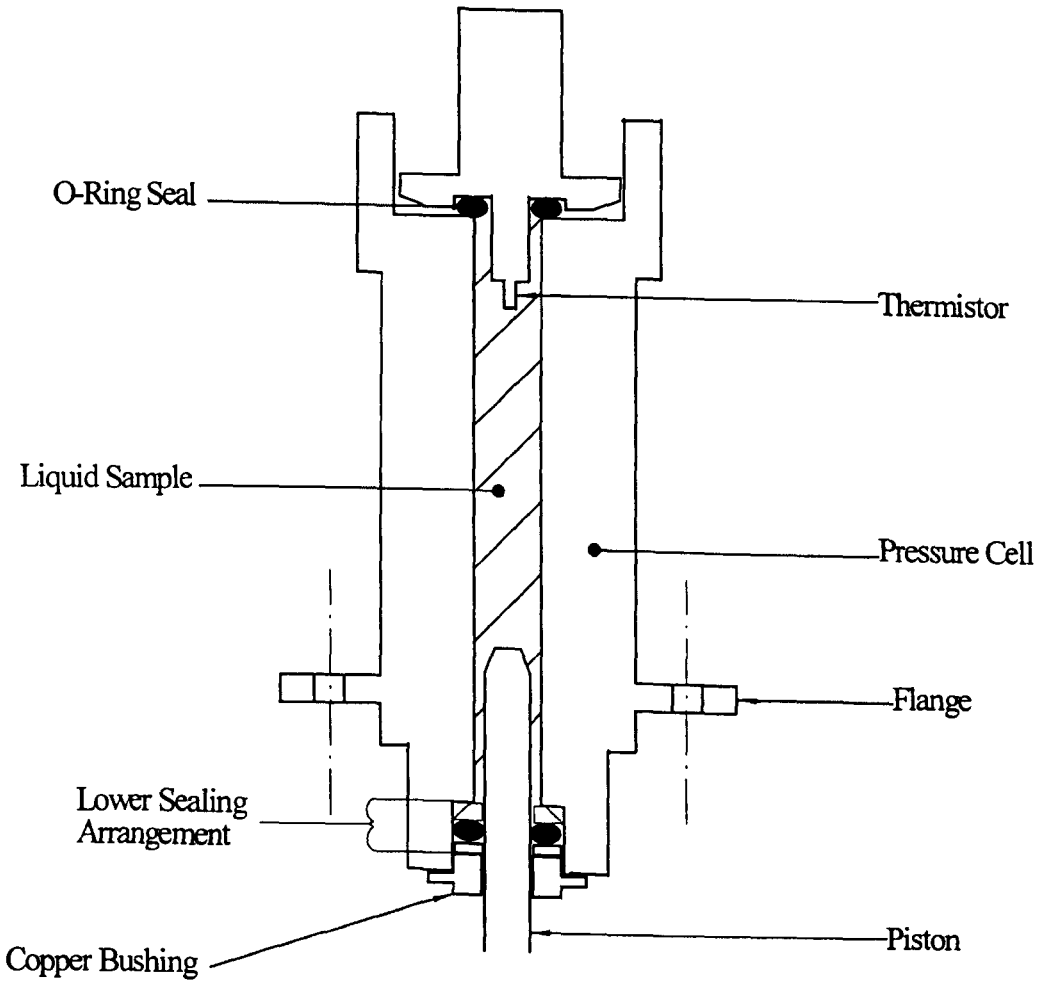

Figure 2.1 Micro-PVT Cell

As the rod is pushed into the cell by the stepper motor, the body of the Micro-PVT moves up relative to the cell, which is at a fixed height. The displacement caused by the advancement of the rod is measured by a length gauge, the body of which is also at a fixed height. The displacement thus measured is recorded on to a personal computer via a pre-amplification and pre-processing block. Displacement is then converted to volume via a mathematical function built into the operating software. The main components of the Micro-PVT are shown in Figure 2.2.

In the introductory paragraph to this section, the cross-sectional area of the high pressure cell was assumed constant for descriptive purposes. However, given the magnitude of the pressures developed, the steel will alter shape slightly as will the rubber o-rings. These volume changes due to material deformation are supposedly accounted for by a mathematical function built in to the software, but in order to obtain highly accurate results it is necessary to calibrate the rig with respect to fluids of known volumetric behaviour.

2.2.2 - Accuracy of Volume Displacement Gauge and Pressure Measurement

Having established the need for calibration due to the Micro-PVT recorded volume ratio being different to the true volume ratio, a methodology for calibrating the instrument was then determined. Firstly, one must consider which variables are measured accurately by the device. Volume is measured indirectly via the displacement of the rod which is measured using a digital length gauge. The length gauge has a resolution of 0.1μm. A check on the linearity was made by comparing displacements from this with a micrometer head using the experimental set up as shown in Figure 2.3. Although the micrometer head was only marked every 0.01mm

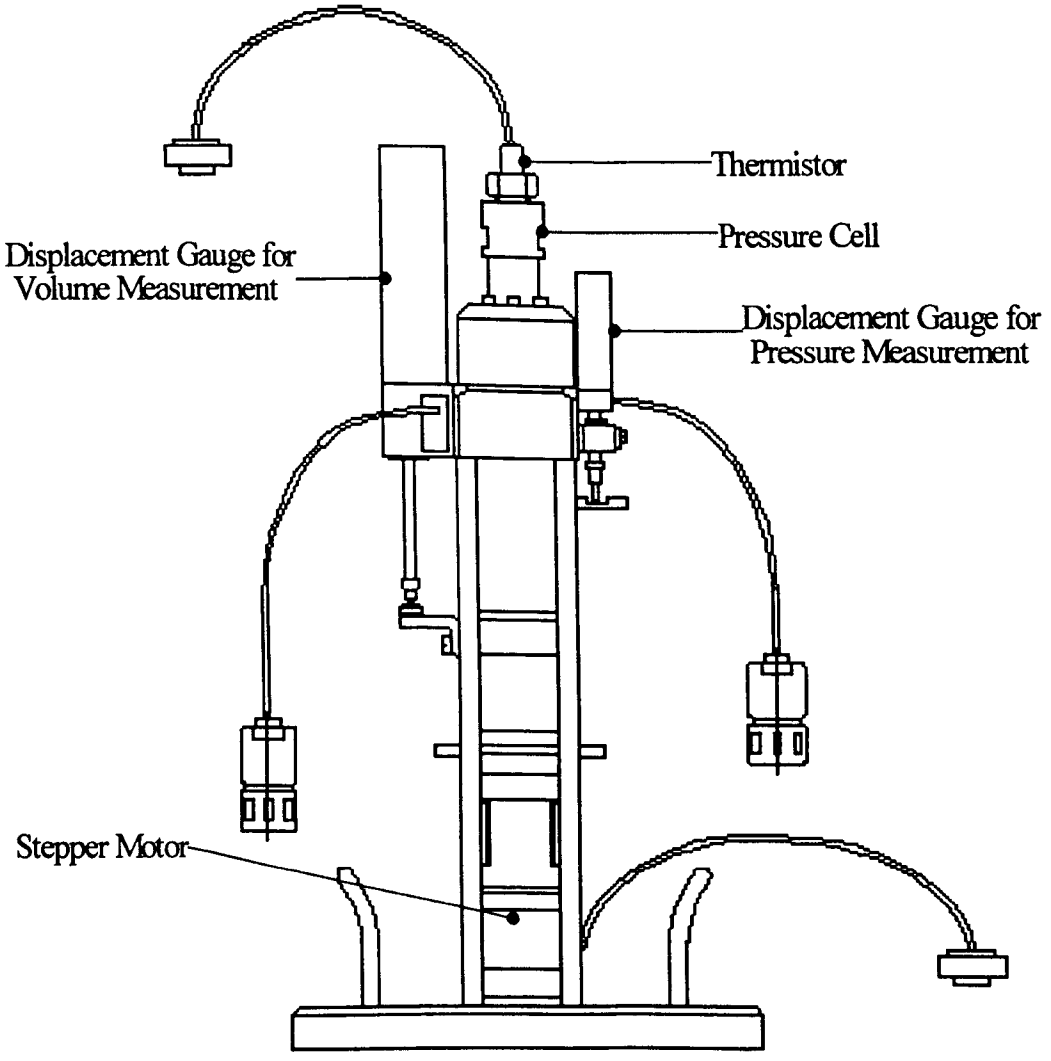

Figure 2.2 Micro-PVT Apparatus

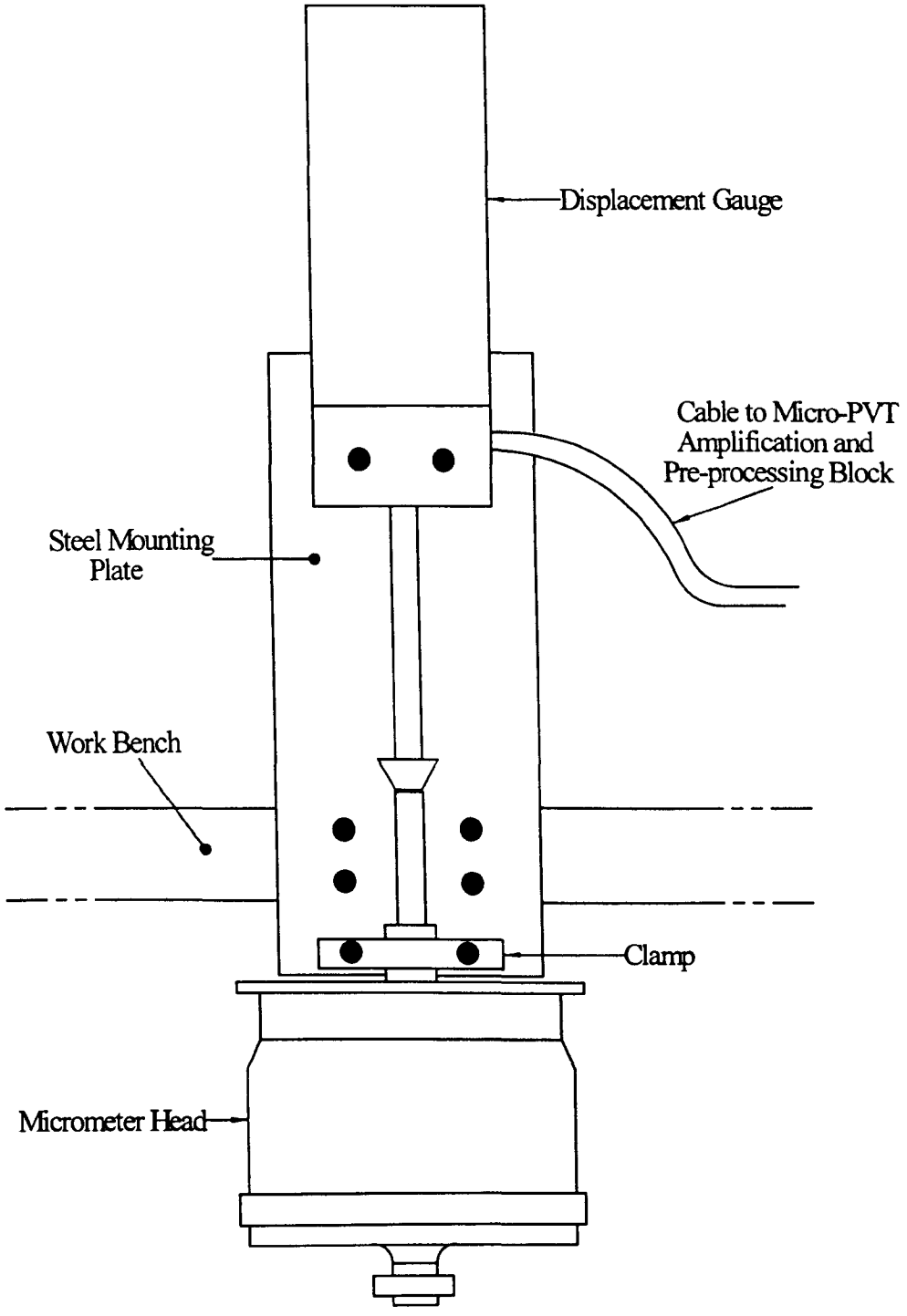

Figure 2.3 Apparatus for comparison of displacement gauge measurement

measurement may be considered more accurate than this by judging the intervals by eye. This is obviously insufficient for a comparison of resolution of the Micro-PVT length gauge, but adequate for a check of the linearity of response of the gauge. Adjusting the micrometer head in steps of 1mm, the displacement reading recorded by the Micro-PVT was found to be consistent well within the resolution of the micrometer head. This indicates that the length gauge does have a linear response with respect to changes in displacement.

Developed pressure is measured indirectly by measuring the displacement of a spring which compresses as a reaction to the pressure pushing downwards on the rod[20.]. Pressure values are then computed via a calibration function built into the Micro-PVT software. In order to confirm that these recorded pressures are correct, a high pressure adapter was fitted to the cell and to this a calibrated piezo-resistive pressure gauge was fitted to directly measure the fluid pressure as shown in Figure 2.4. Agreement between the pressure recorded indirectly by the Micro-PVT and the pressure measured by the gauge in direct contact with the fluid can only be described as reasonable at best as seen from the results presented in Table 2.1. This test does not give a true measure of the directly measured pressure as there was a problem with leakage due to the use of a lead washer which underwent plastic deformation and allowed the fluid to leak. Leakage via the deformed lead washer caused the pressure in the cell to drop off rapidly and therefore only the maximum pressures recorded by the Micro-PVT and piezo-resistive gauge were compared. Pressure measured by the piezo-resistive gauge was programmed via the high pressure viscometer operating software to update only once every five seconds and it is

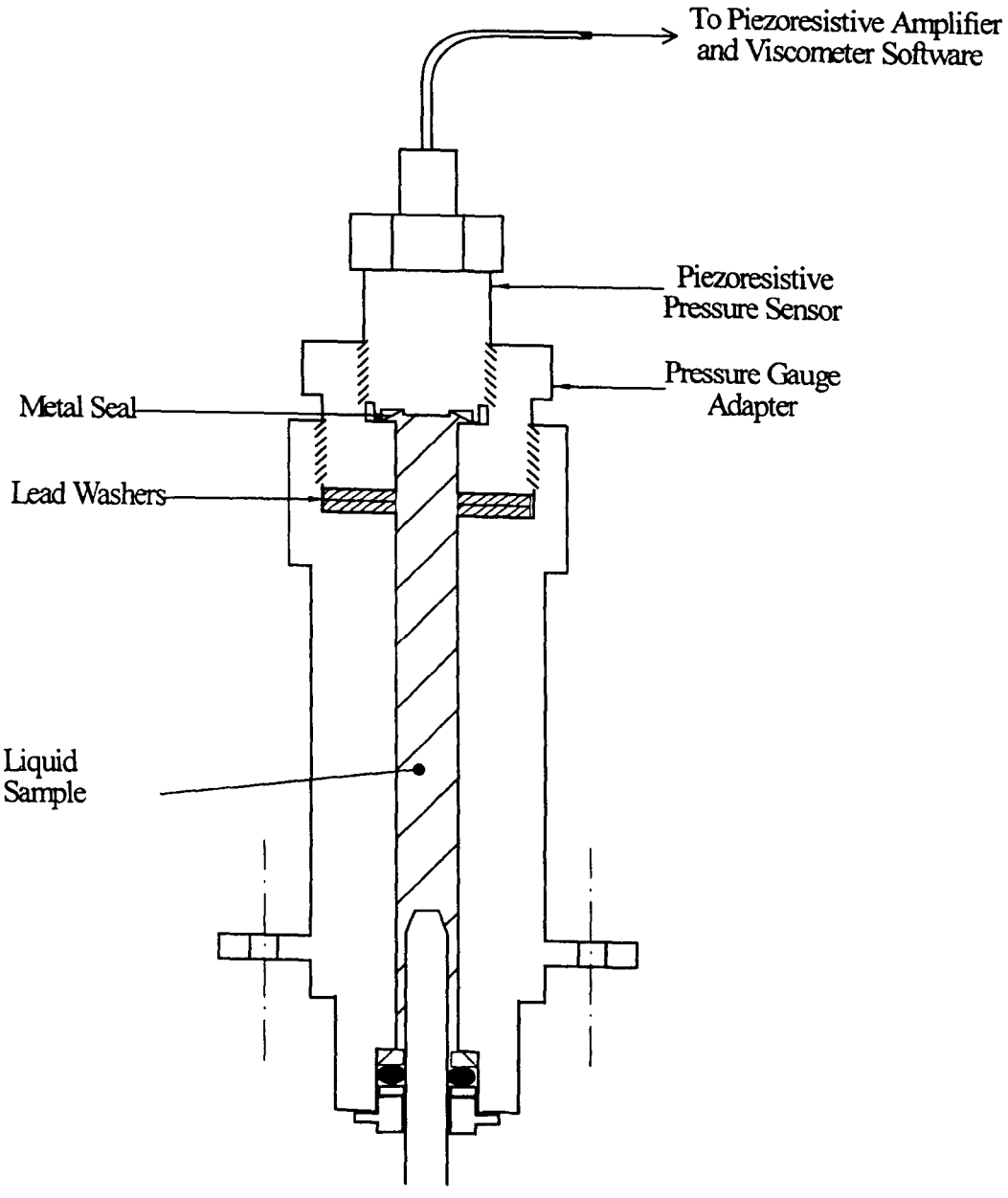

Figure 2.4 Apparatus for comparison of pressure measurement

therefore unlikely that the maximum recorded by the piezo-resistive gauge would coincide with the maximum recorded by the Micro-PVT.

Table 2.1 Comparison of pressure measured by Micro-PVT with fluid pressure measured by Kistler piezo-resistive pressure gauge

Micro-PVT Pressure (MPa)	100.1	150.7	200.1	250.0	300.6	502.0
Kistler Pressure (MPa)	97.1	148.4	195.2	244.5	297.5	494.7

Comparison with the data of Landau and Wurflinger[21.] for n-dodecane, reproduced graphically in Figure 2.5, shows that the Micro-PVT apparently over-predicts the freezing pressure of n-dodecane. It should be noted however that for the reference data[21.], the data are recorded at 160 and 170MPa and it can be implied that the freezing pressure lies between these at 25^{0}C but no exact freezing pressure is given. Pressures recorded by the Micro-PVT on the depressurisation run as the sample melts are apparently closer to the Landau data. This attempt at comparing pressure measurement with the pressure at which an accurately measured physical phenomenon occurs initially appears to be a valid comparison, but one must also take into account the fundamental difference between the way in which the data have been obtained. Landau and Wurflinger's method of PVT measurement, as described in an English paper[16.], is also a compressive method, but point values are measured which allows the sample to reach a thermodynamic equilibrium at constant temperature. With the rod being constantly driven into the high pressure cell of the Micro-PVT, a stable equilibrium cannot be achieved. It is the compression of the fluid which causes the pressure to develop and this developed pressure may cause the sample to freeze. As the volume is still being reduced by means of the continuous

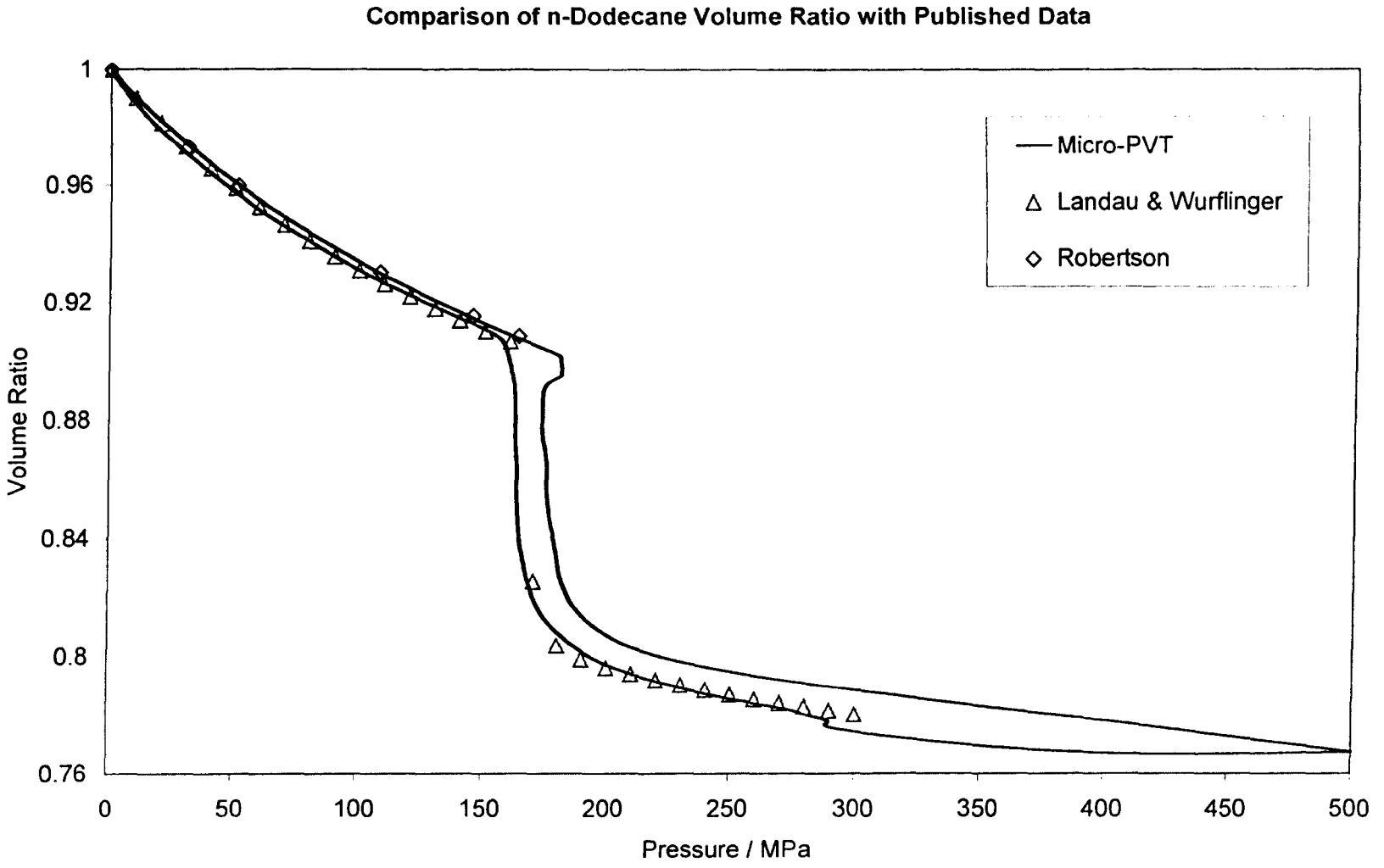

Figure 2.5 Micro-PVT n-dodecane comparison

advancement of the stepper motor, the fluid will not be allowed to attain equilibrium and hence the equilibrium freezing pressure cannot be accurately recorded.

If one assumes that the difference between the apparent freezing pressure recorded by the Micro-PVT upon compression and expansion is due to physical effects associated with solidification and liquefaction rather than any hysteresis with the pressure gauge itself then the data compare quite well. In the Landau paper values for volume change upon freezing and the latent heat of fusion are given at various pressures allowing for a freezing pressure to be calculated at 25^0C by application of the Clausius-Clapeyron equation. From this method the freezing pressure at 25^0C is found to be approximately 165.8MPa which lies between the respective Micro-PVT recorded values for expansion and compression (~163-172MPa). Again, this test of the pressure gauge accuracy proves inconclusive, but it does highlight the difference between freezing and melting and the pressures that these are recorded to occur at for any given temperature by the Micro-PVT.

2.2.3 – Micro-PVT Calibration

Assuming both pressure and displacement measurement to be correct, one can proceed to devise a function for calculating volume in terms of these two variables. One method for calculating the volume would be to use a first principles approach and calculate the volume from the dimensions of the cell and components with corrections for pressure and temperature. A complete stress analysis of the cell and components yields a complicated expression with many terms involving pressure and displacement. Whilst this does not present a problem for calculation with a modern computer, it does require all the dimensions to be measured with extreme accuracy

plus accurate values of the material properties such as Young's modulus and Poisson's ratio. Also, any variation in the seals between runs would not be accounted for through such an approach. Theoretically, any discrepancy caused by inaccuracies in material dimensions or properties values could be accounted for by calibration. In this case finding the constant terms for the calibration function is made difficult due to volume being a complicated function of pressure and rod displacement with it being difficult to separate these to give an equation for volume as a function of pressure plus a function of displacement.

An alternative method for calculating volume from pressure and displacement values can be envisaged through the following portrayal of the system. Volume occupied by the fluid in the cell at any pressure will be equal to the cylindrical volume of the cell less the volume occupied by the rod and thermistor. The rod itself can effectively be separated into two components; the portion in the cell at atmospheric pressure (V_{rod0}) and the portion in the cell which is introduced as the compression proceeds (V_{rodP}). As the compression proceeds, the change in volume of the cell, thermistor and V_{rod0} will be a function of developed pressure only. Change in V_{rodP} volume is a function of displacement and to a lesser extent pressure. Change in V_{rodP} volume due to pressure can be calculated from the change in length and diameter of the rod at pressure via stress strain relations, but may be considered negligible.

The preceding discussion considers the case of a single isothermal compression. A change in temperature will result in different values of initial volume, V_0, and initial length gauge displacement, x_0, being recorded by the Micro-PVT. Differences in these parameters with temperature is a consequence of the

system of measuring developed pressure. As the temperature increases, the developed pressure rises and the only way of restoring atmospheric pressure in the cell is to expand the sample by moving the rod downwards. Therefore V_{rod0} and x_0 do not have constant values but vary according to the temperature and fluids studied.

The simplest way to account for the change in the initial position of the rod at atmospheric pressure is to calculate V_{rod0} as a pseudo initial rod volume;

$$V_{rod0} = \frac{\pi d^2}{4} x_0 \tag{2.3}$$

where x_0 is the initial displacement of the volume encoder recorded by the Micro-PVT. Although this is in no way representative of the true volume occupied by the rod, it does account for changes in starting position of the rod. From the x and P values a function can be calculated to account for the variation in material volume with pressure;

$$f(P) = V_0 - V_{rod} - V_{ref} \tag{2.4}$$

V_0 is the initial volume calculated by the Micro-PVT and is here taken to represent the initial volume of fluid in the cell. V_{rod}, the pseudo rod volume at any pressure is calculated from $\frac{\pi d^2}{4}(x - x_0)$. d is the diameter of the rod which the manufacturer quotes as 3.626mm. V_{ref} is equal to the product of the volume ratio of a reference fluid and the atmospheric pressure volume recorded by the Micro-PVT;

$$V_{ref} = \left(\frac{V}{V_0}\right)_{ref} (V_0)_{\mu-PVT} \tag{2.5}$$

Reference fluid volumetric values used for calculating $f(P)$ were 2,2,4-trimethylpentane at 40 and 65^{0}C, toluene at 25 and 50^{0}C and water at 25, 50 and 75^{0}C. These fluids were chosen as accurate pressure-volume-temperature

measurements have been made across the pressure range by Malhotra and Woolf[22.] for 2,2,4-trimethylpentane, Harris et al.[23.] for toluene plus the water data determined by the International Association for the Properties of Steam[24.]. The fluids also adequately cover the range of compressibility of interest in this study. Measurements of 2,2,4-trimethylpentane were also made at 80^0C but displayed inconsistent behaviour compared to the other fluids and conditions when calibration calculations were made. For this reason the 80^0C iso-octane data, which represents a volume change greater than that expected of a typical diesel fuel, were not used when calculating the calibration function from the averages of the fluids.

When $f(P)$ is calculated for the three fluids and plotted against pressure the functions are seen in Figure 2.6 to be smoothly decreasing above 50MPa, but below 50MPa the $f(P)$ values follow no particular trend compared with the 50-250MPa range. For this reason, when fitting a polynomial to describe $f(P)$, only the data between 50 and 250MPa are considered. A calibration function to cover the entire range of compressibility can be evaluated from an average of the $f(P)$'s for the different reference fluids and conditions. The initial irregular $f(P)$ data means that the intercepts for the different $f(P)$ equations are somewhat different for the different fluids, leading to a large initial offset for each of the fluids when data calculated from the $f(P)$ polynomial is compared with the reference data. This initial offset is clearly shown in the error plot, Figure 2.7.

Comparing a theoretical volume ratio with the reference volume ratio according to;

$$g(P) = \left(\frac{1}{V_o}\right)_{meas}\left[(V_o)_{meas} - \frac{\pi d^2}{4}(x_p - x_o)\right] - \left(\frac{V}{V_o}\right)_{ref} \qquad (2.6)$$

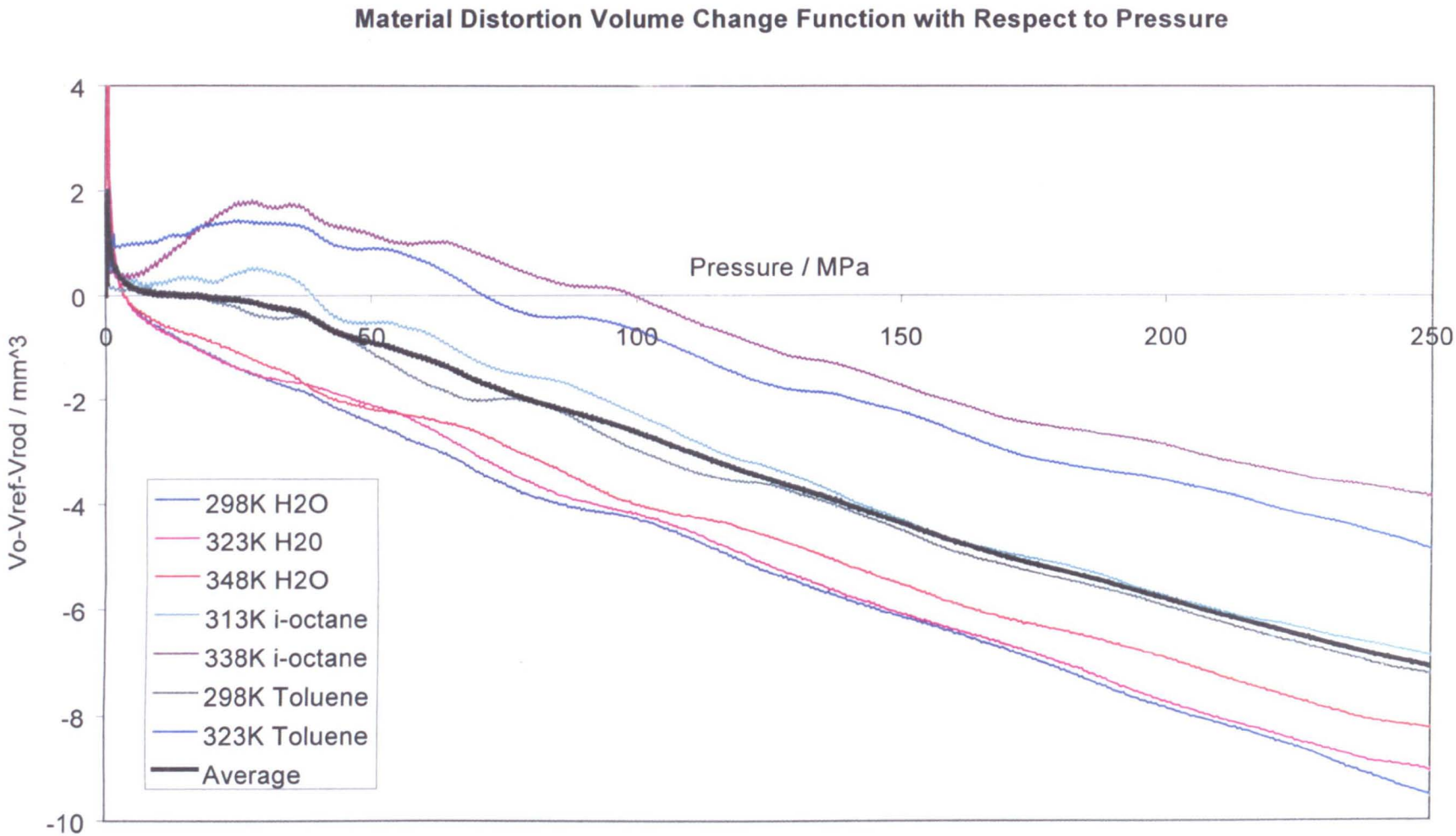

Figure 2.6 Variation of (V_0-V_{rod}-V_{ref}) with respect to pressure

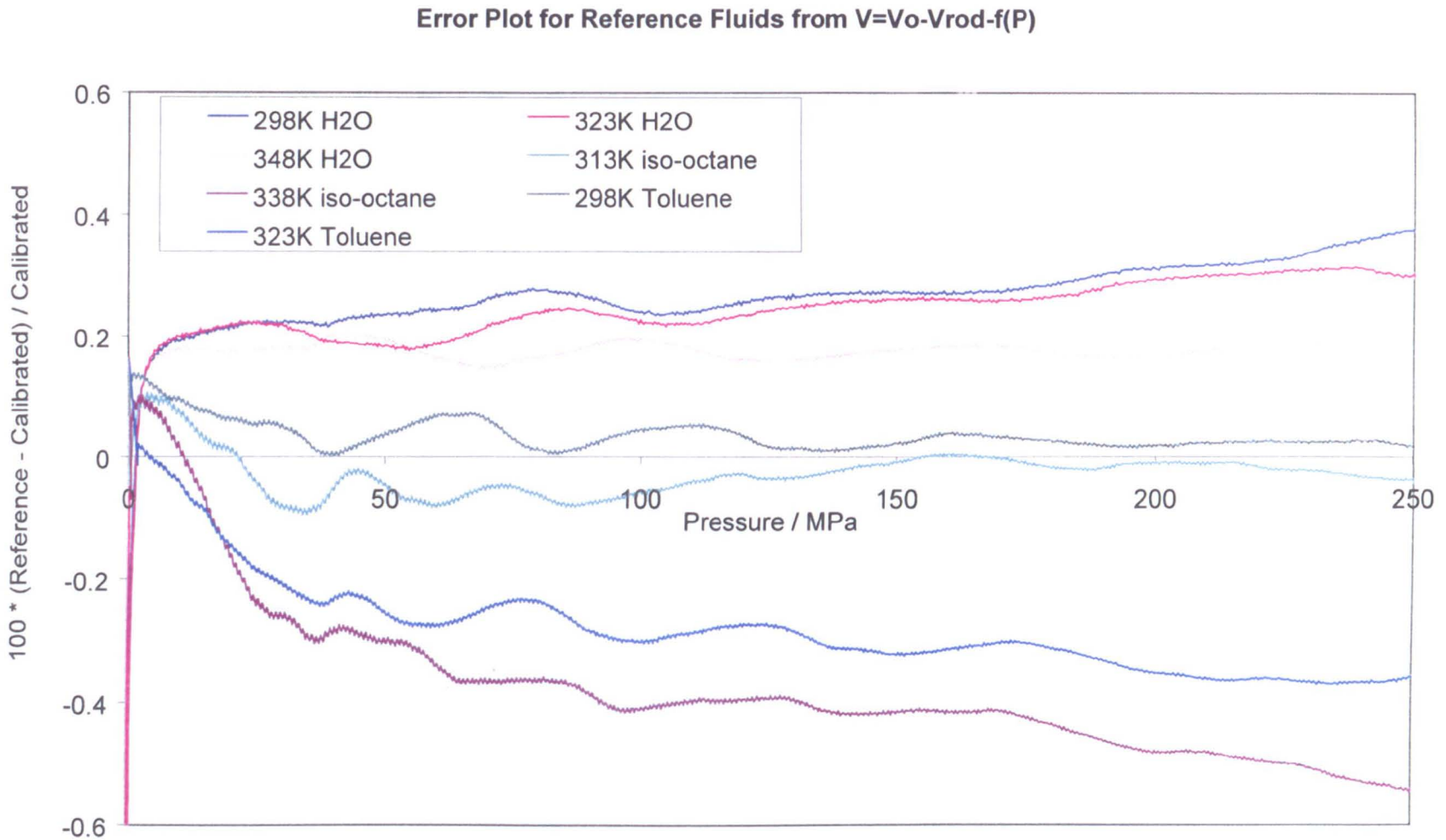

Figure 2.7 Error in measurement when $f(P)$ calibration function is applied

then the general trend obtained for $f(P)$ is once more observed; inconsistent behaviour in the 0.1-50MPa region with approximately parallel lines observed beyond this region. As the lines are approximately parallel in the higher pressure region then it should be possible to obtain consistent error plots in this region for fluids across the compressibility range, albeit with higher errors in the low pressure range. To collapse the parallel lines onto one another it is necessary to add on another function to $g(P)$, this time a function of atmospheric volume value, V_0. A pseudo value of $g(P_{atm})$ is obtained for each fluid by fitting $g(P)$ between 50 to 250 MPa with a straight line and extrapolating this back to atmospheric pressure. $g(P_{atm})$ is then plotted as a function of V_0 and the straight line fit through this becomes the correction factor to be added to $g(P)$ to compensate for the irregular low pressure data.

Adding the correction factor on, one can now write;

$$h(P) = \left(\frac{1}{V_o}\right)_{meas}\left[(V_o)_{meas} - \frac{\pi d^2}{4}(x_P - x_o)\right] - \left(\frac{V}{V_o}\right)_{ref} - (c_{v0} + c_{v1}V_o) \quad (2.7)$$

where the coefficients c_{v0} and c_{v1} were obtained from the straight line fit of $g(P_{atm})$ against V_0. An average value of $h(P)$ can be found from the reference fluids. This average function is plotted against pressure and fitted with a quadratic. Substituting $h(P)$ in the above equation and re-arranging, the volume ratio of any fluid can be found from the equation;

$$\left(\frac{V_P}{V_o}\right)_{correct} = \left[\frac{(V_o)_{meas} - \frac{\pi d^2}{4}(x_P - x_o)}{(V_o)_{meas}}\right] - \left[c_{v0} + c_{v1}(V_0)_{meas}\right] - \left(c_{P0} + c_{P1}P + c_{P2}P^2\right) \quad (2.8)$$

where c_{P0}, c_{P1} and c_{P2} are coefficients found from the plot of $h(P)$ vs. pressure. The error plot for the reference fluids using this method is given in Figure 2.8. From this

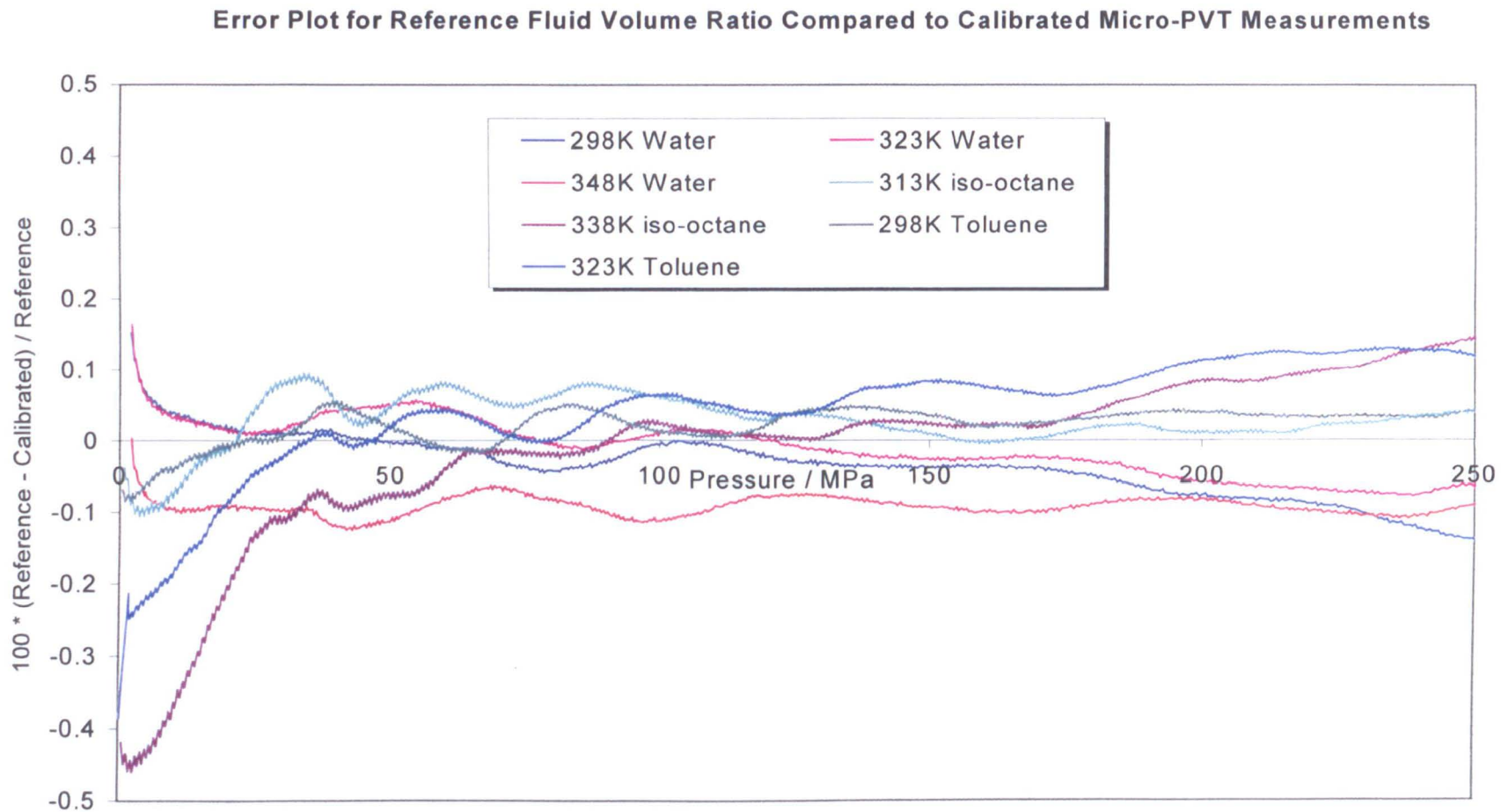

Figure 2.8 Micro-PVT error in measurements after calibration

plot it is seen that the measurements of the reference fluids are largely within ±0.1% of accurate literature data. The largest errors are found at the lowest pressures where error from mechanical factors such as seal slippage is likely to be the greatest. In this low pressure range, the largest error is observed for iso-octane at 65^{0}C. This fluid is, however, more compressible than any diesel fuel likely to be encountered.

2.2.4 – Determination of V_0 and x_0

Initial values of fluid volume, V_0, and initial length encoder displacement, x_0, were taken as those recorded by the Micro-PVT at atmospheric pressure. As there is no pressure effect on the materials of construction this is a reasonable approximation. Despite this there is still a need to use an indirect approach to obtain these parameters such that they are consistent with displacement measurements at pressures above atmospheric. One reason for this is due to the dynamic nature of the device which could cause a small movement of the lower seals at the start of the run due to the initial movement of the rod through the seals. Although only a small effect, this would represent a significant amount of volume change over a limited change in pressure due to the small volumes involved with this method.

Another reason for using an indirect approach for determining V_0 and x_0 is that for a number of trials, the system did not start at atmospheric pressure. Before every set of measurements the rod was advanced two or three times at high speed to try to ensure any gross movement of the seals occurred before the measurements were made as well as compression of any minor bubbles of air into solution. Often the decompression did not reach atmospheric pressure; instead an indicated pressure was reached at which volume would continue to expand with no corresponding

decrease in pressure. A similar effect was found when expanding a sample after a temperature change to try to restore atmospheric pressure. This anomalous behaviour could possibly be due to the use of a spring as the means of pressure measurement. Any slight movement of the spring or difference in relaxation rate between compression and decompression could cause the problem described. Should this prove to be the case, this is evidently a short term problem in terms of small differences between trials. However, the bulk properties of the spring should be more consistent over a longer time period. Small deviations are also accounted for between fluid sample changes by re-establishing the displacement of the spring prior to filling with the sample.

A typical plot of the anomalous behaviour at low pressure is shown in Figure 2.9. This example clearly shows the effect of the pressure not returning to atmospheric on the previous trial. The initial large volume change with no change in developed pressure also indicates that either air was admitted to the cell on the decompression or vacuum conditions existed within the cell. The extent of volume change suggests the former condition occurred. Displacement measurements corresponding to the volume change show analogous behaviour. As the change in volume with respect to pressure is approximately linear in the low pressure region, it follows that a reasonable linear extrapolation of results beyond the spurious region but below pressures where non linear development of pressure with respect to volume starts to become significant can be made to estimate equivalent atmospheric volume and displacement values.

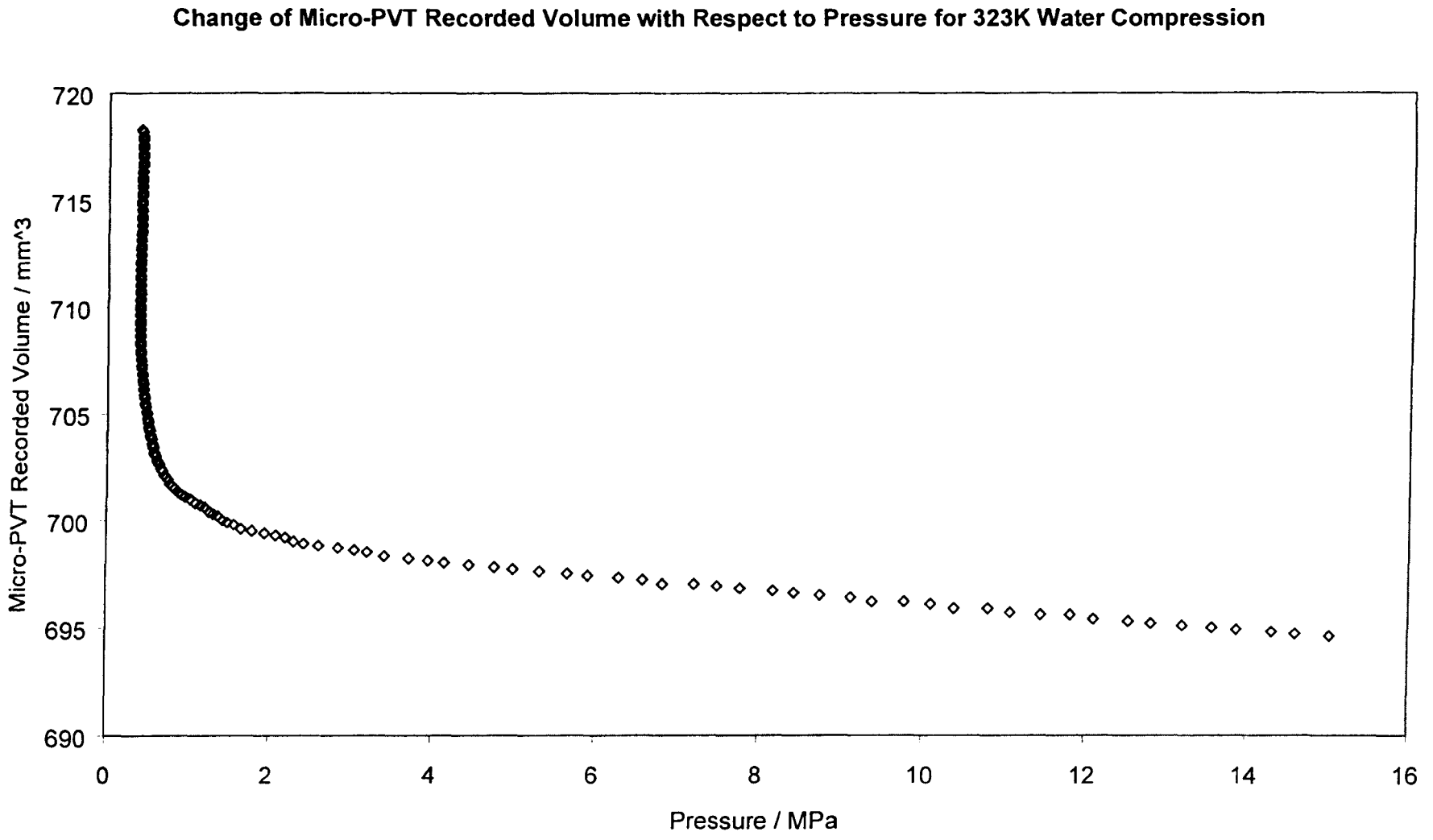

Figure 2.9 Low pressure behaviour of Micro-PVT apparatus

2.2.5 – Analysis of Uncertainty

Having developed the working equation (2.8) for the Micro-PVT, and estimation techniques for the initial volume and encoder displacement, V_0 and x_0 respectively, an estimate of the uncertainty of measurement can now be made. Compression data of a typical diesel fuel (Fuel C; see Chapter 6) at 75^0C were used for this analysis. Uncertainty of the extrapolated values V_0 and x_0 was estimated by considering the deviation of the slope and intercept of the lines required to encompass all the data from the slope and intercept of the line of best fit which was used to extrapolate the data. These uncertainties in the fit were combined to give the uncertainty in V_0 and x_0 reported in Table 2.2. A similar method was employed to estimate the uncertainty of the coefficients c_{vi} and c_{pi} used in (2.8). In the calculation of volume ratio data from the calibration equation (2.8), the compressive and expansive effects of pressure and temperature upon the diameter of the rod, d, are not considered. The uncertainty value assigned to d is therefore calculated to account for these effects upon the rod material. Belonenko et al.[5.] claim an accuracy of 10^{-4}mm in the measurement of displacement. The Micro-PVT software records displacement values to 10^{-3}mm. An uncertainty of $5\text{x}10^{-4}$mm is therefore given to x_p to account for round-off error. Belonenko et al.[5.] also claim an accuracy of 0.1% for recorded pressure. The uncertainty sources were assumed to have the probability distributions listed in Table 2.2.

The input uncertainties are unlikely to be at their extreme values simultaneously, therefore the uncertainties were combined by taking the square root of the sum of squares. The uncertainty in the calibration equation due to the uncertainty of its inputs was assumed to have a normal distribution. Combining the

Table 2.2 Uncertainty analysis of Micro-PVT volume ratio measurement

Source of Uncertainty	Nominal Value	Expanded Relative Uncertainty	Expanded Absolute Uncertainty	Probability Distribution	Divisor	Standard Uncertainty	Sensitivity Coefficient	Contribution to Uncertainty	Contribution Squared
$(V_0)_{meas}$ / (mm^3)	7.255×10^{2}	2.387×10^{-4}	1.732×10^{-1}	Normal	2	8.661×10^{-2}	-6.267×10^{-5}	-5.428×10^{-6}	2.946×10^{-11}
D / (mm)	3.626×10^{0}	1.986×10^{-4}	7.200×10^{-4}	Bias	1	7.200×10^{-4}	-7.019×10^{-2}	-5.053×10^{-5}	2.554×10^{-9}
x_P / (mm)	-1.542×10^{1}	-3.243×10^{-5}	5.000×10^{-4}	Rectangular	$\sqrt{3}$	2.887×10^{-4}	-1.423×10^{-2}	-4.109×10^{-6}	1.688×10^{-11}
x_0 / (mm)	-2.436×10^{1}	-4.741×10^{-4}	1.155×10^{-2}	Normal	2	5.774×10^{-3}	1.423×10^{-2}	8.218×10^{-5}	6.753×10^{-9}
c_{V0}	-1.680×10^{-1}	-5.952×10^{-3}	1.000×10^{-3}	Normal	2	5.000×10^{-4}	-1.000×10^{0}	-5.000×10^{-4}	2.500×10^{-7}
c_{V1} / (mm^{-3})	2.380×10^{-4}	6.723×10^{-3}	1.600×10^{-6}	Normal	2	8.000×10^{-7}	-7.255×10^{2}	-5.804×10^{-4}	3.369×10^{-7}
c_{P0}	8.890×10^{-4}	9.899×10^{-1}	8.800×10^{-4}	Normal	2	4.400×10^{-4}	-1.000×10^{0}	-4.400×10^{-4}	1.936×10^{-7}
c_{P1} / (MPa^{-1})	-5.880×10^{-5}	-3.231×10^{-2}	1.900×10^{-6}	Normal	2	9.500×10^{-7}	-2.496×10^{2}	-2.371×10^{-4}	5.624×10^{-8}
c_{P2} / (MPa^{-2})	4.860×10^{-8}	2.181×10^{-1}	1.060×10^{-8}	Normal	2	5.300×10^{-9}	-6.231×10^{4}	-3.303×10^{-4}	1.091×10^{-7}
P / (MPa)	2.496×10^{2}	1.000×10^{-3}	2.496×10^{-1}	Rectangular	$\sqrt{3}$	1.441×10^{-1}	-2.428×10^{-5}	-3.499×10^{-6}	1.224×10^{-11}
Combined Uncertainty		2.224×10^{-3}	1.955×10^{-3}		2	9.773×10^{-4}			9.552×10^{-7}

input uncertainties gave an uncertainty of 0.22% in the measured value of volume ratio. Uncertainty in the measurement of pressure, temperature and atmospheric pressure density will also contribute to the uncertainty in elevated pressure density. Temperature was accurate to 0.05K[5.1] and the atmospheric density measurements made by ITS Testing Services (UK) were accurate to 0.06%. Considering the effects of these uncertainties on the uncertainty of elevated pressure density using a similar analysis as presented in Table 2.2, gave an overall uncertainty in elevated pressure density of 0.23%.

At least three repeat measurements were made at each temperature for each fluid. The repeatability was typically better than 0.1% between repeats.

2.2.6 – Mechanical Hysteresis

When applying the calibration function to the data recorded by the Micro-PVT and also when calculating the calibration function from the raw data, only the data from the compression and not the decompression have been considered. There is a hysteresis effect between the compression and decompression trials which increases with speed of compression. Part of this difference could be due to a lag between the platform which the encoder measures relative to moving downwards but the encoder rod not falling at the same rate as the platform moves. During the compression the platform moves upwards with the body of the Micro-PVT which will force the encoder rod to move at the same rate. For the decompression the platform is moving in the opposite direction and the encoder falls against the platform under the influence of gravity. Any friction between the encoder rod and the housing will cause a lag in the fall of the rod. Therefore at equivalent pressures

two different displacement readings result when comparing the compression and decompression trials, leading to slightly different pressure-volume curves for the two modes. As any proposed lag is obviously dependent on the rate at which the encoder falls, it follows that the hysteresis would not be observed when comparing upwards and downwards movements of the micrometer head using the test described earlier as the encoder is allowed to come to rest on the rod of the micrometer head.

2.2.7 – Thermodynamic Hysteresis

Using a low speed of compression (0.07 rpm rod rotational speed), the compression is considered to be pseudo-isothermal. A continuous method such as the Micro-PVT cannot be truly isothermal as the fluid is never allowed to attain equilibrium at any given volume / developed pressure. To allow for continuous measurement whilst undertaking a compression which is approaching isothermal, the fluid is compressed at a very slow rate. A constant temperature is maintained in a large volume temperature bath and the fluid from this is circulated round the Micro-PVT pressure vessel at a fast rate. By using a small fluid sample volume any small temperature rise which occurs during the compression is taken up by the circulating fluid where the rise in heat content of the temperature bath and therefore temperature rise of the circulating fluid is negligible due to the large mass of this heat sink. In this way the fluid within the cell is maintained at the temperature of the heat bath.

Further to the principle that led to the use of a low speed for a compression approaching isothermal, it follows that by increasing the speed of compression the compression will be further from isothermal and closer to the isentropic condition. At a high compression speed there would be less time available for heat transfer from

the surroundings. For the condition of the compression taking place instantaneously, heat transfer being a time dependent phenomenon would not occur and any temperature rise of the fluid would be due to the work done in compressing the fluid. Instantaneous compressions not being possible with the Micro-PVT apparatus, an approximation to an isentropic volume change may be made by compressing the fluid as quickly as possible. Compression rate is limited by the stepper motor which rotates at a maximum of 20rpm. Trials may be made at this speed and the resultant data analysed to establish how close the Micro-PVT comes to making an isentropic compression.

By definition an isentropic process is reversible thus any change made between the initial and final state would be witnessed on the return from the final to initial state. For a compression this would mean that at any volume during compression the temperature and pressure recorded upon pressurisation would be equal to the temperature and pressure on the depressurisation at the same volume. Using the measurement technique employed here, such behaviour would not be recorded even if the physical condition was fulfilled in the compression – decompression cycle. This is due to the hysteresis effect on both the volume and pressure measurement gauges. Both pressure and volume are derived from measurements of displacement. Therefore both of these measurements will be subject to the mechanical hysteresis discussed previously.

Another check on departure from the isentropic condition can be made by analysis of the pressure-temperature curves. Instrument effects will again prevent this test from being a true measure of the thermodynamic condition of the compression. As well as the previously discussed hysteresis of the pressure

measurement, there will also be an amount of lag associated with the thermistor. Although the response time is not quantified here, it will be less than that for other PVT measurement techniques due to the temperature gauge being in direct contact with the liquid sample. Ignoring the lag, which is likely to be minimal over small temperature increments, the difference between temperature recorded on compression and on decompression would indicate that the trial is not isentropic as heat is evidently being transferred from the system. Heat transfer occurs due to the efficiency of the circulating fluid at removing heat from the system and also because the compression is not fast enough to prevent the transfer of heat from the system.

It can be seen from Figure 2.10 that initially there is an acceleration phase in the compression as the stepper motor accelerates before reaching the pre-set speed which is then held constant. During this initial acceleration period the temperature rise with respect to pressure for all speeds is equal as the pressure is developing at the same rate due to the fluid being compressed at the same rate until the constant speed is attained. Temperature decreases in a similar fashion on the decompression due to the acceleration of the motor in the reverse direction. Due to these acceleration phases, the Micro-PVT can never provide a true isentropic compression regardless of the final motor speed. The acceleration phase on the decompression will prevent the depressurisation temperature curve following that of the pressurisation, but even when the motor is retracted at the constant maximum speed there is evidence that this is not fast enough for the isentropic condition. It can be seen from Figure 2.10 that at the lower pressures the temperature begins to rise on decompression, and this is particularly pronounced on a cycle which was recorded to

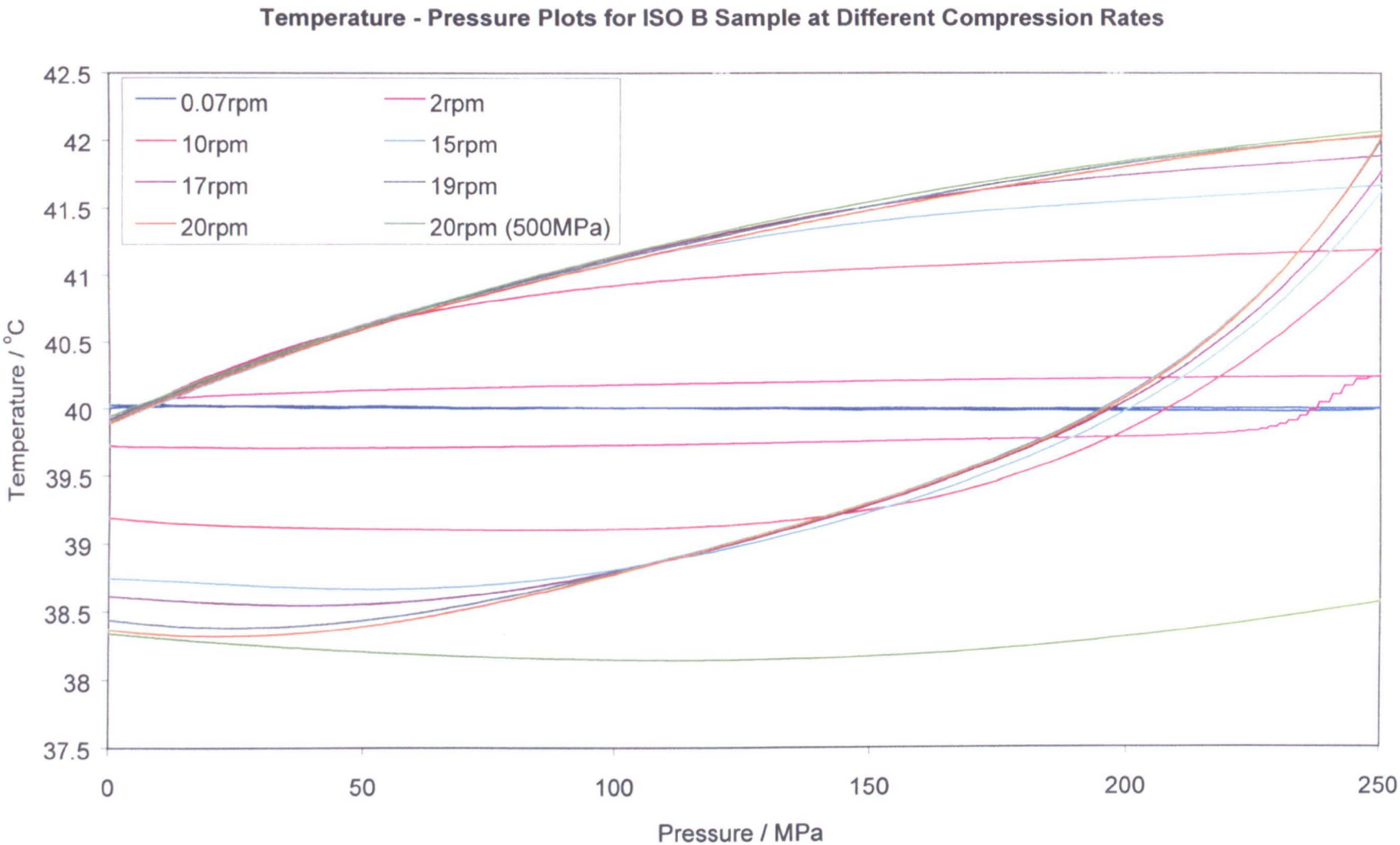

Figure 2.10 Effect of compression speed upon temperature hysteresis

500MPa and back. This temperature rise is due to heat being absorbed into the system from the surroundings which signifies that the cycle is not isentropic.

Chapter 3.

Viscosity Measurement

3. Viscosity Measurement

3.1 Method

In this work the coefficient of dynamic viscosity of liquids at elevated pressure was determined by measuring the rate at which a solid sinker falls through a liquid under the influence of gravity. Viscosity is related to the time taken for the sinker to travel through a fixed length as explained through the force balance presented in Appendix A. With reference to Figure 3.1, the fixed length over which the sinker is timed is the distance between the two detection coils. The coils consist of approximately 230 turns of lacquered copper wire. Each coil is of approximately equal resistance. Both the coils together form one arm of an alternating current bridge circuit which is balanced by means of a variable inductor and variable resistor with respect to two fixed resistors. When the sinker passes through the coils a nickel-iron sinter core glued inside the sinker changes the inductance of the coils causing the bridge circuit to unbalance. The bridge circuit and associated electronics produce a peak on a DC trace as the sinker passes through each set of coils. These peaks are detected, as described by Glen[13.], and signal a timer to start and stop when the sinker passes through the upper and lower coils respectively.

Viscosity measurements are made with the viscometer installed in the pressure vessel as shown in Figure 3.2. The pressure vessel is mounted in a well stirred oil bath to provide a constant temperature for measurement. Pressure is generated using an air-hydro pump at pressures up to 200MPa. An intensifier is used to generate pressures above this. Details of the pressure generation circuit are given

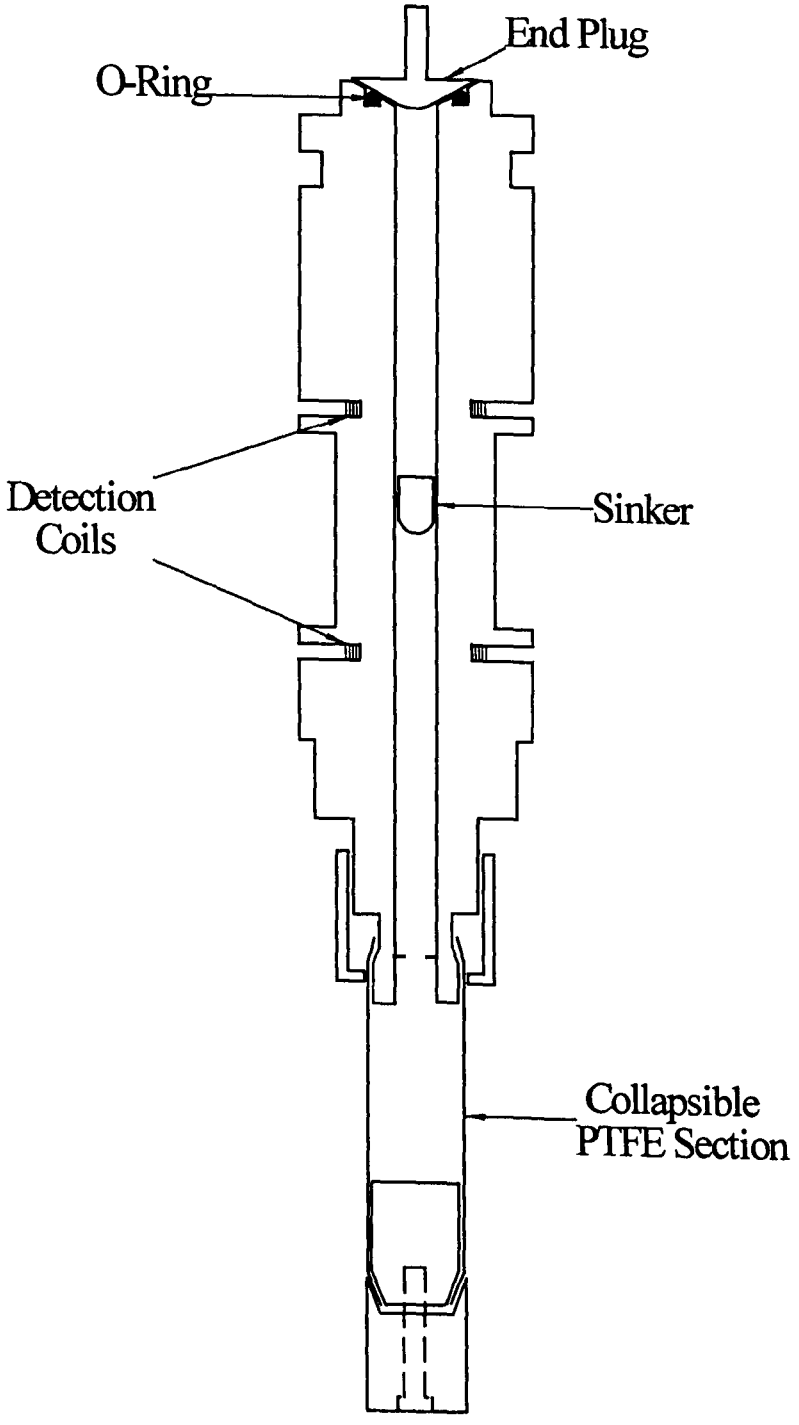

Figure 3.1 Falling Sinker Viscometer

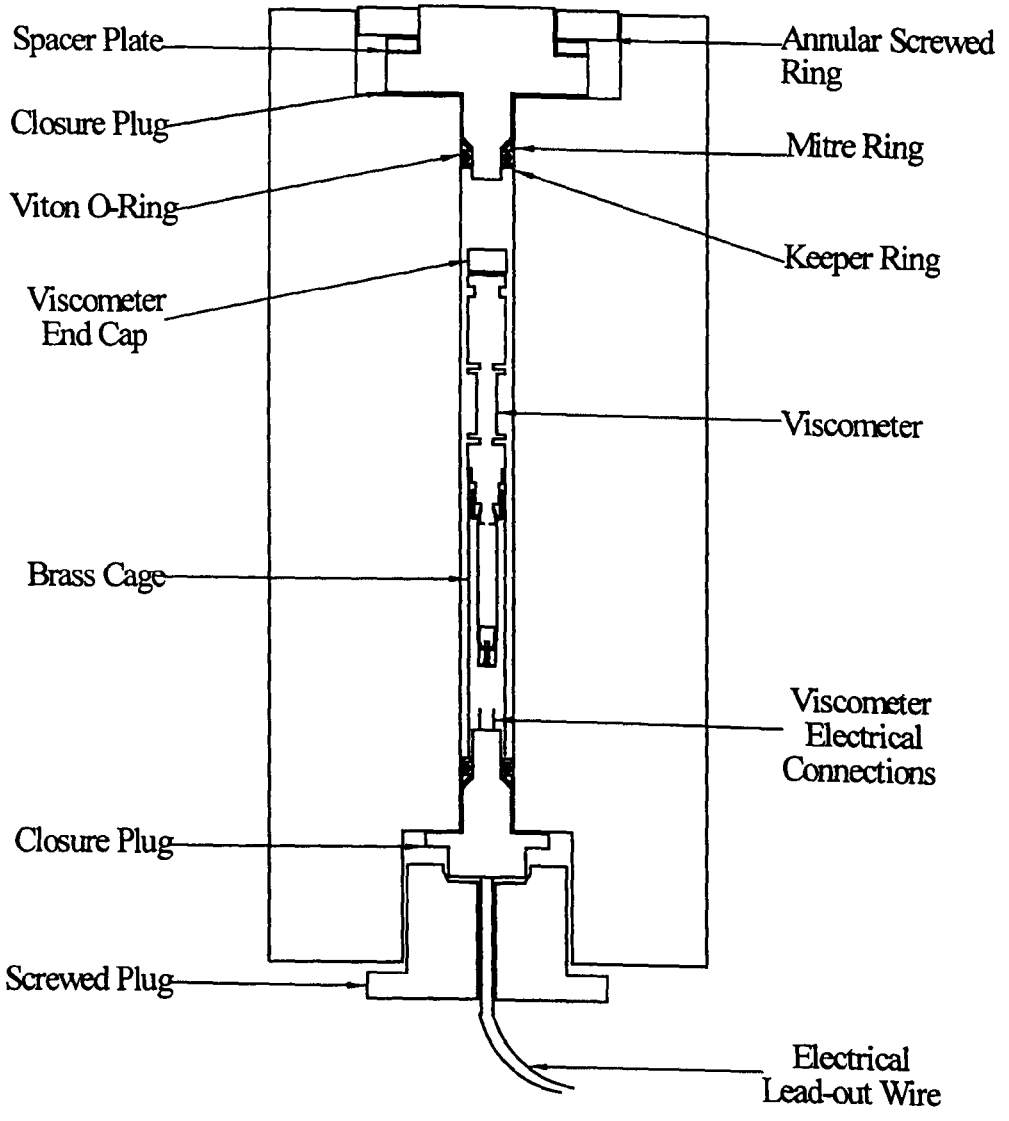

Figure 3.2 Assembled Viscometer in Pressure Vessel

by Glen[13.]. Sealing of the vessel is provided by an arrangement of o-rings and mitre rings proposed by Glen[13.].

The viscometer employed throughout can be considered a versatile instrument for viscosity measurement in terms of the range of viscosity over which it is valid. Isdale[25.] suggests that this method gives better accuracy at low viscosity than a rolling ball method since it avoids the possibility of the ball moving in a sticking and slipping fashion, or spinning. Perhaps the most accurate high pressure apparatus for the measurement of low viscosity is the vibrating wire viscometer[26.]. This method is subject to uncertainty at the highest viscosities due to the large excitation required at these viscosities possibly generating eddies in the fluid. It has been suggested that this phenomenon could occur at viscosities above 300mPa.s[27.].

3.2 Detection of Freezing

One incidental feature which has been noted from the falling body method of measurement is the detection of freezing in mixtures. This is highlighted by measurements made of a diesel fuel with no additives at 25^{0}C. Volumetric measurements of the fuel by the Micro-PVT give a smooth curve with no sharp changes in volume at constant pressure, which would be indicative of freezing, as shown in Figure 3.3. When fall time measurements at 255MPa were made in the viscometer, repeatability was found to be poor. A repeat measurement conducted after holding the viscometer at pressure over an extended time interval gave a fall time over two times longer than measurements made on the previous occasion, despite the pressure having dropped only very slightly due to small imperfections with the sealing. This final fall time measurement does not fit the straight line of the

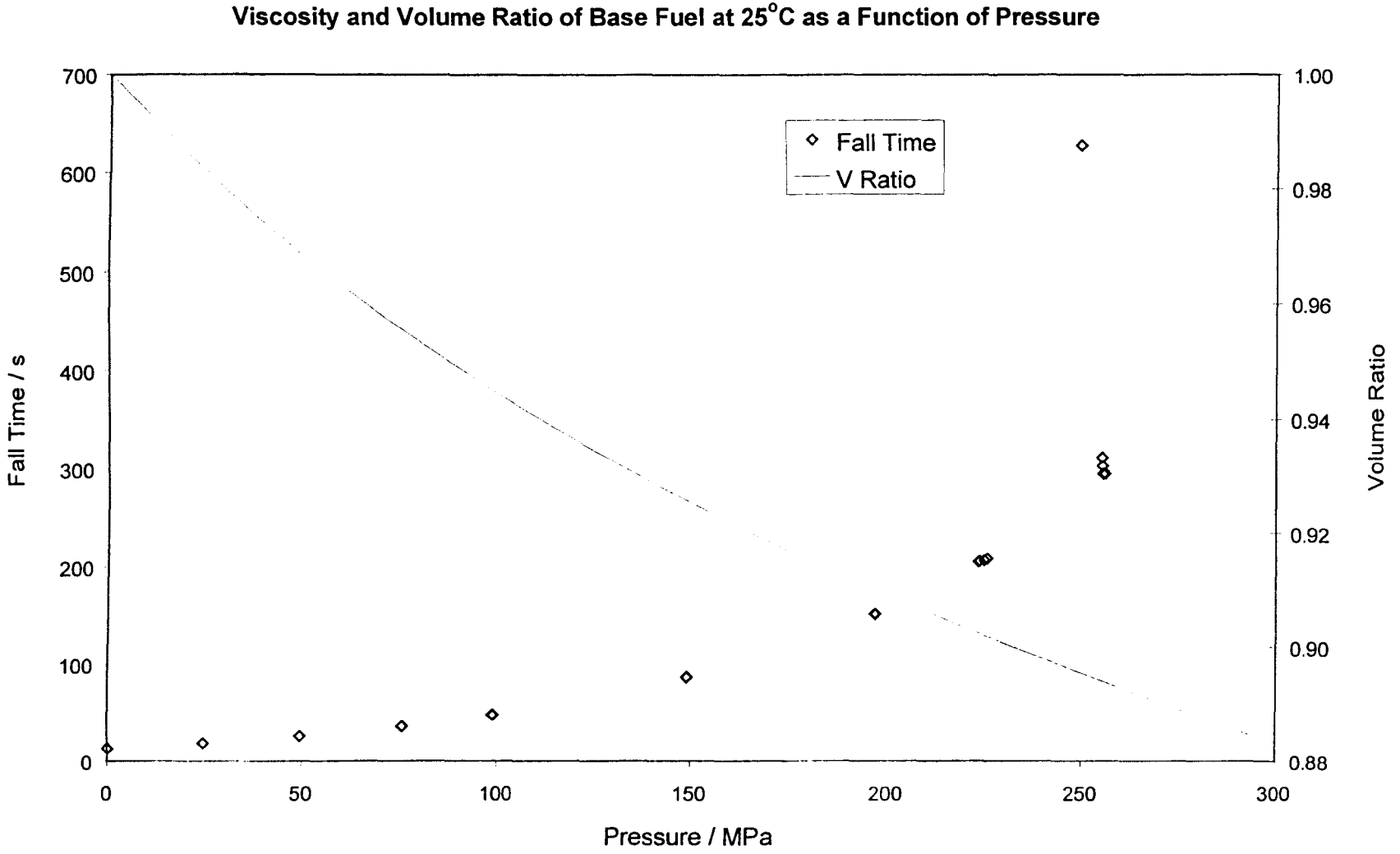

Figure 3.3 Comparison of viscometer and Micro-PVT measurements of Fuel A at 25^0C

logarithm of fall time as a function of pressure as prior measurements do, as seen from Figure 3.4. Such a result suggests that a phase change has occurred although not to the extent that the entire sample has frozen, since this would prevent the sinker from falling through the fuel. It is therefore concluded that one or more of the heavier components of the fuel has frozen out of the mixture causing the sinker movement to be retarded. That the fall time is far longer at a slightly lower pressure after leaving the system at elevated pressure for a long time may be due to the heavy component preferentially freezing in the narrow gap between sinker and tube wall when the phase equilibrium is allowed to establish over time. The initial assumption of poor repeatability would thus be due to the system not being at equilibrium.

In the fuel injector this finding is of limited relevance as the temperature will be higher and the processes too fast for a thermodynamic equilibrium to be obtained. However, from a thermodynamic viewpoint, these measurements provide useful information on the nature of freezing in mixtures and the detection of this. Detection of freezing by analysis of volume changes would require a very accurate PVT device to measure a small volume change at constant pressure as a single component freezes out of the mixture. A continuous PVT measurement method would be inappropriate for this purpose as the system cannot attain equilibrium. Consideration would also need to be given to annuli providing preferential sites for freezing to occur. A phase change such as the one recorded here may also be detectable by the vibrating wire method. If the freezing component froze onto the vibrating wire element, this would change the density of the element which would affect the apparent viscosity measurement.

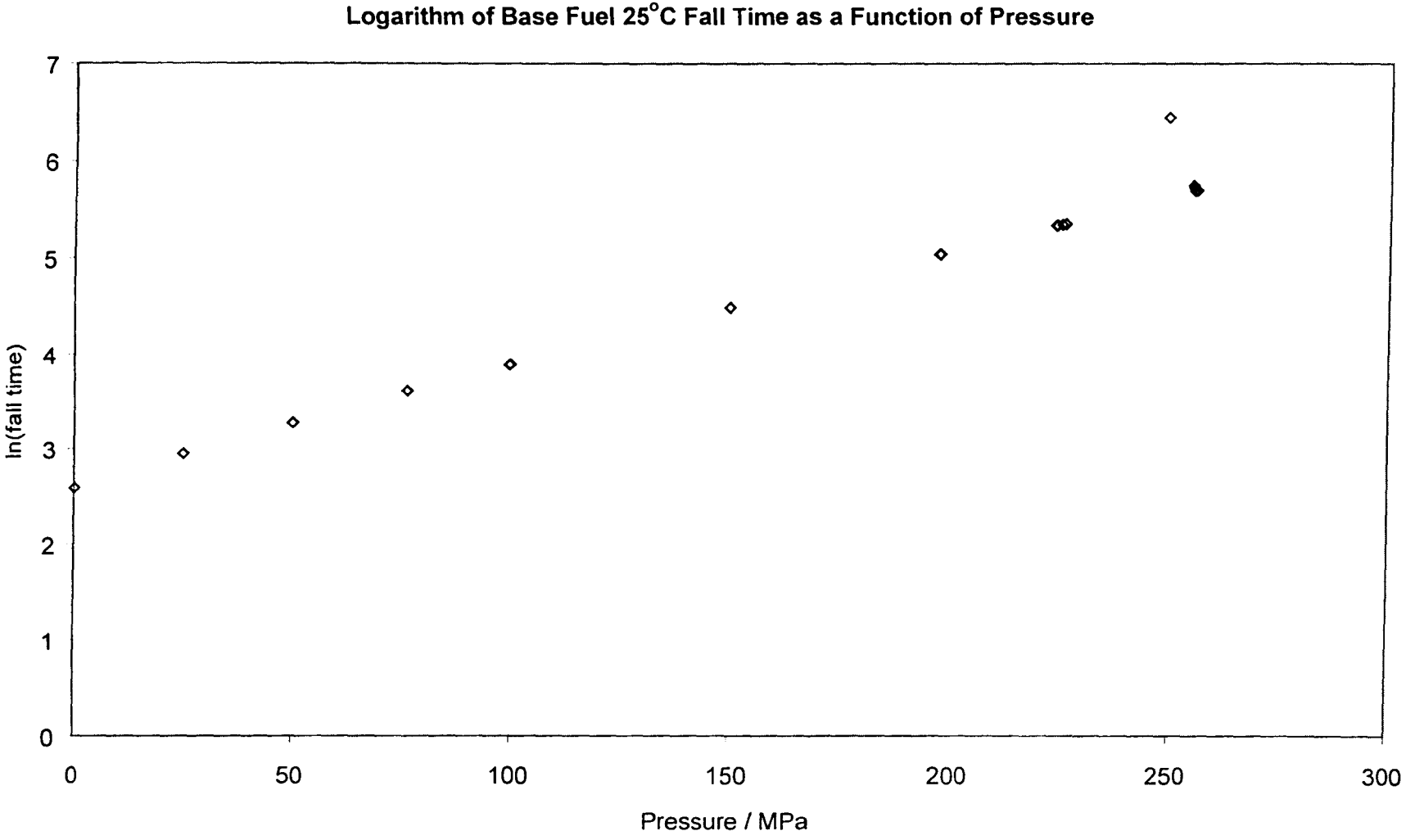

Figure 3.4 Indication of freezing by plot of logarithm of fall time

3.3 Temperature Measurement and Control

Two platinum resistance thermometers (PRT's) are used for measuring temperature in the oil bath surrounding the pressure vessel of the falling body viscometer. These are located as close as possible to the pressure vessel and in the well stirred oil bath the temperature recorded from the thermometers can be assumed to be representative of the temperature of the outer wall of the pressure vessel. Temperature within the oil bath can be held to within 0.02K by means of a Eurotherm temperature controller. Due to the thermal inertia effect associated with a thick-walled steel pressure vessel, the corresponding variation in temperature within the bore of the vessel where the viscometer and the fluid sample are contained is significantly less. Measurements of temperature conducted by inserting a thermometer directly in the vessel bore gave stability to within ±0.002K for a corresponding temperature variation of 0.02K in the oil[27.].

Tests conducted at 50^0C to investigate temperature profiles throughout the bath and vessel showed that mounting the thermometers in close proximity to the stirrers led to the temperature measurement being subject to unstable local temperature effects induced by the stirrers. Instability in temperature measurement was also caused when the thermometers were mounted on a bracket at the rear of the oil bath which was subject to vibration from the rear stirrers. At the front of the oil bath it was possible to mount the thermometers to a bracket attached to a structural member in the bath which was not subject to vibration. Temperature agreement between the thermometers using this configuration was of the order of 1mK. Temperature agreement when the thermometers were placed to the front and rear of the vessel was less than 10mK, but the thermometer at the rear was subject to the

vibration mentioned. Agreement in temperature measurement between a thermometer positioned at the front of the oil bath and one directly in the bore of the vessel was of the order of a few milliKelvin. This is satisfactory considering that any small temperature change in the oil bath will take a long time to affect the temperature in the pressure vessel due to thermal lag as the heat transfers through the thick steel wall of the vessel.

3.3.1 – PRT Calibration

Resistance was measured for each of the PRT's at temperatures of 0 to 160°C in increments of 20K where temperature was measured using a PRT previously calibrated to National Standards using reference points of the International Temperature Scale of 1990 (ITS-90)[28.]. From these data the resistance ratio, $R(T_{90})/R_0$ could be calculated at each temperature. $R(T_{90})$ is the resistance of the PRT at the given temperature T_{90}, and R_0 is the resistance of the PRT at the temperature of the triple point of water (273.16K). Resistance ratios $W(T_{90})$ obtained for the PRT's are then compared with the resistance ratios of ideal platinum, $W_r(T_{90})$, as calculated from the equation:

$$W_r(T_{90}) = C_0 + \sum_{i=1}^{9} C_i \left\{ \frac{T_{90} - 754.15K}{481K} \right\}^i \tag{3.1}$$

The difference between the actual PRT resistance and the ideal resistance, $W(T_{90})$-$W_r(T_{90})$ was plotted as a function of $W(T_{90})$-1, thus allowing for a calibration function to be found of the form:

$$W(T_{90}) - W_r(T_{90}) = a(W(T_{90}) - 1) + b(W(T_{90}) - 1)^2 \tag{3.2}$$

Using the parameters a and b found from the calibration, the resistance found from the PRT's can be converted to ideal resistance ratios through back calculation and this then allows the ITS-90 temperature to be calculated from

$$T_{90} = 273.15 + D_0 + \sum_{i=1}^{9} D_i \left\{ \frac{W_r(T_{90}) - 2.64}{1.64} \right\}^i \tag{3.3}$$

Values of C_0, C_i, D_0 and D_i used in equations (3.1) and (3.3) are found from the reference[28.] and are valid for calibrations in the range 273.15 to 1234.93K. Values of R_0, a and b for the two PRT's are presented in Table 3.1.

Table 3.1 Calibration coefficients for viscometer platinum resistance thermometers

PRT	R_0	a	b
1	100.01453	-0.020447	-5.7472×10^{-4}
2	100.00618	-0.021714	-5.6893×10^{-4}

3.4 Pressure Measurement and Calibration

Viscometer pressure is measured by a piezo-resistive pressure gauge manufactured by Kistler. Voltage output of the gauge as a function of pressure was measured by Transducer Laboratories Limited. Due to non-linearity over the pressure range from 0-500MPa it was necessary to split the data into two ranges with separate fits of voltage as a function of pressure between 0-150MPa and 150 to 500MPa. Coefficients to relate pressure to voltage through quadratic equations in the two ranges are given in Table 3.2.

Table 3.2 Calibration coefficients for viscometer pressure gauge

Pressure Range (MPa)	a_0	a_1	a_2
0-150	0	51.517	0.1406
150-500	-2.5644	53.900	-0.4287

3.5 Viscometer Calibration

From the force balance presented in Appendix A, it was found that viscosity can be calculated from a measurement of fall time provided that fluid and sinker density are known at the condition of measurement along with tube and sinker dimensions. With these parameters known, viscosity would then be found from equation (A.17). Due to the form of this equation, any surface irregularities or slight inaccuracy in measurements of tube or sinker radii will cause a large change in the predicted value of viscosity. It is therefore better practice to calibrate the instrument with fluids of known viscosity and density and use these measurements to find viscosity from an equation of the form;

$$\eta = \frac{t\left(1-\frac{\rho_f}{\rho_s}\right)}{A\left[1+2\alpha(T-T_0)\right]\left[1-2\beta(P-P_0)\right]} \tag{3.4}$$

where A is equivalent to;

$$A = \frac{2\pi L_{s0} L_{t0}}{mg\left[\ln\frac{r_2}{r_1} - \frac{r_2^2 - r_1^2}{r_2^2 + r_1^2}\right]} \tag{3.5}$$

Theoretically, therefore, A will be constant throughout if the assumption of laminar flow used in the derivation of the equation was valid. Measurements made with calibration fluids gave rise to the curve of A as a function of t^* reproduced in Figure 3.5. Noting that A tends toward a constant value at longer fall times with the

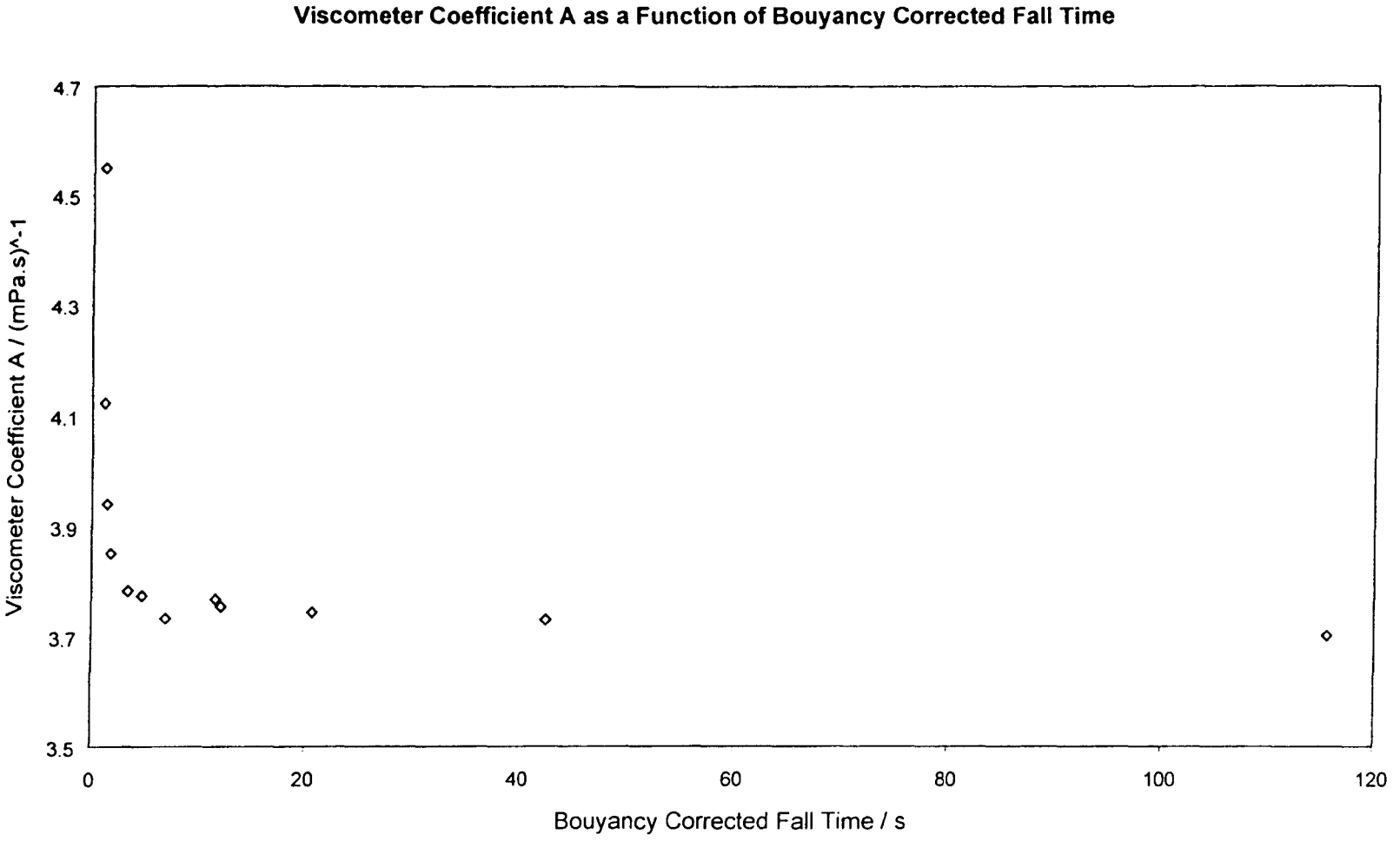

Figure 3.5 Variation of viscometer coefficient with buoyancy corrected fall time

change of A being steepest at short fall times where velocity is highest, it is likely that the variability of A is due to the flow being non-laminar with a transition towards the laminar flow regime for longer fall times. It may thus be appropriate to relate the variation of A to Reynolds' number. Although both Isdale[25.] and Glen[13.] investigated the variation of the viscometer constant with respect to Reynolds' number, they and later workers[11,12.] using the same method obtained their eventual calibration function with respect to buoyancy corrected fall time.

Bird et al.[29.] define Reynolds number in an annulus as;

$$\mathrm{Re} = \frac{2r_2\left(1-\frac{r_2}{r_1}\right)u_{ave}\rho}{\eta} \tag{3.6}$$

Average velocity will be equal to the ratio of flow rate to flow area;

$$u_{ave} = \frac{Q}{\pi\left(r_2^{\,2} - r_1^{\,2}\right)} \tag{3.7}$$

(3.6) and (3.7) can be combined with (A.13) to give annular Reynolds' number in terms of measured sinker velocity;

$$\mathrm{Re} = \frac{2r_1^{\,2}}{r_2 + r_1} u_{\mathrm{sin\,ker}} \frac{\rho}{\eta} \tag{3.8}$$

Figure 3.6 shows the plot of A from equation (3.4) as a function of Reynolds' number when A and Re are found from the calibration fluid measurements. A clustering of data points are seen at low Reynolds number as A tends towards a constant value whilst the points at high Reynolds number are more spread out. Taking an appropriate power of Reynolds number, Re^n, and plotting A as a function of this causes the plot to be more spread out at lower values of Reynolds number, allowing a more accurate fit to the data. Despite this a value of n could not be found to

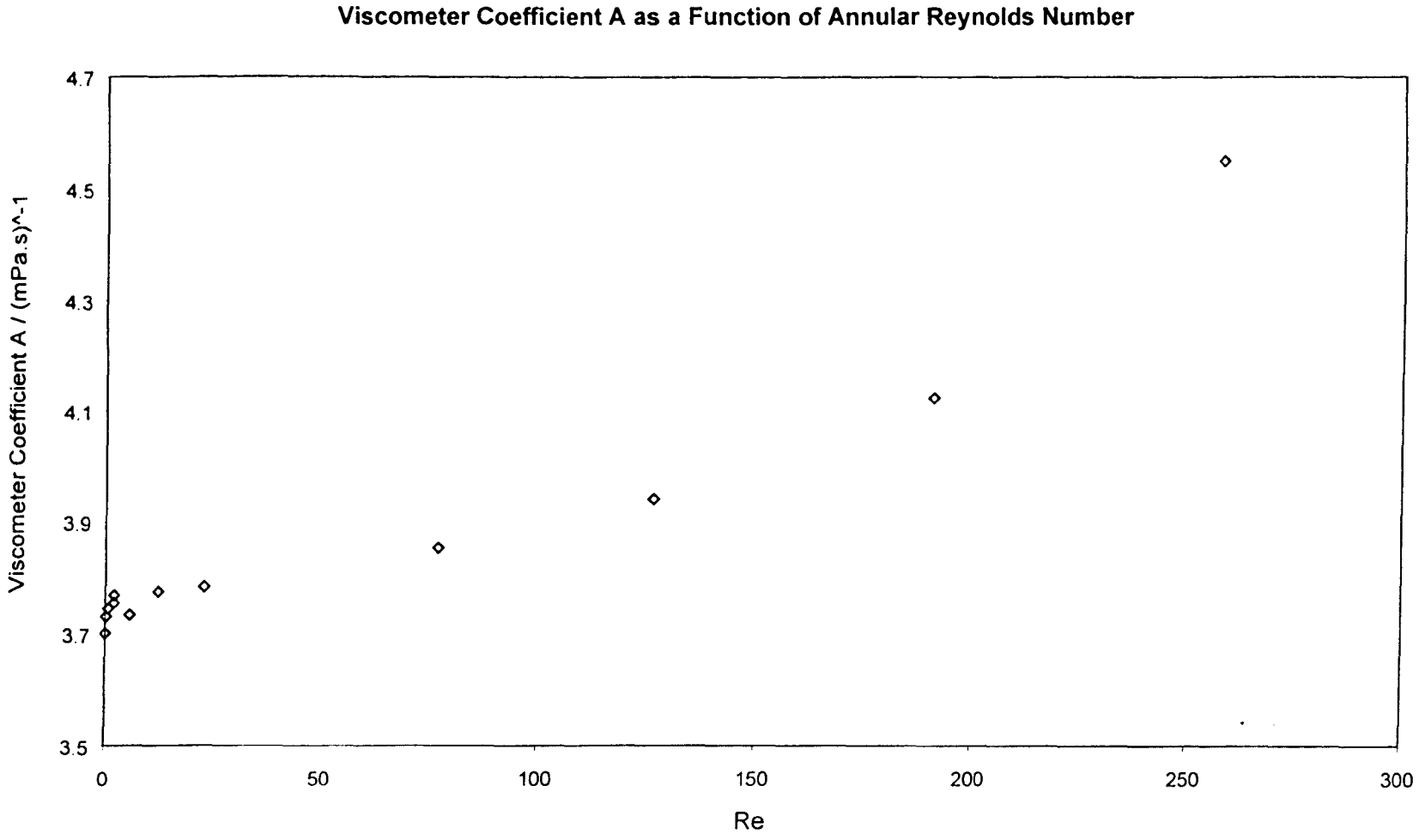

Figure 3.6 Variation of viscometer coefficient with annular Reynolds number

reconcile the data in a single smooth trend. The data were therefore split into two sets (low Reynolds number and high Reynolds number) which were then fitted using two individual straight line fits. A was thus fitted to a function of the form $A=a(\mathrm{Re}^b)+c$ with the values of a, b and c shown in Table 3.3.

Table 3.3 Coefficients for fitting the viscometer constant A to the equation $A=a(\mathrm{Re}^b)+c$

Range of Re	a / $(\mathrm{mPa.s})^{-1}$	b	c / $(\mathrm{mPa.s})^{-1}$
0<25	0.0978	0.1	3.645
25<260	7.024×10^{-7}	2.5	3.792

Data used for the calibration and the error in values of A calculated using the fitting routine described above are presented in Table 3.4. At a Reynolds number of zero, the equation reduces to $A=c$, i.e. $3.645\mathrm{mPa}^{-1}$. The theoretical value of A calculated from measurements of instrument dimensions is $4.364\mathrm{mPa}^{-1}$. The sinker length was taken as the length from the tip of the sinker nose to the tail. Given that the flow is not immediately fully developed as was assumed in the derivation of the theoretical constant A value, the effective length of the sinker over which the flow is laminar will be less than the sinker length. For example, if the flow is not assumed fully developed until the cylindrical section of the sinker, excluding the hemispherical nose section, the effective length would be about 80% of the total length. As A is directly proportional to sinker length, A would become $3.491\mathrm{mPa}^{-1}$, a difference of 4.4% compared to the estimated A. Given the effect of slight measurement inaccuracies on the final value of A and the assumption regarding fully developed flow, this represents a reasonable agreement between the two values.

Table 3.4 Viscometer Calibration Data

Liquid	Temperature / K	Density / kgm^-3	Viscosity / mPa.s	Fall time / s	t^* / s	Re	A	Calculated A	% Diff
Iso-octane	298.14	687.9	0.4718	2.089	1.817	77.00	3.852	3.829	0.61
	323.17	666.6	0.3588	1.618	1.414	126.7	3.941	3.919	0.56
	348.17	644.5	0.2816	1.323	1.162	191.0	4.122	4.146	-0.58
	373.15	621.2	0.2269	1.171	1.034	258.1	4.550	4.544	0.13
Hexadecane	298.15	770.2	3.0679	13.529	11.561	2.047	3.768	3.750	0.49
	323.17	753.0	1.8429	8.026	6.884	5.618	3.734	3.761	-0.73
	348.19	735.8	1.2364	5.425	4.670	12.110	3.775	3.770	0.11
	373.13	718.6	0.8927	3.913	3.381	22.719	3.783	3.779	0.12
S20 Oil	298.16	854.7	31.223	137.82	115.57	0.022	3.702	3.712	-0.28
	323.16	838.9	11.374	50.448	42.451	0.161	3.731	3.726	0.12
	348.16	823.0	5.525	24.524	20.707	0.670	3.745	3.739	0.16
	373.17	807.1	3.215	14.265	12.086	1.943	3.755	3.749	0.15

From the calibration procedure described above viscosity can be found from fall time through equation (3.4) with A as a function of Reynolds number. Robertson[12.] showed that systematic errors in viscosity measurements from the falling body viscometer used here could be reduced by using an accurate atmospheric viscosity measurement in a 'ratio' method with the atmospheric viscosity found from fall time and equation (3.4). For the calibration equation as a function of annular Reynolds number, the ratio method yields;

$$\eta = \frac{t^{*}\eta_0\left[a\left(\frac{2r_{1_0}^{\ 2}}{r_{2_0}+r_{1_0}}\frac{L_{t_0}}{t_0}\frac{\rho_{l_0}}{\eta_0}\right)^{b}+c\right]}{\left[a\left(\frac{2r_{1_P}^{\ 2}}{r_{2_P}+r_{1_P}}\frac{L_{t_P}}{t_P}\frac{\rho_{l_P}}{\eta_P}\right)^{b}+c\right]\left[1-2\beta(P-P_0)\right]t_0^{*}} \tag{3.9}$$

3.6 Analysis of Uncertainty

A summary of the uncertainty analysis for the high pressure falling body viscometer is presented in Table 3.5. This uncertainty analysis was derived using data from the measurement of viscosity of Fuel C (see Chapter 6) at 75^{0}C and 439.36MPa. The analysis summarised in Table 3.5 combines the contributions of the input uncertainties to the overall output uncertainty in the working equation (3.9) by quadrature as the inputs are uncorrelated. Separate uncertainty analyses were made of t^{*}, t^{*}_0, A_0, and A_P which are all functions of more than one input, with each input having its associated uncertainty.

Buoyancy corrected fall times are a function of the measured fall time, liquid density and sinker density. An uncertainty analysis for sinker density is made from the inputs to this which are given in equations (A.19) and (A.20). The viscometer

Table 3.5 Uncertainty analysis of relative high pressure viscosity measurement

Source of Uncertainty	Nominal Value	Expanded Relative Uncertainty	Expanded Absolute Uncertainty	Probability Distribution	Divisor	Standard Uncertainty	Sensitivity Coefficient	Contribution to Uncertainty	Contribution Squared
t^* / (s)	1.830×10^{2}	2.929×10^{-3}	5.360×10^{-1}	Normal	2	2.680×10^{-1}	2.653×10^{-4}	7.109×10^{-5}	5.054×10^{-9}
η_0 / (Pa.s)	1.228×10^{-3}	5.000×10^{-3}	6.140×10^{-6}	Rectangular	$\sqrt{3}$	3.545×10^{-6}	3.953×10^{1}	1.401×10^{-4}	1.963×10^{-8}
A_0 / ({mPa.s}$^{-1}$)	3.771×10^{0}	1.231×10^{-2}	4.641×10^{-2}	Normal	2	2.320×10^{-2}	1.287×10^{-2}	2.986×10^{-4}	8.918×10^{-8}
t^*_0 / (s)	4.723×10^{0}	2.727×10^{-3}	1.288×10^{-2}	Normal	2	6.439×10^{-3}	-1.025×10^{-2}	-6.599×10^{-5}	4.355×10^{-9}
A_p / ({mPa.s}$^{-1}$)	3.706×10^{0}	9.539×10^{-3}	3.535×10^{-2}	Normal	2	1.768×10^{-2}	-1.297×10^{-2}	-2.293×10^{-4}	5.258×10^{-8}
β_{Ti} / (MPa^{-1})	3.075×10^{-6}	2.500×10^{-1}	7.688×10^{-7}	Normal	2	3.844×10^{-7}	4.279×10^{1}	1.645×10^{-5}	2.705×10^{-10}
P / (MPa)	4.394×10^{2}	1.000×10^{-3}	4.394×10^{-1}	Normal	2	2.197×10^{-1}	2.993×10^{-7}	6.575×10^{-8}	4.324×10^{-15}
P_0 / (MPa)	1.013×10^{-1}	9.869×10^{-3}	1.000×10^{-3}	Rectangular	$\sqrt{3}$	5.774×10^{-4}	-2.993×10^{-7}	-1.728×10^{-10}	2.986×10^{-20}
Combined Uncertainty		1.704×10^{-2}	8.272×10^{-4}		2	4.136×10^{-4}			1.711×10^{-7}

coefficient, A, is a function of the inputs to annular Reynolds number and the fitting coefficients a, b and c.

Uncertainty in the calculation of A_P is presented in Table 3.6. An optimal value of b was found which gave the best straight line fit of $A=f(Re^b)$ from the calibration data. Uncertainty values of a and c were estimated from the difference of slope and intercept of the straight line fits needed to cover all the calibration data and the line of best fit used to fit the data. Uncertainty in tube radius was found from the difference in measured values at different positions in the bore. Relative uncertainty in sinker radius was assumed to be the same as that of the tube. A larger uncertainty was assigned to the distance between the mid-points of the coils, L_t, as this was measured with less accuracy. Uncertainty in the change of material dimensions with pressure and temperature due to uncertainty in measurement of these parameters and the material properties was also taken into account in the final calculation of uncertainty of the instrument dimensions. Fall time uncertainty was taken to be at the level of repeatability of the measurements. At least three repeat fall time measurements were made at each temperature and pressure for each fuel, with repeatability within 0.2%. Uncertainty from repeatability is far greater than the resolution of the timer which operated at 120MHz. Liquid density uncertainty was taken to be higher than that recorded by the Micro-PVT as this was an extrapolation beyond the maximum measured pressure, as detailed in Chapter 6. Uncertainty in the viscosity value used to calculate Reynolds number is a conservative estimate of uncertainty in using the viscometer as an absolute instrument based on the measurements of previous workers[11-12,25].

Table 3.6 Uncertainty analysis of elevated pressure viscometer coefficient, A_P

Source of Uncertainty	Nominal Value	Expanded Relative Uncertainty	Expanded Absolute Uncertainty	Probability Distribution	Divisor	Standard Uncertainty	Sensitivity Coefficient	Contribution to Uncertainty	Contribution Squared
a / (mPa.s)$^{-1}$	9.780×10^{-2}	2.360×10^{-1}	2.308×10^{-2}	Rectangular	$\sqrt{3}$	1.333×10^{-2}	6.275×10^{-1}	8.362×10^{-3}	6.992×10^{-5}
b	1.000×10^{-1}	0	0	Rectangular	$\sqrt{3}$	0	0	0	0
c / (mPa.s)$^{-1}$	3.645×10^{0}	7.400×10^{-3}	2.697×10^{-2}	Rectangular	$\sqrt{3}$	1.557×10^{-2}	1.000×10^{0}	1.557×10^{-2}	2.425×10^{-4}
$r_{1T,P}$ / (m)	3.702×10^{-3}	5.632×10^{-4}	2.085×10^{-6}	Normal	2	1.043×10^{-6}	2.504×10^{0}	2.611×10^{-6}	2.984×10^{-12}
$r_{2T,P}$ / (m)	3.870×10^{-3}	5.632×10^{-4}	2.180×10^{-6}	Normal	2	1.090×10^{-6}	-8.103×10^{-1}	-8.831×10^{-7}	r_1, r_2 correlated
$L_{tT,P}$ / (m)	3.046×10^{-2}	5.784×10^{-3}	1.762×10^{-4}	Normal	2	8.809×10^{-5}	2.010×10^{-1}	1.770×10^{-5}	3.133×10^{-10}
t_P/ (s)	2.226×10^{2}	2.000×10^{-3}	4.452×10^{-1}	Rectangular	$\sqrt{3}$	2.570×10^{-1}	-2.754×10^{-5}	-7.079×10^{-6}	5.011×10^{-11}
$\rho_{l,P}$ / (kg.m^{-3})	9.449×10^{2}	5.000×10^{-3}	4.725×10^{0}	Normal	2	2.362×10^{0}	6.480×10^{-6}	1.531×10^{-5}	2.343×10^{-10}
η_P / (Pa.s^{-1})	4.945×10^{-2}	5.000×10^{-2}	2.472×10^{-3}	Rectangular	$\sqrt{3}$	1.427×10^{-3}	-1.208×10^{-1}	-1.725×10^{-4}	2.974×10^{-8}
Combined Uncertainty		9.539×10^{-3}	3.535×10^{-2}		2	1.768×10^{-2}			3.125×10^{-4}

Uncertainty in measured viscosity from the high pressure viscometer, using the working equation (3.9), was found from the uncertainty analysis to be 1.70%. Uncertainty in viscosity due to uncertainty in temperature and pressure measurement is combined with the uncertainty of the viscometer to give an overall uncertainty of 1.74% in elevated pressure viscosity.

Chapter 4.

Density Correlation and Prediction

4. Density Correlation and Prediction

4.1 Corresponding States Principle – Previous Work

4.1.1 - Background

One of the more versatile methods for the prediction of dense fluid thermodynamic properties is that of Lee and Kesler[30]. Unlike other methods the Lee and Kesler method uses the published critical property and acentric factor data directly without the calculation of intermediary characteristic parameters. For example, the method of Hankinson and Thomson[31] and later Thomson et al.[32] for liquid density prediction requires the determination of a characteristic volume for the fluid of interest. Similarly, the method of Soave[33], based upon the equation of state of Redlich and Kwong[34] requires the calculation of a correction factor for the fluid of interest.

Based upon the three parameter corresponding states principle, the method of Lee and Kesler calculates the compressibility factor of the fluid of interest with respect to those of a simple fluid and a reference fluid. Three parameter corresponding states was used as the two parameter corresponding states method was found to be inadequate for estimating pressure-volume-temperature relations of non-ideal fluids. The original two parameter corresponding states principle relates intermolecular separation and energy of one ideal fluid to that of another by appropriate scaling parameters. In order to take account of the departure from ideality Pitzer[35] introduced a third parameter: the acentric factor.

Pitzer noted that the only substances which displayed corresponding behaviour, that is to say those with similar intermolecular potential curves, were

argon, krypton, xenon and methane. Correspondence between these fluids, termed simple fluids, was attributed to their spherical shape and an absence of quantum effects. Two parameter corresponding states theory does not hold for non-spherical polyatomic molecules as there is no longer a single attractive centre co-incident with the geometric centre. For example, in the case of a long chain hydrocarbon with branching, attractions will be between the methyl groups of the molecules. Thus, the attractions are no longer between the molecular centres as is assumed when a theoretical description of the intermolecular pair potential energy curve is made for simple spherical molecules.

4.1.2 – Acentric Factor

Pitzer defined a model for a branched molecule by taking into account attractive effects between parts of the molecule away from its centre. From the intermolecular curve produced by this model it was seen that the potential minimum was narrowed compared to the simple case. With consideration of this finding and its implications for entropy, Pitzer established that change in vapour pressure with respect to temperature would be steeper for complex molecules compared to simple molecules.

Taking into account this finding regarding vapour pressure, Pitzer et al.[36] defined a third parameter for the corresponding states theory to account for attractions between non-central parts of the molecule. This third parameter was termed the acentric factor and was defined as ω=-log(P_r)-1 where P_r is the reduced vapour pressure at a reduced temperature of 0.7. Reduced vapour pressure as a

function of reduced temperature is the same for the simple fluids. At T_r=0.7, P_r=1 for the simple fluids and therefore these have an acentric factor of zero.

Plots of compressibility factor as a function of acentric factor were made for the range $0.8<T_r<4$ and $0<P_r<9$. Observing that these lines were approximately linear, it was proposed that $Z=Z^{(0)}+\omega Z^{(1)}+\ldots$ which may be expanded as deemed necessary by curvature. Terms $Z^{(n)}$ were proposed to be functions of reduced temperature and pressure. Rather than using a general equation to define these functions precisely, tables of values of $Z^{(0)}$ and $Z^{(1)}$ were presented as functions of T_r and P_r. From this study the properties of a fluid may be estimated from those of a simple fluid with deviations accounted for by change in intermolecular energy via critical temperature, intermolecular separation via critical pressure (critical volume cannot be accurately measured and is therefore not used for modelling purposes) and molecular shape by acentric factor.

4.1.3 – Analytical Method for Three Parameter Corresponding States

Lee and Kesler attempted to define an equation of state using the three parameter corresponding states principle which could be solved analytically rather than graphically or by use of tables of values. Compressibility factor of the fluid of interest was defined by;

$$Z = Z^{(0)} + \frac{\omega}{\omega^{(r)}}\left(Z^{(r)} - Z^{(0)}\right) \tag{4.1}$$

Rather than defining $Z^{(0)}$ and $Z^{(r)}$ by arbitrary functions of reduced temperature and pressure, these parameters represented the compressibility factors of a simple and a reference fluid. Thus at a given temperature and pressure the compressibility factor of the fluid of interest was equal to the compressibility of the simple fluid at

equivalent reduced temperature and pressure plus a deviation term defined in terms of acentric factor. Octane was chosen as a reference fluid, this being the heaviest hydrocarbon having suitably comprehensive thermodynamic data at the time. Compressibility factors of the simple and reference fluid were calculated using an equation of state based upon that of Benedict et al.[37]. In order that compressibility factors were valid across the whole fluid region, the constants in the modified Benedict-Webb-Rubin equation were determined with the constraint that vapour and liquid fugacities were equal at saturation and the first and second derivatives of pressure were zero with respect to volume at the critical point.

Using the constraints set out above Lee and Kesler defined their equation such that different properties of the fluid could be calculated in a thermodynamically consistent manner. Applying such constraints on the model may be the cause of the predictive properties of the equation being limited when any single property, for example liquid density, is considered. This is most readily demonstrated for the case of n-octane. As this was chosen as the reference fluid the equation for compressibility factor reduces to $Z=Z^{(r)}$. $Z^{(r)}$ was previously defined by fitting n-octane data to the modified Benedict-Webb-Rubin equation of state and therefore compressibility factor calculated by this method should be accurate to the fitting abilities of this equation. Comparing calculated compressibilities with measured compressibilities in the subcooled liquid and dense phase the average absolute deviation was quoted as 1.87% in the range $0.66<T_r<0.96$ and $0.2<P_r<8.2$. Extending the pressure range well beyond the recommended maximum of ten times the critical pressure, the deviation of the function can be analysed at high pressure when compared with the results of Dymond et al.[38]. Error at each temperature

increases in an approximately linear fashion with respect to pressure up to 300MPa as detailed in Figure 4.1. Beyond this pressure, rate of change of error with respect to pressure decreases to the extent that the error goes through a local maximum. Volume ratio rather than density has been compared to remove initial error due to incorrect prediction of atmospheric density. From plots of error as a function of pressure it is observed that the trend of error with respect to pressure is nearly identical for the temperatures considered. Within the range of atmospheric to $10P_c$ (~25MPa) the slope of error with respect to pressure is steep suggesting that even within the specified range of applicability the pressure dependence of the fit could be improved by making the equation thermodynamically less general. Predictions of volume change with respect to pressure for other liquid alkanes have errors of similar orders of magnitude to that of n-octane, as shown in Figure 4.2.

Despite the errors in predicted change in liquid volume with respect to pressure being quite large, even over the limited range of 0-$10P_c$, the validity of the Lee-Kesler equation must not be overlooked on two counts. Firstly, the error increases in a regular fashion when the equation is used far beyond the stated limit of pressure. Secondly, the magnitude of error for components studied is broadly similar to that of the reference fluid suggesting that the assumption of three parameter corresponding states has a degree of validity.

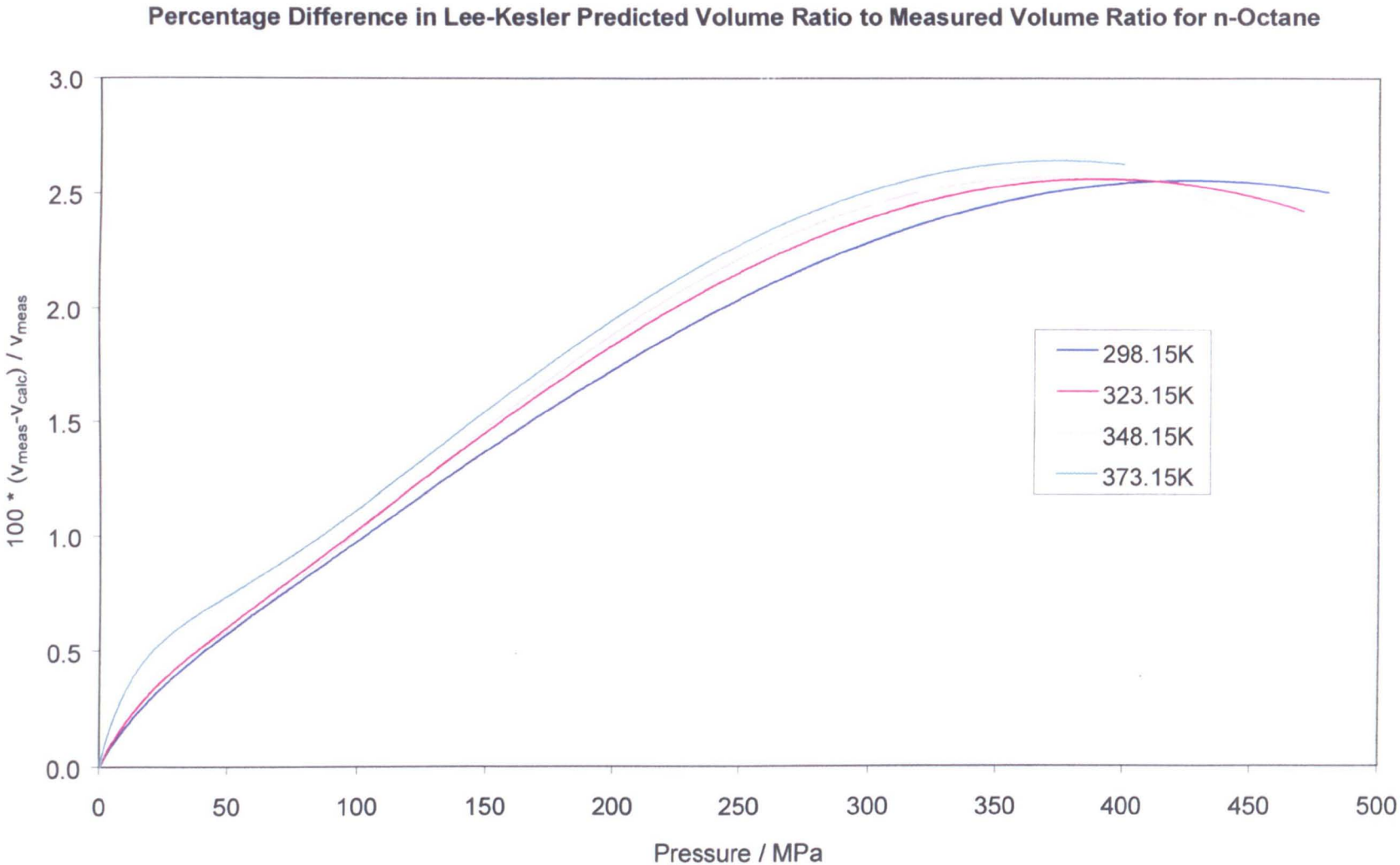

Figure 4.1 Error in prediction of n-octane liquid volume ratio change by Lee-Kesler correlation

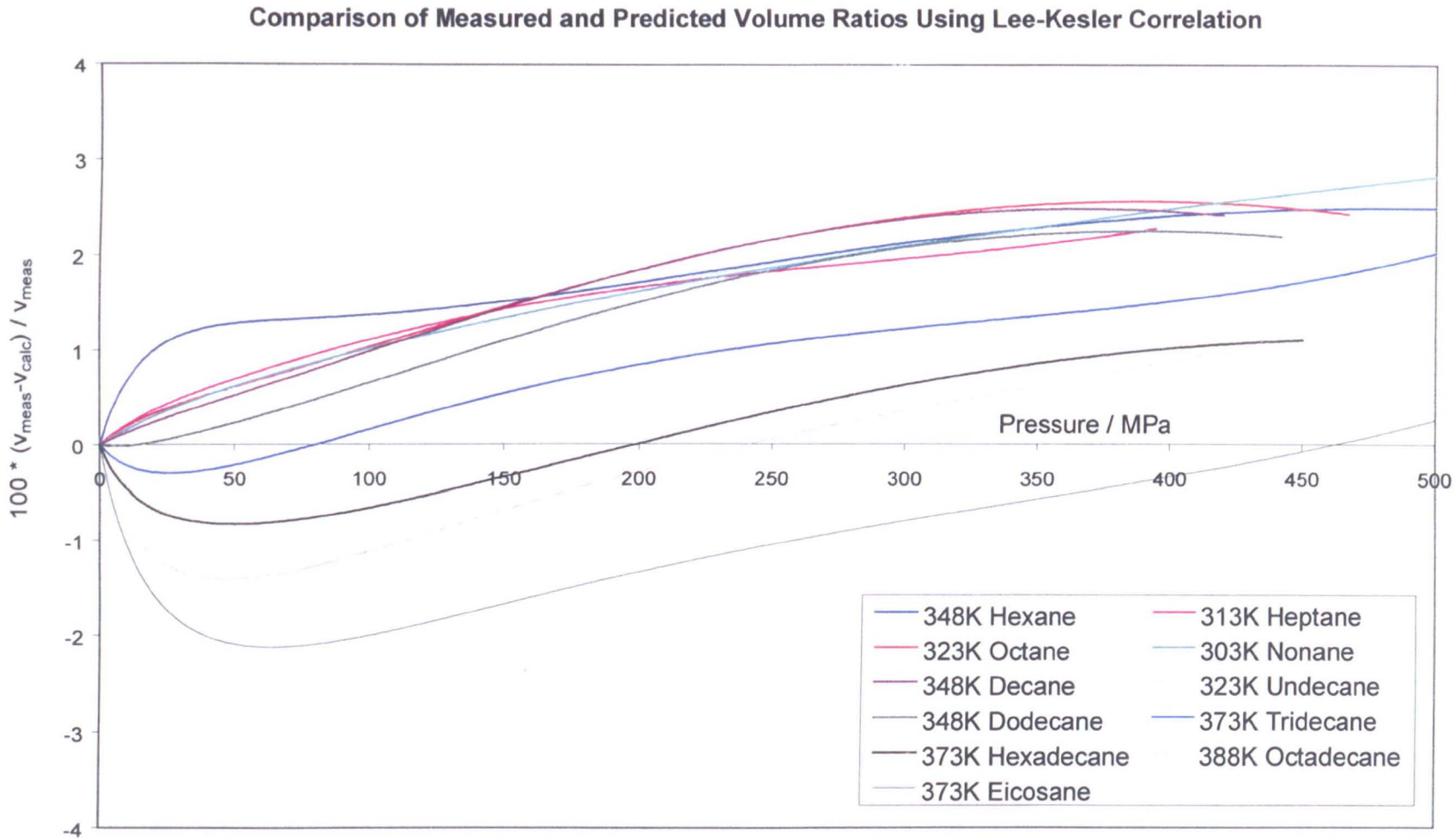

Figure 4.2 Percentage error in Lee-Kesler prediction of n-alkane volume ratio

4.2.1 – Extension of the Pressure Range for Compressed Liquid Compressibility

One approach to improving the prediction of liquid density at elevated pressure would be to use reference data covering the liquid region only, over as wide a range of pressure possible. For the reference fluid the octane data of Dymond et al.[38] could be used with those of Harris et al.[23]. As the reference fluid is only being considered in the liquid phase, fitting the data to a BWR type equation is unnecessary. Instead the volumetric behaviour can be represented by the modified Tait equation with the C parameter constant and B as a function of temperature as suggested in the review of Dymond and Malhotra[39]. This yields the equation;

$$Z = \left(P \times 10^{-6}\right) v_0 (RT)^{-1} \left[1 - C \log_{10}\left(\frac{B+P}{B+0.1}\right)\right] \tag{4.2}$$

to describe compressibility as a function of temperature and pressure. P is the pressure in MPa, T is absolute temperature in Kelvin. v_0 can be expressed as the following function of temperature in units of m^3/mol;

$$v_0 = (k_0 + k_1 T + k_2 T^2)\frac{M}{1000} \tag{4.3}$$

Coefficients for equations (4.2) and (4.3) are given in Table 4.1.

The range of pressure covered by the simple fluid can be extended by using the equation of state of Tegeler et al.[40] for argon which has an acentric factor of approximately zero. Whilst this equation correlates argon thermodynamic data up to 1000MPa, in the corresponding states application the pressure range is limited by the phase behaviour of argon. For example the triple point temperature is 0.556 times the critical temperature which sets the lower limit of the fluid estimation at a

relatively high temperature. With this limiting constraint the Lee-Kesler simple fluid correlation is preferable as this is valid over a wider range, being calculated from mainly argon, krypton and methane properties.

Table 4.1. Coefficients for calculation of v_0 and Tait B ($=b_0+b_1T+b_2T^2$) and C

Fluid	$k_0 \times 10^3$ / m^3kg^{-1}	$-k_1 \times 10^6$ / $m^3kg^{-1}K^{-1}$	$k_2 \times 10^9$ / $m^3kg^{-1}K^{-2}$	b_0 / MPa	b_1 / $MPa.K^{-1}$	$b_2 \times 10^3$ / $MPa.K^{-2}$	C
Octane	1.2108	0.17870	3.0794	393.28	-1.5726	1.6936	0.216

Due to the limiting temperature constraint, comparison of the original Lee-Kesler correlation to the correlation with different equations for reference fluid pressure-volume-temperature behaviour can only be made at certain conditions. For the argon reference fluid to be above its triple point the fluid of interest would need to have a relatively low critical temperature and be studied at a relatively high temperature. Hexane measurements at 348.15K and 373.15K fulfil these requirements as do measurements of iso-octane density at the same temperatures by Dymond and co-workers[41,42]. For these considered cases the reduced temperatures are 0.685, 0.735, 0.640 and 0.686 respectively, corresponding to argon freezing pressures of 84, 118, 53 and 84 MPa respectively where freezing pressure is calculated from the equation presented by Tegeler et al.[40]. Despite the phase change from liquid to solid, the equation of state predicts a smooth change in argon volume ratio with respect to pressure beyond the freezing pressure. Prediction of volume ratio of the fluid of interest as a function of pressure using the alternative equations for prediction of simple and reference fluid density do not represent an improvement in prediction compared to the original Lee-Kesler equation. This

suggests that the use of these reference fluids might not be appropriate for the prediction of liquid hydrocarbon properties.

The low freezing pressure of argon at relatively high reduced temperatures may explain why the correlation using the argon equation of state does not provide a good representation of high pressure properties. Poor prediction of low pressure properties cannot be readily ascribed to a phase change higher up the pressure range. Both the original Lee-Kesler equation and the equation proposed specifically with the aim of more accurate prediction of dense liquid properties show a steep rise in error with respect to pressure up to only a few times the critical pressure of the fluid of interest.

In each of the cases tested the predicted volume ratio decreases at a greater rate with respect to pressure than the measured values. At the molecular level this would suggest that the molecules are predicted to move closer to one another upon pressure increase than is actually the case. Comparing the volume ratio of argon as a function of reduced pressure with n-octane at equivalent reduced temperature shows that argon is a very compressible fluid with volume decreasing relatively sharply with respect to pressure as shown in Figure 4.3. Using this as a reference fluid for long chain hydrocarbons as found in diesel fuels may therefore be inappropriate, particularly if there is any large deviation from linearity in the curve of Z as a function of acentric factor at the lowest values of acentric factor.

A similar exercise in re-fitting the Lee-Kesler simple and reference fluid data was carried out by Munoz and Reich[43.]. This study retained the constraints of Lee and Kesler regarding the critical point and phase equilibria, but was intended to produce an improved representation of liquid phase density by the data regression

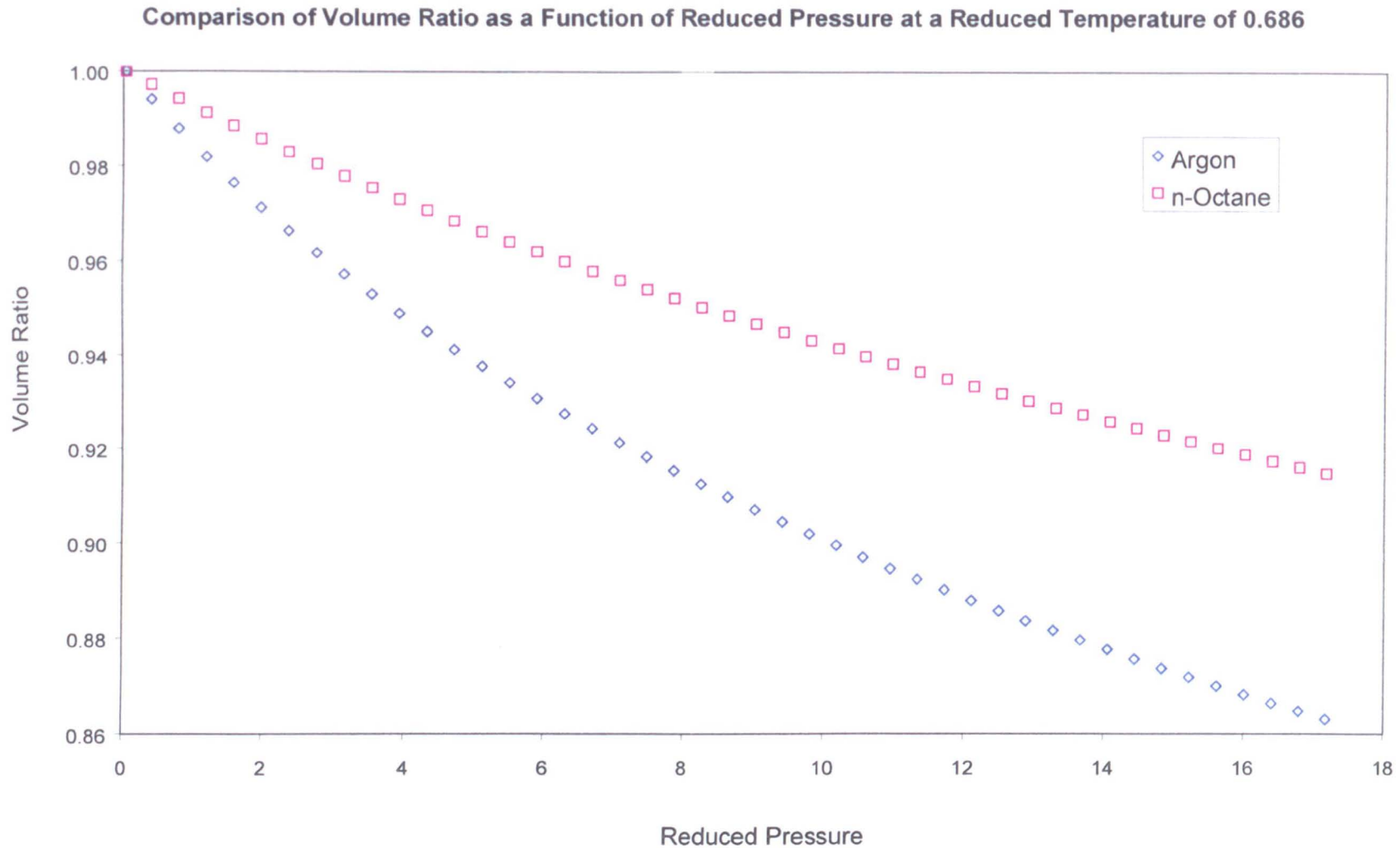

Figure 4.3 Comparison of argon and octane volume ratio at equivalent reduced pressure and temperature

method employed. Results published show that average liquid density errors are still large, particularly for longer chain n-alkanes.

4.2.2 – Alternative Reference Fluids for Three Parameter Corresponding States

Smith et al.[44] draw attention to the point that the Lee-Keseler equation is an interpolation of the supposed straight line relation between acentric factor and compressibility utilising the special case of $\omega^{(0)}=0$ as one of the reference points. For a more general case of two fluids being chosen as the reference fluids r_1 and r_2, the interpolation equation is

$$Z = Z^{(r_1)} + \left(\omega - \omega_{r_1}\right)\left(\frac{Z_{r_2} - Z_{r_1}}{\omega_{r_2} - \omega_{r_1}}\right) \tag{4.4}$$

One may therefore chose any pair of components for a corresponding states type equation. In selecting a pair of components for the prediction of liquid hydrocarbon densities at elevated pressure certain factors should be considered. For the principle to work adequately over a broad range of temperature and pressure the reference fluids must have accurate PVT data available over a wide range of conditions. As the method is an interpolation it would also be advantageous if the fluids chosen as reference fluids covered the range of acentric factors likely to be encountered in real fluid systems. A gas chromatography analysis of a diesel fuel has shown that the n-alkanes follow a normal type distribution between C_9-C_{24} with C_{15} being most abundant by mass fraction. n-Alkanes between C_{10} to C_{19} individually constitute more than 1% mass to the total diesel fuel mixture which gives an indication of what choice of chain length for the reference components might give the best representation of the fuel. With consideration of these constraints iso-octane and

heptadecane are chosen as the reference fluids. Measurements of iso-octane liquid phase PVT relations have been made by both Malhotra and Woolf[22.] and Dymond et al.[42.] which cover the range $0.51<T_r<0.69$ and $0<P_r<195$. Measurements of heptadecane liquid phase compressions were made by Doolittle et al.[45.] in the range $0.44<T_r<0.91$ and $0<P_r<368$. These are then fitted to Tait style equations for compressibility factor (4.2) as before with C constant and B and v_0 functions of temperature. Data at the highest temperature are excluded from the fit of the heptadecane data decreasing the range to a maximum of T_r=0.71. This noticeably improves the fit of the data. Coefficients for v_0, B and C for iso-octane and heptadecane are given in Table 4.2.

Table 4.2 Coefficients for calculation of v_0 and Tait B ($=b_0+b_1T+b_2T^2$) and C

Fluid	$k_0 \times 10^3$ / m^3kg^{-1}	$-k_1 \times 10^6$ / $m^3kg^{-1}K^{-1}$	$k_2 \times 10^9$ / $m^3kg^{-1}K^{-2}$	b_0 / MPa	b_1 / $MPa.K^{-1}$	$b_2 \times 10^3$ / $MPa.K^{-2}$	C
Iso-Octane	1.3549	1.0667	4.6851	300.94	-1.1327	1.0926	0.207
Heptadecane	1.1382	0.047394	1.8780	316.76	-0.93033	0.69114	0.203

n-Alkane PVT properties predicted using the corresponding states equation with alternative reference fluid data are largely within 0.5% of the measured values as shown in Figure 4.4. Notable exceptions are hexane and eicosane, both of which have acentric factors outside the range of the reference fluids. Hexane in particular causes some doubt as to the validity of the three parameter corresponding states theorem as its acentric factor is 0.2979 which is nearly identical to that of iso-octane (0.3035 – both values from PPDS[46.]). Apart from these, there is no over-riding regular trend of error with respect to pressure or chain length suggesting that the equation is satisfactory for n-alkanes. In comparison the original Lee-Kesler

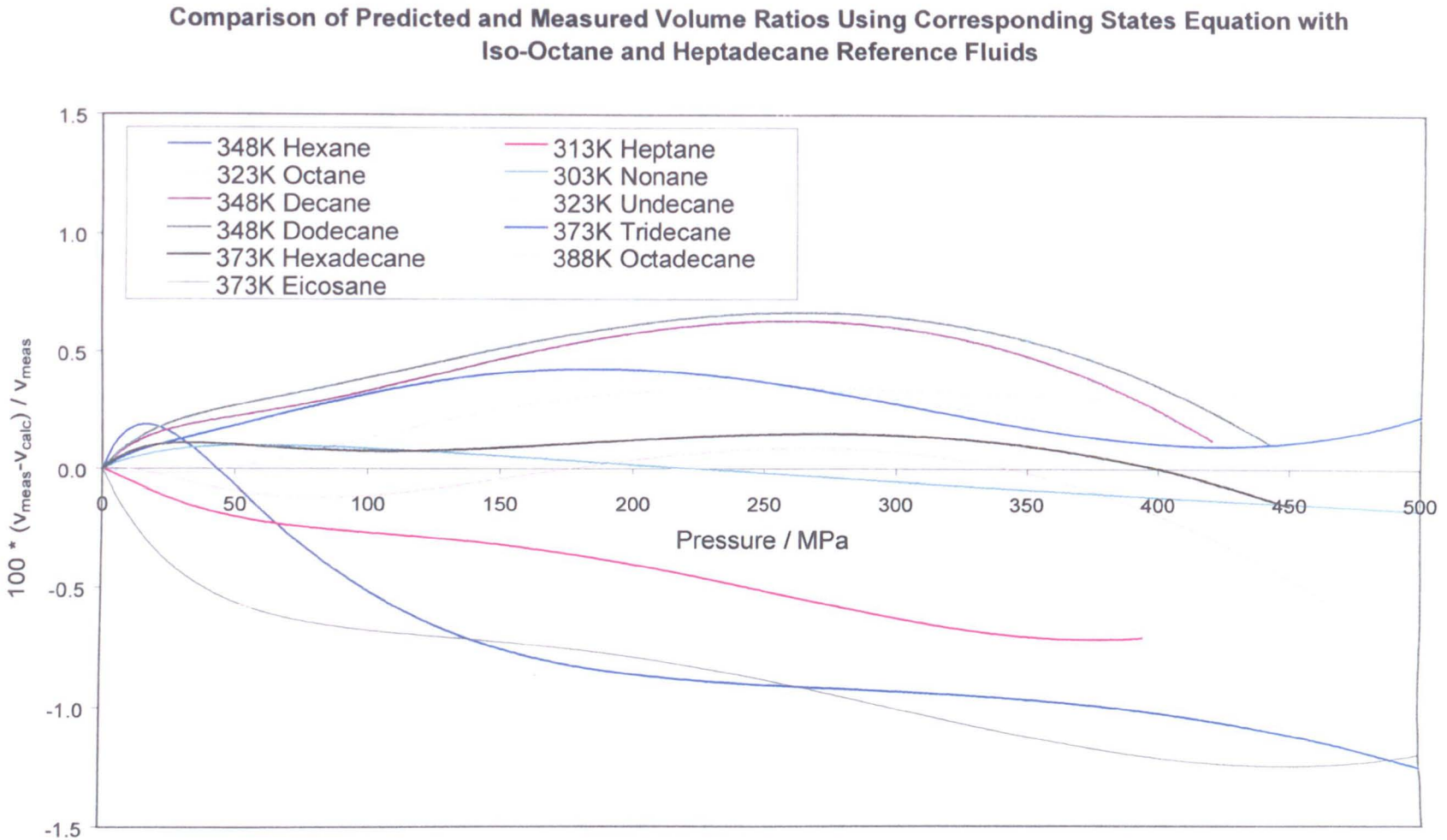

Figure 4.4 Percentage error in liquid volume ratio prediction by alternative reference fluids in corresponding states scheme

correlation shows a general increase in error with respect to pressure for all the cases considered.

4.2.3 – Testing of Non- n-Alkane Liquids

Testing for the applicability of branched alkanes to the theorem is limited by both a lack of knowledge of acentric factor and critical properties and a dearth of volumetric data measured over a wide range of temperature and pressure for comparison with the predicted values. Tait parameters of some branched alkanes are presented in a review of data by Cibulka and Takagi[47.]. Of the compounds studied only the lower molecular weight compounds have readily available critical properties and acentric factor value data. From this limited resource it is seen, with reference to Figure 4.5, that volumetric properties of C_6 molecules are again poorly predicted with the exception of 3-ethyl pentane. Prediction of 2,2,3-trimethyl butane volume is satisfactory over the limited pressure range considered. The main finding of this limited comparison is that the use of alternative reference fluids apparently represents an improvement in the prediction of branched alkane volumetric properties compared with the original Lee-Kesler correlation.

Another limited comparison can be undertaken for aromatics with reference to another review collated by Cibulka and Takagi[48.]. Once more the prediction of the compression of the C_6 molecule gives a large error. For the components analysed which according to the gas chromatography analysis are to be found in significant quantities, the error is at a more acceptable level as shown in Figure 4.6.

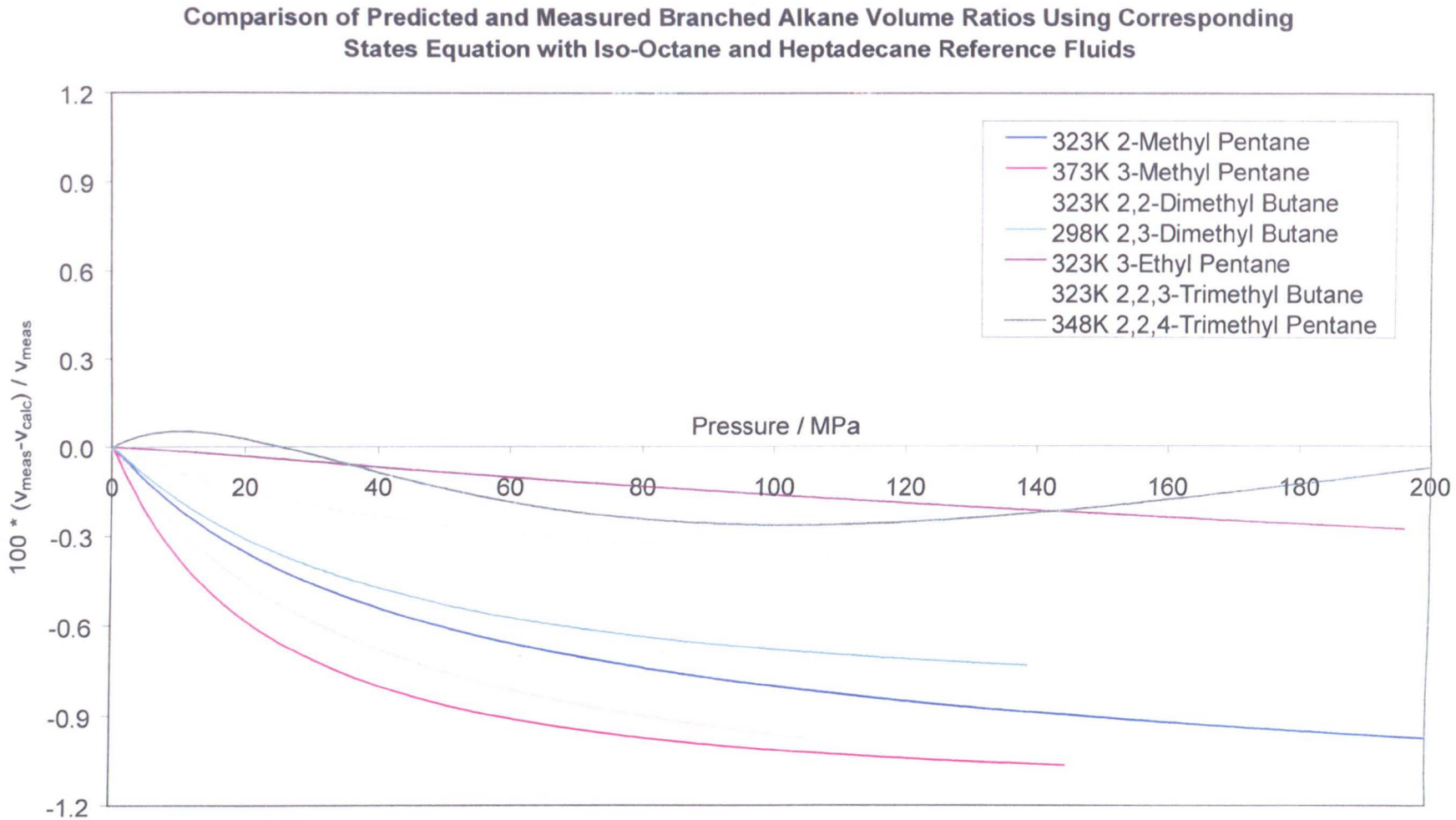

Figure 4.5 Error in prediction of some branched alkanes using corresponding states

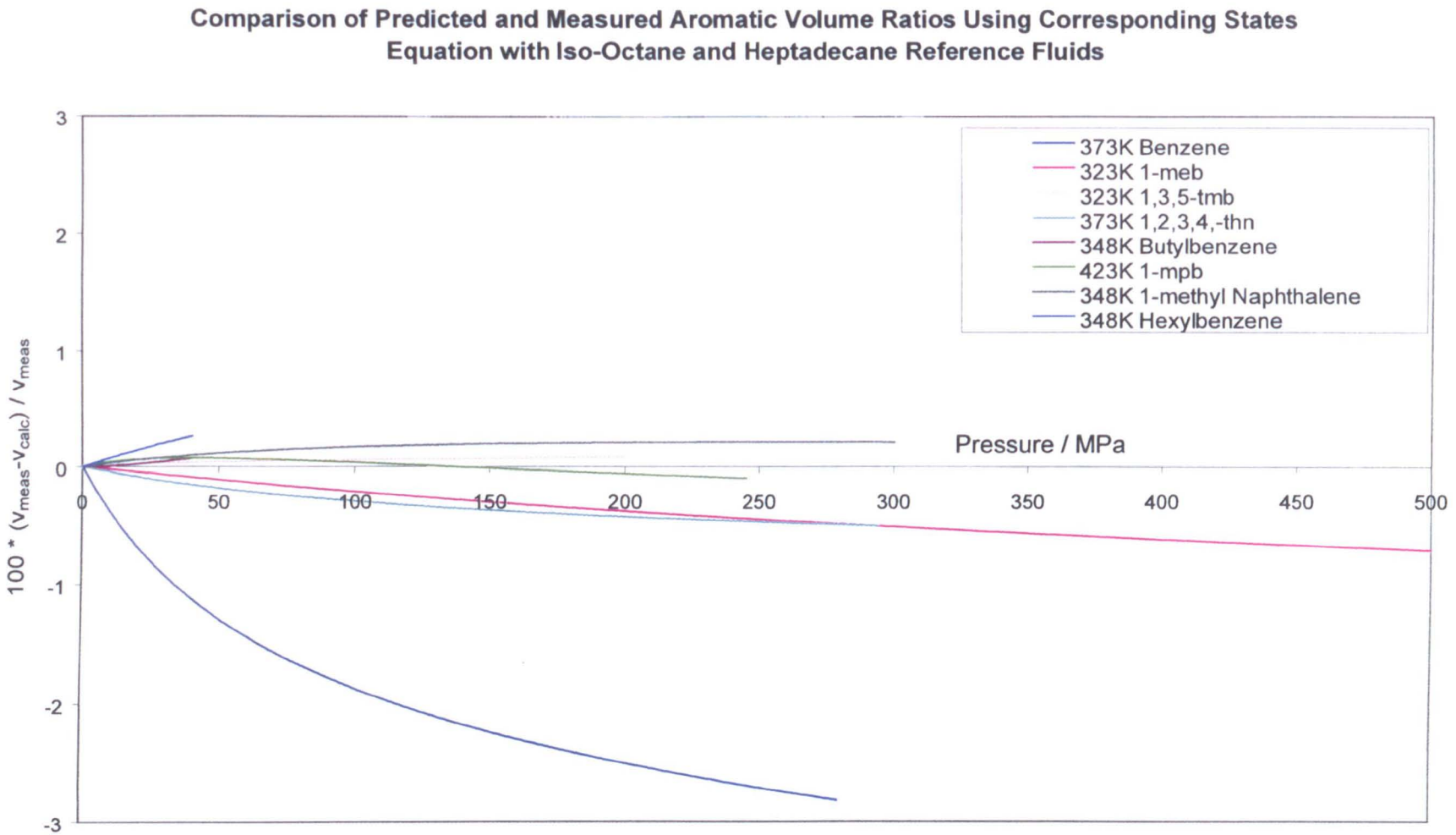

Figure 4.6 Error in prediction of some aromatics using corresponding states

4.3.1 – Estimation of Critical Properties

From the above trials of the corresponding states scheme, it is clear that in many cases the use of such an approach for the prediction of the extent of liquid compressions is limited by a lack of critical property and acentric factor data. For pure components, group contribution methods, such as those described by Reid et al.[49.], may be used to provide an estimate of critical properties. A group contribution method can also be used for the estimation of boiling point and from this acentric factor can be estimated from an equation presented by Lee and Kesler[30.]. Estimates of critical data and acentric factor for mixtures can be made using the mixing rules reviewed by Reid et al.[49.]. Estimation of mixture critical pressure in particular is a complex process requiring characteristic parameters for the individual components. It was noted by Reid that estimation of mixture critical pressure can also often be unreliable.

Estimation of mixture properties using the method outlined above assumes that the mixture is defined in terms of molecular species. For a complex diesel fuel mixture containing many unidentified components, a different approach is required. A number of correlations have been proposed for the estimation of critical properties from normal boiling point and specific gravity at 60^0F. A review of these methods is presented by Korsten[50.].

A problem with using critical properties correlations where normal boiling point is used as an input is that no mixture has a unique boiling point. Instead a boiling point is estimated from distillation data. This can be done by taking a

volume average boiling point which may be defined as the average of the temperatures at which 10, 30, 50, 70 and 90% of the mixture is in the vapour phase. The volume average can further be converted to a molar average using an empirical correction factor, for example using the method of Nelson[51]. There will therefore be a difference in the value of the boiling point dependent upon which definition of the average boiling point is used. Additional uncertainty is added in many cases by the necessity of measuring the high temperature data under vacuum to prevent cracking of heavy fuel components. Measurements in vacuum must then be corrected to give an equivalent atmospheric pressure temperature.

Problems with cracking at high temperature can be avoided by using a simulated distillation. This was performed for two fuel samples using the IP406[52] method, whilst the standard distillation was performed to the ASTM D86[53] standard. A straightforward comparison of the results is impossible due to the actual distillation temperatures being measured over increments of percentage volume of original sample in the condensate whilst the simulated distillation uses a mass percent basis. An idea of the differences between the two methods can be obtained by comparing the range of temperatures encompassed by both methods for the same refinery fuel sample with no additives. A simple comparison of the initial boiling point of the actual distillation with the 0.5 mass percent temperature of the simulated distillation gives temperatures of 165.9^{0}C and 116^{0}C respectively. At the other end of the temperature range, the actual distillation has a final boiling point of 341^{0}C whilst the simulated distillation predicts that 99.5% by mass of the mixture will be in the vapour phase at 391^{0}C. Thus the simulated distillation predicts that boiling will occur over a much wider range than is actually observed. Despite this, the average

boiling points are similar. Ignoring the difference of mass and volume basis, the D86 method gives an average boiling point of 268.2^{0}C and the IP406 method 269.2^{0}C when the temperatures at 10, 30, 50, 70 and 90% volume / mass in vapour phase are averaged. Comparisons between D86 and IP406 methods for the base refinery fuel with handling additives plus a double dose of performance additives gives similar findings.

4.3.2 – Implementation of Corresponding States Scheme from Guessed Boiling Point

Rather than assuming that a boiling point derived from distillation data provides a true measure of boiling point, it may be better to use additional measures of density to employ a scheme whereby the measured ratio of two densities, ρ_2/ρ_1 at temperature T_2 and T_1 and pressure P_2 and P_1 respectively is found equivalent to the calculated ratio $(Z_1T_1P_2)/(Z_2T_2P_1)$. This latter ratio is found using values of the compressibility factor Z calculated using the corresponding states scheme with guess values of critical temperature, critical pressure and acentric factor. These three parameters represent three unknowns with only one equation;

$$\frac{\rho_2}{\rho_1} = \frac{Z_1T_1P_2}{Z_2T_2P_1} \tag{4.5}$$

However, as all three parameters can be related to normal boiling point using a suitable correlation scheme, the iteration is now to solve the above equality with only one unknown.

The procedure for estimating the PVT behaviour of a fluid over a range of conditions from two measurements of density, starts by guessing a value for normal boiling point. For convenience, one of the measurements can be the density found from the specific gravity at 60^{0}F, which was required as an input in the critical

correlation schemes mentioned earlier. Critical properties and acentric factor are calculated by using the guessed boiling point and the specific gravity in a correlation scheme. Compressibility factors of the reference fluids are calculated at equivalent temperature and pressure equal to the product of the reduced temperature / pressure of the fluid of interest and the critical temperature / pressure of the reference fluid. Reduced conditions of the fluid of interest are calculated using the critical properties estimated from the guessed boiling point. Compressibility factor of the fluid is then calculated using the calculated acentric factor and equation (4.4). Fluid compressibility factor is evaluated at T_1 and P_1 and T_2 and P_2 and the calculated density ratio compared with the measured. This process is repeated using an iterative procedure varying normal boiling point until the calculated quantity is within a specified tolerance of the measured quantity. The solution method described is presented in diagram form in Figure 4.7. Critical temperature and pressure and acentric factor are evaluated using the final value of normal boiling point and these can be used in the corresponding states scheme to find compressibility at any temperature and pressure. Prediction of absolute values for compressibility factor is poor, but when the scheme is used to calculate the ratio of compressibility factors and from this density by $\rho = \rho_{meas} \frac{Z_{meas} T_{meas} P}{Z T P_{meas}}$ where subscript '*meas*' indicates measured values, prediction is reasonable.

From tests of the scheme using various pure fluids and mixtures it was found that prediction of atmospheric density as a function of temperature was reasonable when a measured atmospheric density value was used in conjunction with the specific gravity measurement at 60^0F. This did not give as good prediction at elevated pressure as using a measurement at a pressure greater than atmospheric in

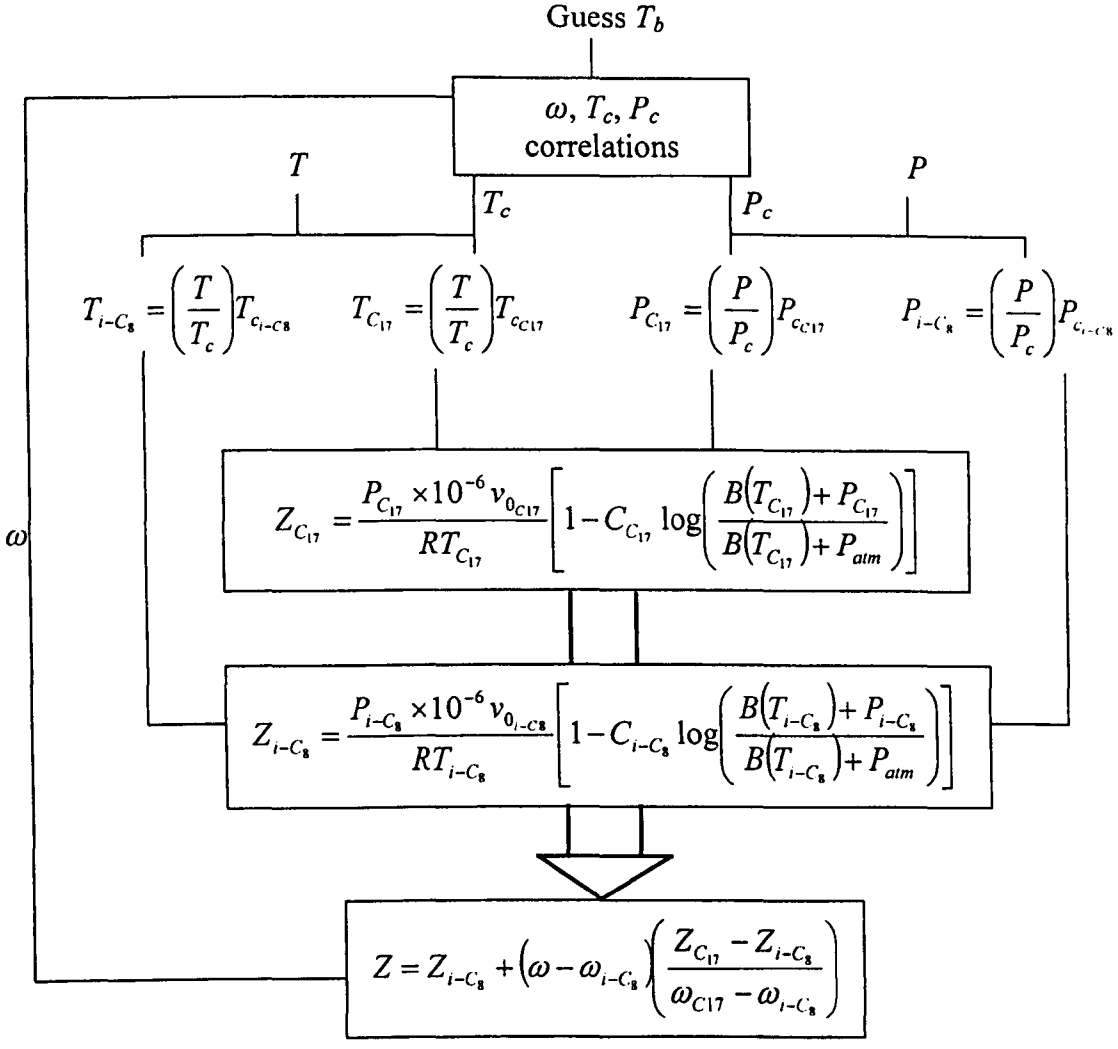

- Calculate Z using above routine at T_1, P_1 and T_2, P_2 to give calculated compressibility factors Z_1 and Z_2.
- Compare measured ratio $\frac{\rho_2}{\rho_1}$ to calculated ratio $\frac{Z_1 T_1 P_2}{Z_2 T_2 P_1}$.
- Adjust T_b until set of T_c, P_c and ω are obtained which give $\frac{\rho_2}{\rho_1} - \frac{Z_1 T_1 P_2}{Z_2 T_2 P_1} \approx 0$.

Figure 4.7 Algorithm for estimation of boiling point required to correlate measured densities using corresponding states method

conjunction with the atmospheric value but this latter method gave worse prediction of initial atmospheric pressure density as a function of temperature. To give a better prediction of density at any temperature and pressure the specific gravity measurement should be combined with a measurement of density at atmospheric pressure and elevated temperature and a measurement of density at the same elevated temperature and a pressure above atmospheric. From these measurements two sets of critical property and acentric factor values are found, neither of which represents the true parameters of the fluid. One set allows for the prediction of density at atmospheric pressure and any temperature and the other gives prediction of the density at elevated pressure using the density predicted at atmospheric pressure and the calculated ratio of atmospheric and elevated pressure compressibility factor values calculated using the second set of critical property and acentric factor values.

4.3.3 – Critical Correlations and Testing

Various critical property correlations have been used to test the applicability of the scheme described in the preceding section. For petroleum distillates Korsten[50.] highlights the main correlation types as being exponential laws, polynomial equations and equations which estimate the critical data of a fluid mixture from the perturbation of the properties of a reference system. Riazi and Daubert's critical correlation is tested as being representative of the exponential type correlations. The critical correlation of Cavett is chosen as an empirical method represented by polynomial fits of critical temperature and logarithm of critical pressure. Kesler and Lee's correlation is of a similar type to that of Cavett but has a certain degree of theoretical justification behind it as described by Korsten[50.]. A

perturbation theory correlation presented by Twu[54.] is also used as a correlation scheme for the estimation of the critical parameters in the corresponding states theory.

Comparison of the predictive ability of the corresponding states scheme with different critical property correlations is made for n-alkanes to allow direct comparison with the Lee-Kesler equation as before and also the corresponding states equation using published critical properties. When the critical properties were assumed unknown, two measurements of density were used in conjunction with the specific gravity at 60^0F as described previously. Density measurements were typically taken at 50^0C and atmospheric and approximately 30MPa pressure. These conditions were chosen as measurements can be made at these points using a standard commercially available vibrating tube densimeter. When specific gravity was not measured at 60^0F this was linearly interpolated or extrapolated from atmospheric density data. It is seen from Table 4.3 that the overall average absolute deviation for n-alkane density prediction is reduced by using additional measurements of density to define false critical points to correlate the pressure-volume-temperature behaviour of a liquid compared to the proposed corresponding states scheme using measured critical data. Predicted densities are compared with reference data quoted in Table 4.4. Of the methods tested the corresponding states scheme utilising the critical correlation of Twu[54.] gives the best fit of the data. This is to be expected as the correlation of Twu was devised to accurately yield the critical properties of n-alkanes with other fluid critical properties found by a perturbation expansion of the n-alkane critical properties.

Table 4.3 Average Absolute Percentage Deviations from measured data for n-alkanes

	Volume Ratio AA%D		Density AA%D			
	Measured Critical Properties		Critical Correlation in Iterative Scheme			
Fluid	Lee-Kesler	C17 - i-C8 Corresponding States	Twu	Kesler & Lee	Cavett	Riazi & Daubert
Hexane	1.615	0.744	0.435	0.368	0.365	0.648
Heptane	0.842	0.414	0.129	0.086	0.114	0.374
Octane	1.179	0.099	0.118	0.204	0.101	0.208
Nonane	0.751	0.064	0.198	0.400	0.120	0.448
Decane	1.352	0.390	0.204	0.222	0.295	0.266
Undecane	0.720	0.150	0.221	0.179	0.547	0.194
Dodecane	1.152	0.354	0.182	0.131	0.137	0.115
Tridecane	0.804	0.166	0.237	0.229	0.388	0.236
Hexadecane	0.429	0.089	0.119	0.162	0.224	0.127
Octadecane	0.764	0.399	0.068	0.126	0.226	0.077
Eicosane	4.001	0.781	0.565	0.808	0.435	0.567

Table 4.4 Range of conditions for fluids examined and sources of measured data.

Fluid	T_{min} (K)	T_{max} (K)	P_{max} (MPa)	No. Points	Reference
Hexane	298.15	373.15	564	31	41
Heptane	303.15	373.15	500	33	60
Octane	278.15	348.14	480	100	38, 23
Nonane	303.15	423.15	500	40	60
Decane	298.31	373.11	420	19	38
Undecane	303.15	423.15	500	44	60
Dodecane	298.27	373.21	502	32	38
Tridecane	303.15	473.15	500	55	60
Hexadecane	298.15	373.15	451	27	41
Octadecane	333.15	408.15	551	53	9
Eicosane	373.15	573.15	500	55	60
Class 1 Diesel	298.10	348.00	421	74	59
Low Sulphur Diesel	298.10	347.90	203	26	59
ISO4113 Fluid	298.00	347.90	208	32	59
0.5 iso-octane/0.5 toluene	313.15	348.15	346	40	22
0.4 hexadecane / 0.6 hexane	298.15	373.15	450	23	41
Benzene	298.09	373.16	391	30	61
Oct-1-ene	298.15	373.15	265	36	62
9(2-Phenylethyl) heptadecane	310.95	352.55	689	51	9
Diesel Oil	293.15	353.15	140	60	58
Rapeseed Metyhl Ester Oil	293.15	353.15	140	60	58
Sunflower Methyl Ester Oil	293.15	353.15	140	60	58
Normalised Testing Fluid (ISO4113)	293.15	353.15	140	60	58

Absolute percent average deviations in the prediction of density of mixtures, including diesels, are presented in Table 4.5. Also included for comparison are benzene, which was not well predicted from the published critical properties; oct-1-ene to show the validity of the method to an alkene for which high pressure densities have been measured; and 9(2-phenylethyl)heptadecane to provide an example of the application of the scheme to a pure component for which no critical property or boiling point data have been published. It is seen that a similar magnitude of error is given from the corresponding states scheme regardless of the critical correlation chosen. Use of the correlation of Riazi and Daubert gives the lowest errors for mixtures but did not solve for the aromatic containing two component mixture or pure benzene. This may be due to the tolerance set on the iterative scheme, but as the other methods are unaffected by aromatics it may be the case that this method could fail for a mixture with high aromatic content. This method also gave the highest average absolute percent deviation when applied to n-alkanes. Of the remaining three correlations, the Kesler and Lee correlation appears to give the most consistent AAD regardless of molecular type and on this basis could be considered as the method of choice for the iterative corresponding states method.

Values of the pseudo critical parameters and pseudo acentric factors resulting from the iterative corresponding states method are presented in Tables 4.6 to 4.9. The subscript *atm* indicates the pseudo properties found from the iterative process to correlate the two atmospheric measurements and provide prediction of density ratio with respect to temperature for any temperature of the liquid. Similarly, the subscript *P* refers to the pseudo properties found from the iterative process to correlate two measurements at the same temperature but different pressures as described earlier.

These pseudo properties are used in the corresponding states scheme for the prediction of density ratio with respect to pressure. Calculation of absolute values of density from the pseudo properties presented is poor. Instead, absolute values of atmospheric density at any temperature are found from the measured density and predicted ratio of atmospheric densities at the temperature of interest and the temperature of the measured atmospheric density. This calculated atmospheric density value at the temperature of interest can then be used to calculate the density at elevated pressure from the density ratio predicted from the corresponding states scheme using the set of pseudo properties which were found to correlate the two measurements at the same temperature but different pressures.

Table 4.5 Average Absolute Percentage Deviations from measured data for various fluids

	Density AA%D			
	Critical Correlation Used in Iterative Scheme			
Fluid	Twu	Kesler & Lee	Cavett	Riazi & Daubert
Class 1 Diesel	0.137	0.149	0.110	0.137
Low Sulphur Diesel	0.092	0.113	0.087	0.101
ISO4113 Fluid	0.043	0.068	0.054	0.041
0.5 iso-octane/0.5 toluene	0.395	0.290	0.148	No Solution
0.4 hexadecane / 0.6 hexane	0.172	0.113	0.359	0.118
Benzene	0.432	0.212	0.107	No Solution
Oct-1-ene	0.220	0.260	0.266	0.098
9(2-Phenylethyl) heptadecane	0.208	0.182	0.349	0.206
Diesel Oil	0.167	0.150	0.248	0.172
Rapeseed Methyl Ester Oil	0.086	0.083	0.082	0.089
Sunflower Methyl Ester Oil	0.134	0.127	0.094	0.092
Normalised Testing Fluid	0.099	0.100	0.113	0.090

The Visual Basic program used for the estimation of liquid density at any temperature and pressure from two density measurements, specific gravity at 60^0F and a guessed value of boiling point, is presented in Appendix B. In the program shown, the critical correlation of Kesler and Lee is used. For density prediction

Table 4.6 Pseudo critical parameters from iterative corresponding states scheme with critical correlations of Twu

Fluid	$T_{c,atm}$ (K)	$P_{c,atm}$ (MPa)	ω_{atm}	$T_{c,P}$ (K)	$P_{c,P}$ (MPa)	ω_P
Hexane	504.58	3.0678	0.2899	475.03	3.6779	0.2015
Heptane	540.02	2.7458	0.3460	508.15	3.2890	0.2487
Octane	559.04	2.6484	0.3582	548.59	2.8036	0.3256
Nonane	579.42	2.5064	0.3844	591.58	2.3496	0.4243
Decane	597.83	2.3788	0.4105	641.16	1.8942	0.5639
Undecane	740.07	1.1870	0.9673	648.03	1.8863	0.5551
Dodecane	744.08	1.1696	0.9437	672.16	1.7079	0.6177
Tridecane	745.38	1.1739	0.9154	692.17	1.5691	0.6723
Hexadecane	753.46	1.1739	0.8757	725.88	1.3802	0.7493
Octadecane	754.80	1.2073	0.8410	755.54	1.2019	0.8445
Eicosane	686.86	1.8757	0.5430	749.02	1.2924	0.7853
Class 1 Diesel	808.05	0.9972	0.9697	755.98	1.3959	0.7327
Low Sulphur Diesel	825.20	1.0424	0.9486	788.17	1.3284	0.7820
ISO 4113 Fluid	818.36	1.0069	0.9654	767.02	1.4065	0.7349
0.5 iso-Octane / 0.5 Toluene	530.36	3.8626	0.2098	430.51	7.3345	0.1332
0.4 Hexadecane / 0.6 Hexane	751.50	1.1374	1.0769	620.42	2.1117	0.4854
Benzene	538.50	5.7400	0.1823	427.17	11.8236	0.1978
Oct-1-ene	545.62	3.0150	0.2882	542.59	3.0677	0.2805
9(2-Phenylethyl) Heptadecane	665.50	2.9156	0.3653	827.31	1.1586	0.8931
Diesel Oil	819.85	1.0520	0.9388	796.74	1.2252	0.8324
Rapeseed Methyl Ester Oil	870.66	1.0660	0.9941	824.46	1.4255	0.7920
Sunflower Methyl Ester Oil	877.38	1.0299	1.0215	824.76	1.4349	0.7896
Normalised Testing Fluid (ISO4113)	814.78	1.0236	0.9528	787.46	1.2255	0.8255

Table 4.7 Pseudo critical parameters from iterative corresponding states scheme with critical correlations of Kesler and Lee

Fluid	$T_{c,atm}$ (K)	$P_{c,atm}$ (MPa)	ω_{atm}	$T_{c,P}$ (K)	$P_{c,P}$ (MPa)	ω_P
Hexane	502.73	3.0090	0.2767	481.35	3.4388	0.2396
Heptane	538.61	2.6808	0.3358	516.94	3.0799	0.2896
Octane	559.60	2.5714	0.3685	611.11	1.7939	0.5171
Nonane	582.26	2.3949	0.4105	667.59	1.2837	0.6975
Decane	600.18	2.2739	0.4444	691.35	1.1625	0.7700
Undecane	744.03	0.8105	0.9859	687.23	1.2917	0.7315
Dodecane	737.09	0.9244	0.9309	703.91	1.2081	0.7818
Tridecane	728.82	1.0462	0.8744	706.75	1.2442	0.7772
Hexadecane	723.78	1.2346	0.8084	722.69	1.2447	0.8037
Octadecane	693.98	1.6321	0.6639	747.61	1.1028	0.8898
Eicosane	722.25	1.4013	0.7591	740.36	1.2278	0.8369
Class 1 Diesel	767.46	1.1809	0.8938	714.28	1.7099	0.6710
Low Sulphur Diesel	775.80	1.3219	0.8553	744.37	1.6326	0.7237
ISO 4113 Fluid	770.85	1.2608	0.8701	729.55	1.6715	0.6974
0.5 iso-Octane / 0.5 Toluene	534.14	3.7828	0.2669	464.52	5.2650	0.1873
0.4 Hexadecane / 0.6 Hexane	761.04	0.6394	1.0921	678.18	1.2948	0.7147
Benzene	538.69	5.5209	0.1798	488.66	6.5814	0.1515
Oct-1-ene	549.02	2.9491	0.3296	532.16	3.2619	0.2947
9(2-Phenylethyl) Heptadecane	685.60	2.5544	0.4832	788.25	1.3579	0.8577
Diesel Oil	767.62	1.3625	0.8313	758.49	1.4502	0.7922
Rapeseed Methyl Ester Oil	822.13	1.2882	0.9220	781.45	1.6719	0.7492
Sunflower Methyl Ester Oil	832.41	1.2124	0.9651	781.70	1.6811	0.7467
Normalised Testing Fluid (ISO4113)	773.91	1.2237	0.8875	751.59	1.4308	0.7897

Table 4.8 Pseudo critical parameters from iterative corresponding states scheme with critical correlations of Cavett

Fluid	$T_{c,atm}$ (K)	$P_{c,atm}$ (MPa)	ω_{atm}	$T_{c,P}$ (K)	$P_{c,P}$ (MPa)	ω_P
Hexane	503.07	3.0662	0.2858	479.78	3.5311	0.2141
Heptane	540.64	2.6922	0.3666	509.80	3.2127	0.2790
Octane	563.58	2.5650	0.4031	541.28	2.9075	0.3431
Nonane	584.38	2.4428	0.4359	578.81	2.5219	0.4214
Decane	602.01	2.3466	0.4621	681.76	1.4385	0.6647
Undecane	613.34	2.3107	0.4752	688.84	1.4577	0.6646
Dodecane	880.98	0.6618	1.1454	738.03	1.1367	0.7697
Tridecane	874.00	0.6763	1.1171	747.74	1.1158	0.7815
Hexadecane	651.59	2.1895	0.5173	780.74	1.0109	0.8357
Octadecane	676.47	1.9862	0.5621	811.09	0.9035	0.9002
Eicosane	716.68	1.6148	0.6479	783.48	1.0788	0.8156
Class 1 Diesel	880.65	0.7581	1.0693	783.82	1.2040	0.7792
Low Sulphur Diesel	876.43	0.8331	1.0153	821.69	1.0898	0.8416
ISO 4113 Fluid	881.43	0.7857	1.0525	791.72	1.2247	0.7788
0.5 iso-Octane / 0.5 Toluene	534.21	3.5867	0.2700	500.56	4.0078	0.1992
0.4 Hexadecane / 0.6 Hexane	909.51	0.6451	1.2463	591.81	2.4915	0.4356
Benzene	539.05	4.5671	0.1969	536.58	4.5815	0.1933
Oct-1-ene	550.16	2.9370	0.3484	533.48	3.1916	0.3061
9(2-Phenylethyl) Heptadecane	687.88	2.6258	0.4840	861.90	0.9479	0.9373
Diesel Oil	657.99	2.7942	0.4468	829.60	1.0247	0.8710
Rapeseed Methyl Ester Oil	901.02	0.8784	1.0350	857.27	1.0877	0.8776
Sunflower Methyl Ester Oil	902.39	0.8772	1.0384	857.42	1.0926	0.8761
Normalised Testing Fluid (ISO4113)	873.49	0.8057	1.0261	824.87	1.0082	0.8725

Table 4.9 Pseudo critical parameters from iterative corresponding states scheme with critical correlations of Riazi and Daubert

Fluid	$T_{c,atm}$ (K)	$P_{c,atm}$ (MPa)	ω_{atm}	$T_{c,P}$ (K)	$P_{c,P}$ (MPa)	ω_P
Hexane	501.91	3.1496	0.2521	417.79	6.4757	0.0766
Heptane	536.11	2.7720	0.3020	435.42	6.2777	0.0870
Octane	558.13	2.6154	0.3294	622.48	1.7034	0.5281
Nonane	575.62	2.5039	0.3512	656.15	1.4968	0.6155
Decane	595.76	2.3315	0.3847	684.84	1.3484	0.6972
Undecane	749.73	0.9936	0.9970	690.31	1.3744	0.6885
Dodecane	751.27	1.0297	0.9625	709.75	1.2875	0.7453
Tridecane	753.49	1.0545	0.9414	715.10	1.2951	0.7448
Hexadecane	757.04	1.1256	0.8848	737.33	1.2485	0.7867
Octadecane	758.76	1.1678	0.8547	758.41	1.1700	0.8530
Eicosane	686.21	1.7949	0.5375	752.61	1.2486	0.7972
Class 1 Diesel	802.37	1.0805	0.9575	760.12	1.3364	0.7524
Low Sulphur Diesel	817.24	1.1281	0.9282	789.44	1.2924	0.7957
ISO 4113 Fluid	810.21	1.1041	0.9430	770.55	1.3448	0.7546
0.5 iso-Octane / 0.5 Toluene	N/A	N/A	N/A	N/A	N/A	N/A
0.4 Hexadecane / 0.6 Hexane	753.57	0.9279	1.0750	674.75	1.4323	0.6528
Benzene	N/A	N/A	N/A	N/A	N/A	N/A
Oct-1-ene	544.43	3.1051	0.2732	590.83	2.2517	0.3950
9(2-Phenylethyl) Heptadecane	663.93	2.7546	0.3560	822.77	1.1857	0.8877
Diesel Oil	812.91	1.1314	0.9223	793.25	1.2456	0.8267
Rapeseed Methyl Ester Oil	865.24	1.0937	0.9938	830.94	1.2821	0.8285
Sunflower Methyl Ester Oil	865.78	1.0967	0.9914	831.63	1.2846	0.8275
Normalised Testing Fluid (ISO4113)	807.15	1.1145	0.9319	784.51	1.2464	0.8203

using the iterative corresponding states method, but with one of the other critical correlations mentioned, the desired critical correlation is simply substituted into the program in place of that of Kesler and Lee.

For high accuracy n-alkane density estimation the method of Assael et al.[55.] will give density prediction to within 0.2% for the range of temperature and pressure stated in that paper. This is however limited to n-alkanes only or other homologous series which have been studied[56.]. Prediction of mixture density by the method of Assael et al.[55.] is also very good, but was only applied to members of the same homologous series. Similalrly, the correlation scheme of Aalto and Keskinen[57.] provides reasonable prediction of elevated pressure liquid density but requires a set of parameters unique to each fluid. If these parameters are known for each fluid in a mixture then this method may be extended to cover mixtures of fluids of different series. For fluids where the parameters are unknown it would be necessary to determine these from experimental data. Measurement is also a necessity for the corresponding states method as presented here. Only liquid density measurements are required in this proposed scheme, whereas the method proposed by Aalto and Keskinen, which is in turn based upon the Hankinson-Brobst-Thomson[31,32.] method, requires measurements of density and critical properties. The corresponding states method can also be applied from direct measurements of mixture density without the application of mixing rules. From the published table of average absolute deviations it would appear that this method does not provide as good prediction of density as the corresponding states method, but the data assessed by Aalto and Keskinen covers a wider range.

4.4 Comparison with Data of Rodriguez-Anton et al.

Diesel fuel density over a range of temperature and pressure has also been measured by Rodriguez-Anton et al.[58.] by means of a vibrating tube densimeter. Results are presented in a Tait style equation. In place of the usual Tait B parameter, a term C is included and is given as the following function of temperature; $C = C_5 e^{-C_6(t-15)}$ where t is the temperature in degrees Celcius. Density results are also plotted as isotherms as a function of pressure. Using the form of equation given in the paper gives results which do not agree with the graphical values. Using a linear form of equation with the same coefficients C_5 and C_6 gives results which are in better agreement with the graphical results but do not work as well when used with the proposed corresponding states method. Included in the fuels tested was an ISO4113 fluid. Comparison with previous NEL measurements using the Micro-PVT[59.] shows good agreement with atmospheric pressure density values. In order to obtain densities at the same temperatures as those of Rodriguez-Anton et al., the NEL data were estimated at 20, 40, 60 and 80^{0}C from measurements at 75^{0}C using the semi-theoretical scheme described in this chapter. Disagreement between measured high pressure values is up to approximately five times as great when the linear form of equation for estimation of the 'C' parameter is used compared to the exponential form. This suggests that the exponential form is the correct form in this context despite being non-standard and giving densities which disagree with those plotted in the same paper.

Assuming that the equation presented in the paper is correct, then the densities calculated from the Tait style equation can be used to test the proposed

corresponding states scheme. For the purposes of calculating average absolute differences, the predicted values are compared with the measured values fitted by the Tait style equation in 10MPa increments from atmospheric to 140MPa. Average absolute deviations in predicted values using each of the four critical correlations chosen for study are presented in Table 4.5.

Chapter 5.

Viscosity Correlation and Prediction

5. Viscosity Correlation and Prediction

5.1 Empirical Viscosity Prediction

Abbot et al.[63.] highlight the use of the API nomograph as the industry standard for the prediction of the viscosity of a wide range of oils at 100 and 210^{0}F. In their work, the authors formed equations to represent the nomograph at the two temperatures. The equations were also used with additional data to extend the range of specific gravity and boiling point covered by the nomograph. Kinematic viscosity was fitted from the nomograph and additional viscosity data by the following equation;

$$\log \nu = A(K,^\circ API) + \frac{B(K,^\circ API)}{^\circ API + C(K)} \tag{5.1}$$

A, B and C are functions of the API specific gravity, $^\circ API$, and Watson characterisation factor[64.], K. Despite the empirical fit being at only two temperatures, the errors found from the equations are large compared with experimental data for pure hydrocarbons, petroleum fractions and waxy lubes. This suggests the large degree of difficulty in predicting viscosity from a limited number of input parameters, in this case specific gravity at 60^{0}F and boiling point, as

$$^\circ API = \frac{141.5}{SG} - 131.5 \text{ and } K = \frac{T_b^{1/3}}{SG}.$$

Noting that the logarithm of the kinematic viscosity of liquids at the same boiling point is a linear function of API specific gravity, Twu[65.] uses a corresponding states form of equation to relate kinematic viscosity to $^\circ API$ by means of reference fluid data. The equation with two reference fluids r_1 and r_2 is thus;

$$\ln(\nu) = \ln(\nu^{(r_1)}) + \frac{^\circ API - ^\circ API^{(r_1)}}{^\circ API^{(r_2)} - ^\circ API^{(r_1)}} \left[\ln(\nu^{(r_2)}) - \ln(\nu^{(r_1)})\right] \tag{5.2}$$

This equation was then simplified to;

$$\nu = \nu^{(r_1)}\left[\frac{\nu^{(r_2)}}{\nu^{(r_1)}}\right]^{(1/2)(K-10)} \tag{5.3}$$

Twu determined reference fluid kinematic viscosities from the plots of Watson et al.[64.] with the reference fluids being chosen to have K values close to those expected in petroleum fractions. These reference fluids, which do not represent experimental data of real fluids, have viscosity fitted by means of a function with respect to boiling point. Coefficients of the equation were only determined at 100 and 210^{0}F, which does not allow for calculation at other temperatures, but does allow direct comparison with the work of Abbot et al.[63.]. Viscosities predicted by the method of Twu at equivalent values of K and $^{\circ}API$ were consistently better than the predictions from the correlation of Abbot. Once again, the method is of limited use for predicting fuel viscosity over a range of temperatures and pressures, but it does show that a method can be improved by limiting the range of hydrocarbons studied. This in turn highlights the difficulty of obtaining a general fit for viscosity of hydrocarbon mixtures.

An attempt at obtaining a general form of equation to relate viscosity to both temperature and pressure was made by Cameron[66.]. This work combines the viscosity law of Vogel for prediction of viscosity with respect to temperature, with a simplified form of the Eyring equation for viscosity variation with pressure. The form of equation resulting from this is;

$$\eta_{P,T} = ke^{\left(\frac{b+AP}{T+\theta}\right)} \tag{5.4}$$

Parameters k, b and θ are constants and A is a function of temperature. Alternative values can be used to give better prediction with respect to temperature or pressure

only. Detailed results of errors in viscosity prediction are not presented, however it was noted that the diesel oils studied showed anomalous behaviour compared to the other oils considered.

Johnston[67] assumes a basic relationship between zero pressure and elevated pressure viscosity of the form;

$$\eta_P = \eta_0 e^{\alpha_P P} \tag{5.5}$$

Johnston also assumed viscosity varied with temperature according to the equation;

$$\eta = A e^{\frac{E_v}{CRT}} \tag{5.6}$$

This equation assumes an energy of activation E_v is required for viscous flow to occur. A is a function of temperature and pressure, C is a constant and R is the universal gas constant. Differentiating (5.6) with respect to pressure at constant temperature then differentiating with respect to temperature at constant pressure, the resulting equation is;

$$\left(\frac{d\ln\eta}{dP}\right)_T = -\frac{\beta E_v}{\alpha_T 2CRT^2} \tag{5.7}$$

α_T is the coefficient of thermal expansivity of the liquid, $\alpha_T = \frac{1}{V}\left(\frac{dV}{dT}\right)_P$, and β the isothermal coefficient of compressibility, $\beta = -\frac{1}{V}\left(\frac{dV}{dP}\right)_T$.

Noting that the natural logarithm form of (5.6) gives a straight line with respect to temperature at atmospheric pressure, it follows that the term E_v/C can be determined from measurements of viscosity at atmospheric pressure. Stated in this manner, it is evident that equation (5.6) is equivalent to the Andrade equation form at constant pressure. Taking the logarithm of both sides of (5.5) and differentiating

with respect to pressure, it is found that the left hand side of (5.7) is equivalent to the pressure viscosity coefficient of (5.5), α_P. Therefore, if the pressure-volume-temperature behaviour of the fluid is known over the range of interest α_T and β can be found, allowing calculation of α_P at any pressure and temperature from (5.7). Viscosity at elevated pressure is then found with respect to that at atmospheric from (5.5). Error in viscosity prediction is not given; rather error in the viscosity pressure coefficient is given. It is not possible to back calculate this to viscosity error without knowledge of a viscosity ratio at a given pressure. In their conclusions the authors do not make great claims for the accuracy of this equation attributing the error to the simple form of equation (5.6). Another error source (mentioned in a discussion section after the main text of the paper) is the use of an empirical correlation for the prediction of bulk modulus. No high pressure density measurements were made corresponding to the viscosity measurements in the paper, therefore error introduced by the differentiation of volume with respect to pressure and temperature from empirical estimates of bulk modulus data could result in a large error in the final calculation of viscosity.

5.2 Semi-Theoretical Viscosity Prediction

Ozdogan and Yucel[68.] present a semi-theoretical viscosity correlation for predicting petroleum viscosity based on a combination of hard sphere theory and corresponding states theory. A reduced viscosity is defined in this work as;

$$\eta^* = \eta T_c^{1/6} M^{-1/2} P_c^{-2/3} \tag{5.8}$$

Reduced fluid viscosity defined by (5.8) was taken to be equal to the theoretical reduced viscosity of a monatomic liquid plus a reduced viscosity correction term for

the real polyatomic fluid. The monatomic reduced viscosity was given as a function of reduced temperature. The correction term for a petroleum fraction is calculated from a weight fraction average of the correction terms of the alkanes, alkenes, aromatics and cycloalkanes present in the petroleum. Correction terms for each of these classes were presented in an earlier paper[69.] as functions of reduced temperature and reduced boiling point.

Viscosity predicted by the method for 42 petroleum samples covering a wide range of composition of the respective hydrocarbon classes was found to be reasonable. Although comparisons were made at 40^0C only, in this method this represents a reasonable range of reduced temperatures of the fuels studied. Critical properties and molecular weight of the fuels were estimated from the volume average boiling point of the mixtures using the correlations of Riazi and Daubert. The coefficients required for the correction factors determined in the original study[69.] were found from consideration of atmospheric results only. Although it would be possible to determine the correction factor in terms of reduced temperature, reduced boiling point and reduced pressure, the scope of the coefficients thus determined would be limited by the range of data available at elevated pressure. For example, there is a very limited amount of data for branched hydrocarbons at elevated pressure. Whether the exercise would be worthwhile is also questionable for two reasons. The corresponding states method when used in conjunction with critical correlations, relies on an accurate boiling point measurement. A mixture has no boiling point and any figure given for this parameter is a spurious estimation. Secondly, despite the study only covering atmospheric viscosity, the average

deviations predicted by Assael et al.[70,71] are in many cases better over a wider range of conditions than those presented by Yucel and Ozdogan[68].

5.3 Molecular Theories

Viscosity of a fluid can be readily observed by considering the bulk effect on a fluid when a shear rate is applied to the fluid; however a more complete understanding of what causes the fluid to have the viscosity it does under given conditions will be better obtained by considering what is happening within the fluid at a molecular level. Various theories have been proposed to explain qualitatively what molecular events occur within a fluid to cause the resistance to shear exhibited at the macroscopic level. These theories are then treated mathematically to enable estimations of fluid viscosity to be made from consideration of molecular movements.

5.3.1 – Energy Theories

One treatment of molecular movement in a fluid considers that a certain activation energy is required before flow will occur. This theory was advocated by Eyring[72] and is based on the assumption that the viscosity of a liquid is determined by the propensity of molecules to acquire an activation energy which would remove a molecule from its original equilibrium position to a new equilibrium position. As this is a rate process, the viscosity was treated analogously to reaction rate theory which leads to viscosity being described by an Arrhenius type equation with viscosity proportional to exponential of reciprocal temperature.

Eyring's equation follows the same basic mathematical form as the viscosity equation proposed by Andrade[73];

$$\eta = Ae^{b/T} \tag{5.9}$$

In a letter following the paper, Andrade[74.] presents the theory that transfer of momentum between adjacent layers of molecules is caused by temporary unions between molecules within the separate layers. These unions are opposed by the energy of molecular motion. As this energy increases with respect to temperature it follows that the number of unions decreases, and therefore the viscosity also decreases upon a temperature increase. Viscosity as treated here is dependent on probability, in this case the probability that a union between molecules in adjacent layers will occur. This probability is also temperature dependent and therefore the simplified Boltzmann equation (5.9) as proposed by Andrade provides the link between the qualitative and quantitative theory.

5.3.2 – Free Volume Theories

Cohen and Turnbull[75.] considered the molecules of a liquid to be hard spheres contained within cages, the difference between the molecular volumes and cage volumes being equivalent to the free volume of the liquid. They assumed that the free volume per cage was a random value throughout the liquid. For diffusion of molecules through the liquid to occur, a molecule would need to move from its original cage to a neighbouring cage with a free volume large enough to accommodate the additional molecule. Thus the problem is once more one of probability, in this case the probability that a given molecule has a free volume large enough to allow diffusion to occur as opposed to the probability that a molecule has an activation energy for flow as proposed by Eyring[72.]. Viscosity derived from diffusion as defined by Cohen and Turnbull is given by the formula;

$$\eta = (ga_0 ua^*)^{-1}\left(\frac{3\pi}{kT}\right)^{-1} e^{\gamma\frac{v^*}{v_f}} \qquad (5.10)$$

Terms in the first bracket relate to molecular properties, whilst temperature is accounted for in the second bracketed term. From Cohen and Turnbull's theory viscosity is given as a function of the ratio of a critical volume (v^*) required for diffusion to occur to the free volume (v_f) with a constant γ to account for overlap of free volume between cages.

A less rigorous approach to relating viscosity to free volume was made prior to Cohen and Turnbull's work by Doolittle[76]. In this case the free volume was taken to be the difference between the molar volume of liquid at the conditions considered and the theoretical molar volume of the liquid at 0K. Analysis of the results led Doolittle to establish a logarithmic relation between viscosity and free volume. Viscosity as a function of free volume was therefore given by;

$$\eta = Ae^{B\frac{v_0}{v_f}} \qquad (5.11)$$

A and B are constants established from the linear relation between logarithm of viscosity and the ratio of theoretical 0K volume, v_0, to the free volume, v_f. This empirical formula is seen to be of the same form as the formula derived by Cohen and Turnbull (equation 5.10) from theoretical consideration of molecular movements, with the latter including a temperature term introduced from the Stokes-Einstein relation of diffusion to viscosity.

Despite later attempts to relate the coefficients of equation (5.11) to molecular weight of a homologous series[77] the equation is still an empirical fit and therefore the extension of the equation to correlate data of other molecular types will be limited to the range of viscosity data available. A model with greater scope for

prediction should therefore consider the physical situation first with the mathematics developed around this. Such a philosophy would suggest that the works of Eyring[72.] and Cohen and Turnbull[75.] will be worthy of further study. However, when actual experimental data is studied, as was done by Hildebrand[78.], then it can be argued that the theory is contradicted by experimental evidence. Hildebrand modified an equation of Batschinski to give viscosity as the following function of relative free volume;

$$\frac{1}{\eta} = B\frac{V - V_0}{V_0} \tag{5.12}$$

From this equation Hildebrand proposed that various theories, such as those reviewed above, are physically unrealistic as they would not predict the observed degree of fluidity at low values of V compared to V_0. Whilst Hildebrand used equation (5.12) to correlate data, its usefulness as a predictive tool is limited.

5.3.3 – Hard Sphere Theory

From the observations of Hildebrand[78.] it would appear that a different molecular theory is necessary. Rather than considering molecular movement in the liquid phase as completely different to that in the gaseous phase, one can start by assuming that some previous description of the gas phase is fundamentally correct and using this as a basis for describing liquid behaviour. In their book Assael et al.[79.] outline the work of Maxwell who considered the movement of molecules between adjacent planes in a dilute gas when a shear force is applied. The equation resulting from Maxwell's study was;

$$\eta_0 = \frac{2}{3}\frac{(mkT)^{1/2}}{\pi^{3/2}\sigma^2} \tag{5.13}$$

Equation (5.13) was derived on the assumption that the molecules within a fluid do not interact with one another. For the case of a dilute gas with attractions and repulsions between molecules, Reed and Gubbins[80.] summarise the solution method of Chapman and Enskog who solved the equation of Boltzmann to arrive at an equation similar in form to (5.13);

$$\eta_0 = \frac{5}{16}\frac{(mkT)^{1/2}}{\pi^{3/2}\sigma^2\Omega^{(2,2)^*}} \tag{5.14}$$

With further application of the Boltzmann equation, theoretical viscosity for a dense fluid can be related to the dilute gas case (5.14) by the equation;

$$\frac{\eta_E}{\eta_0} = \frac{1}{g(\sigma)} + 0.8\frac{b}{V} + 0.761 g(\sigma)\left(\frac{b}{V}\right)^2 \tag{5.15}$$

The subscript 'E' is used to denote that this is a theoretical dense fluid viscosity as proposed by Enskog. Rather than applying the theory directly, Dymond[81.] proposed that the theoretical terms be used in a reduced viscosity method. Reduced viscosity coefficient is calculated from;

$$\eta^* = \left(\frac{\eta}{\eta_E}\right)\left(\frac{\eta_E}{\eta_0}\right)\left(\frac{V}{V_0}\right)^{2/3} \tag{5.16}$$

$g(\sigma)$, the radial distribution function can be established in terms of molar volume, V, and the second virial coefficient of a hard sphere fluid, $b = \frac{1}{3}\left(2\pi N_A \sigma^3\right)$, by means of the equation of state of Carnahan and Starling[82.] to give;

$$g(\sigma) = \frac{1 - 0.5\frac{b}{4V}}{\left(1 - \frac{b}{4V}\right)^3} \tag{5.17}$$

The above expression allows equation (5.15) to be defined in terms of hard sphere diameter and molar volume and along with equation (5.14) can be used to define the reduced viscosity in terms of macroscopically observable parameters. As the theoretical viscosity is derived from a system of hard spheres, the collision integral, $\Omega^{(2,2)*}$, in equation (5.14) is unity. From the definitions presented, the reduced viscosity can now be written as;

$$\eta^{*}_{\exp} = \frac{16}{5}\pi^{1/2}(2N_A)^{1/3}\left(\frac{1}{MRT}\right)^{1/2} V^{2/3}\eta \qquad (5.18)$$

Subscript 'exp' refers to equation (5.18) being in a form which can be used to find the reduced viscosity coefficient from experimental data. The reduced viscosity derived above will correlate liquids whose molecules display the same transport behaviour as an assembly of hard spheres. To test the applicability of the hard sphere theory to the liquid system of interest, experimental data for V and η are used to calculate η^* using (5.18). If the curve of $\log(\eta^{*}_{exp})$ as a function of $\log(V)$ obtained from (5.18) can be super-imposed on the theoretical hard sphere curve found from (5.16) then the liquid corresponds to the hard sphere theory.

In order that the experimental curve can be easily compared with the theoretical curve, universal curves of hard sphere transport properties have been correlated with respect to the ratio of molar volume to hard sphere volume. Universal theoretical curves were found by Assael et al.[83.] from a combination of computational study of ideal hard spheres, experimental measurements of methane and argon which can be taken as nearly spherical, and measurements of n-alkanes which extend the range of the curves. These curves are given as seventh order

polynomials of reciprocal reduced volume where reduced volume is taken as the ratio of molar to estimated hard sphere volume.

Although the above theory is strictly only applicable to fluids which display similar behaviour to a system of hard spheres, the correlation scheme can be modified to correlate the properties of fluids composed of non-spherical molecules. In order to correlate the transport properties of n-alkanes, Dymond and Awan[84.] introduced a factor, R_η, to account for non-sphericity and translational-rotational coupling. The experimental reduced viscosity (5.18) can now be compared to the universal reduced curve as follows;

$$\log_{10}\left(\frac{\eta^*_{exp}}{R_\eta}\right) = \sum_{i=0}^{7} a_{\eta i}\left(\frac{1}{V_r}\right)^i \qquad (5.19)$$

Coefficients $a_{\eta i}$ for the universal curve of viscosity are listed by Assael et al.[83.].

Using this method of comparison of the universal seventh order curve to the experimental reduced viscosity curves, Assael and co-workers successfully correlated the transport properties of pure n-alkane[70.], aromatic hydrocarbon[71.] and alcohol liquids[56.] over wide ranges of temperature and pressure. The correlation method was also extended to mixtures of n-alkanes[85.] by taking the V_0 and R_η parameters for the mixture to be mole fraction averages of the pure component values. Mixture viscosity prediction was within 5% when compared with atmospheric pressure, but for those mixtures for which high pressure data were available, the prediction was worse, although still reasonable. Assael et al.[79.] later stated that whilst a reasonable fit of the data may be obtained for mixtures from the same homologous series, the mixing rules cannot be satisfactorily applied to mixtures of different classes of compounds.

In all the comparisons made by Assael and co-workers described above, the parameters V_0 and R_η were found graphically by comparing the horizontal and vertical displacements necessary to super-impose the experimental reduced viscosity curve onto the theoretical reduced viscosity curve. In all cases except for the alcohols from CH_3OH to $C_5H_{11}OH$ R_η was found to be a constant for each fluid with V_0 a function of temperature. For the short chain length alcohols R_η displayed a temperature dependency. Assuming that these alcohols are unique in R_η displaying temperature dependence, then an alternative, numerical method can be established for the determination of the correlation parameters V_0 and R_η.

To determine V_0 at a given temperature at the same time as determining R_η requires measurements of density and viscosity at that temperature at atmospheric and an elevated pressure. An initial guess value of R_η is taken and used to calculate the left hand side of (5.19) using the atmospheric properties. A guess value of V_r is made and used to calculate the right hand side of (5.19) using the atmospheric density value. V_r is then adjusted using an iterative scheme until the difference between the left and right hand sides of (5.19) is within a specified tolerance. From the final value of V_r, V_0 is found and used to calculate V_r using the elevated pressure density. Theoretical reduced viscosity is calculated using this value of V_r. A guess value of R_η is used in conjunction with the elevated pressure data to calculate the left hand side of (5.19). An iterative method of varying R_η is then used until both sides of (5.19) are equal. At this point the same value of V_0 has been used to correlate the atmospheric and elevated pressure data with different values of R_η. This procedure is itself then used in an iterative routine which changes the initial guess value of R_η until the difference between this initial guess value and the final calculated value of

R_η are equal. A program written in Visual Basic code to implement this solution scheme is given in Appendix C.

5.3.4 – Application of Hard Sphere Theory

Once R_η has been established using the method described above, this is taken as a constant for the fluid regardless of temperature. If the method is used to predict viscosity at other temperatures it is necessary to establish V_0 at the temperature of interest. V_0 will be found at any temperature by solving (5.19) using the calculated value of R_η with atmospheric data at the temperature to be studied. Before attempting to apply this solution scheme to diesel fuels, dodecane and a limited number of mixtures of known composition were tested as a check on the validity. For consistency the R_η value was found for each fluid using data at 50^0C and atmospheric and ~100MPa pressure. Density values used throughout were predicted from the corresponding states scheme using the Kesler and Lee correlation for critical property estimation as described earlier. Average absolute percentage deviations for data predicted by the method are given in Table 5.1.

Values of V_0 and R_η found from the iterative scheme to correlate the measurement of viscosity at atmospheric with a single high pressure value, and subsequently used for viscosity prediction at other temperatures and pressures, are presented in Table 5.2. The parameters published in this table should not be ascribed any physical significance. Unlike the values of V_0 calculated by previous workers to correlate all the transport properties, those presented in Table 5.2 have been established from viscosity measurement only, for the sole purpose of fitting viscosity data. As the molecular weights of the diesel fuels are unknown, a value of 200 was

used throughout. Calculated viscosity is very insensitive to changes in molecular weight, with the error in calculated viscosity changing by an insignificant amount when molecular weight is increased by an order of magnitude.

Table 5.1 Average errors from hard sphere theory predictions of elevated pressure viscosity using numerical solution for V_0 and R_η

Fluid	Temperature / K	Max. Pressure / MPa	N°. Points	AA%D	Ref.
Dodecane	298.27	119.2	4	0.269	86
	323.35	261.9	7	0.427	86
	348.10	422.5	10	1.19	86
	373.21	501.6	11	4.96	86
0.5 Mole Fraction Octane – Dodecane Mixture	298.20	238.6	7	1.78	86
	323.22	395.6	9	0.328	86
	348.17	502.0	11	3.20	86
	373.17	505.5	11	9.47	86
0.5 Mole Fraction iso-Octane – Dodecane Mixture	298.15	241.4	7	1.37	87
	323.14	397.2	7	0.964	87
	348.03	503.4	8	2.82	87
	372.85	502.5	8	8.03	87
0.8 Mole Fraction Hexadecane – 0.2 Mole Fraction Hexane	298.09	39.5	7	0.784	11
	323.21	156.6	10	0.969	11
	348.09	300.4	9	1.90	11
	373.17	446.1	10	6.95	11
Class 1 Diesel	298.12	405.4	16	35.7	59
	323.03	401.7	20	16.4	59
	348.04	420.5	38	5.00	59
Low Sulphur Diesel	298.12	147.3	7	9.69	59
	322.88	200.7	9	3.83	59
	347.85	202.5	9	10.1	59
ISO 4113	297.99	204.4	10	18.7	59
	322.89	207.6	9	3.78	59
	347.87	207.9	13	10.1	59

With reference to Table 5.1, it is seen that the error for dodecane and the mixtures of known composition is significantly higher at 373K compared to the other temperatures. More insight into the nature of the error can be had by displaying the error at 373K for the fluids in graphical format as shown in Figure 5.1. These show that the error tends to sharply reach a maximum value with respect to pressure before either remaining at an approximately constant value or decreasing at a slow rate with

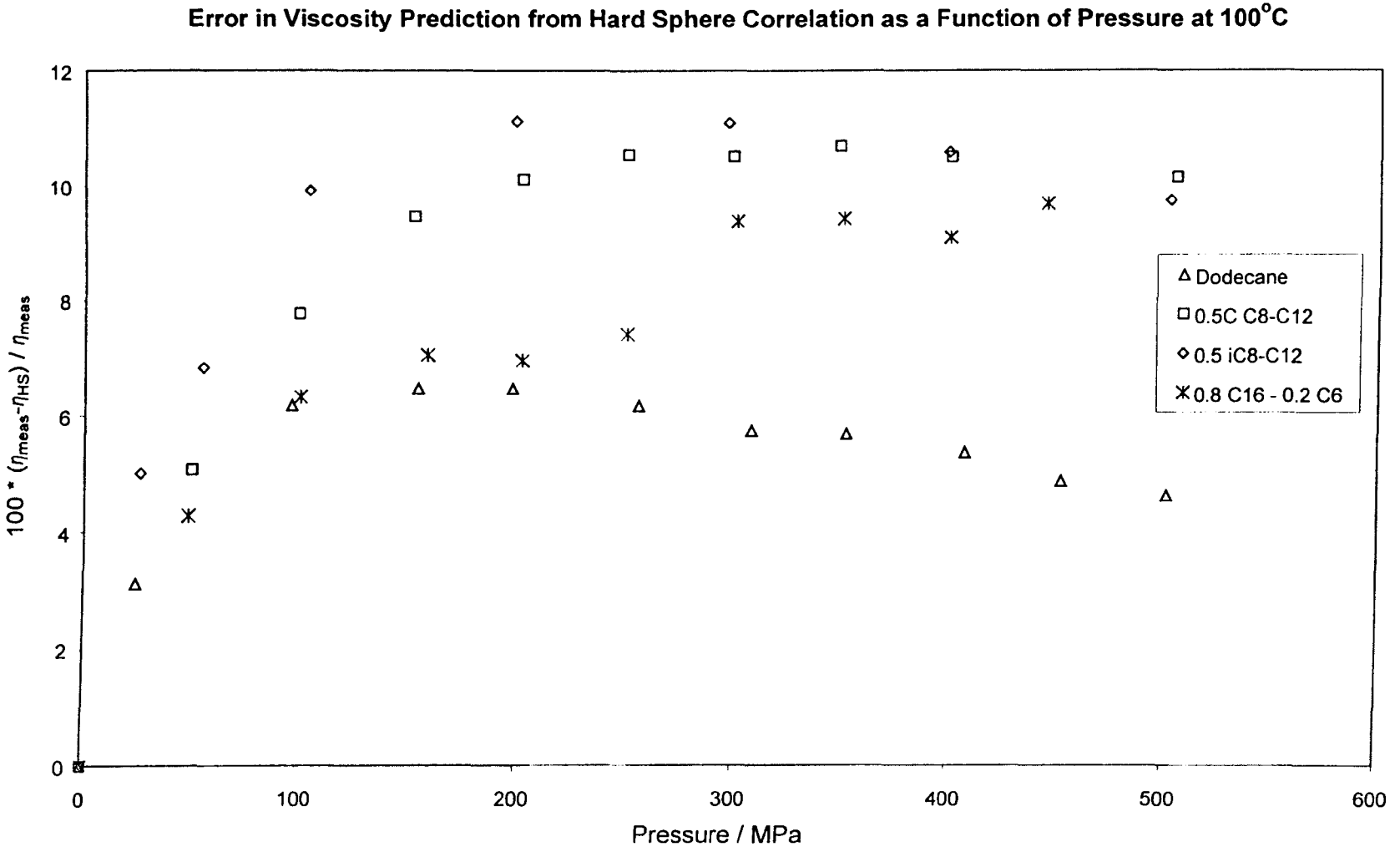

Figure 5.1 Error in viscosity prediction from hard sphere theory for dodecane and mixtures of known composition at 100^0C

respect to pressure. When considered with the other results, it would appear that the method gives reasonable prediction of viscosity except at the highest values of free volume as seen from the rate of change of error with respect to pressure at the lower pressures for the highest temperature considered.

Table 5.2 Pseudo V_0 and R_η values from numerical hard sphere scheme

Fluid	T (K)	V_0 (m^3mol^{-1})	R_η
Dodecane	298.27	1.9071×10^{-4}	1.6551
	323.35	1.8791×10^{-4}	
	348.10	1.8557×10^{-4}	
	373.21	1.8341×10^{-4}	
0.5 Mole Fraction Octane – Dodecane Mixture	298.20	1.8881×10^{-4}	1.5858
	323.22	1.8611×10^{-4}	
	348.17	1.8368×10^{-4}	
	373.17	1.8130×10^{-4}	
0.5 Mole Fraction iso-Octane – n-Dodecane Mixture	298.15	1.9150×10^{-4}	1.4457
	323.14	1.8894×10^{-4}	
	348.03	1.8671×10^{-4}	
	372.85	1.8442×10^{-4}	
0.8 Mole Fraction Hexadecane – 0.2 Mole Fraction Hexane Mixture	298.09	1.9079×10^{-4}	2.1377
	323.21	1.8731×10^{-4}	
	348.09	1.8458×10^{-4}	
	373.17	1.8186×10^{-4}	
Class 1 Diesel	298.12	1.8777×10^{-4}	1.0062
	323.03	1.8576×10^{-4}	
	348.04	1.8521×10^{-4}	
Low Sulphur Diesel	298.12	1.8924×10^{-4}	0.8096
	322.88	1.8688×10^{-4}	
	347.85	1.8611×10^{-4}	
ISO 4113	279.99	1.8936×10^{-4}	0.8182
	322.89	1.8760×10^{-4}	
	347.87	1.8660×10^{-4}	

Prediction of viscosity by the hard sphere method gave a scatter of error as a function of pressure for pure fluids and mixtures of known composition, except for the 100^0C data as discussed above. When applied to the diesel fuel results of Glen[59] there appear to be definite trends of error with respect to pressure, as shown

in Figure 5.2. Here the error increases continually as a function of pressure over the ranges studied at the lowest temperature of 25^{0}C. At 50^{0}C the error is acceptable at lower pressures before rising steeply beyond ~125MPa. 75^{0}C results appear to go through a minimum before showing a similar increase in error with respect to pressure. The regular trends of error found suggest that a reasonable estimation of diesel fuel viscosity can be made by using the hard sphere theory with an empirical fit of error. Although the errors were seen to be regular with respect to pressure, pressure is not a fundamental variable in hard sphere theory. Viscosity was instead proposed as a function of the free volume. Any fit of the error should therefore be a function of the free volume if it is to be consistent with the hard sphere scheme. To account for changes in the hard sphere volume for different fluids and temperatures, the relative free volume, $\frac{V - V_0}{V_0}$, is considered. Error for the three fuels as a function of relative free volume is plotted in Figure 5.3.

Plots of error in predicted viscosity from the hard sphere theory as a function of relative free volume, presented in Figure 5.3, indicate that either the hard sphere theory is inapplicable to diesel fuels or the numerical solution method used to implement this is unreliable. As there are errors of the magnitude shown then it is evident that direct application of the hard sphere theory is not appropriate for diesel fuels. The failure of the method when applied to diesel fuels is also highlighted by the difference in the isotherms of error. For a given fluid, the error plots differ greatly for the different temperatures considered. If a fluid corresponds to the hard sphere theory then the predicted viscosity would be equal at equivalent values of free volume regardless of temperature.

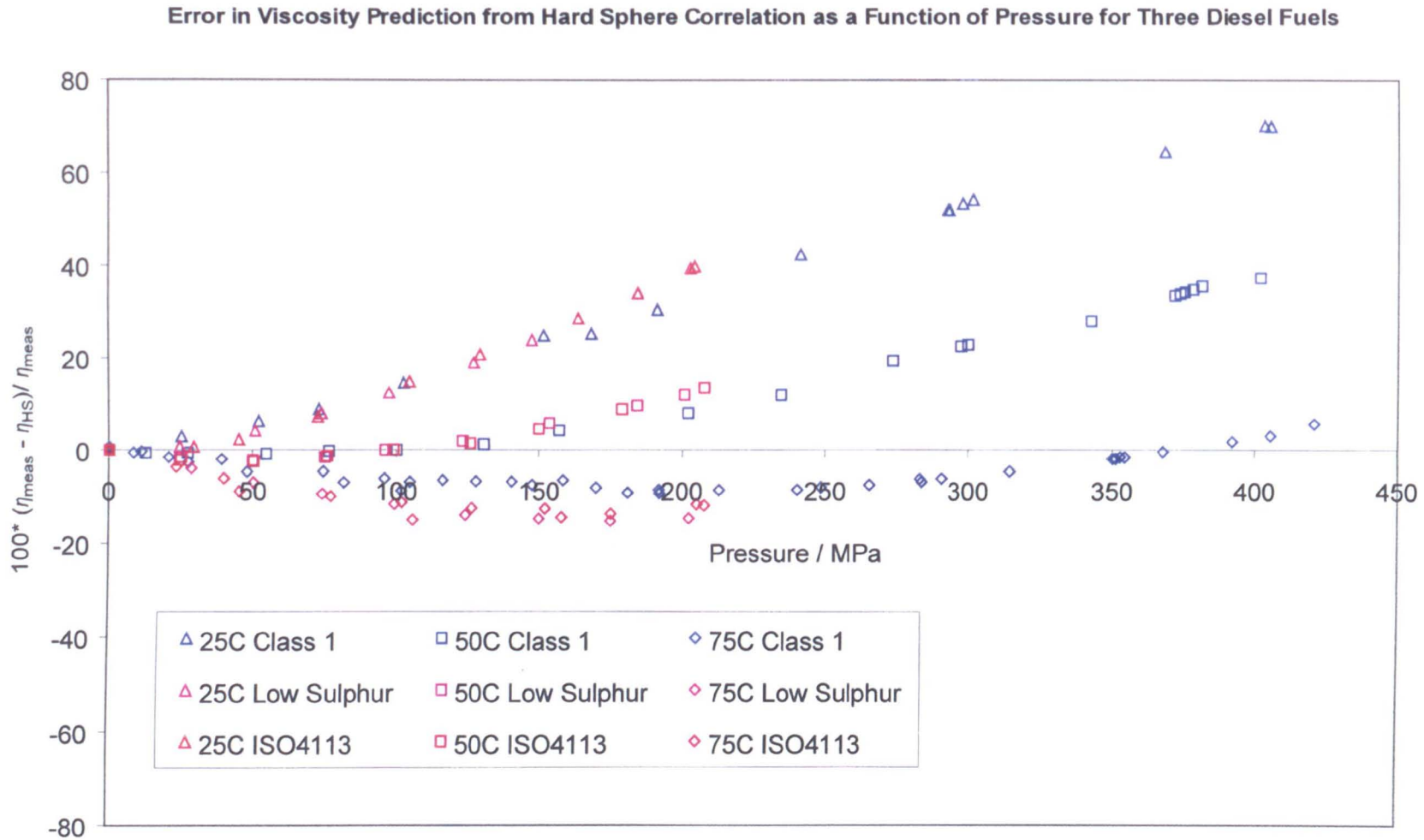

Figure 5.2 Trends of error in hard sphere prediction for diesel fuels with respect to pressure

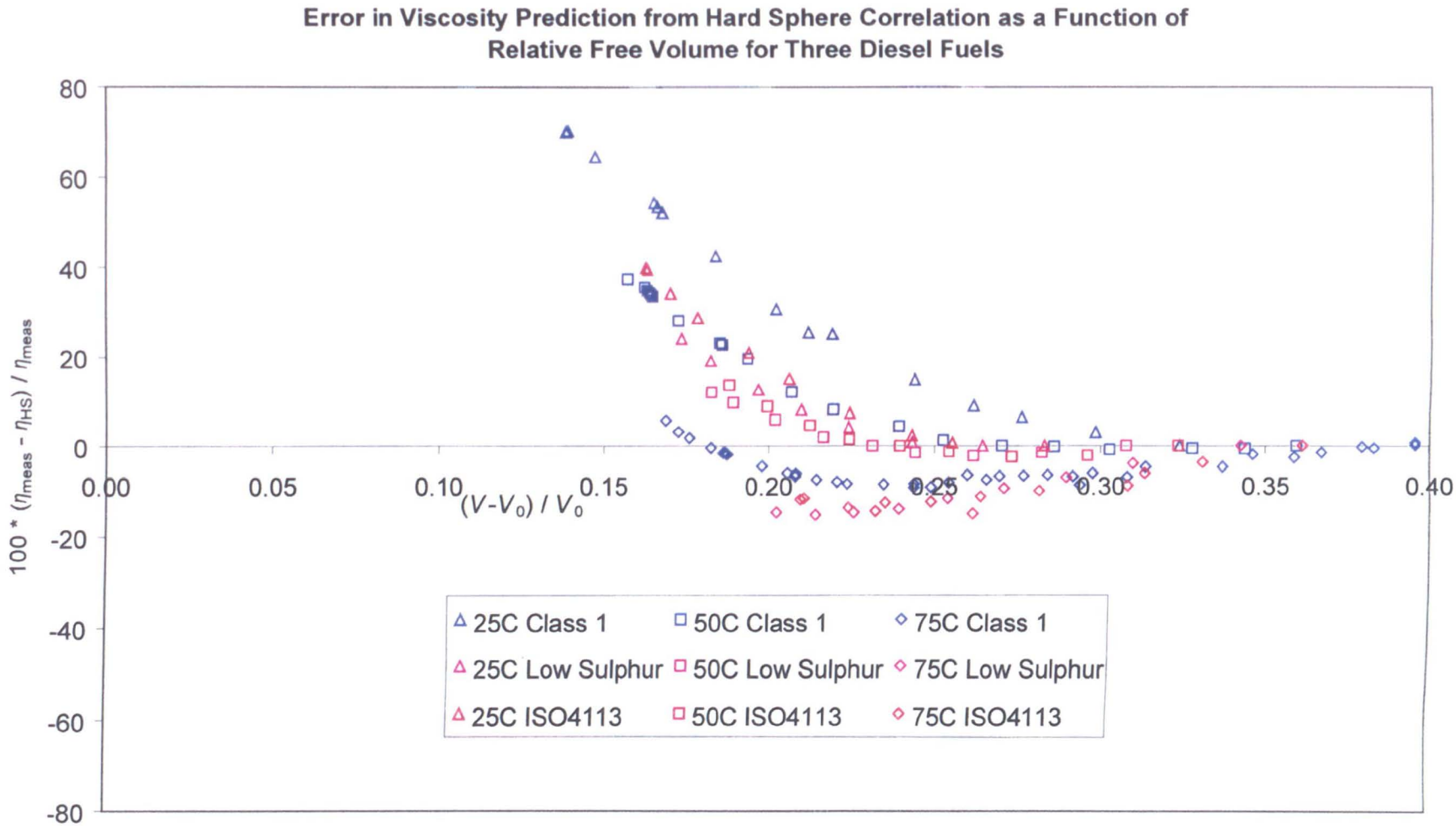

Figure 5.3 Trends of error in hard sphere prediction for diesel fuels with respect to relative free volume

Analysing Figures 5.2 and 5.3 together, both show a change in the behaviour of error with respect to temperature. However, Figure 5.2 shows regular plots of error for different fluids at the same temperature whereas Figure 5.3 does not. This could be indicative of poor estimation of V_0 for different fluids as the isotherms need to be moved along the abscissa to make Figure 5.3 analogous to Figure 5.2 where a regular trend is seen at each temperature for all fluids. Probable inaccurate prediction of V_0 between different fluids as suggested by consideration of Figures 5.2 and 5.3 together could be due to the method of solution used. The graphical method for estimating V_0 and R_η might offer greater accuracy, but this could not be done from limited measurement as proposed here. Therefore using relative free volume estimated by numerical solution as a basis for an empirical fit of error would not offer as simple a fit as with respect to pressure. Although not a satisfactory solution from a theoretical viewpoint, this is more likely to yield better accuracy in prediction provided that it is only used for corrections for fluids of a similar type to those from which the original correction was derived.

Error in viscosity prediction at 25^{0}C and pressures below 50MPa is acceptable; beyond 50 MPa the error increases approximately linearly for the three fluids considered here. The error can therefore be fitted by a straight line and corrected viscosity found from;

$$\eta_{corr_{25}} = \frac{\eta_{HS}}{1 - \dfrac{0.190P - 4.374}{100}} \tag{5.20}$$

Similarly at 50^{0}C a correction can be applied for the linear increase in error beyond 125MPa;

$$\eta_{corr_{50}} = \frac{\eta_{HS}}{1 - \frac{0.130P - 15.375}{100}} \tag{5.21}$$

Error is quite large between 100 and 200MPa at 75^{0}C for the low sulphur diesel and the ISO4113 fluid. This appears to represent a minimum of error. The Class 1 fuel has less error in predicted viscosity in this range before gradually increasing as the pressure is increased. Despite an apparent transition to a linear dependence of error upon pressure, the magnitude of error is not large in the higher pressure region considered. Therefore no correction term is derived at this temperature.

From the findings presented above, it appears that error in hard sphere prediction decreases with respect to temperature. No higher temperature results were published by Glen[59.] to test whether applying the hard sphere theory with no correction term gives reasonable results beyond 75^{0}C; this is tested using results found from measurements made in this work. At temperatures below 75^{0}C, correction terms could only be derived from the measurements at 25 and 50^{0}C. Thus it was not possible to estimate the behaviour of error with respect to temperature by fitting the linear coefficients of the pressure correction terms as functions of temperature. While empirical corrections allow the theory to be applied to complex mixtures of fluids, the study presented here highlights the limitations of the scope of such empirical corrections. Corrections to the idealised hard sphere system, derived from theoretical considerations would allow the theory to predict viscosity over a wider range of conditions and fluid types.

5.3.5 – Limiting the Scope of a 'Universal' Reduced Viscosity Curve

Rather than use an empirical correction to correct the viscosity calculated from the hard sphere theory, one might consider defining a 'universal' curve of more limited scope than that presented by Assael et al.[83.]. A pseudo universal reduced viscosity curve averaged from the curves of reduced viscosity as a function of relative free volume of a number of diesel fuels, should intrinsically provide less deviation of reduced viscosity of a given diesel fuel from the 'universal' case. Plots of the experimental reduced viscosity curves at 25, 50 and 75^{0}C of the Class 1 fuel are compared in Figure 5.4 as a function of relative free volume with the universal reduced viscosity curve of Assael et al.[83.]. This figure once more highlights the point made earlier that the hard sphere theory as applied to diesel fuel has failed to a certain degree as the curves at the different temperatures are not co-incident. Agreement of the curves at higher values of relative free volumes shows that the iterative scheme has worked as a numerical method, and does allow reasonable prediction of experimental reduced viscosity from the values of V_0 and R_η established by this method from limited measurement, over certain ranges.

V_0 and R_η were found relative to the universal reduced viscosity curve and could not be used as a basis for an independent pseudo universal diesel curve. If one was to develop such a curve, the value of V_0 would need to be found by comparison of experimental reduced transport data with the same quantities found from hard sphere theory. Assael et al.[83.] stress the importance of correlating at least two transport properties simultaneously if a consistent set of values of V_0 are to be found for the fluid at different temperatures. Therefore additional measurements of the self

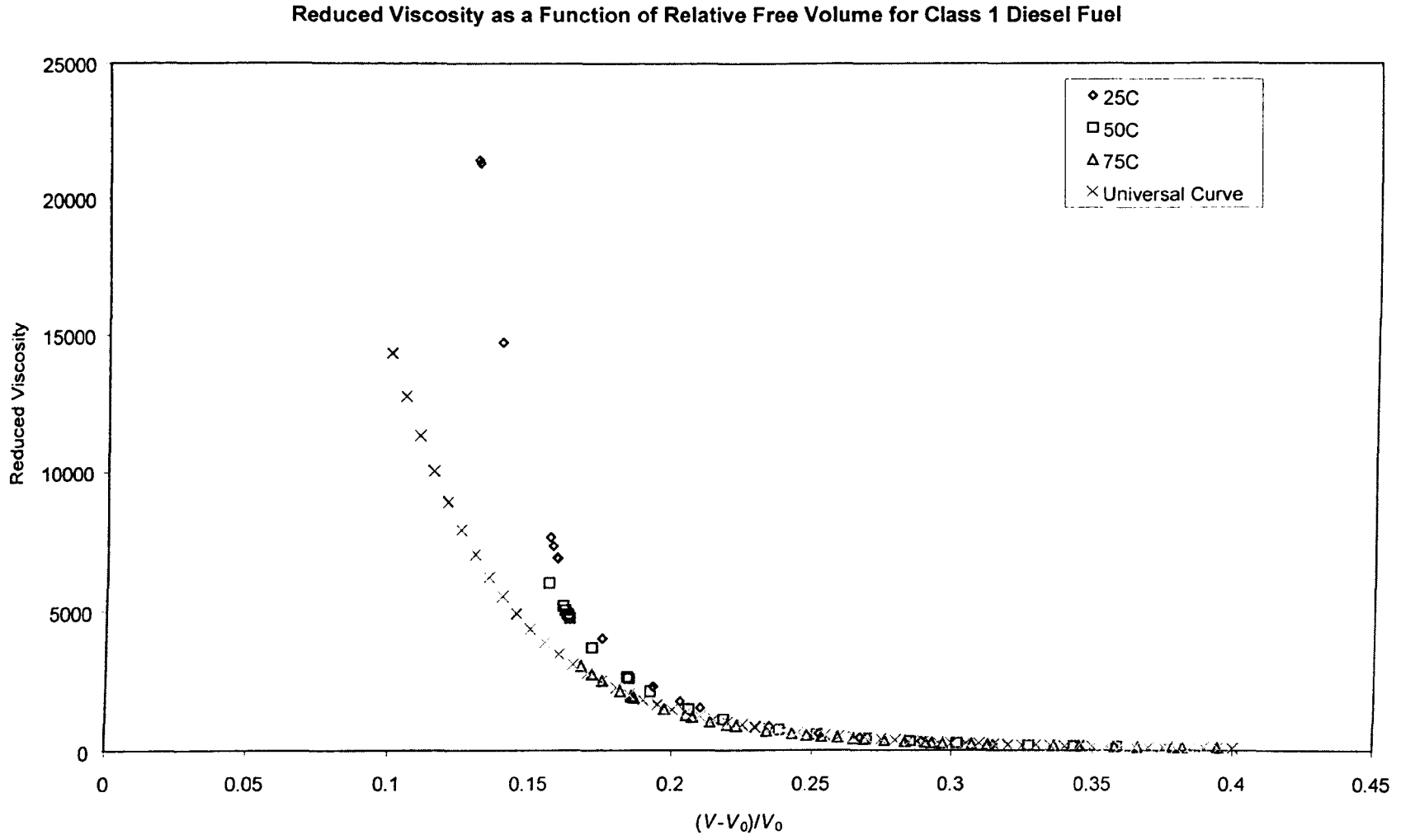

Figure 5.4 Comparison of experimental reduced viscosity of Class 1 diesel fuel with universal reduced viscosity

diffusion coefficient or the thermal conductivity of the fluid would be required for this exercise.

Assuming that sufficient experimental data were obtained to proceed with the analysis, values of V_0 would be found by comparison with the theoretical reduced transport properties. In the case of reduced viscosity, the theoretical term would be calculated from (5.16) with the right hand side multiplied by R_η to account for molecular roughness and non-spherical shape. Again, this parameter was found relative to the universal reduced viscosity curve of Assael et al.[83.] and would need to be determined independently to provide an independent pseudo universal diesel curve. To attempt to correct the difference between an assembly of regular hard spheres and a mixture of various molecules with different non-spherical shapes and interactions using a single correction factor is perhaps over optimistic. Thus either a new set of correction factors would be needed to correct for non-spherical and mixture effects, or the theoretical model would need to be changed to a more complex model than an assembly of hard spheres. This would also lead to the experimental reduced viscosity coefficient (5.18) being redefined. Given the potential variability in diesel composition and the effect that this could have on a theoretical model of the mixture, the additional complexity of this method will not necessarily be justified when it has already been shown that a reasonable viscosity prediction can be had by comparison with the universal hard sphere curve, given by Assael et al.[83.], plus an empirical correction.

A more straight-forward approach, ignoring how the universal hard sphere curve was derived, would be to simply change the coefficients of the polynomial equation to provide a better fit of an average curve of the fluid of interest. Once

again, this leads to the problem of defining a new curve from values of V_0 and R_η which have been derived relative to the universal curve defined by Assael et al.[83]. This approach would also lead to a discrepancy between comparing a reduced viscosity coefficient which has been defined in terms of the hard sphere theory with a pseudo universal curve which has been fitted from data which takes no account of the molecules being related to hard spheres. The universal curve of Assael et al. does take account of this, even when non-spherical n-alkanes were used to extend the range of the curve. In defining the non-spherical n-alkane extension to the curve, V_0 and R_η were adjusted to give agreement with the curve established from molecular dynamic simulation and measured data of spherical molecules, such as CCl_4. The seventh order polynomial fit of this universal curve was subsequently used for the correlation of the properties of other n-alkanes[70], aromatic hydrocarbons[71] and n-alcohols[56] without changing the coefficients of the universal curve. This proves the validity of the approach, and that the shape of the curve defined by the polynomial coefficients reported by Assael et al.[83] is a good general representation of the universal reduced viscosity as a function of reduced volume. This also reinforces the argument that it is better to use the universal reduced viscosity curve of Assael et al., which has been defined in a consistent manner with respect to the hard sphere theory, than to attempt to develop a pseudo 'universal' curve of limited application.

5.4.1 – Collision Integral

It was found from the above results that the hard sphere theory cannot be directly applied to complex mixtures without fluid specific empirical corrections, despite previous success in correlating non-spherical molecules. If such a theory is to be extended to fuel mixtures, one must consider the reasons why diesel viscosity data cannot be correlated by the method in its current form. It is seen from Figure 5.2 that error in prediction for each of the fuels is similar along isotherms. The change in shape of error as a function of pressure at the different temperatures suggests that the effect of temperature may not be adequately accounted for in the present method. In the derivation of the hard sphere theory for application to dense liquids, it was assumed that there was no interaction between the hard spheres and therefore the collision integral in (5.14) was assumed to be unity. Neufeld et al.[88] found collision integrals to be a function of temperature. As error in viscosity estimation was earlier shown to be temperature dependent it may follow that molecular interactions in the diesel mixtures do have a significant effect on the calculated viscosity and should be accounted for through a collision integral term.

Neufeld et al.[88] presented a general equation for reduced collision integrals with respect to reduced temperature. The equation for the $\Omega^{(2,2)^*}$ collision integral is;

$$\Omega^{(2,2)^*} = \frac{1.16145}{\left(T^*\right)^{0.14874}} + \frac{0.52487}{e^{0.77320T^*}} + \frac{2.16178}{e^{2.43787T^*}} \qquad (5.22)$$

An additional sine term can be used, but omission of this gives little change in the accuracy of the equation, particularly at higher values of T^*. Reduced temperature,

T^*, is defined here by $T^*=T(k/\varepsilon)$. Incorporating the collision integral into the experimental reduced viscosity (5.18) gives;

$$\eta^*_{exp} = \frac{16}{5}(2N_A)^{1/3}\pi^{1/2}\left(\frac{1}{MRT}\right)^{1/2}V^{2/3}\eta\Omega^{(2,2)^*} \qquad (5.23)$$

To test the validity of the hypothesis that including a collision integral term can correct the temperature effect for error in diesel viscosity prediction, the experimental viscosity term defined by (5.23) can be used in a solution scheme with (5.19). With this scheme the problem is now to find values of V_0 and k/ε which correlate the viscosity data. As the temperature effect should be accounted for by the collision integral, V_0 is now assumed constant. Solution of (5.19) now involves finding constant values V_0 and k/ε to correlate viscosity data. As these are both constant for the fluid, the solution scheme can now be viewed as using two measurements to give two equations with V_0 and k/ε as two unknowns.

A computer program was written to implement the above scheme using a similar algorithm to that used for the solution of V_0 and R_η; this program is presented in Appendix D. The program started from an initial guess value of k/ε which was used to find a value of V_0 such that both sides of (5.19) were approximately equal when data at a given temperature were used. This V_0 was then used to calculate a k/ε value which would give equality of (5.19) when a second set of data were used. This process was repeated until the initial assumed value and final calculated value of k/ε were approximately equal. Thus the correlating parameters V_0 and k/ε can be established from two atmospheric pressure measurements.

It was found that it was necessary to implement the solution scheme in the form above. The alternative method of attempting to find an iterated value of k/ε

equal to the original guess was unsuccessful due to the sensitivity of this parameter to changes in V_0. Analysing the method, a 0.15% change in V_0 was found to give a 20% change in the value of k/ε. This meant that although the measurements were correlated using values of V_0 which were equal within a specified tolerance, when viscosity was calculated back from the correlation parameters significantly larger errors were found for the former of the two measurements used to establish V_0 and k/ε.

Error in predicted viscosity with respect to pressure by this method was very large as seen from the equimolar octane - dodecane mixture error plot given in Figure 5.5. It is seen that the error by this method, although large, is regular with respect to temperature and also appears to show a regular rate of change with respect to pressure. However, the isotherms are seen to cross at lower pressures which could give some difficulty in establishing a function to estimate change of error with respect to temperature. In contrast the isotherms of error with respect to relative free volume display greater curvature, but have a more consistent displacement between each other even at the highest free volumes as shown by Figure 5.6. Therefore despite the previous analysis of error of diesel fuels using the hard sphere theory being undertaken with respect to pressure, relative free volume appears to provide a more appropriate basis for study in this instance. This could be due to the simpler binary mixture studied here, or it could be that the different algorithm gives a more reliable estimation of V_0.

Error as a function of free volume was fitted by polynomial equations at 25, 50 and 75^{0}C for the octane-dodecane mixture. It is seen from Figure 5.6 that the curvature of error of viscosity prediction with respect to relative free volume

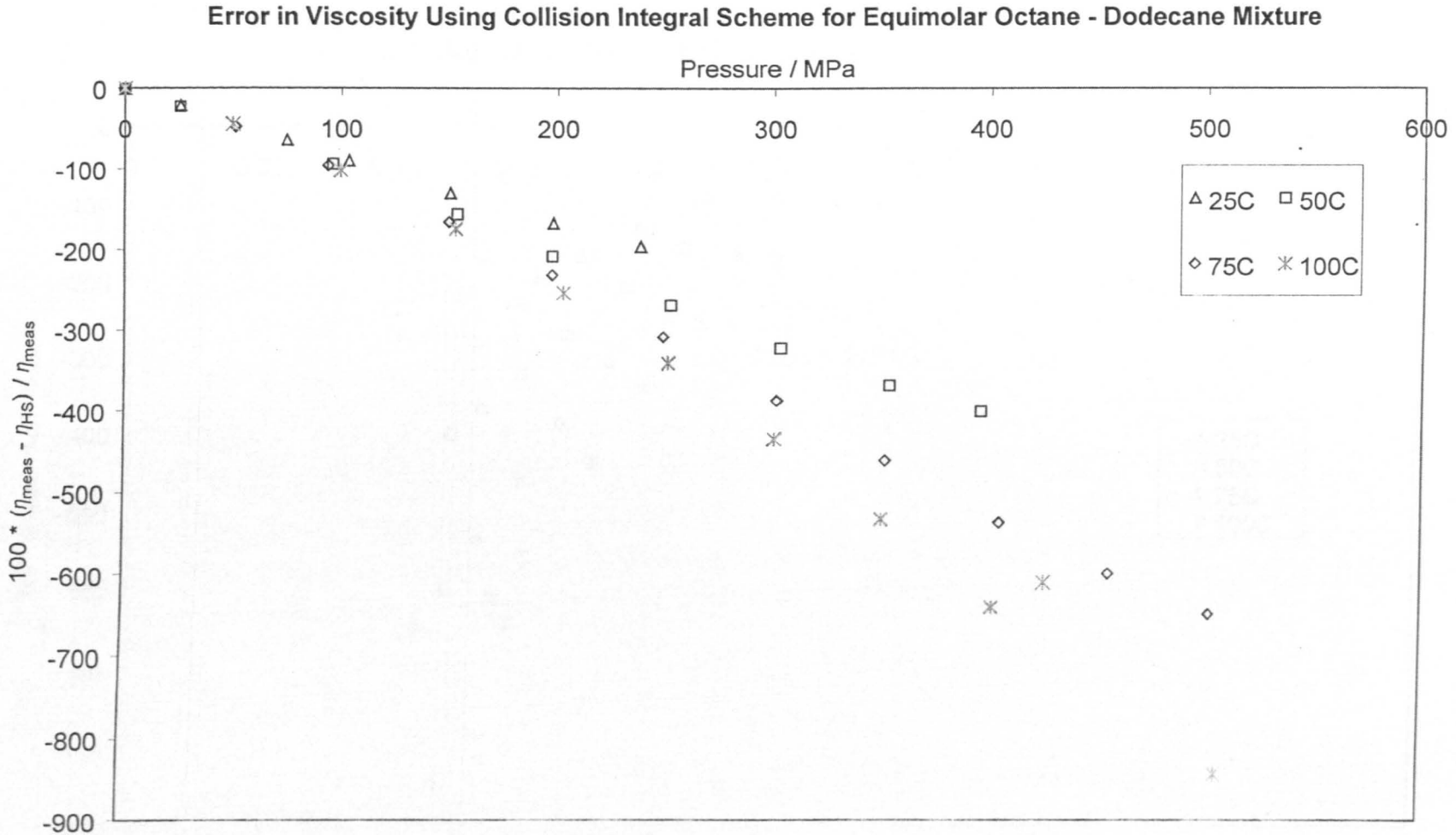

Figure 5.5 Error in prediction of octane-dodecane mixture viscosity using hard sphere theory with collision integral term

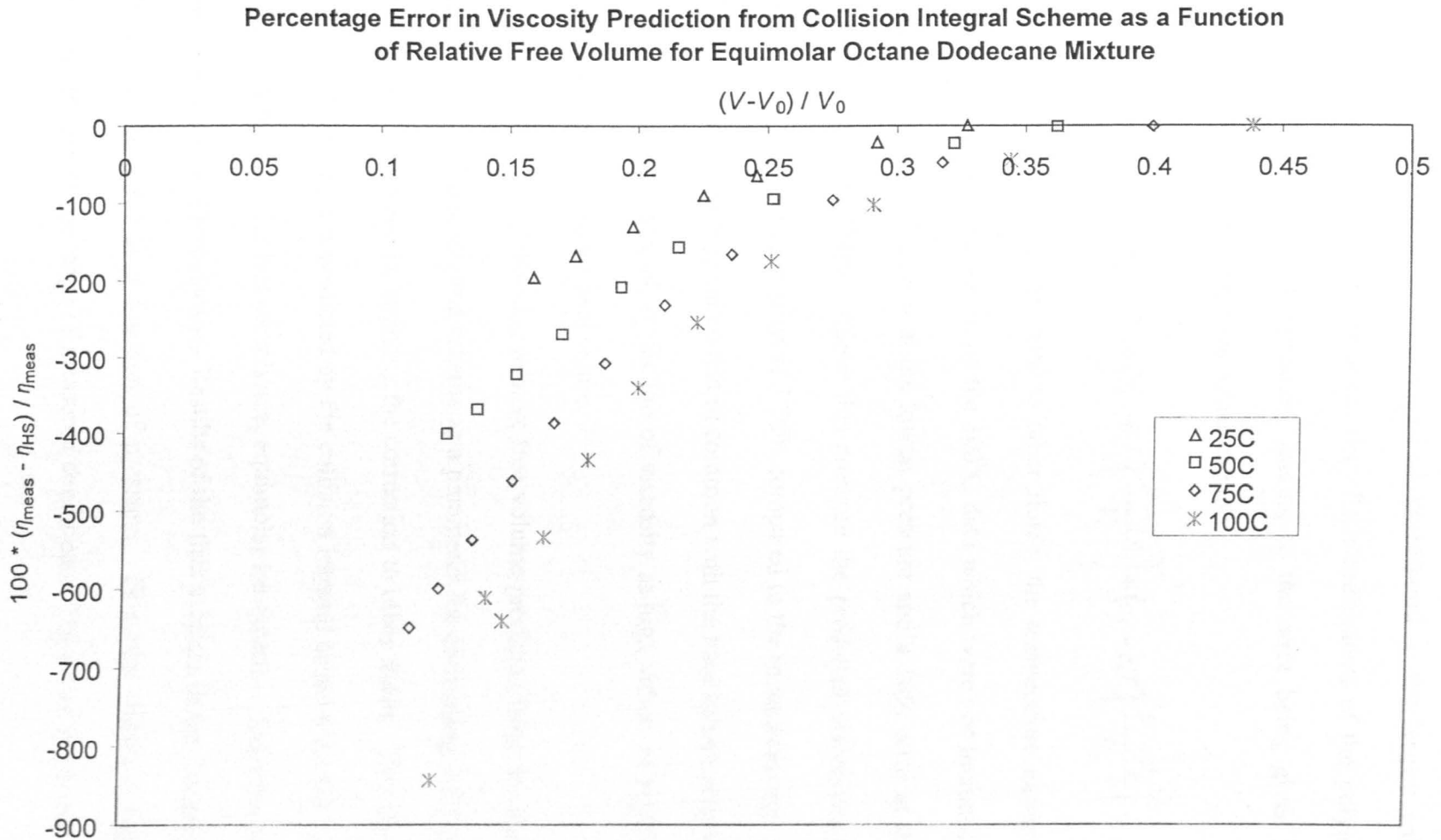

Figure 5.6 Error in collision integral scheme viscosity prediction as a function of relative free volume

increases greatly at the largest values of relative free volume. In this analysis, the region of greatest curvature is not considered; this is excluded from the fit by simply excluding the atmospheric data points which correspond to the largest values of relative free volume. Reasonable linear fits of the coefficients of the polynomials were made with respect to temperature, leading to the error being given by the following function of temperature and free volume;

$$100\left(\frac{\eta_{meas}-\eta_{pred}}{\eta_{meas}}\right)=(a_0+a_1T)+(b_0+b_1T)\left(\frac{V-V_0}{V_0}\right)+(c_0+c_1T)\left(\frac{V-V_0}{V_0}\right)^2 \qquad (5.24)$$

Before applying the correction term to other fluids, the temperature extrapolation ability of the equation was tested on the 100^0C data which were not included in the fit. This test gave a 72% error at the lowest pressure and a 16% error at the next lowest pressure of 49.7MPa. Above this pressure the predicted viscosities had an absolute average percent deviation of 3.76% compared to the measurements. On the basis of this single test it appeared that in common with the hard sphere scheme used without the collision integral, prediction of viscosity at high values of relative free volume is not as good as at lower values.

The validity of choosing relative free volume predicted from the numerical solution of the collision integral scheme as a parameter for correlating corrections to this scheme is best tested by applying the correction to other fluids. This correction was applied to the results predicted by the collision integral scheme for the 0.8 mole fraction hexadecane – 0.2 hexane mixture, equimolar iso-octane – dodecane mixture, octane, dodecane, and hexadecane. Results of the first mixture in the list are plotted in Figure 5.7 as error as a function of pressure. This plot shows a large, but consistent error over the range of measured conditions. The other fluids considered

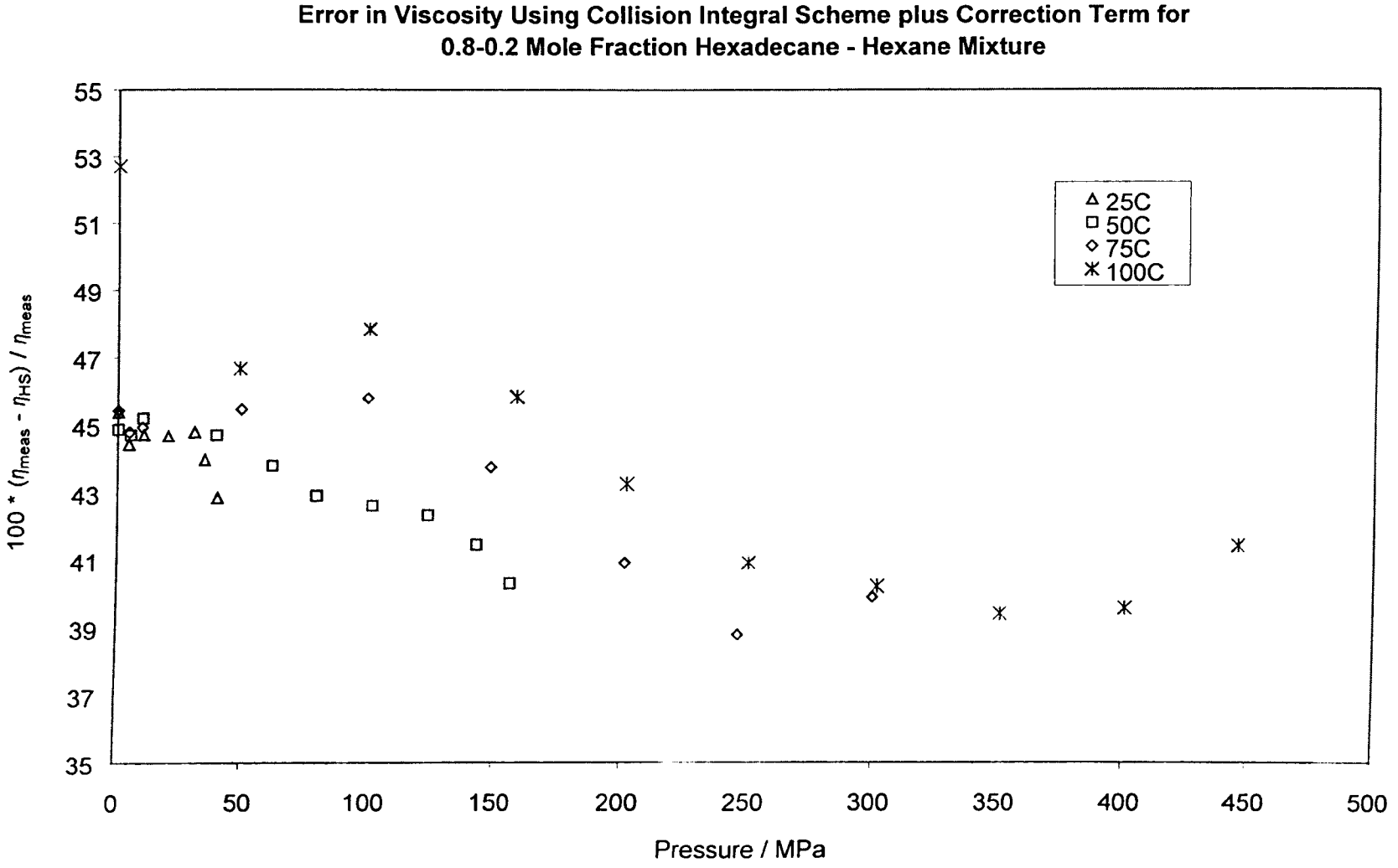

Figure 5.7 Example of consistent error obtained through collision integral scheme with correction factor

in this study also display a consistent error when compared to the measured results. Assuming the error to be constant, it follows that an additional correction term can be found by comparing another measured viscosity with the viscosity at the condition of measurement predicted through use of equations (5.19), (5.23) and (5.24). When percentage error in prediction is calculated for the additional measurement, the correction term is simply;

$$\eta_{meas} = \left(\frac{100}{100 - \%error}\right)\eta_{calc} \tag{5.25}$$

Referring to the term $\frac{100}{100-\%error}$ as a correction factor to the collision integral scheme presented here, then this correction factor can be considered as a form of shape factor to account for non-spherical shape. This possible explanation for the offset is given some weight by consideration of the relative values of correction factor for the pure fluids considered, compared with relative values of acentric factor and the hard sphere non-sphericity term R_η. Values of these terms are presented in Table 5.3.

Table 5.3 Comparison of collision integral correction factor to non-sphericity terms

Fluids compared	Collision Integral Correction Factor Ratio	Ratio of Acentric Factors	Ratio of R_η Values
Octane-Dodecane	0.619	0.692	0.757
Octane-Hexadecane	0.497	0.536	0.565
Dodecane-Hexadecane	0.802	0.775	0.747

None of the terms in Table 5.3 are directly comparable; the collision integral correction factor corrects relative to the equimolar octane-dodecane system as

discussed earlier whereas the acentric factor, ω, and R_η are relative to spherical molecules. ω and R_η cannot be directly compared either as the former was developed from thermodynamic considerations and the latter is a true shape factor. Despite this, the similar magnitudes of the three parameters suggest that the correction factor for the collision integral, found here from average error and equation (5.25), is a form of shape factor.

Despite the large errors found when the collision integral scheme was initially applied directly to the alkane liquids and mixtures, this method has proven to be of some practical use due to the regular behaviour of the errors and the ability to correct for these. It should be noted however, that whilst data for five of the six fluids could be correlated using atmospheric data at 25 and 50^0C (plus an additional measurement to calculate the correction factor (5.25)), it was necessary to use the atmospheric measurements at 50 and 75^0C to obtain solution for V_0 and k/ε for hexadecane. When tested on diesel fuels only the ISO4113 fluid could be successfully correlated using this method. Results for this were poor suggesting that for complex mixtures it is not just the lack of a temperature dependent parameter for molecular interactions which causes the hard sphere theory to fail.

In the immediate context of using a collision integral method to correlate diesel properties, this study has yielded little of direct importance. When the behaviour of the model is considered when applied to alkanes and binary mixtures, this method could be of some use in the study of transport theory for correlating pure components and mixtures of pure components by relating the bulk fluid property to both the molecular distance property (V_0) and a molecular energy term (k/ε).

5.4.2 – Non-Uniform Molecular Shape

Disregarding the effect of molecular interactions may introduce some error into the hard sphere correlation method. For diesels, the greater effect causing the scheme to fail is likely to be that the mixture can in no way approximate to an assembly of regular hard spheres. It was noted earlier that Dymond and Awan[84.] correlated liquid alkane transport properties by correcting using a factor R_η to account for non-sphericity of the molecules. It was also shown that this factor could not be used to correlate diesel viscosity. To understand why this should be, one can visualise the case of a fluid composed of uniform, non-spherical molecules. Here the case of the molecules as cuboids of length d, equivalent to the diameter of an equivalent system of hard spheres is considered. Height and breadth are taken to be constant proportions of the length, xd and yd respectively. The volume of each molecule would then be xyd^3, with xy constant. The equivalent hard sphere would have volume $(\pi d^3)/6$. As the ratio between the spherical and non-spherical volumes is constant, the simplest method for correcting for non-sphericity in a uniform fluid is to apply a constant correction factor.

If the case of a fluid mixture of non-uniform molecular shapes is now considered, it is obvious that there is no longer a single constant to account for non-sphericity. It was shown by Assael et al.[85.] that for a mixture of molecules of the same homologous series, viscosity could be correlated by mole fraction averages of the V_0 and R_η values of the components of the mixture. This approach predicted liquid viscosity within 5% for two ternary and three quaternary n-alkane mixtures. Only atmospheric measurements were available for comparison of these ternary and quaternary mixtures, but given the range of components covered and the success of

the method when applied to binary mixtures over a wide range of conditions, the mole fraction average method is proven to be a valid approach at least when applied to n-alkanes. Failure of this averaging method when applied to compounds of different molecular types[79.] could possibly be attributed to two effects. Firstly, branching of molecules could affect the movement of molecules past one another. Secondly, interactions between unlike molecules, such as aromatics and alkanes, are not accounted for by a simple molecular average of V_0 and R_η.

The first of these suggestions has already been investigated to a small extent by the choice of the iso-octane – dodecane mixture as one of the liquids studied earlier. With reference to Figure 5.1 it is seen that the error in the viscosity predicted from the hard sphere theory is similar for both the equimolar n-octane – dodecane mixture and the equimolar iso-octane – dodecane mixture. Hard sphere correlation viscosities were found for these mixtures by considering the fluid as one component and finding V_0 and R_η by numerical means as described earlier. Although this is a different method with less physical significance than the mixing laws of Assael et al.[85.], both rely on a single value of V_0 and a single value of R_η to correlate the data and therefore the finding that error is similar for the normal and iso-octane mixtures should not be invalidated on account of the solution method used.

5.4.3 – Aromatic-Aliphatic Mixture Effects

If the failure of the application of the hard sphere theory to mixtures is caused by unaccounted for interactions between aromatics and non-aromatics then it may be possible to account for this without directly considering some form of interaction correction factor to the hard sphere theory. Assuming that it is possible to

correlate both classes with single values of V_0 and R_η for each, then viscosity for each class would be calculated from the correlation parameters and viscosity of the mixture from a viscosity mixing rule. For example, Dymond et al.[89.] correlated the viscosity of hexane and toluene separately using hard sphere theory. However, mixtures of toluene and hexane were correlated over a wide range of pressure and temperature using the mixing rule of Grunberg and Nissan[90.].

Whilst it is an interesting possibility to extend this method to combining mixtures of aliphatics and aromatics, testing of the method is not possible without knowing the volume behaviour and average V_0 and R_η of each of the classes of compounds. An attempt could be made at estimating viscosity of each class if detailed composition data is available for the fuel. V_0 and R_η for each class would be found from molecular weight averages of the individual components within the class. Viscosity would then be found by combining the classes through a mixing rule.

Using the correlations presented by Assael et al.[70.] V_0 and R_η of the n-alkanes can be found as a function of chain length and temperature. Assuming that these functions extrapolate satisfactorily, V_0 and R_η can be found for each component identified in the diesel fuel then combined using the mole fraction average. A similar method is not possible for other hydrocarbon series. This is due to both a lack of identification of all components within the fuel and limited viscosity data over a wide range of conditions from which V_0 and R_η may be found. For example, aromatic data studied by Assael et al.[71.] was limited to chain lengths from 6 to 9. The published correlation for V_0 does not represent the data in the accompanying table. Using the tabulated data to fit V_0 with respect to temperature and carbon number, then it still proves a difficult task to find a function which extrapolates realistically based on

three data points (benzene represents the start of the aromatic series and is excluded due to the anomalous behaviour associated with the first member of a series). Rather than attempting to base aromatic behaviour upon that displayed by three carbon numbers and assuming that all aliphatics have similar viscosity behaviour to the n-alkanes, it may be better to consider the diesel viscosity in terms of deviation from n-alkane behaviour. This deviation can then be considered in terms of other species present in the diesel fuel.

5.4.4 – Deviation of Diesel Viscosity from n-Alkane Viscosity

Before attempting to find viscosity of the alkanes present in the diesel from hard sphere theory, it is necessary to have an accurate knowledge of their density. Alkane atmospheric densities from methane to hexadecane are given by Assael et al.[70.] as functions of reduced temperature and critical density. Calculating density then plotting as isotherms against reciprocal carbon number, the trends are well fitted by quadratic equations. Checking the extrapolation of atmospheric density as a function of carbon number for eicosane at 100^0C compared to the measurements of Doolittle[60.] it is found that the predicted atmospheric density is within 0.1% of the measured value. This density can be used in combination with the equation given by Assael et al. to fit the Tait B parameter[55.] to estimate density as a function of pressure for the normal alkanes. Critical temperature is required for the Tait B correlation and this is estimated by extrapolation with respect to carbon number. Predicted volume ratios of eicosane at 100^0C with respect to pressure were compared with the measurements of Doolittle, and found to agree very well. At the conditions considered, many of the n-alkane components detected within the diesel will be in

the solid phase when considered as individual components. For the purposes of comparing fluid mixture properties, the components are taken to be in a theoretical liquid phase with density behaviour estimated by extrapolation as described. Theoretical liquid density of each alkane can now be estimated at the temperature and pressure of interest. Density for each is combined with the mole fraction of each in the mixture and used to find the equivalent alkane mixture density at the condition of interest. Having established V_0 and R_η using the method described earlier, it is now possible to calculate viscosity for the alkane portion of the diesel fuel.

With this method for estimating the viscosity of the alkane fraction of a diesel now established, the alkane components of the fuel can be used as a reference mixture within the fuel. Deviation from alkane behaviour could then be empirically related to the fractions of different classes of compounds present in the diesel. Deviation functions could possibly be derived from mixtures of aliphatics and aromatics, or branched, cyclic and unbranched molecules with known composition. This would require more tests of diesels where composition of alkanes were known. More tests of mixtures of few components with known composition composed of the various classes of hydrocarbons would also be useful to give more insight into possible interaction parameters between, for example, alkanes and aromatics.

5.4.4.1 – Diesel Composition

A general model for viscosity derived from theory would be preferable to an empirical correlation limited to, for example, certain distillation ranges for fuels from a specific region. The problem with obtaining such a general model derived from molecular theory is the potential degree of characterisation of the fuel necessary to

implement the model. Ideally, if a function was derived from one fuel relating deviation of alkane behaviour to the proportion of aromatics and other aliphatic groups present, then this function would be applicable to all fuels. This is unlikely to occur due to different refinery techniques used to obtain the fuel potentially resulting in a different spread of components within the classes.

Despite the potential variation in the composition of diesel fuels, Ozdogan and Yucel[68.] obtained reasonable estimates of viscosity using a method relating atmospheric pressure viscosity to different hydrocarbon types present. Similarly, for elevated pressure viscosity it might be possible to successfully apply the hard sphere theory for diesel prediction provided that the relative amounts of alkanes, non-alkane aliphatics and aromatics are known as characterisation parameters for the fuel. Instead of using a molecular weight averaging method for combining viscosities of the different hydrocarbon types, diesel viscosity could be defined by the deviation of the diesel viscosity from the alkane fraction as discussed previously. This deviation would then be a function of the amounts of aliphatics and aromatics present;

$$\eta = \eta_{alk} + f_1(x_{aliphatics}) + f_2(x_{aromatics}) \tag{5.26}$$

Basic forms of the functions f_1 and f_2 could be established from studies of the viscosity of mixtures of alkanes and other hydrocarbon types. When applied to diesels, coefficients of the functions would be optimised from limited measurement using numerical methods.

Chapter 6.

Results and Analysis

6. Results and Analysis

6.1 Fuels Measured

Density and viscosity over a range of conditions were measured for eleven diesel fuels. The fuels tested were a fuel from a British refinery with no performance or handling additives (Fuel A); the same fuel with handling additives but no performance additives (Fuel B); and the same fuel with both handling and performance additives (Fuel C). A fuel from another British refinery was tested with no performance or handling additives (Fuel W); this fuel with handling additives (Fuel X); the same fuel with both handling and performance additives (Fuel Y); and the same fuel with handling and performance additives and approximately 5wt% rape methyl ester (Fuel Z). An ISO4113 standard fuel mixture previously used in a fuel injection test rig (ISOA) and a previously unused ISO4113 mixture (ISOB) were tested. A retail fuel sample from South East England was tested (SE Retail) as was a fuel from Kansas (Kansas).

Density measurements at atmospheric pressure were made according to ASTM D4052 by ITS Testing Services (UK) of West Thurrock. Atmospheric viscosities were measured according to the IP 71 method, also by ITS Testing Services (UK). Atmospheric data for the eleven fuels are given in Table 6.1.

6.2 Density

6.2.1 – Fitting of Density Results

Change in volume ratio with respect to temperature and pressure was measured for all the fuels by the Micro-PVT apparatus. Measurements of volume

Table 6.1 Atmospheric density (ρ), kinematic viscosity (ν) and dynamic viscosity (η) measurements. Subscripts denote temperature in degrees Celcius.

	Fuel A	Fuel B	Fuel C	Fuel W	Fuel X	Fuel Y	Fuel Z	ISO A	ISO B	SE Retail	Kansas
	Density / kgm^{-3}										
ρ_{15}	832.9	833.7	833.7	832.7	832.7	832.7	835.0	829.0	823.8	829.3	850.4
ρ_{25}	825.9	826.6	826.8	825.7	825.7	825.7	828.0	825.7	817.0	822.4	843.1
ρ_{40}	815.4	816.2	816.3	815.1	815.2	815.2	817.4	815.2	806.6	811.9	832.7
ρ_{50}	808.5	809.3	809.3	808.1	808.1	808.1	810.5	808.1	799.5	805.0	825.8
ρ_{75}	790.9	791.8	792.0	790.5	790.5	790.5	792.7	790.5	781.8	787.4	808.0
ρ_{100}	-	-	773.6	-	-	-	-	-	762.4	-	790.9
ρ_{125}	754.4	-	755.2	-	-	754.2	756.5	-	743.2	-	772.6
	Kinematic Viscosity / cSt										
ν_{25}	3.668	-	3.809	-	-	3.212	3.376	-	3.437	-	3.323
ν_{40}	2.634	2.714	2.720	2.420	2.434	2.451	2.520	2.824	2.582	2.575	2.445
ν_{50}	2.209	-	2.267	-	-	2.049	2.102	-	2.165	-	2.062
ν_{75}	1.529	-	1.551	-	-	1.416	1.451	-	1.481	-	-
ν_{100}	-	-	1.138	-	-	-	-	-	1.087	-	1.045
ν_{125}	0.8974	-	0.9005	-	-	0.8363	0.8463	-	0.8636	-	0.8424
	Dynamic Viscosity / mPa.s										
η_{25}	3.029	-	3.149	-	-	2.652	2.795	-	2.808	-	2.802
η_{40}	2.148	2.215	2.220	1.973	1.984	1.998	2.060	2.302	2.083	2.091	2.036
η_{50}	1.786	-	1.835	-	-	1.656	1.704	-	1.731	-	1.703
η_{75}	1.209	-	1.228	-	-	1.119	1.150	-	1.158	-	-
η_{100}	-	-	0.8804	-	-	-	-	-	0.8288	-	0.8265
η_{125}	0.6770	-	0.6801	-	-	0.6307	0.6402	-	0.6418	-	0.6508

change with respect to pressure from this device show a small amount of scatter about the expected smooth variation with pressure. This is a measurement artefact of the Micro-PVT apparatus, due either to slight irregularity in the motion of the piston into the cell, or the response of the pressure sensor. Figure 6.1(a) shows a detailed section of the pressure-volume curve for Fuel C at 25^0C. These data can be smoothed by fitting the data through bulk modulus coefficients then re-calculating volume from the obtained coefficients. A smooth form of the data is of use when calculating derived properties such as isothermal compressibility. Hayward[91,92] describes the use of bulk modulus for fitting volume data with respect to pressure, and also explains the different definitions employed. Here, volume ratio results were used to calculate isothermal secant bulk modulus values, $\overline{K}_T$, for each fuel;

$$\overline{K}_T = \frac{P - P_0}{1 - \left(\frac{V}{V_0}\right)} \tag{6.1}$$

$\overline{K}_T$ can be fitted by a polynomial equation with respect to pressure at each temperature;

$$\overline{K}_T = k_0 + k_1 P + k_2 P^2 + \ldots \tag{6.2}$$

Isothermal secant bulk modulus calculated from equation (6.1) for Fuel C at 25^0C is shown as a function of pressure in Figure 6.2. It is seen that the function is irregular at lower pressures, but smooth further up the range beyond 50MPa. For this reason, the lower pressure data were not used when determining the coefficients for equation (6.2). Ranges of pressure used for fitting the equation and the isothermal bulk modulus coefficients, k_0, k_1 and k_2 for all fuels measured are given in Table 6.2.

Comparison of Volume Ratio from Micro-PVT Displacement Measurements with Volume Ratio from Bulk Modulus

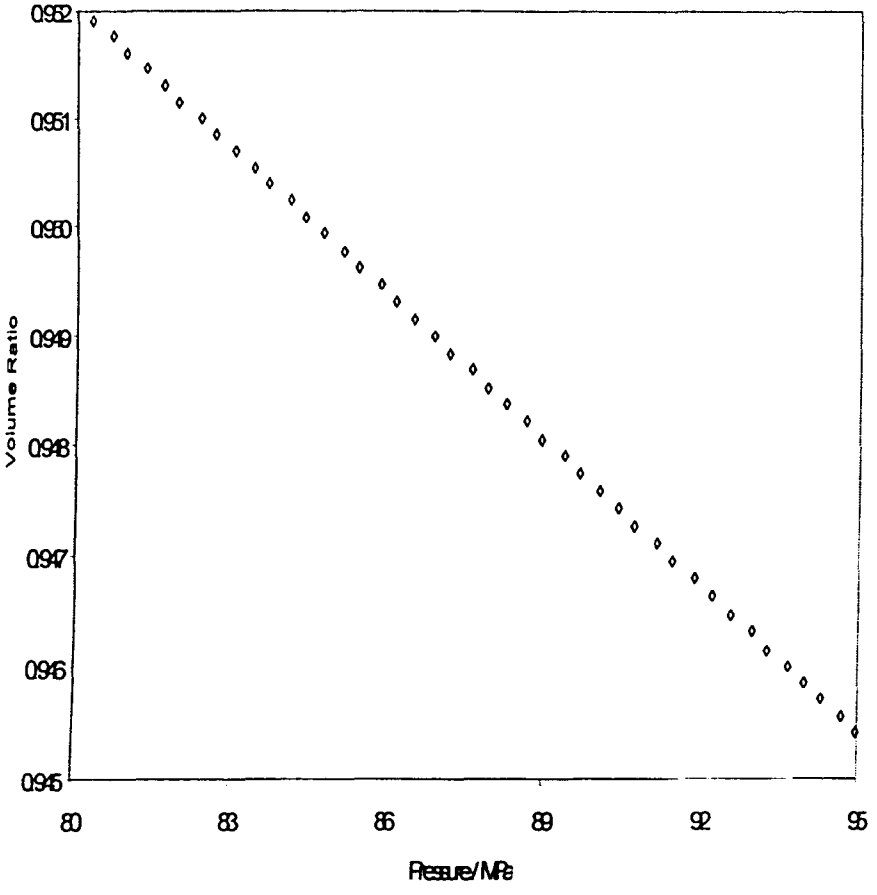

Figure 6.1(a). Volume ratio from Micro-PVT measurements

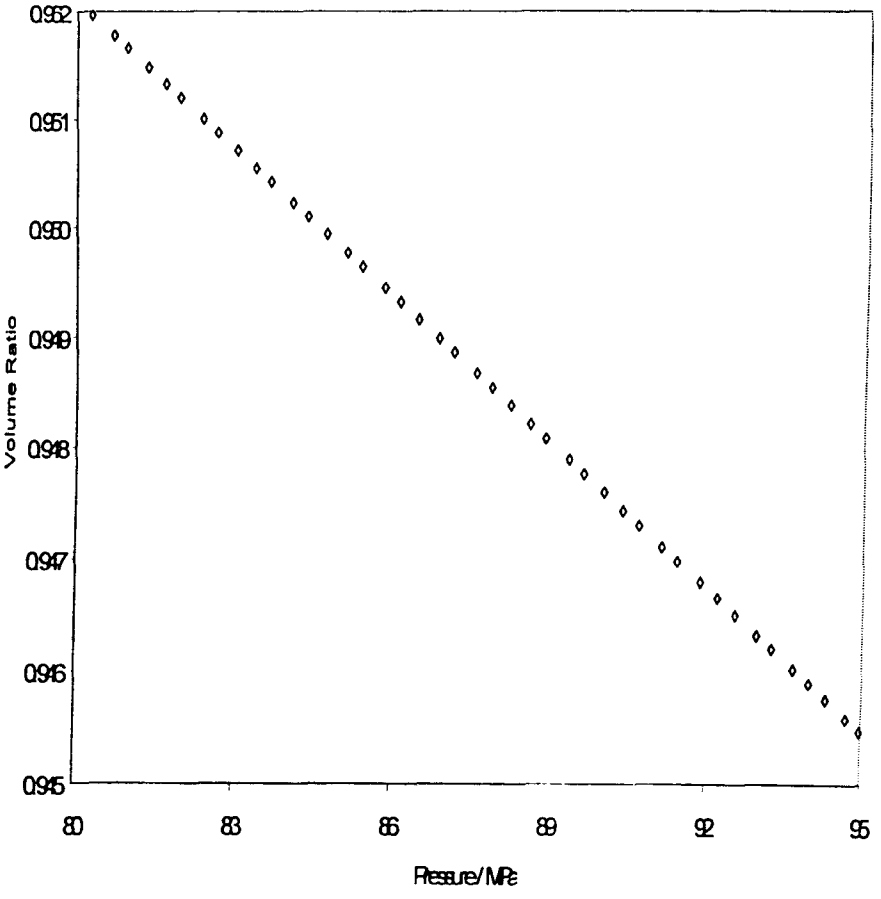

Figure 6.1(b). Volume ratio derived from bulk modulus fit

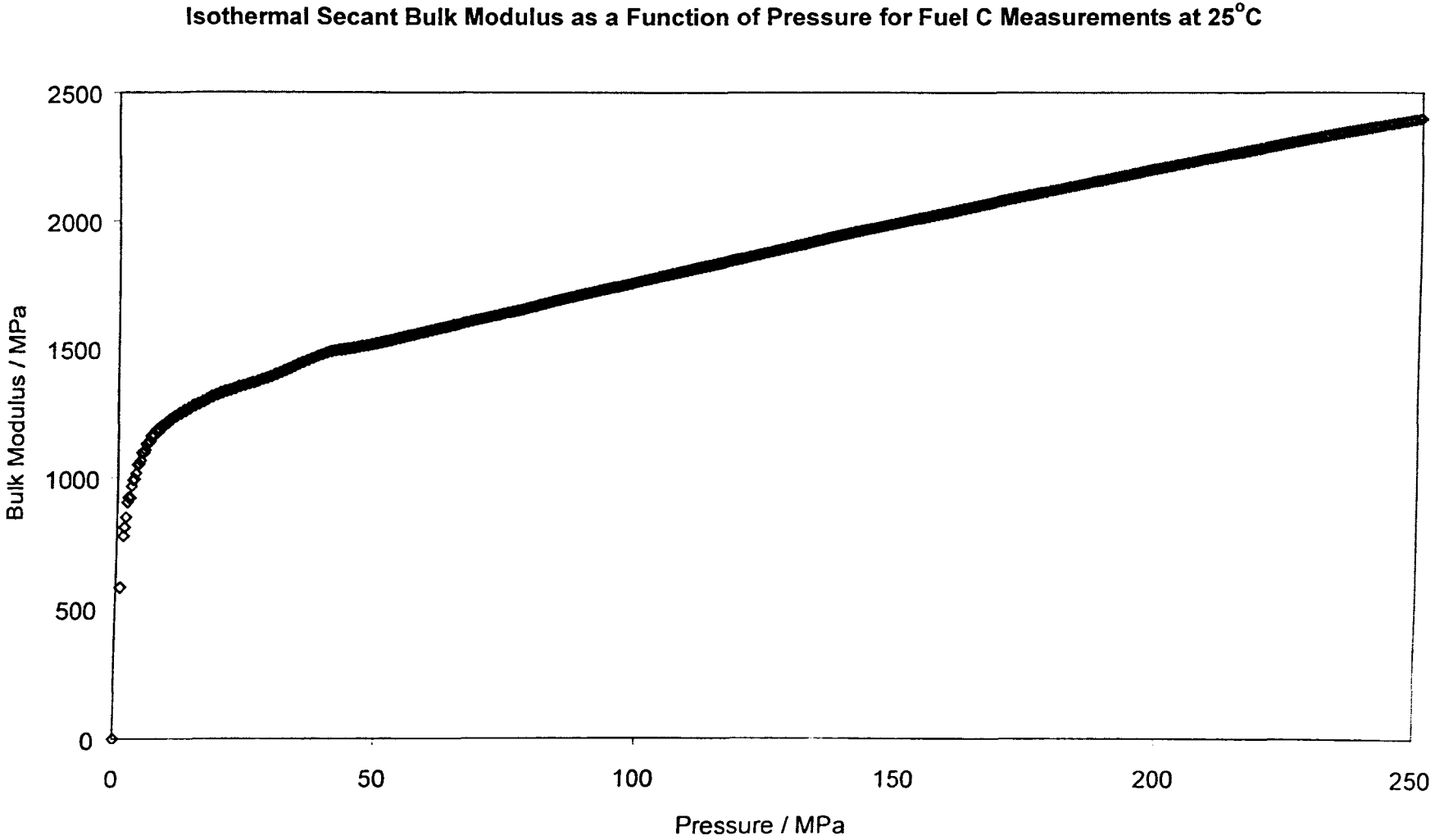

Figure 6.2 Typical form of bulk modulus with respect to pressure for a diesel fuel using volume data from Micro-PVT

Table 6.2 Bulk modulus coefficients for fuels measured and range over which bulk modulus was fitted

Fuel	T / °C	k_0 / MPa	k_1	$-k_2 \times 10^3$ / MPa^{-1}	Range / MPa
Fuel A	25	1148.2	6.0614	4.8698	50-250
Fuel A	50	943.37	6.2802	5.7127	50-250
Fuel A	75	792.96	6.2248	5.7624	50-250
Fuel B	25	1159.3	6.1183	5.0504	50-250
Fuel B	50	924.65	6.6073	6.5433	50-250
Fuel B	75	783.61	6.4004	6.0676	50-250
Fuel C	25	1259.5	5.3547	3.1533	50-250
Fuel C	50	1056.0	5.7864	4.4615	50-250
Fuel C	75	868.60	6.0832	5.3430	50-250
Fuel W	25	1211.0	5.6074	3.5780	50-300
Fuel W	50	1058.9	5.4755	3.4925	50-300
Fuel W	75	824.87	6.0851	5.0584	50-300
Fuel X	25	1245.0	5.3460	3.4106	50-300
Fuel X	50	1008.8	5.8290	4.4281	50-300
Fuel X	75	812.25	6.0238	4.9179	50-300
Fuel Y	25	1253.0	5.3332	3.1350	50-300
Fuel Y	50	1026.9	5.6780	3.9713	50-300
Fuel Y	75	870.78	5.6894	4.1921	50-300
Fuel Z	25	1265.8	5.3416	3.1145	50-300
Fuel Z	50	1018.3	5.7855	4.2104	50-300
Fuel Z	75	823.15	6.0066	4.7889	50-300
ISO A	25	1242.7	5.5391	3.7458	50-250
ISO A	40	1150.8	5.4239	3.6650	50-250
ISO A	50	1025.7	5.9125	4.8809	50-250
ISO A	75	841.91	6.0452	5.2999	50-250
ISO B	25	1159.0	5.7012	3.7913	50-300
ISO B	50	999.62	5.7040	4.0434	50-300
ISO B	75	828.81	5.7649	4.2964	50-300
SE Retail	25	1201.6	5.8616	4.6422	50-300
SE Retail	50	1025.2	5.7367	4.1518	50-300
SE Retail	75	835.49	5.8706	4.6075	50-300
Kansas	25	1229.1	5.8202	4.1156	50-300
Kansas	50	997.35	6.1588	4.9513	50-300
Kansas	75	818.19	6.2556	5.2272	50-300

6.2.2 – Comparison of Calculated and Measured Density

Densities predicted from the corresponding states solution scheme with limited measurement were generally in close agreement with the measured density data. Measurements of density at 50^0C and 0.1 and 30MPa pressure were used in conjunction with the specific gravity at 60^0F as input parameters to the corresponding states method. It has previously been mentioned that the boiling point used for the correlation of these measurements and consequent prediction of density at other conditions, is applied here as a mathematical variable with no physical relevance. To test the validity of the solution method, the initial guessed boiling point is altered. If the method of solution is valid then large changes in the guessed boiling point should have a minimal effect upon the predicted density. Using the stated measurements as inputs, guessed boiling point was varied between 900 and 1300^0R for all the fuels measured. Variation of guessed boiling point led to only a small variation in predicted density for all fuels with the exception of Fuel A, Fuel B and the Kansas fuel which were sensitive to the value of guessed boiling point. Using measurements of density at 25^0C and 0.1 and 30MPa gave more accurate predictions of density for these fuels.

Average absolute percentage deviations for the predictions compared to the measurements are given in Table 6.3. The predictions were made from the limited measurements as described in the preceding paragraph. Measured values were calculated using the atmospheric density data of Table 6.1 and the bulk modulus coefficients of Table 6.2. Comparisons were made in 10MPa increments from atmospheric pressure to the maximum pressure quoted in Table 6.2. Pseudo critical

parameters used in the predictions are given in Table 6.4. The explanation of the meaning and usage of the parameters presented in Table 6.4 is given in section 4.3.3.

Table 6.3 Average absolute percentage deviation of predicted density compared to measured density

Fuel A	Fuel B	Fuel C	Fuel W	Fuel X	Fuel Y
0.151	0.143	0.108	0.151	0.240	0.188
Fuel Z	ISO A	ISO B	SE Retail	Kansas	
0.284	0.093	0.162	0.206	0.180	

Table 6.4 Pseudo critical parameters from iterative corresponding states scheme with critical correlations of Kesler and Lee

Fluid	$T_{c,atm}$ (K)	$P_{c,atm}$ (MPa)	ω_{atm}	$T_{c,P}$ (K)	$P_{c,P}$ (MPa)	ω_P
Fuel A	772.05	1.2721	0.8678	687.44	2.2111	0.5421
Fuel B	773.43	1.2664	0.8716	709.54	1.9381	0.6152
Fuel C	762.81	1.3640	0.8247	730.65	1.6931	0.6932
Fuel W	771.23	1.2778	0.8647	718.56	1.8201	0.6501
Fuel X	771.23	1.2778	0.8647	687.43	2.2090	0.5425
Fuel Y	773.28	1.2594	0.8739	710.11	1.9205	0.6195
Fuel Z	771.87	1.2915	0.8608	688.15	2.2256	0.5401
ISO A	752.52	1.4209	0.7939	733.36	1.6174	0.7155
ISO B	756.34	1.3379	0.8248	707.38	1.8594	0.6298
SE Retail	759.73	1.3543	0.8239	710.77	1.8767	0.6296
Kansas	798.60	1.1865	0.9350	715.02	2.0501	0.5967

Additional insight into the predictions compared to the measured density can be obtained from graphical representation of error with respect to pressure. Figure 6.3 shows an amount of regularity in the graphs of error with respect to pressure and temperature for the three fuels considered. As all three show similar behaviour at the same temperatures and pressures, there may be a combined temperature and pressure effect which causes this difference. Although the differences are small, there are definite trends. It may therefore be worth some further study into whether this regularity is due to a temperature effect with the Micro-PVT or is caused by the prediction method used.

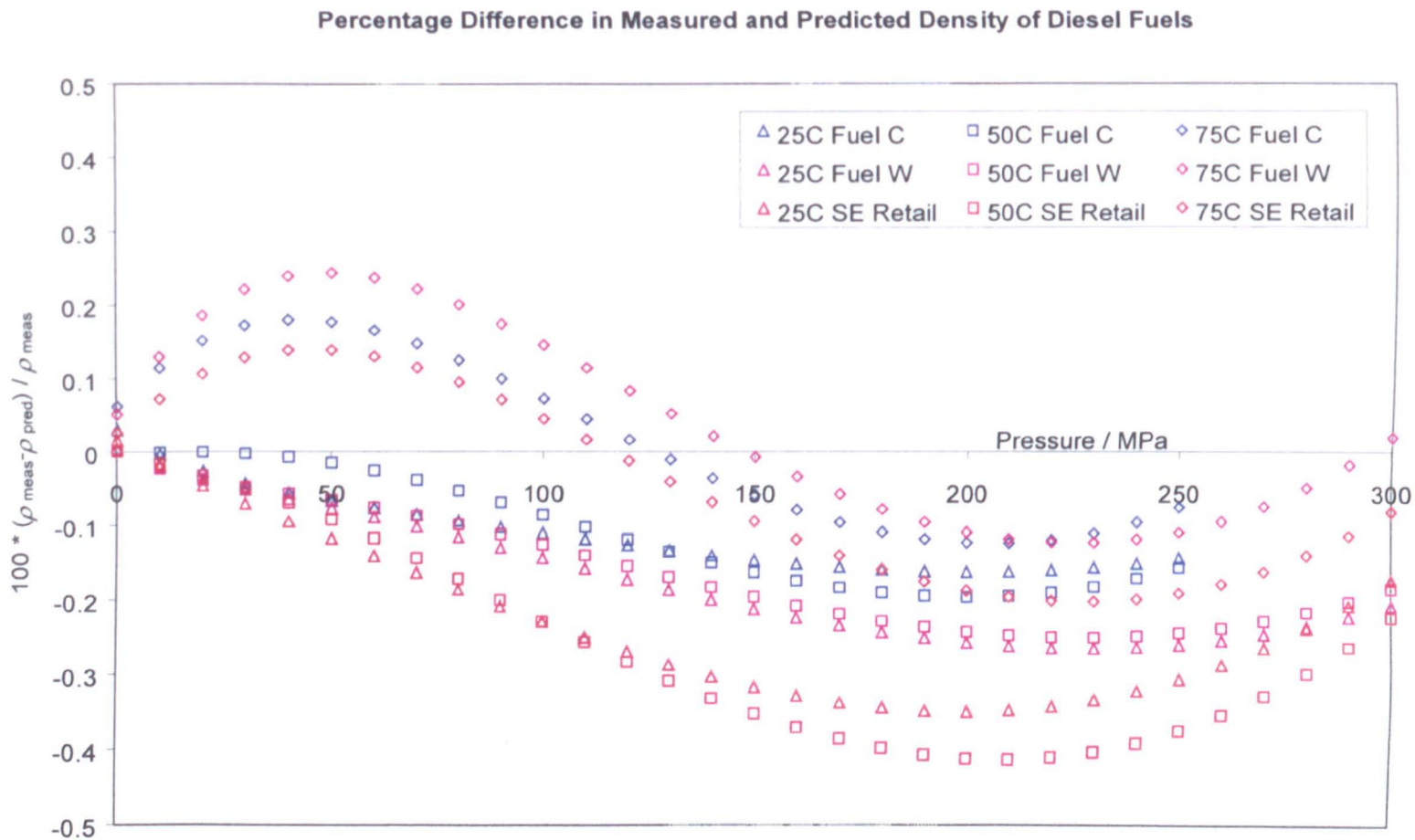

Figure 6.3 Typical difference in prediction and measurement for three fuel samples

6.2.3 – Reasons for Instability of Solution Method

One possible explanation for the inaccuracy could be that the measured densities at 50^0C were inaccurate, perhaps due to a poor fit of the bulk modulus in the low pressure region. This does not give an adequate explanation of the instability of the predicted densities with respect to guessed boiling point which is more likely due to a weakness in the solution method used. The method of false position is used as the iteration method. Boiling point is varied in this scheme until the difference between the measured and calculated ratios of equation (4.5) is approximately zero. The value of boiling point required to do this is bracketed between two guess values of boiling point; one which gives a positive difference between calculated and measured parameters, the other giving a negative difference. This 'correct' boiling point is then found by iteration using the equation;

$$T_{b_2} = \frac{T_{b_0} diff(T_{b_1}) - T_{b_1} diff(T_{b_0})}{diff(T_{b_1}) - diff(T_{b_0})} \tag{6.3}$$

The function *diff* is the difference between the measured density and the calculated quantity of equation (4.5) evaluated at the given boiling point. In the first instance T_{b0} is a guessed value for boiling point and T_{b1} is the initial guess plus an increment of temperature. Visual Basic program code used to implement this method is given in Appendix B. This program was written to decrease and increase the value of boiling point, that is to say the bracket which the solution is contained in is expanded in both directions until the product $diff(T_{b1})*diff(T_{b2})$ is negative. In the program the temperature increment was 50R. Anomalous behaviour of the method was noted throughout. An example of this was when a guess boiling point of 900R was used for a particular fuel. The bracket was extended until T_{b0} was 800R and T_{b1} was

1050R. From (6.3), T_{b2} was found to be 917.5R. Altering the boiling point in increments of 50R it follows that T_{b2} should have either been between 1000 and 1050R or the product $diff(T_{b1})*diff(T_{b2})$ should have been negative from the initial guess values of 900 and 950R. Failure to satisfy either condition is possibly due to the complex nature of the calculation procedure which may give an irregular trend if *diff* was plotted as a function of T_b. Other solution methods involving differentiation of *diff* with respect to T_b, such as Newton's method cannot be easily applied here due to the complex function involved.

With this possibility of failure having been established and no alternative numerical technique available to efficiently overcome the problem, a check on consistency of results is advisable. From the comparisons of prediction with measurements of the diesel fuels conducted, it appears that if the solution is stable with respect to changes in guessed boiling point, the predicted values are close to the measured. However, if predicted density shows a large variation when the guessed boiling point is altered, then without further measurement one cannot tell which prediction is close to the actual liquid density. In this case it is suggested that a further measurement be taken at an alternative temperature. Whether this problem would arise at all using measurements from a vibrating tube densimeter has not been tested. If the instability of the method presented is a function of the accuracy of the measurement, then vibrating tube measurements should be better than measurements from the Micro-PVT. The latter device gives better measurements at the high end of the pressure range than at lower pressures due to mechanical considerations such as seal slippage at the start of a trial.

Although not identified as a problem in this work, should it be found that the method gives poor prediction of density with respect to temperature but not pressure, a good estimate of density over a range of temperatures from a single measurement of density at 15^{0}C may be made using Petroleum Measurement Table 53B according to ASTM Standard D1250-80[93.]. Density at 25, 40, 50, 75, 100 and 125^{0}C were predicted by ITS Testing Services using this method. Comparison of predictions with measurements at 25, 40, 50 and 75^{0}C gave an average absolute percentage deviation of 0.025% for measurements of the eleven fuel samples.

6.3 Viscosity

6.3.1 – Viscosity Measurements

Fall time measurements were made in the falling cylinder viscometer over a range of pressure for Fuel A, Fuel C, Fuel Y, Fuel Z and the Kansas Fuel. Viscosity found from these measurements and density values at the conditions of measurement are presented in Tables 6.5 to 6.9.

6.3.2 – Density Data for Buoyancy Correction

From the force balance presented in Appendix A relating viscosity to measured fall time, it was found that it was necessary to know the density of the fluid at the conditions of measurement to provide a correction for buoyancy force acting on the sinker. Measurements from the Micro-PVT provide this density data when made at the same conditions. For viscosity measurements made at pressures higher than those at which equivalent density measurements are available, a form of extrapolation must be used. Considering the case of Fuel A at 75^{0}C, viscosity

Table 6.5 Viscosity measurements of Fuel A

Temperature / °C	Pressure / MPa	Density / kgm^{-3}	Viscosity / mPa.s
25.00	0.1013	825.9	3.029
25.02	24.84	842.0	4.313
25.02	49.59	855.4	5.939
25.05	75.68	867.4	8.262
25.02	99.00	876.9	10.91
25.04	149.11	894.5	19.65
25.04	196.61	908.9	34.27
25.04	223.73	916.6	46.45
50.04	0.1013	808.5	1.786
50.04	25.50	827.6	2.471
50.04	50.57	842.6	3.276
49.98	100.18	865.7	5.499
50.01	166.59	889.4	10.51
50.02	228.32	908.2	18.73
50.03	256.10	916.2	24.09
50.02	303.71	930.0	36.47
50.00	399.88	948.8	81.84
75.02	0.1013	790.7	1.209
75.05	25.25	810.6	1.661
75.04	50.13	826.5	2.165
75.03	100.29	852.1	3.491
75.02	150.27	872.4	5.369
75.03	190.57	886.2	7.407
75.03	255.22	905.4	12.39
75.03	327.48	923.6	21.04
75.03	405.07	940.4	36.39
75.04	457.24	950.6	52.09
100.03	0.1013	772.5	0.8745
100.06	28.04	796.8	1.204
99.99	51.83	813.2	1.526
99.95	169.69	868.1	4.083
100.02	304.00	908.3	10.10
100.02	356.71	920.9	14.17

Table 6.6 Viscosity measurements of Fuel C

Temperature / °C	Pressure / MPa	Density / kgm^{-3}	Viscosity / mPa.s
25.01	0.1013	826.8	3.149
25.01	23.91	841.3	4.444
25.03	54.79	857.2	6.336
25.04	75.24	866.4	8.044
25.02	101.35	877.0	11.05
25.05	137.70	890.0	16.74
25.01	165.84	899.1	22.96
25.06	212.47	912.8	39.07
25.04	246.32	921.9	65.44
25.05	298.10	935.7	139.6
24.98	341.28	945.3	245.0
50.02	0.1013	809.3	1.835
50.06	22.89	825.2	2.457
49.99	48.94	840.2	3.349
50.01	75.17	853.0	4.496
50.02	100.37	863.7	5.871
50.00	149.77	881.7	9.586
50.00	199.26	897.2	15.47
50.00	251.81	912.3	25.41
49.99	301.62	926.0	40.10
49.98	361.88	939.3	67.70
50.00	439.30	954.6	129.4
75.00	0.1013	792.0	1.228
74.97	49.56	827.4	2.067
74.98	76.47	841.3	2.692
75.03	102.18	852.7	3.624
74.97	134.20	865.0	4.812
75.00	187.25	882.8	7.487
75.02	254.02	902.8	12.28
75.00	307.82	916.9	18.45
74.98	361.70	929.2	27.54
75.00	439.36	944.9	48.53
100.00	0.1013	773.3	0.8804
99.98	37.54	803.4	1.310
99.93	67.85	821.9	1.786
99.87	99.45	837.9	2.361
99.89	140.80	855.6	3.299
99.89	179.77	869.9	4.434
99.91	222.35	883.6	6.003
99.93	253.85	892.7	7.537
99.94	293.70	903.3	9.761

Table 6.7 Viscosity measurements of Kansas fuel

Temperature / °C	Pressure / MPa	Density / kgm^{-3}	Viscosity / mPa.s
25.02	0.1013	843.1	2.802
25.05	26.48	859.5	3.851
25.01	51.20	872.5	5.237
25.03	77.74	884.6	7.272
25.02	103.56	894.9	10.05
25.03	137.74	907.0	15.02
25.02	158.76	913.8	19.62
25.00	195.61	924.9	30.36
24.95	241.85	937.7	53.91
49.99	0.1013	825.8	1.703
50.00	22.65	842.6	2.262
49.99	50.99	859.5	3.146
49.98	74.55	871.2	4.076
50.04	100.75	882.5	5.301
50.02	128.18	892.9	6.909
50.03	191.18	913.3	13.00
50.06	231.84	925.1	19.32
50.00	262.37	933.5	25.98
49.99	301.82	944.3	38.11
75.06	0.1013	808.0	1.139
75.05	26.80	830.6	1.569
75.06	52.28	847.1	2.059
75.05	98.15	869.7	3.173
75.04	127.83	881.5	4.130
75.03	157.47	891.9	5.327
75.03	196.23	904.1	7.305
75.06	245.07	918.4	10.66
75.05	311.46	937.1	18.46

Table 6.8 Viscosity measurements of Fuel Y

Temperature / °C	Pressure / MPa	Density / kgm^{-3}	Viscosity / mPa.s
24.96	0.1013	825.7	2.652
24.94	51.79	854.7	5.493
24.93	81.94	868.3	8.043
24.96	104.16	877.1	10.51
24.97	133.73	887.8	14.70
24.92	169.77	899.5	22.49
24.95	199.17	908.2	31.70
50.03	0.1013	808.1	1.670
50.04	51.22	841.0	2.963
50.04	74.94	852.7	3.798
50.04	98.92	863.1	4.897
50.02	105.49	865.8	5.145
50.04	131.01	875.4	6.640
50.06	157.93	884.6	8.610
50.02	185.86	893.4	11.25
50.03	225.69	905.0	16.47
75.04	0.1013	790.5	1.119
74.99	50.66	826.9	1.911
75.00	74.24	839.5	2.412
75.06	77.12	840.9	2.450
74.99	94.33	848.9	2.905
75.04	104.43	853.2	3.182
75.00	133.24	864.6	4.078
74.99	160.26	874.1	5.129
75.01	190.77	883.9	6.601
75.01	218.98	892.5	8.245

Table 6.9 Viscosity measurements of Fuel Z

Temperature / °C	Pressure / MPa	Density / kgm^{-3}	Viscosity / mPa.s
24.94	0.1013	828.0	2.795
24.93	50.73	856.4	5.379
24.94	74.08	867.0	7.159
24.92	102.23	878.4	10.02
24.94	130.43	888.7	13.93
24.96	151.21	895.6	17.74
24.94	180.90	904.8	24.82
24.97	219.75	915.9	38.36
50.00	0.1013	810.5	1.704
50.01	54.36	845.2	3.239
50.02	77.78	856.6	4.154
50.04	103.76	867.7	5.408
50.02	128.33	877.0	6.846
50.03	156.28	886.6	8.974
50.05	183.93	895.3	11.67
50.07	227.22	908.0	17.49
75.06	0.1013	792.7	1.150
75.03	27.35	815.3	1.632
75.06	77.96	844.8	2.666
75.09	103.77	856.3	3.392
75.05	134.27	868.2	4.397
75.04	165.78	879.0	5.674
75.05	192.20	887.4	7.071
75.05	212.34	893.4	8.290

measurements were made to 457MPa, but volume change was only measured to 250MPa. An estimate of density can be made from the bulk modulus coefficients obtained from the data to 250MPa. These coefficients were used directly to predict higher pressure values. From the curve of volume ratio as a function of pressure, shown in Figure 6.4(a), it would appear that this leads to unusual results beyond the range to which the data were originally fitted. Confirmation of the failure of the direct extrapolation of the bulk modulus coefficients is given by Figure 6.4(b) which shows the compressibility curve obtained by differentiation of volume, expressed in terms of bulk modulus coefficients, with respect to pressure. This figure shows compressibility going through a minimum which is physically unrealistic. Instead, the corresponding states method should be used to predict data outside the range of measurement. Although not validated for diesel fuels at the highest pressures, extrapolation by this means is smooth and compressibility estimated from finite differences shows no obvious anomalous behaviour as shown in Figures 6.5(a) and 6.5(b) respectively. Similarly, as no reliable fit can be made for the bulk modulus coefficients with respect to temperature, density data at 100^0C are also estimated from the corresponding states method.

6.3.3 – Comparison of Predicted and Measured Viscosity

Of the methods of prediction of viscosity of complex mixtures discussed in Chapter 5, the most feasible method likely to obtain a reasonable estimate of diesel viscosity was the numerical solution of the hard sphere theory with an empirical correction derived from other diesels. Hard sphere viscosity with the pressure dependent correction factors found from analysis of previous diesel measurements[59.]

Extrapolation of 25^{0}C Fuel A Bulk Modulus Data

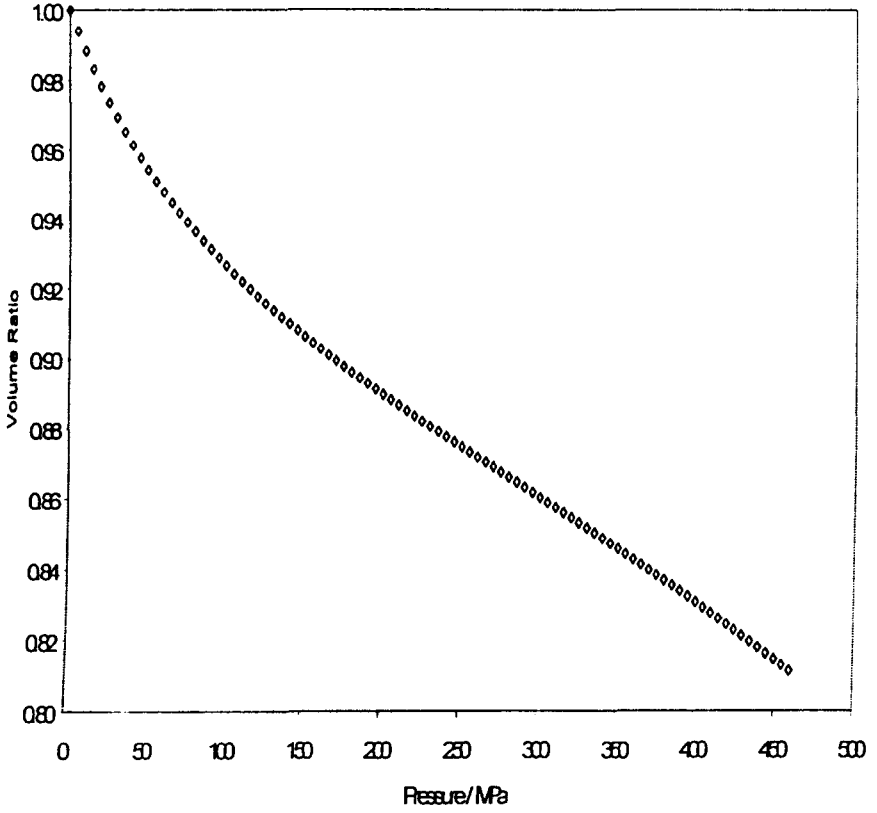

Figure 6.4(a). Extrapolated volume ratio

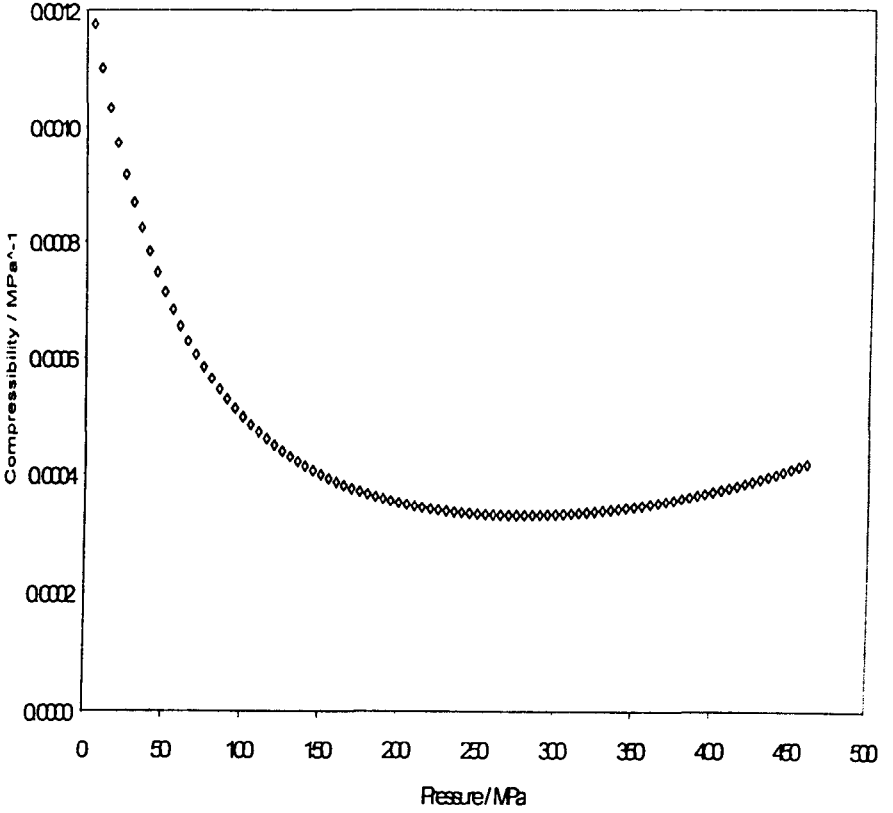

Figure 6.4(b). Extrapolated compressibility

Prediction of 25^{0}C Fuel A High Pressure Data by Corresponding States Method

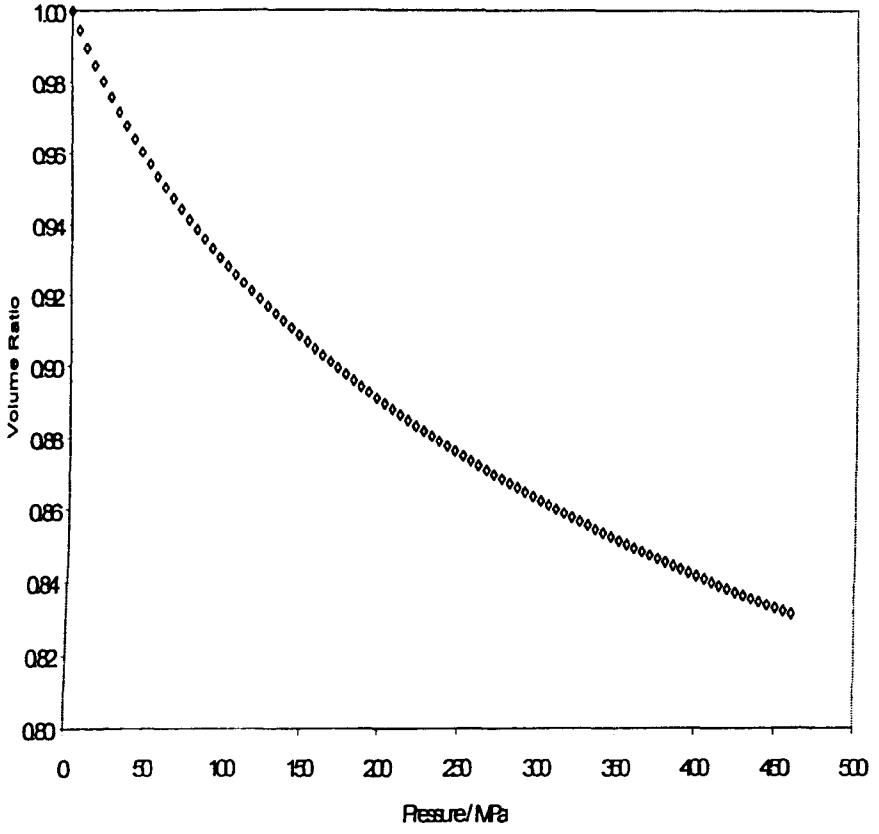

Figure 6.5(a). Predicted volume ratio

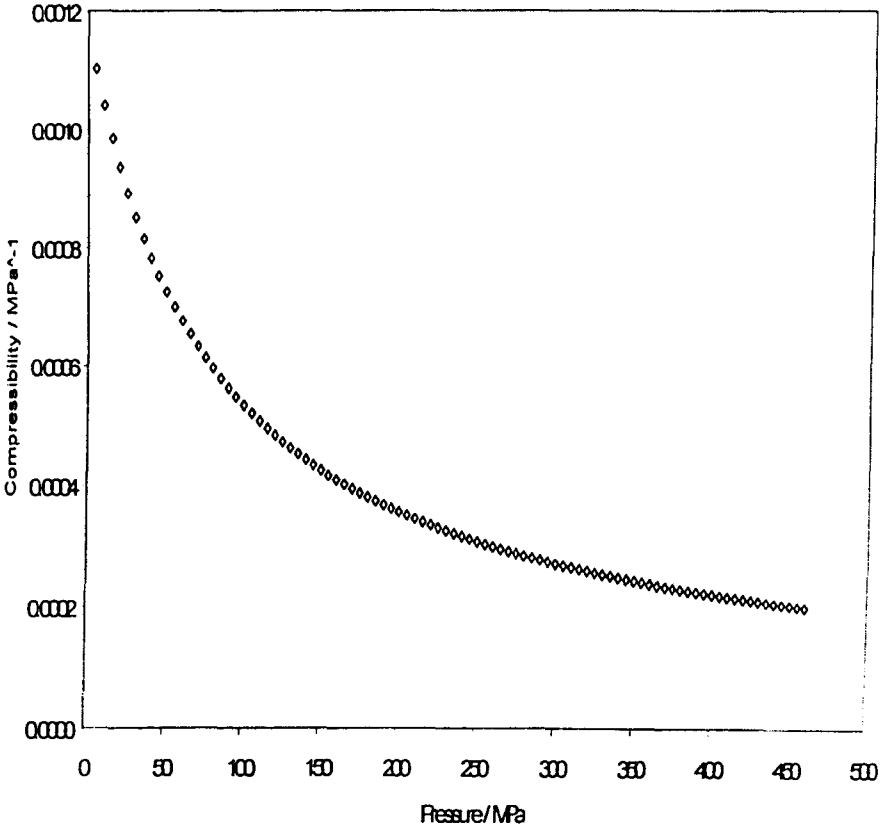

Figure 6.5(b). Predicted compressibility

given by equations (5.20) and (5.21) can now be used for comparison with the current diesel viscosity measurements. Average absolute percentage deviations between the measured and predicted values are given in Table 6.10. Graphs of the differences with respect to pressure are given in Figures 6.6 to 6.10. Values of V_0 and R_η used to predict viscosity are given in Table 6.11. Details of how these pseudo parameters were obtained are given in sections 5.3.3 and 5.3.4.

Table 6.10 AA%D between measured and predicted viscosities of diesel fuels

Temperature (°C)	Fuel A	Fuel C	Fuel Y	Fuel Z	Kansas
25	2.32	10.7	8.39	1.68	5.25
50	2.69	3.82	3.57	2.88	4.52
75	6.74	6.74	3.79	2.85	5.17
100	2.77	10.9	N/A	N/A	N/A

Table 6.11 Pseudo V_0 and R_η values from numerical hard sphere scheme

Fluid	T (K)	V_0 (m^3mol^{-1})	R_η
Fuel A	298.15	1.8382×10^{-4}	1.3995
	323.19	1.8085×10^{-4}	
	348.17	1.7882×10^{-4}	
	373.18	1.7705×10^{-4}	
Fuel C	298.16	1.8585×10^{-4}	1.1876
	323.17	1.8317×10^{-4}	
	348.15	1.8128×10^{-4}	
	373.15	1.7994×10^{-4}	
Fuel Y	298.11	1.8203×10^{-4}	1.4361
	323.18	1.7968×10^{-4}	
	348.19	1.7720×10^{-4}	
Fuel Z	298.09	1.8303×10^{-4}	1.3257
	323.15	1.8048×10^{-4}	
	348.21	1.7841×10^{-4}	
Kansas	298.17	1.8113×10^{-4}	1.1592
	323.14	1.7871×10^{-4}	
	348.21	1.7673×10^{-4}	

Figure 6.6 shows good agreement between the measured and predicted viscosities of the base refinery fuel with no additives to 300MPa at all temperatures.

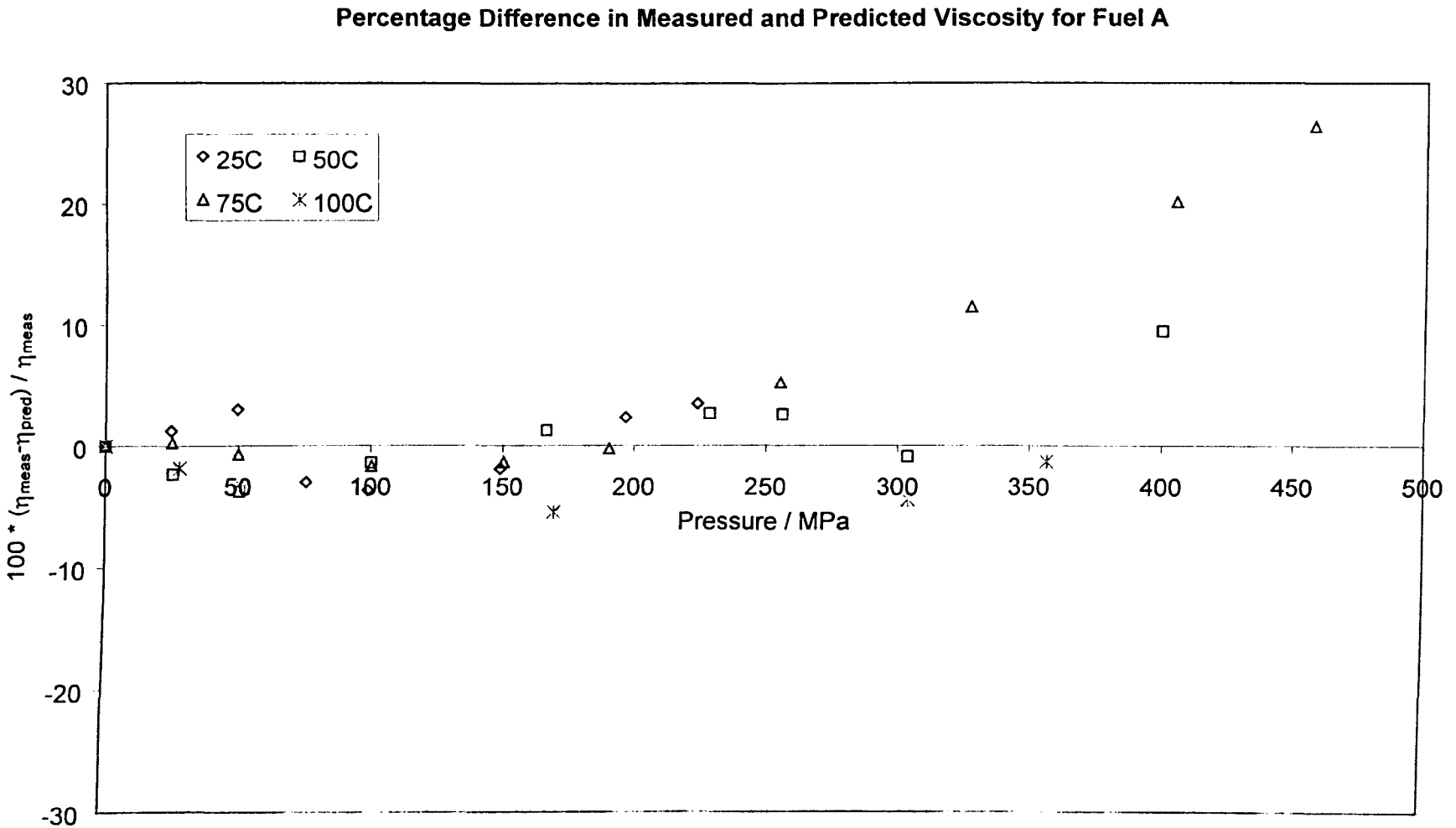

Figure 6.6 Fuel A viscosity comparison

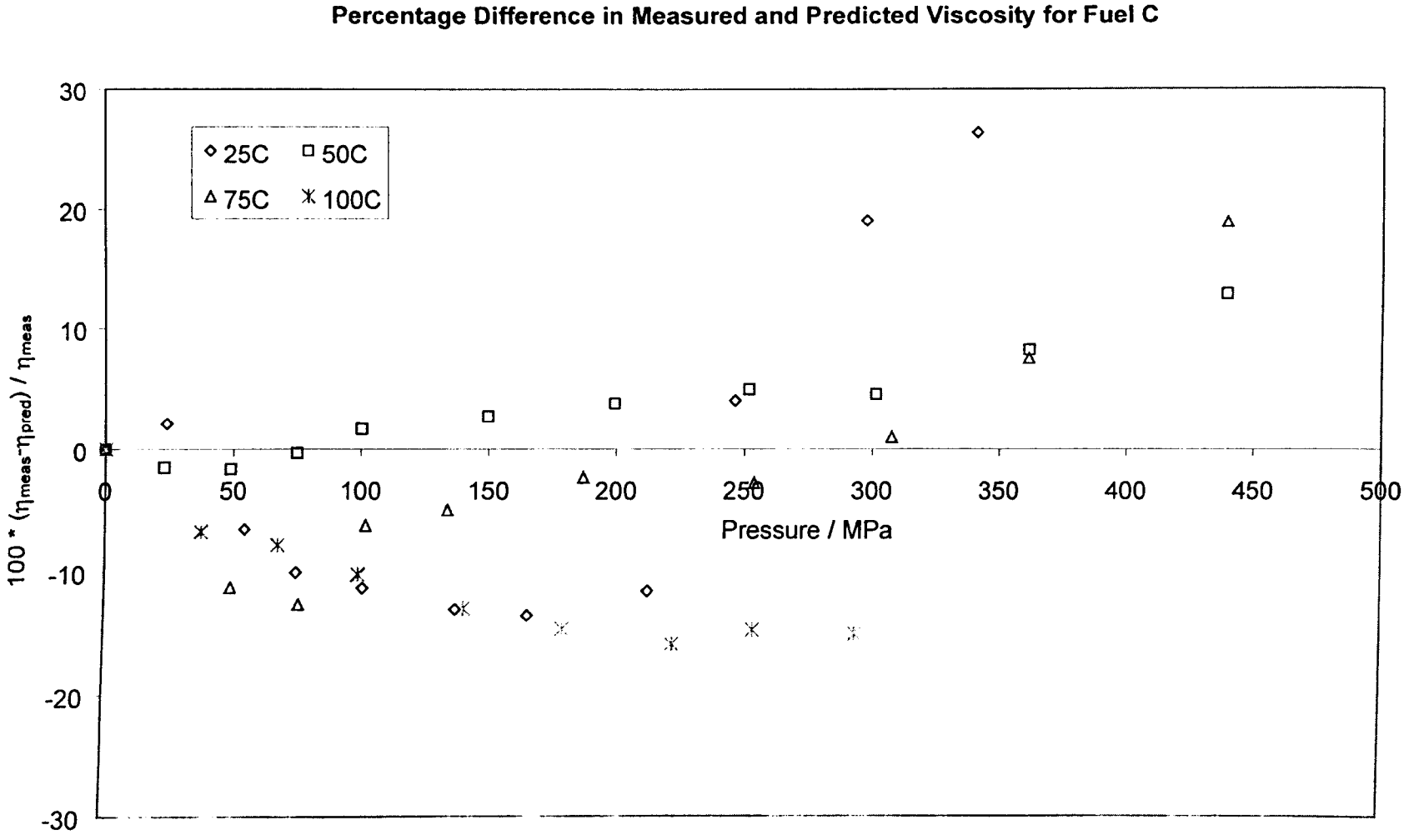

Figure 6.7 Fuel C viscosity comparison

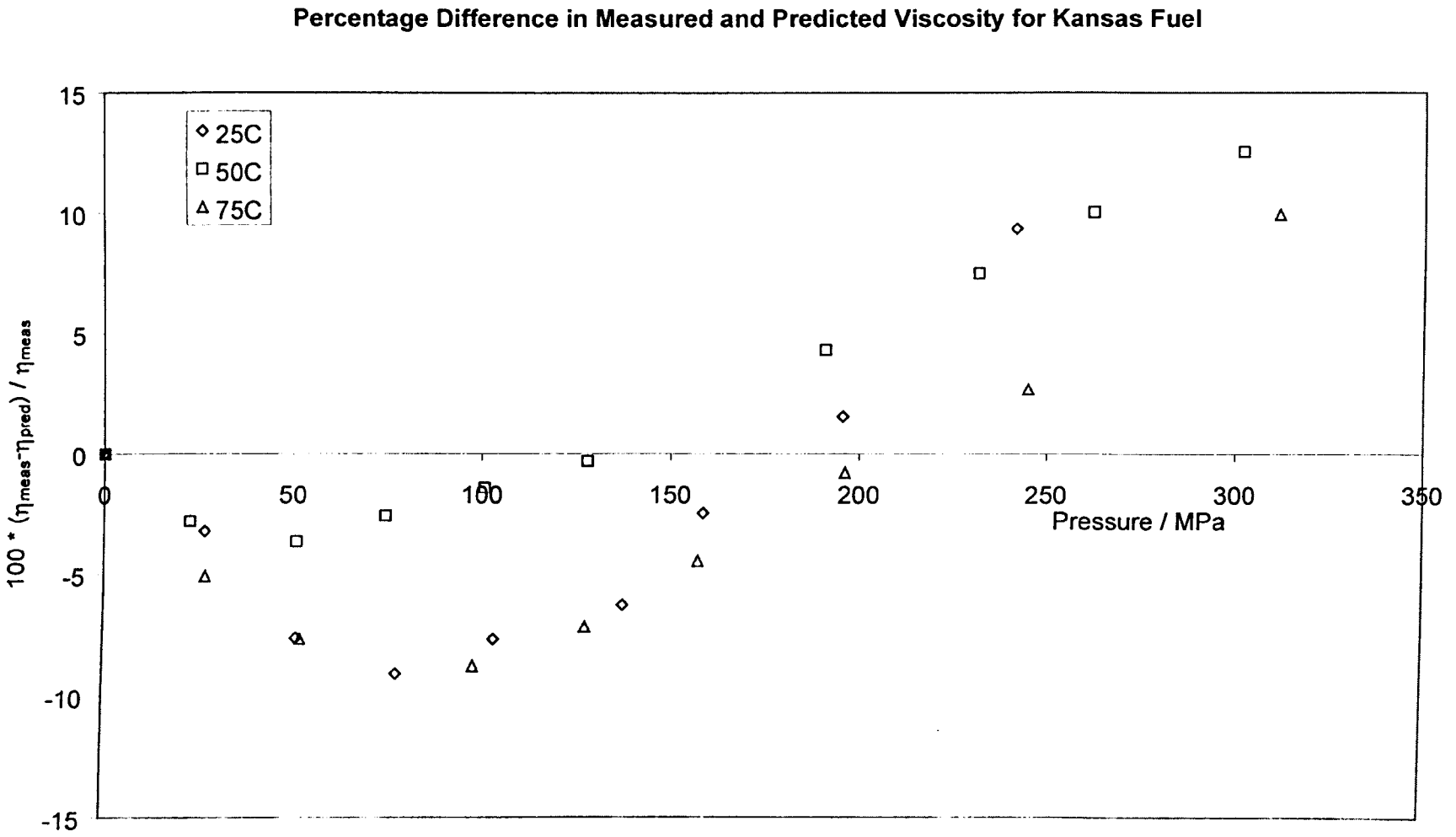

Figure 6.8 Kansas fuel viscosity comparison

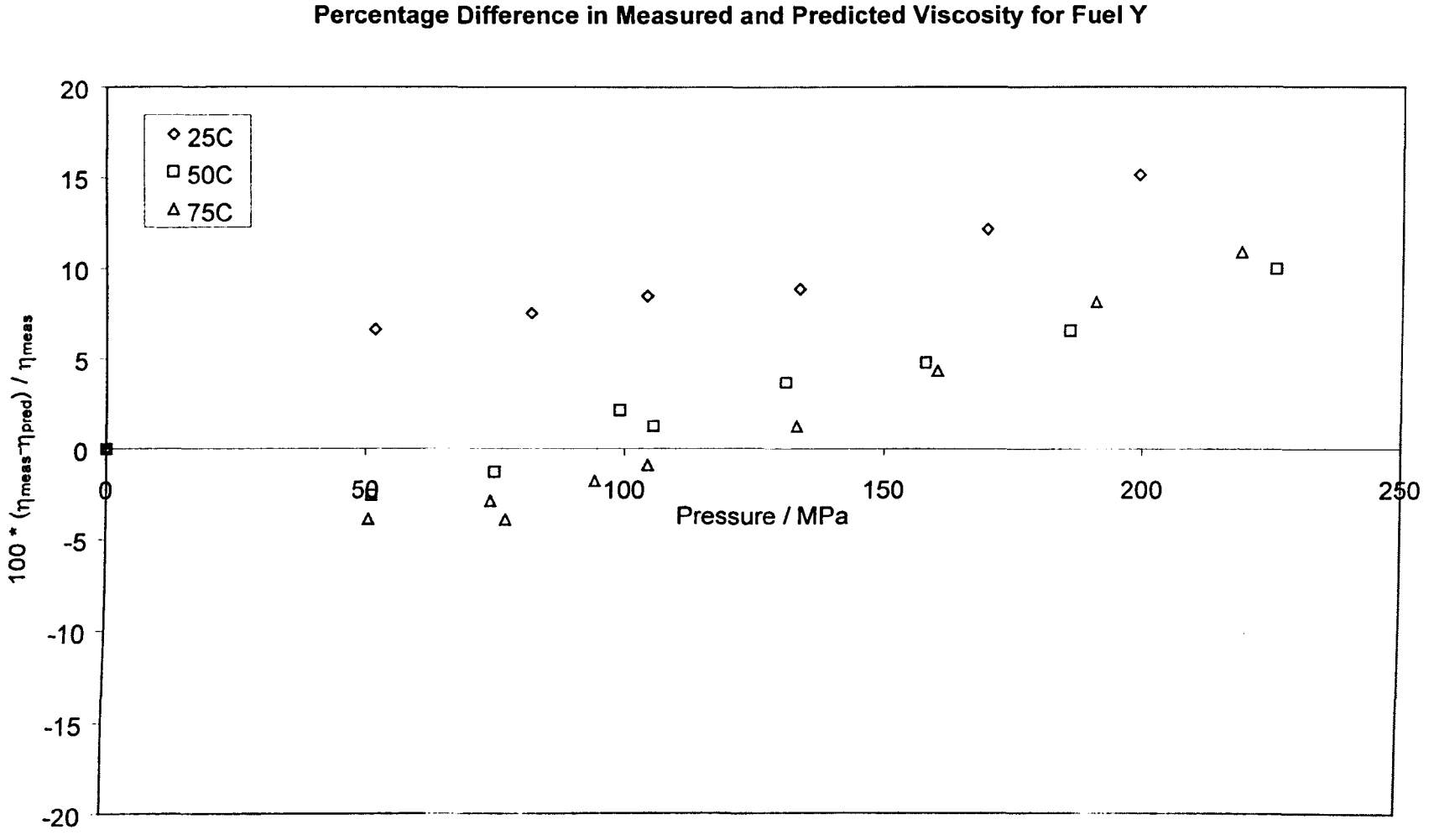

Figure 6.9 Fuel Y viscosity comparison

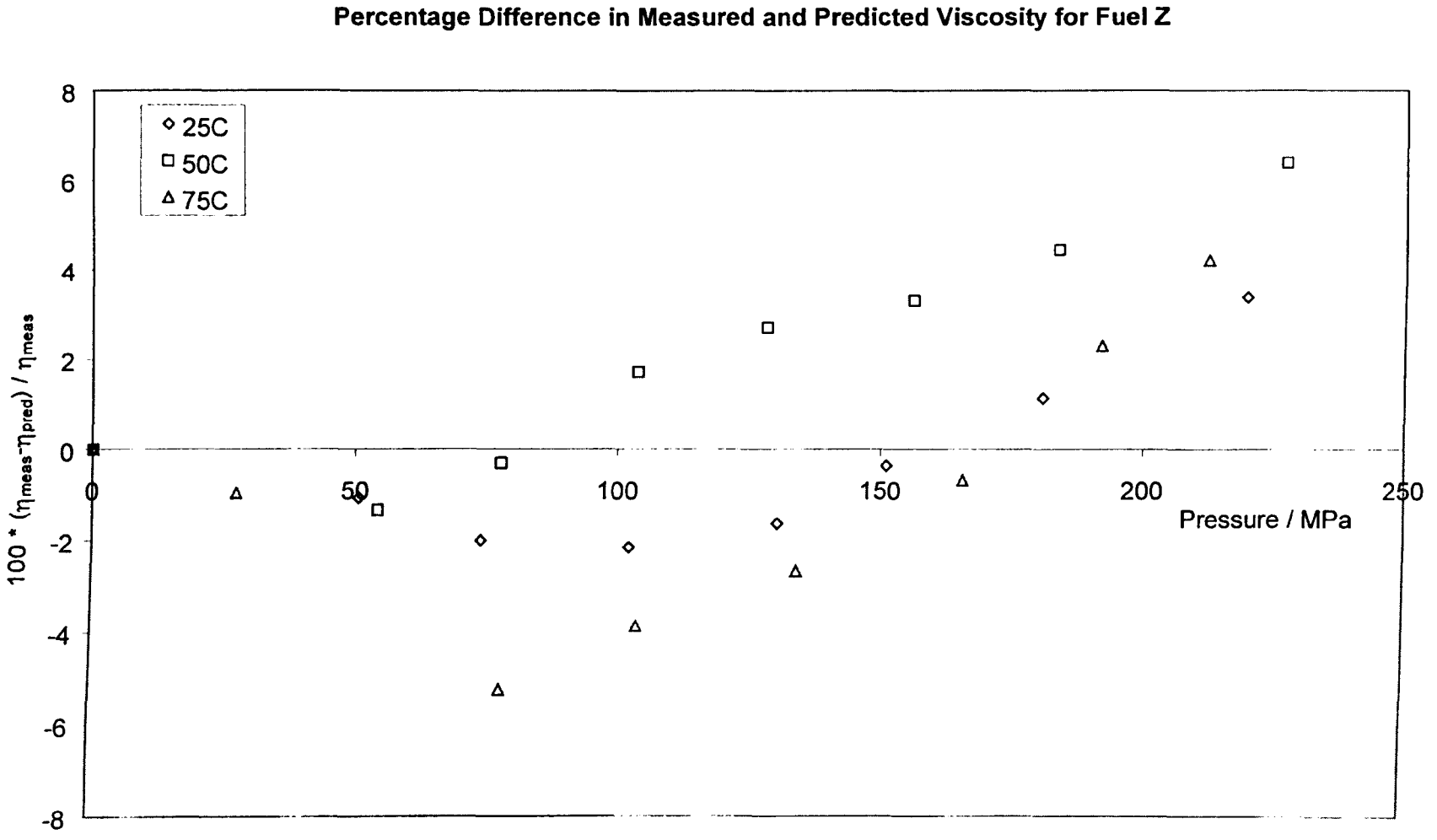

Figure 6.10 Fuel Z viscosity comparison

Prediction is similarly good for the same fuel with handling and performance additives over the same pressure region, but only at 50^0C. At all other temperatures the differences are significantly larger. These large differences between the same prediction method applied to Fuel A and Fuel C highlight the effect that fuel additives have upon not only the viscosity as measured, but also semi-theoretical viscosity predictive methods such as that applied here. This is particularly apparent in Figure 6.11 which shows the difference between measured viscosity and viscosity predicted from the hard sphere method using the program given in Appendix C for all fuels measured here and those measured in a previous study[59].

Another notable feature with the additive containing fuel is the behaviour beyond 200MPa. From 75 to 210MPa percentage difference in measured and predicted viscosity appears to follow a different trend with respect to pressure than the measurements above this pressure. This effect could possibly be due to the additives preventing freezing. It was previously noted that a phase change was detected for Fuel A at approximately 250MPa from fall time measurements in the high pressure viscometer. Fuel C did not show any such behaviour at this pressure. therefore the presence of additives has elevated the freezing pressure of this hydrocarbon mixture. Whether going beyond the freezing pressure of the additive free mixture is the cause of the apparent discrepancy in the trend cannot be established without further work comparing fuels with and without additives to high pressures at low temperature. However, the analogous plot for Fuel C at 50^0C (Figure 6.12) shows a reasonably regular trend across the pressure range; no freezing of Fuel A was discernible from viscosity measurements at this temperature and elevated pressure.

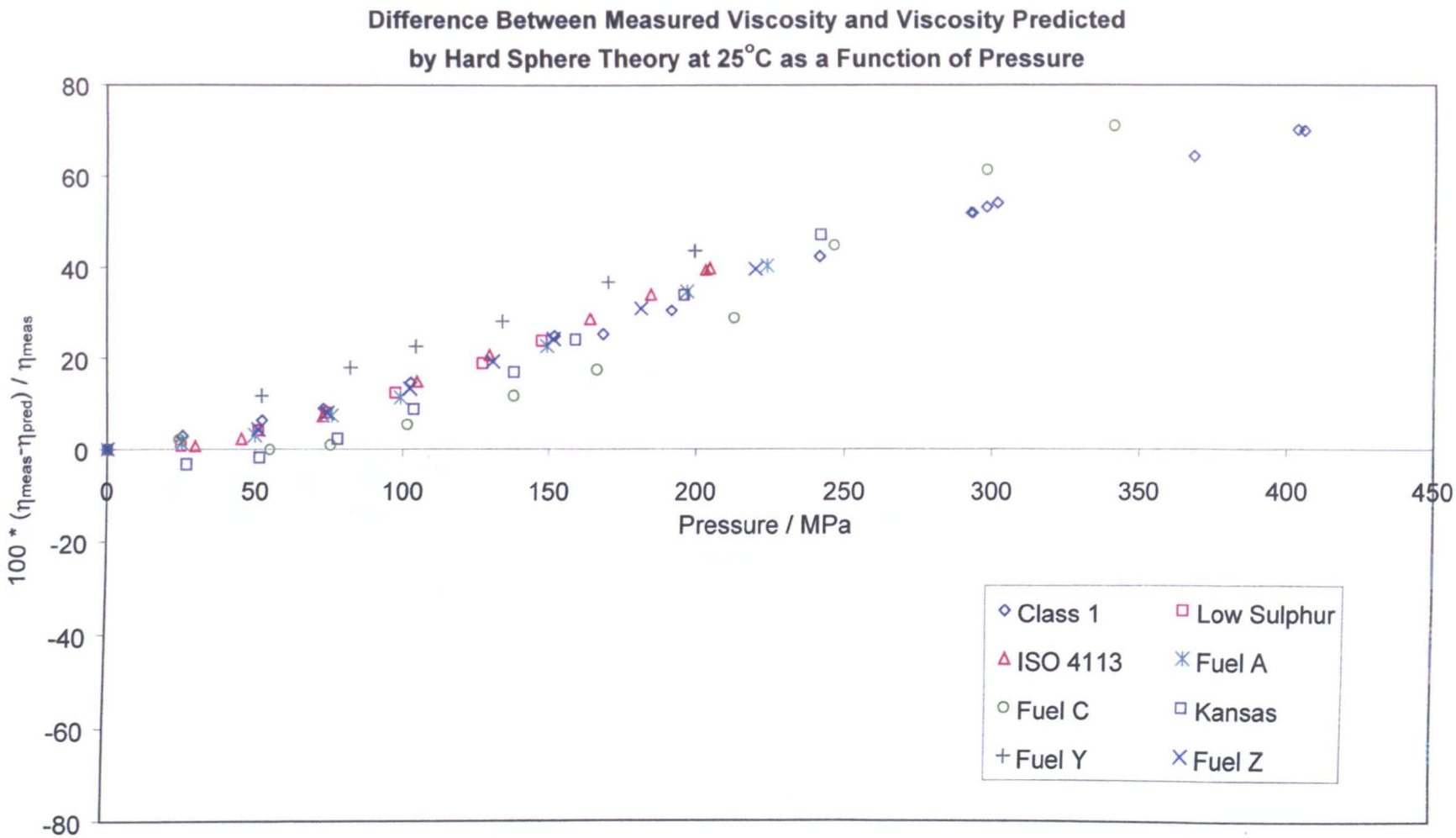

Figure 6.11 Difference in measured viscosity and hard sphere predicted viscosity with respect to pressure for diesel fuels at 25°C

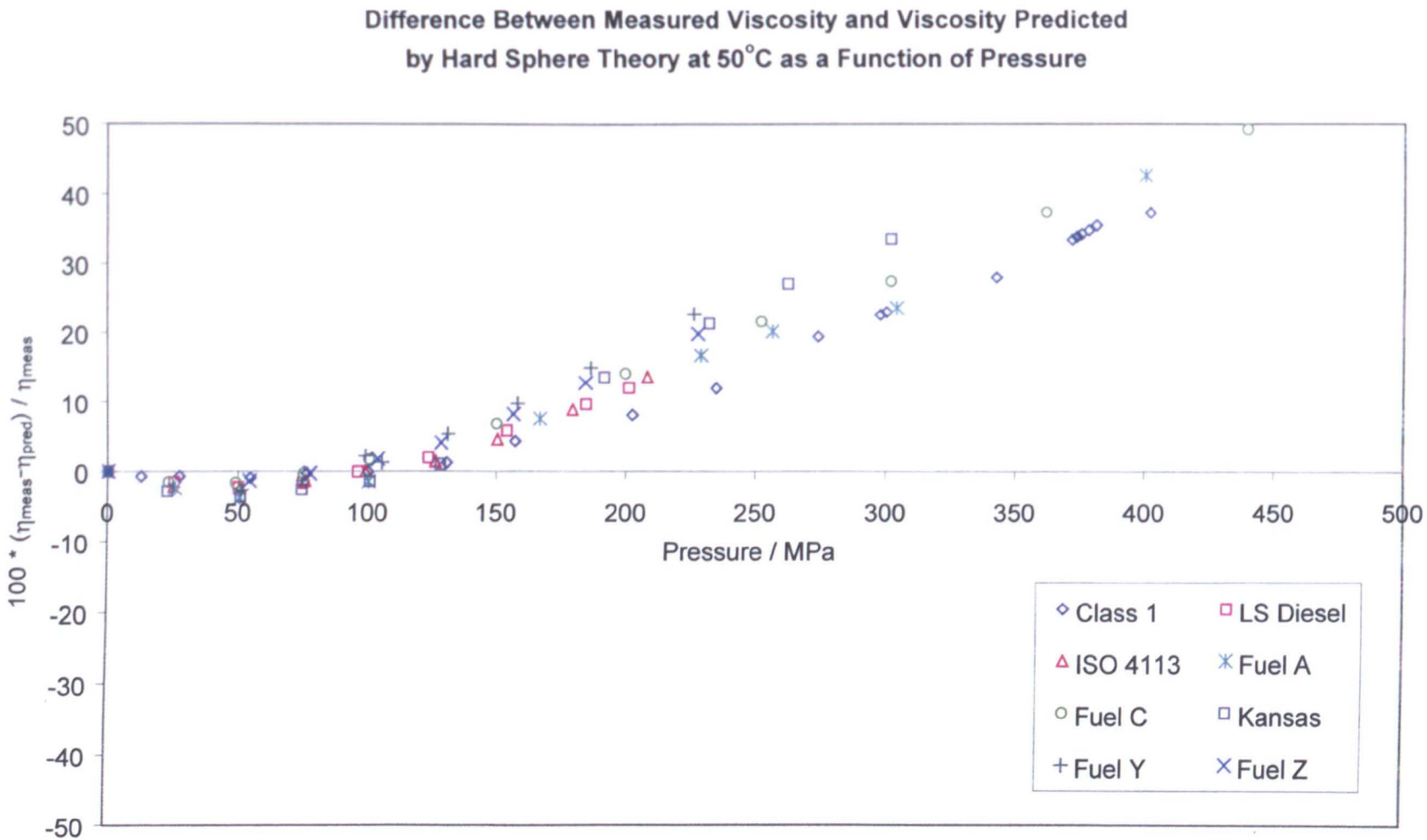

Figure 6.12 Difference in measured viscosity and hard sphere predicted viscosity with respect to pressure for diesel fuels at 50^0C

The effect of this change in behaviour of the difference in measurement compared to the idealised hard sphere prediction can also be implied from comparison with the Class 1 fuel. The Class 1 fuel has a regular slope of difference with respect to pressure at 25^0C as seen from Figure 6.11. When viscosity measurements are compared in Figure 6.13 it is seen that the viscosity of Fuel C increases at a significantly greater rate with respect to pressure at the higher pressures than the Class 1 fuel. No comparable measurements of this Class 1 fuel with no additives are available for comparison with Fuel A. These highest pressures are beyond the range of current practical application for fuel injection equipment, however the results are of some interest for general thermophysical considerations.

At pressures up to 200MPa there is fair agreement between measured viscosity and viscosity predicted from hard sphere theory with the empirical corrections at 25 and 50^0C derived from previous diesel measurements[59]. Errors for Fuel C are significantly larger than those for the other fuels at lower pressures. With this worst case fuel, the predicted viscosity is within about 15% of the measured viscosity across the pressure range to 250MPa. This prediction method therefore gives a reasonable estimate of viscosity at elevated pressure for a number of fuels up to the maximum pressures used in current fuel injection equipment at temperatures up to 100^0C.

These findings indicate that despite the complex nature of diesel fuel mixtures there is potential to use theoretically derived methods such as the hard sphere scheme as a basis for viscosity prediction. This is particularly in evidence for viscosity at 75^0C, in particular below 200MPa, and 100^0C where the method has been applied without any empirical correction factors. This is slightly contradictory to findings

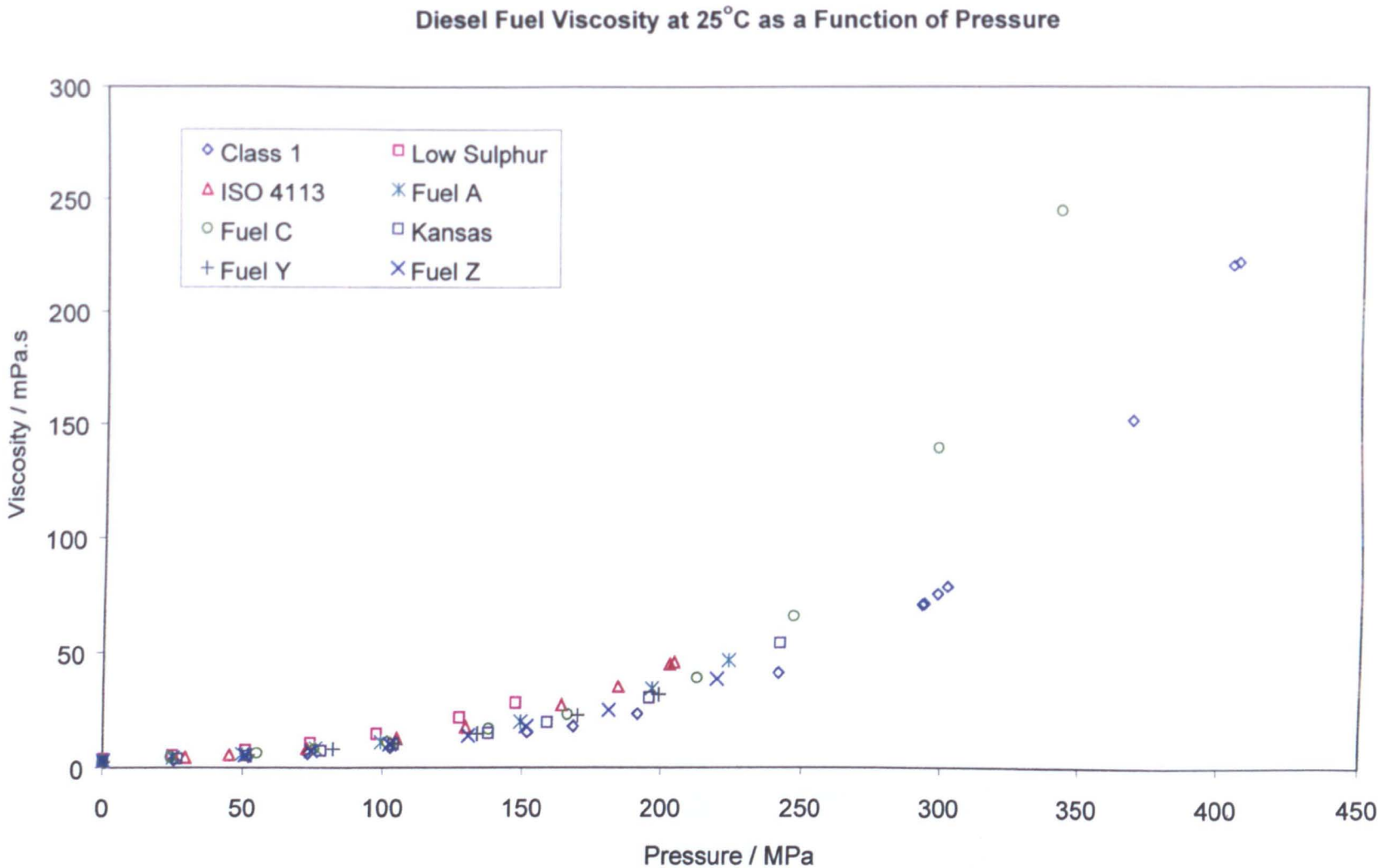

Figure 6.13 Comparison of measured viscosity at 25^{0}C with respect to pressure for diesel fuels

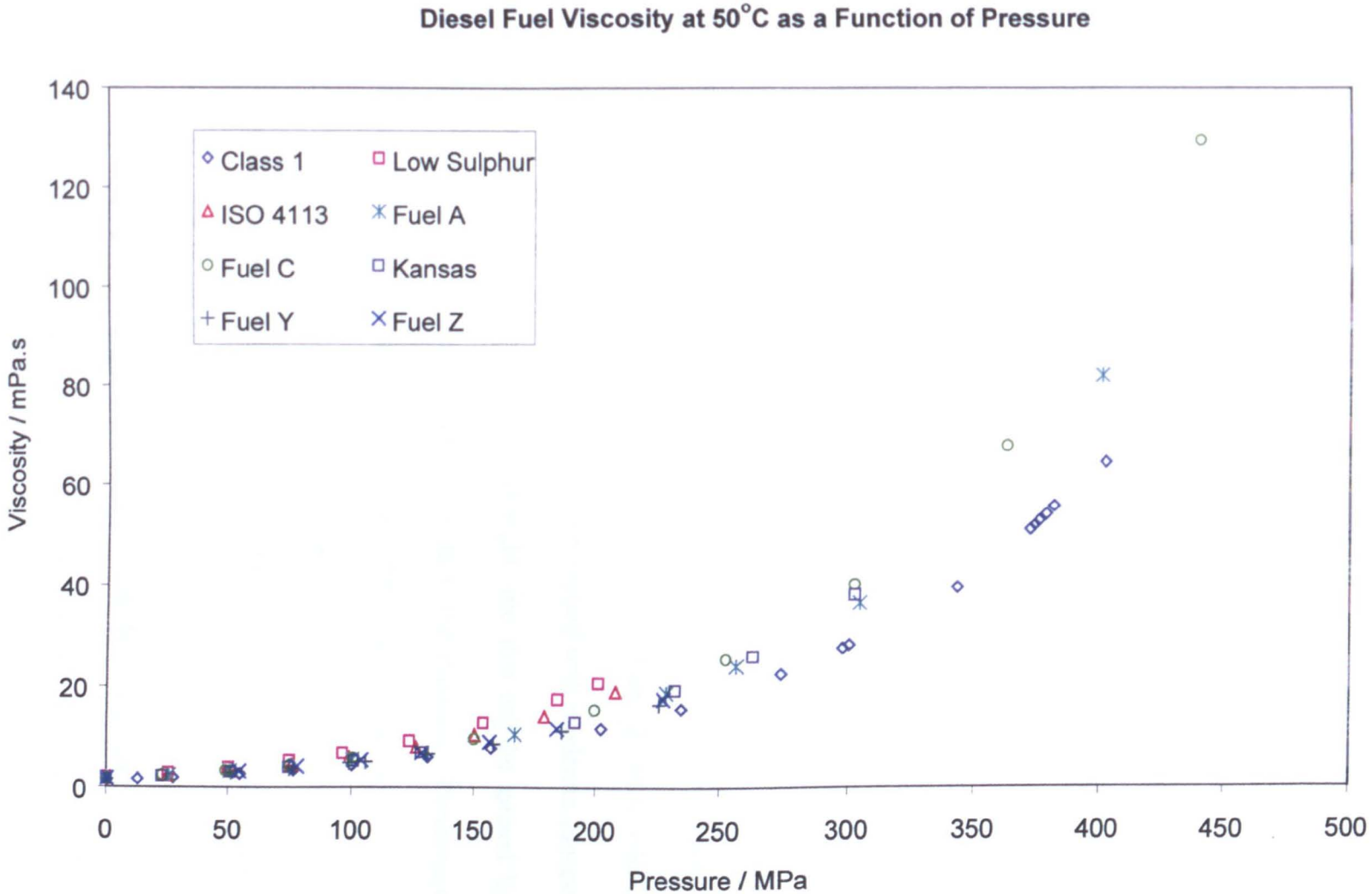

Figure 6.14 Comparison of measured viscosity at 50^0C with respect to pressure for diesel fuels

from previous tests of the numerical solution to the hard sphere method for pure fluids and mixtures of known composition. From these tests it was found that the method was worst at the largest values of free volume. Tests on diesel fuels indicate that prediction is worst at lower temperatures; that is to say at the smallest values of free volume where empirical corrections were necessary. It would be a vast over simplification to imply from this that the numerical solution of the hard sphere theory as proposed has the best predictive ability at intermediate values of free volume. Such a statement would neglect the large differences between predicting viscosity of complex mixtures and the more simple fluids discussed earlier.

6.3.4 – Compositional Effects

Although the hard sphere theory as used here requires corrections at lower temperatures above certain pressures, the ability to fit the error and apply the method to other fuels indicates a degree of validity in this approach. Given the vast number of molecules, all of different size and shape, consideration is here given to why a method derived from consideration of spheres can be applied with moderate success to such an apparently non-uniform mixture. Insight into this can be gained by consideration of analyses of molecules present within the mixture. Percentage abundance of n-alkanes from carbon chain length 9 to 27 present in the mixture was measured by GC-FID (gas chromatography – flame ionisation detector) method on a mass for mass basis. This testing was undertaken by M-Scan Ltd. of Ascot. Results of this analysis are shown in Figure 6.15.

It is seen from Figure 6.15 that the percentage of n-alkanes present in Fuel A follow, very approximately, a bell-shaped distribution with respect to carbon number.

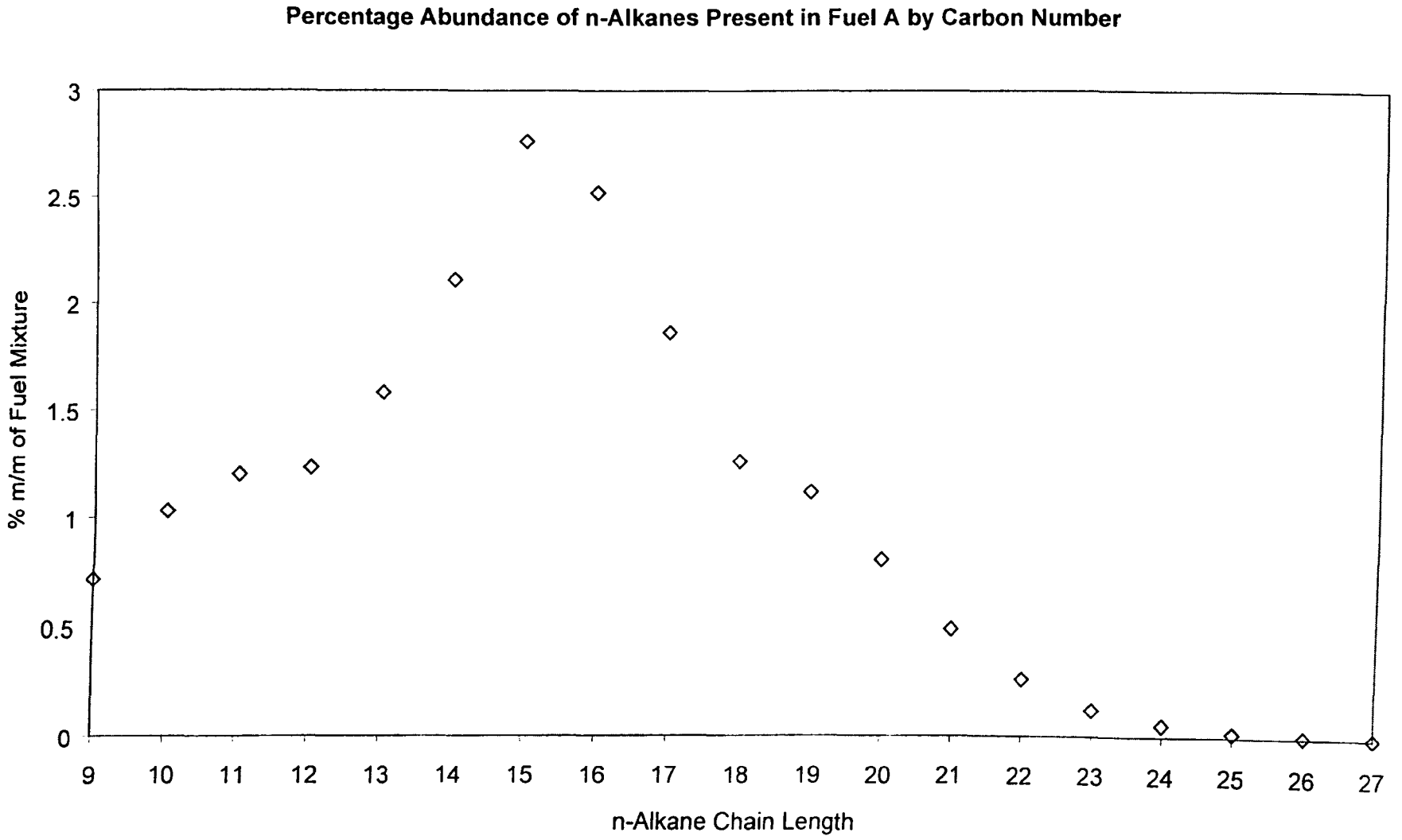

Figure 6.15 GC-FID analysis of n-alkanes present in Fuel A

If this distribution is also followed for the other molecular types present then this could lead to the mixture behaving more like a single molecular type, or at least a mixture of different classes each of which can approximate to a representative average molecule of the different classes. The averaging effect implied from the distribution could possibly explain why the hard sphere theory can be applied to the prediction of diesel fuel viscosity with some success.

6.3.5 – Comparison of Diesel Viscosity with n-Alkane Viscosity

Even if all the molecular types had similar chain length distributions as the n-alkanes, it was previously identified that the hard sphere theory was not recommended for mixtures of unlike molecules. From this it was proposed that the predicted viscosity of a diesel fuel mixture could be related to the theoretical liquid viscosity of the n-alkane mixture present within the fuel. With the n-alkane composition having been identified for Fuel A an indication of the deviation of the diesel viscosity from this can be made. The alkane viscosity was estimated as described in the previous chapter and the difference between this and the diesel viscosity is plotted as a function of pressure. This is shown in Figure 6.16.

Difference in diesel fuel and alkane viscosity is found to be a regularly increasing function of pressure. Difference with respect to temperature does not show such apparent regularity. Use of the alkane deviation scheme as proposed earlier, whilst offering some insight into interaction between groups of hydrocarbons. may prove impractical for diesel fuels if studied primarily as a function of pressure. The basis of the method was that deviation from n-alkane viscosity for a number of diesels and other mixtures of aliphatics and aromatics could be established from

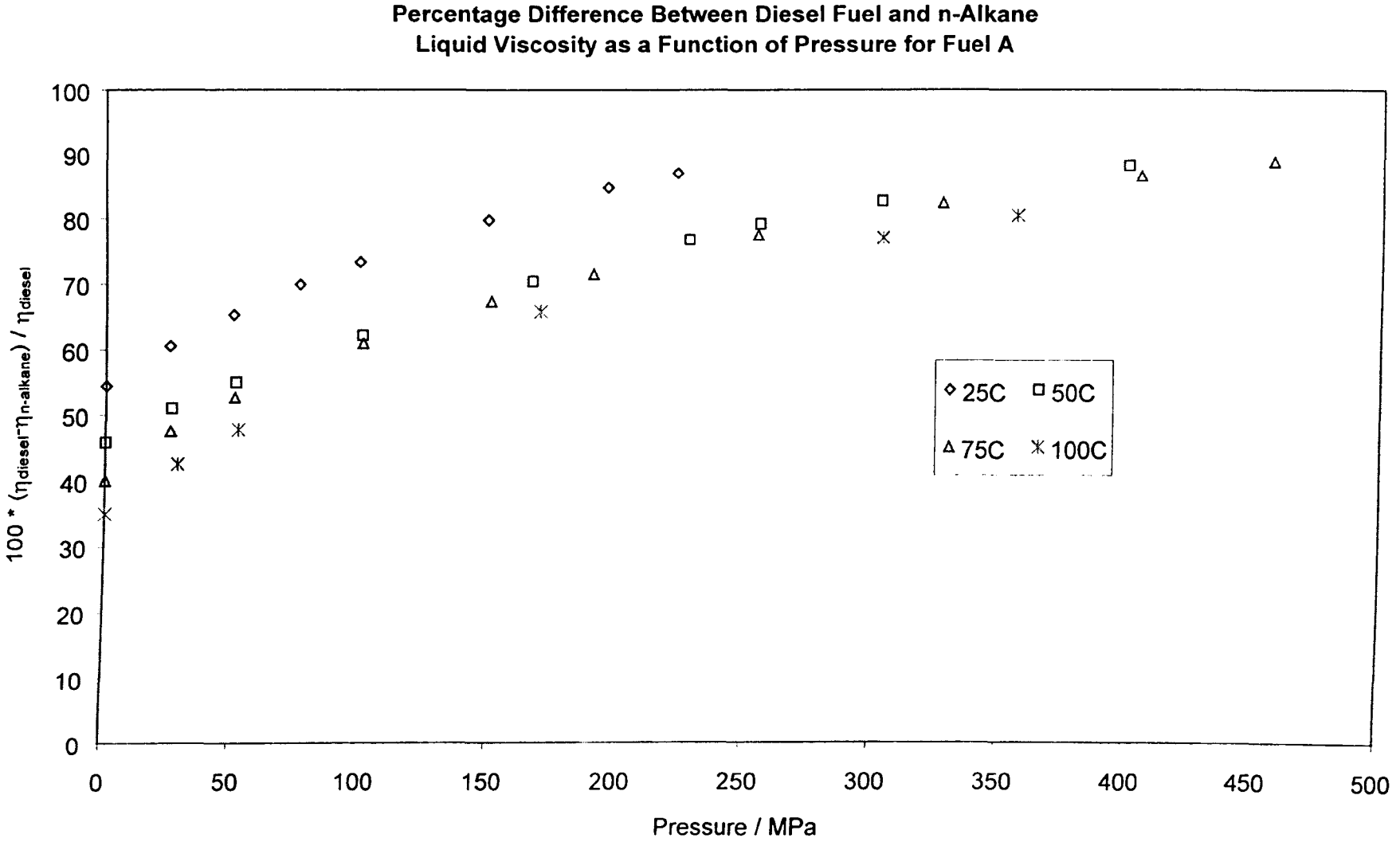

Figure 6.16 Comparison of diesel viscosity with theoretical liquid n-alkane viscosity with respect to pressure

measurement in terms of quantities of molecular species present. As shown from Figure 6.16, without consideration of molecular species, the deviation is a function of both temperature and pressure. Therefore, the fit would involve consideration of the effects of pressure, temperature and composition of the fuel. An empirical fit to this method would require a large amount of measurement to derive. The fit would probably be subject to large uncertainty due to the finding that the deviation function is not just composition dependent, but also pressure and temperature dependent.

The trend of difference between diesel and alkane viscosity is much more regular when fitted as a function of the relative free volume of the theoretical average n-alkane. This is shown for Fuel A in Figure 6.17. When error is plotted in this manner it is found that the error is linear at each temperature. That the lines are not equivalent at all four temperatures once more indicates that the hard sphere method does not satisfactorily correlate complex mixture data. Given that the separation of the isotherms is due to the fact that a complex non-uniform mixture cannot be considered as a system of hard spheres, then perhaps this could be used as a term to account for the non-ideality of the system. Parameters such as change of the slope and intercept of the percentage difference with respect to free volume line could be used for correlation with respect to quantities of molecular species present.

Figure 6.18 shows the difference between mixture and alkane viscosity for three binary mixtures of hexane and toluene. Each of the series in Figure 6.18 is composed of data at 25, 50, 75 and 100^0C. These mixtures do not display the same temperature dependent behaviour as the diesel. In this binary mixture case the isotherms overlap one another resulting in the scatter shown in Figure 6.18. The two significant differences between the binary mixture and the complex diesel mixture

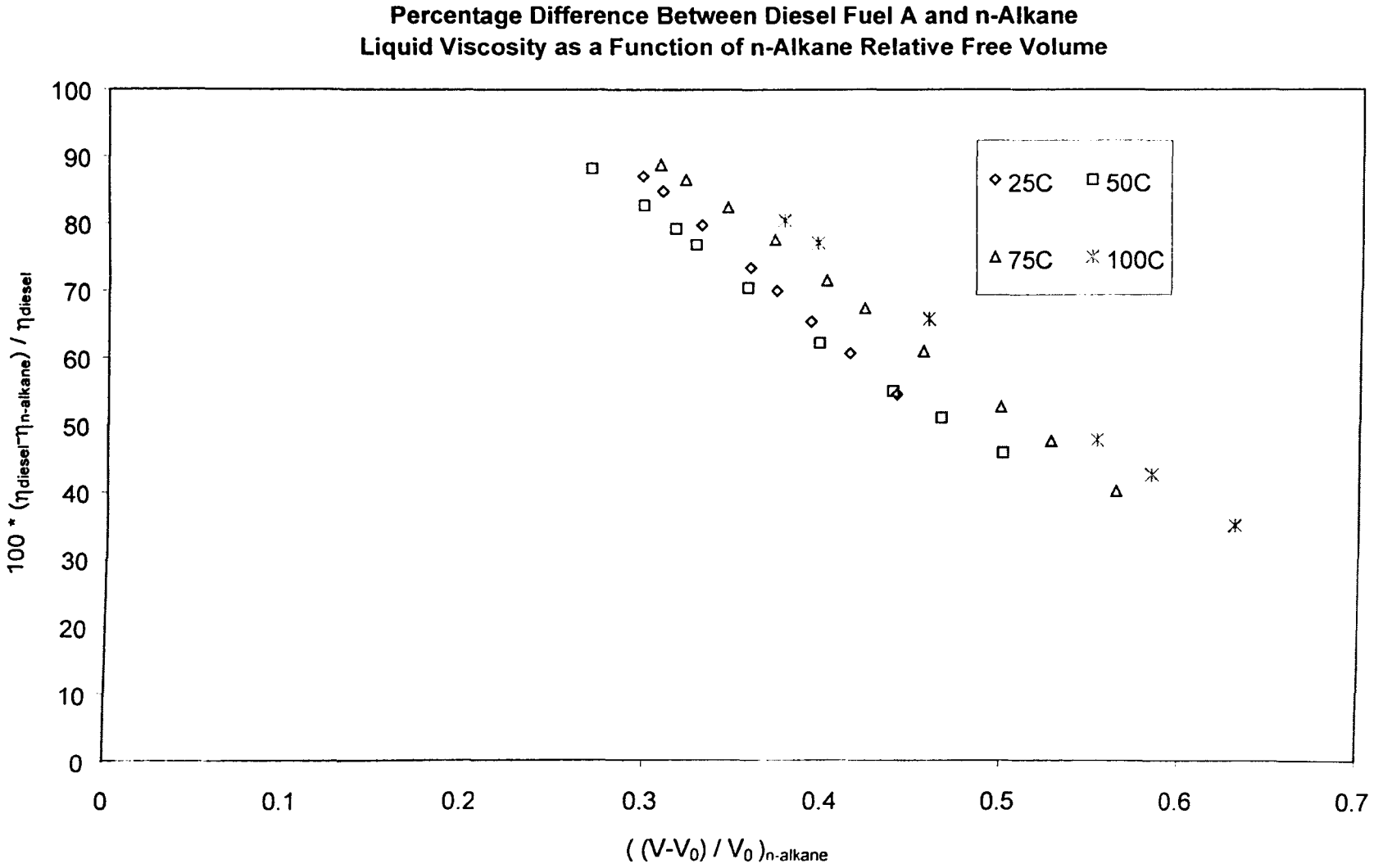

Figure 6.17 Comparison of diesel viscosity with theoretical liquid n-alkane viscosity with respect to n-alkane relative free volume

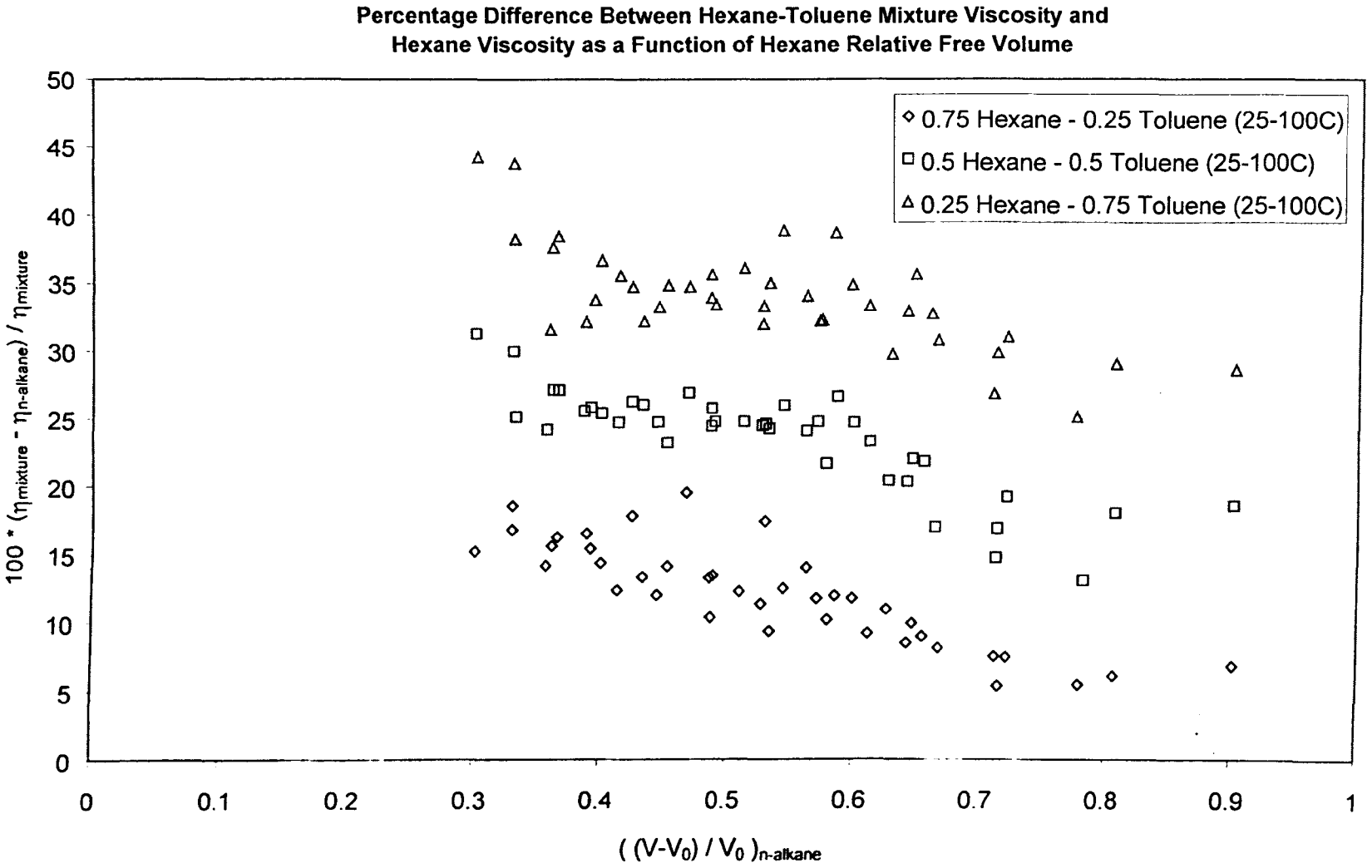

Figure 6.18 Comparison of hexane-toluene mixture viscosity and hexane viscosity with respect to hexane relative free volume

are therefore the overlapping of isotherms displayed by the former case and the more linear trends of the latter.

That the isotherms of difference in mixture and alkane viscosity overlap in the binary mixture suggests that the binary mixture considered here is closer to being a mixture which could be considered as a hard sphere type system. The scatter of this might be a function of a form of difference between the two molecules; this may be more clearly illustrated by considering the case of the diesel.

Although the isotherms of the diesel shown in Figure 6.17 are dissimilar, they each display regular linear behaviour with respect to n-alkane relative free volume. This could be a result of the averaging effect discussed previously. From the processes, such as distillation, used to produce the diesel, there will be certain similarities between the aliphatic and aromatic portions of the fuel, in terms of boiling point for example. Such a proposed similarity could cause the diesel property to be different from the n-alkane property in the regular fashion as shown in Figure 6.17. That this was not as apparent from Figure 6.16 will be due to the plot being with respect to pressure which is not the fundamental variable for liquid viscosity, unlike free volume.

A method relating diesel viscosity to known alkane viscosity on the basis of diesel composition with no measurement of diesel viscosity required may be desirable. However, this method would still require some development from additional measurements as discussed above. If such a method was developed, the degree of characterisation of the fuel is still large; a gas chromatography identifying the quantity of each alkane present would be necessary and the amount of different classes of compound would also need to be measured. Whether this is more useful

than the method requiring limited viscosity measurement as input would depend on how useful the composition data was considered for other purposes, and also the cost of undertaking either set of measurements. Another significant factor in assessing the merits of the methods is the effect of additives upon viscosity prediction; it may be easier to factor this in as another class of compound in the compositional method.

6.3.6 – Extending the Generality of the Empirical Fit of Prediction Error

In the absence of the necessary data to derive a compositional method of viscosity prediction, perhaps the most practical method is to use the hard sphere solution scheme with empirical fits of error as discussed earlier. For a wide range of diesels with different base hydrocarbon composition and additives, the best option may be to accumulate a wide range of data and fit the error to this to give a reasonable average fit for all other cases. Figures 6.11 and 6.12 show that the general trend of error for all fuel measurements is similar to the case where only the measurements reported by Glen[59.] were considered. Again approximately linear trends of error beyond 50MPa are seen at 25^{0}C and beyond 125MPa at 50^{0}C. Average linear functions of error can be found from consideration of the error in the prediction compared from the measurements of Glen[59.] and the measurements presented in this work. Using the same nomenclature as equations (5.20) and (5.21) the viscosity predicted from hard sphere theory incorporating empirical correction terms at 25^{0}C is;

$$\eta_{corr_{25}} = \frac{\eta_{HS}}{1 - \frac{0.206P - 7.122}{100}} \tag{6.4}$$

Similarly at 50^{0}C;

$$\eta_{corr_{50}} = \frac{\eta_{HS}}{1 - \frac{0.133P - 13.936}{100}} \tag{6.5}$$

A comparison of the average absolute percentage deviations was made for all fuels at 25 and 50°C to compare the error in prediction from using the different empirical hard sphere error correlations. Results of the comparison are presented in Table 6.12.

Table 6.12 AA%D of viscosity predicted using hard sphere theory with correction factor 1 (CF1 {5.20 and 5.21}) and correction factor 2 (CF2 {6.4 and 6.5}) at 25 and 50°C compared to measured viscosity

	Class 1	Low Sulphur	ISO 4113	Fuel A	Fuel C	Fuel Y	Fuel Z	Kansas
25°C CF1 AA%D	6.48	1.05	3.11	2.32	10.7	8.39	1.68	5.25
25°C CF2 AA%D	10.1	0.456	2.75	1.65	9.22	9.14	0.790	4.29
50°C CF1 AA%D	1.13	1.21	1.08	2.69	3.82	3.57	2.88	4.52
50°C CF2 AA%D	2.95	1.16	1.22	2.04	2.15	2.64	1.45	3.69

Table 6.12 shows that there is little difference in the average deviation between prediction in measurement when equations (6.4) and (6.5) are used instead of (5.20) and (5.21). This suggests that the corrections derived only from the measurements of Glen[59] represent a reasonable average error for typical diesel fuels. The empirical corrections derived from all the measurements contain more data at higher pressure and are thus likely to provide a better average in the high pressure range.

The additional measurements made in this work allow a more thorough analysis of error in hard sphere predicted viscosity compared to measured viscosity

at 75^0C. Isotherms of error for all the fuels are shown in Figure 6.19. These isotherms display the same trend of error approaching a minimum value before increasing linearly with respect to pressure. Apart from this common qualitative description, there is a large variation in the behaviour between fuels. For example Fuels Y and Z display a transition to the linear form of error with respect to pressure at a significantly lower pressure than the Class 1 fuel and Fuel C. There is also a large spread of error for the different fuels at equivalent pressures. However, in the range of most practical interest for fuel injection equipment manufacturers, to 2kbar, the error is within 15%. No definite trend could be established for error in prediction at 100^0C for the two fuels measured at this temperature. However, error was within 15% as shown from Figures 6.6 and 6.7.

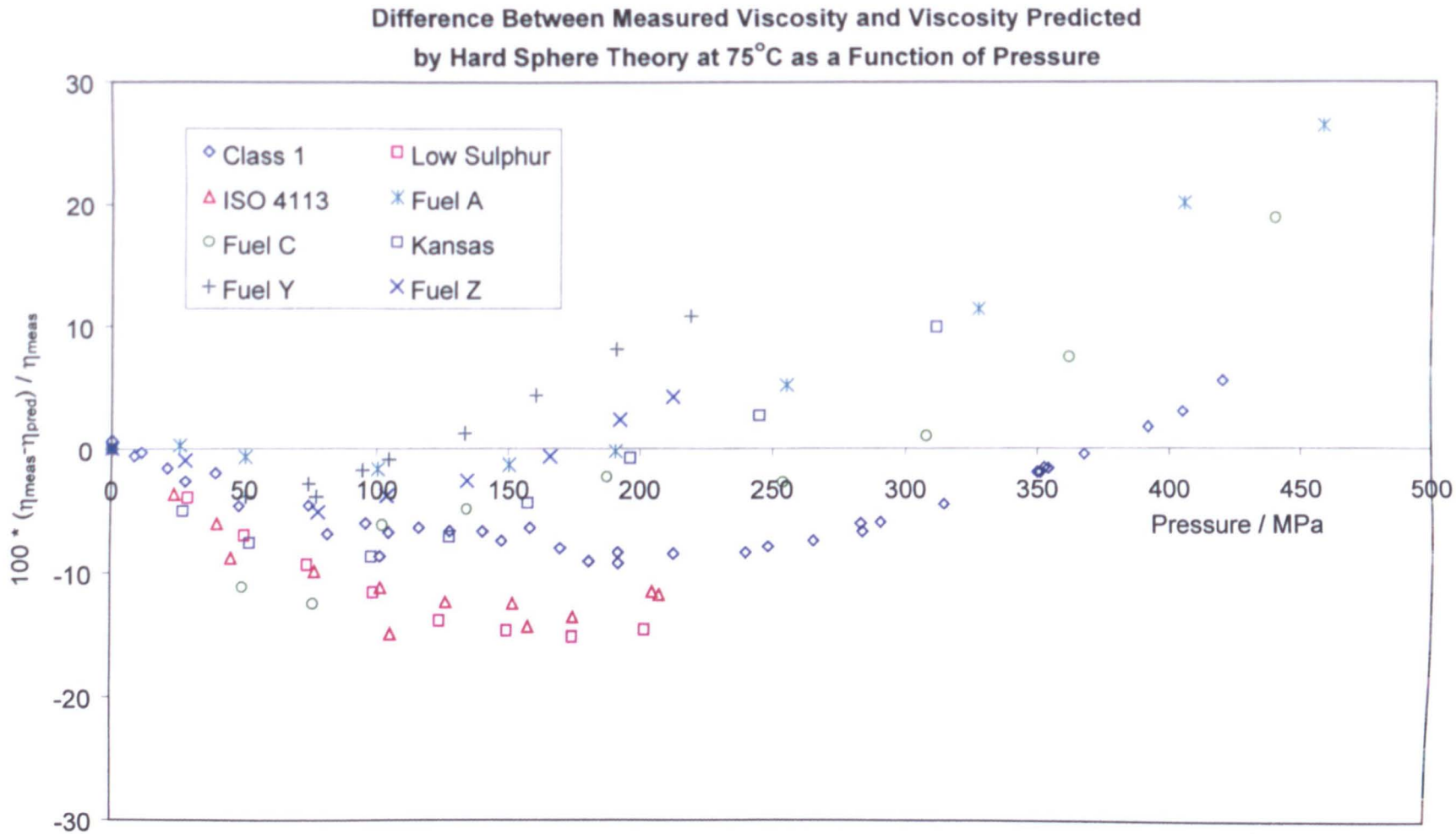

Figure 6.19 Difference in measured viscosity and hard sphere predicted viscosity with respect to pressure for diesel fuels at 75^0C

Chapter 7.

Conclusions

7. Conclusions

One method for meeting stringent legislation for various emission types from compression ignition engines is to use common rail fuel injection equipment (FIE) operated at high pressure. Hydraulic modelling of the common rail FIE at the working conditions requires accurate thermophysical property data of the fuel at the conditions of elevated pressure and temperature. A series of measurements of the density and viscosity of a number of diesel fuels at these non-ambient conditions were made. Mathematical methods, developed from thermophysical theory, for estimating these properties were compared with the measurements.

The Micro-PVT apparatus, a continuously driven compressive technique, was used for measurements of pressure-volume-temperature relationships of liquids. A new calibration method was necessary for this apparatus. Measurements of volume change made by the Micro-PVT were largely within ±0.1% of accepted reference fluid measurements when the new calibration method was applied. An uncertainty analysis gave an overall uncertainty of 0.23% in measured density. A low speed of compression represented a pseudo-isothermal compression. However, the device could not provide a fast enough compression rate to give a compression which could be considered representative of the isentropic case.

Viscosity measurements at high pressure were made using a falling sinker viscometer. To provide a good representation of the viscometer coefficient, A, for the reference fluids, it was necessary to calibrate the viscometer with respect to annular Reynolds number, rather than measured fall time as described by previous workers. An uncertainty analysis of the viscometer gave an overall uncertainty of

1.74% in elevated pressure viscosity. Measurements made in the viscometer of a base refinery fuel with no additives indicated a phase change from liquid to solid which was not detected by the Micro-PVT apparatus at the same condition. This highlights the need to have a measurement technique appropriate to the phenomena to be detected.

The corresponding states method was developed for the prediction of the density of liquids of unknown composition over a wide range of conditions. The method of Lee and Kesler was studied in detail due to the lack of arbitrary 'characteristic parameters' required, the consistency of errors obtained when extrapolated far beyond the suggested pressure limit, and the similarity of the magnitude of errors for other fluids compared to the reference fluid, n-octane. Prediction of liquid volume ratio change with respect to pressure was improved through use of iso-octane and heptadecane as the reference fluids. A notable result when the corresponding states method was applied with i-C_8H_{18} and $C_{17}H_{36}$ as reference fluids, was that the error for hexane was very large despite having a similar acentric factor to the reference fluid iso-octane. This implies that there is scope for improvement of three parameter corresponding states, perhaps through a different parameter to account for molecular shape.

Application of the corresponding states method requires the critical temperature and pressure and acentric factor of the fluid of interest. These parameters are not readily available for many pure fluids, and even less so for mixtures of unknown composition such as diesel fuels. Correlations are available to relate the input parameters to the normal boiling point. However, no mixture has a boiling point, although estimations of this can be made. Rather than use the spurious

parameter of mixture boiling point as an input for the corresponding states method, an iterative method was developed to imply input parameters for the method. This led to a semi-measurement scheme for density prediction to solve $\frac{\rho_2}{\rho_1} = \frac{Z_1 T_1 P_2}{Z_2 T_2 P_1}$ where ρ_1 and ρ_2 are measurements of density at T_1, P_1 and T_2, P_2 respectively. Compressibility factors Z_1 and Z_2 are calculated at the same conditions using a guessed boiling point to establish the critical properties and acentric factor through published correlations. The guessed boiling point is altered by an iterative method until values of the critical properties and acentric factor are found which correlate the measured densities and enable prediction of density at other pressures and temperatures. Tests with various critical correlations showed the correlations of Kesler and Lee to give the most consistent results for a range of different fluid types.

Predictions of diesel density up to 300MPa, using two atmospheric density measurements and one elevated pressure density measurement as inputs to the iterative corresponding states scheme, gave an average absolute deviation of 0.173% for the fuels tested when compared to the density measurements made with the Micro-PVT. Solution of the method was unstable with respect to guessed boiling point in some instances. This was overcome by using a different elevated pressure density measurement as an input. Highly accurate measurements of density at elevated pressure, for example by the vibrating tube method, might lead to more accurate and stable predictions of density.

Reviewing the theory for viscosity prediction, it was found that the hard sphere theory was not only generally accepted as being a physically realistic description of the molecular movements which result in a liquid having a given viscosity, the theory also enabled viscosity to be correlated over a wide range of

temperature and pressure from two parameters, V_0 and R_η. Both parameters can be found by an iterative method of comparing the experimental reduced viscosity with a universal curve of reduced viscosity developed from consideration of the hard sphere case. Values of V_0 and R_η were estimated simultaneously at any given temperature by the iterative method using the atmospheric pressure viscosity and a single elevated pressure viscosity measurement. R_η was considered temperature independent and used to find V_0 at any other temperature from an atmospheric viscosity measurement only. Viscosity of pure fluids and simple mixtures of known composition were reasonably predicted using this method, although not mixtures of different classes, such as n-alkanes and aromatics. Applying the method directly to diesel fuels gave large errors compared to measurements. The errors displayed a certain amount of regularity with respect to temperature and pressure, but not with respect to relative free volume, $\frac{V-V_0}{V_0}$, as would be expected from theory. This may have been due to the method of solution used for obtaining V_0.

Empirical fits of the error in viscosity prediction compared to measurement. as a function of pressure, were made from data for three fuels from a previous study. The fits were made at 25 and 50^{0}C only; 75^{0}C data displayed different behaviour compared to the lower temperatures, with the magnitude of error not as large. Using the iterative hard sphere method plus empirical correction for prediction of viscosity, using atmospheric viscosity and a single elevated pressure viscosity measurement as inputs, an average absolute deviation of 5.07% was found for predicted diesel viscosity to 457.2MPa compared with measurements made in the high pressure viscometer. A more general empirical fit can be obtained by derivation from more fluids. Extending the empirical fit to include the fuels measured here, as well as

from the previous study, gives a slight improvement in estimated diesel viscosity at 25 and 50^{0}C, particularly at the highest pressures. Further measurements at temperatures between 25 and 50^{0}C might also allow determination of temperature dependency of the empirical fit. Reasonable estimates of viscosity at 75 and 100^{0}C were made using the hard sphere method with no correction terms. That the hard sphere theory can be applied to this complex mixture directly at higher temperatures, and corrected at the lower temperatures using a simple empirical correction term, is possibly due to the approximately bell-shaped distribution of molecular species with respect to chain length.

A collision integral term was added to the hard sphere method. This gave very large, but consistent, errors for the pure fluids and mixtures of known composition which this was tested on. Fitting these errors for one fluid as functions of relative free volume and temperature, the empirical fit of error was then used to predict viscosity from the hard sphere – collision integral method for other fluids. Consistent offsets were found for each fluid, which may be a method for accounting for different molecular shapes. Although no solution was reached for diesel fuels, this method might allow some insight into the intermolecular distance and energy parameters for pure fluids.

The very large errors found for diesel fuels when predictions of viscosity by the hard sphere method are compared with measurements, is most likely due to the fuels being composed of many different molecules of different molecular shape and type. This is far removed from the initial assumption of spherical molecules used in the hard sphere theory. The non-uniformity of the mixture also makes it difficult to use a simple non-sphericity parameter to account for the non-spherical shape of all

the molecules present. Instead, the theoretical liquid viscosity of the n-alkanes present in the mixture could be estimated from the hard sphere theory, and deviation of diesel viscosity from this related to the composition of the fuel. From an analysis of a fuel where quantities of n-alkanes in the fuel had been identified, the deviation was found to be linear with respect to relative free volume of the n-alkane. Development of this method would require much extra measurement of fuel viscosity and composition. The linearity of the deviation suggests that this has potential as a prediction method, perhaps due to similarities in the molecular classes present in the fuels as a result of the refinery techniques used.

The study of density and viscosity undertaken in this work was for specific application in simulations of diesel FIE. With computer simulation tools in widespread use throughout the process industries, there is a more general need for fast, accurate models of all physical properties. The effect of inappropriate thermodynamic data and models used in simulations for typical process industry design problems is shown by Whiting[94.]. With the vast numbers of different pure fluids and fluid mixtures produced and used by industry, it is unlikely that a single model for any given physical property will accurately predict the property value for all fluids. Therefore the use of thermophysical models derived from theory with appropriate input parameters implied from limited measurement of the fluid, might yield more reliable estimates of thermophysical property data over a wide range of conditions for any given fluid.

References

[1.] Pischinger, F. F. "The Diesel Engine for Cars - Is There a Future?." Transactions of the ASME: Journal of Engineering for Gas Turbines and Power 120 (1998): 641-647.

[2.] Russell, M. F., Greeves, G., and Guerrassi, N. "More torque, less emissions and less noise." SAE Technical Paper Series.2000-01-0942 (2000):

[3.] Yamaki, Y., Mori, K., Kohketsu, S., Mori, K., Kato, T. "Heavy Duty Diesel Engine with Common Rail Type Fuel Injection System." Japanese Society of Automotive Engineers: IPC-8 Proceedings 1995. 73-78.

[4.] Jansons, M., Lin, S., Choi, D.S., Campbell, S., Rhee, K.T. "Study of High-Pressure Injection DI Diesel Engine." Diesel Engines: Combustion and Emmisions; 1999 SAE International Fall Fuels & Lubricants Meeting & Exposition 1999. 83-98.

[5.] Belonenko, V.N., Troitsky, V.M., Belyaev, Yu.E., Dymond, J.H., and Glen, N.F. . "Application of a Micro-(p, V, T) Apparatus for Measurement of Liquid Densities at Pressures up to 500MPa." Journal of Chemical Thermodynamics 32.9 (2000): 1203-1219.

[6.] Bridgman, P. W. "The Physics of High Pressure." London: G. Bell and Sons, Ltd., 1931.

[7.] Doolittle, A. K., Simon, I., Cornish, R. M., Doolittle, D. B. "Compressions of Liquids." A.I.Ch.E. Journal 6.1 (1960): 150-162.

[8.] Grindley, T., and Lind, J. E., Jr. "PVT Properties of Water and Mercury." The Journal of Chemical Physics 54.9 (1971): 3983-3989.

[9.] Cutler, W.G., McMickle, RH., Webb, W., and Schiessler, R.W. "Study of the Compressions of Several High Molecular Weight Hydrocarbons." The Journal of Chemical Physics 29.4 (1958): 727-740.

[10.] Isdale, J. D., Brunton, W. C., and Spence, C. M. "Bulk Modulus Measurement and Prediction." NEL Report No. 591 1975.

[11.] Young, K. J. "Viscosity Coefficient Measurement and Theoretical Interpretation for Hydrocarbon Mixtures." Ph.D. Thesis, University of Glasgow 1980.

[12.] Robertson, J. "Transport Properties of Non-Electrolyte Liquids and Mixtures." Ph.D. Thesis, University of Glasgow 1983.

[13.] Glen, N. F. "Viscosity Coefficient Measurement at Elevated Pressure." Ph.D. Thesis, University of Glasgow 1985.

[14.] Back, P. J., Easteal, P. J., Hurle, R. L., and Woolf, L. A. "High-precision measurements with a bellows volumometer." Journal of Physics E: Scientific Instruments 15 (1982): 360-363.

[15.] Figuiere, P., Fuchs, A. H., Ghelfenstein, M., and Szwarc, H. "Pressure-Volume-Temperature Relations for Crystalline Benzene." Journal of Physics and Chemistry of Solids 39 (1977): 19-24.

[16.] Landau, R., and Wurflinger, A. "High pressure apparatus for PVT measurements of liquids and plastic crystals at low temperatures." Reviews of Scientific Instruments 51.4 (1980): 533-535.

[17.] Tekac, V., Cibulka, I., and Holub, R. "PVT Properties of Liquids and Liquid Mixtures: A Review of the Experimental Methods and the Literature Data." Fluid Phase Equilibria 19 (1985): 33-149.

[18.] Albert, H. J., and Wood, R. H. "High-Precision Flow Densimeter for Fluids at Temperatures to 700K and Pressures to 40MPa ." Reviews of Scientific Instruments 55.4 (1984): 589-593.

[19.] de Oliveira, C. M. B. P. "Viscosity of Liquid Hydrocarbons at High Pressure." Ph.D. Thesis, Imperial College of Science, Technology and Medicine 1991.

[20.] Belonenko, V., Bunau, E., Funck, T., and Nikolashev, V. "High Pressure Pump System and Method of Operation Thereof." United States Patent No. 5,992,222 1999.

[21.] Landau, R, and Wurflinger, A. "PVT-Daten von Acetonitril, Undecan und Dodecan bis 3kbar und -50C. Druckabhangigkeit der Umwandlungsvolumina, -enthalpien und -entropien." Berichte der Bunsengesellschaft fur Physikalische Chemie 84 (1980): 895-902.

[22.] Malhotra, R., and Woolf, L. A. "Volumetric measurements under pressure for 2,2,4-trimethylpentane at temperatures up to 353.15K and for benzene and three of their mixtures at temperatures up to 348.15K." International Journal of Thermophysics 14.6 (1993): 1153-1172.

[23.] Harris, K. R., Malhotra, R., and Woolf, L. A. "Temperature and density dependence of the viscosity of octane and toluene." Journal of Chemical and Engineering Data 42 (1997): 1254-1260.

[24.] The International Association for the Properties of Water and Steam. "Release on the IAPWS Formulation 1995 for the Thermodynamic Properties of Ordinary Water Substance for General and Scientific Use." (1996)

[25.] Isdale, J. D. "Viscosity of Simple Liquids Including Measurement and Prediction at Elevated Pressure." Ph.D. Thesis, University of Strathclyde 1976.

[26.] Assael, M. J. and Wakeham, W. A. "Vibrating-wire Viscometry on Liquids at High Pressure." Fluid Phase Equilibria 75 (1992): 269-285.

[27.] Glen, N. F. Private Communication, 2001.

[28.] M^{c}Glashan, M. L. "The International Temperature Scale of 1990 (ITS-90)" The Journal of Chemical Thermodynamics 22.7 (1990): 653-663.

[29.] Bird, R. B., Stewart, W. E., and Lightfoot, E. N. "Transport Phenomena." John Wiley & Sons. 1960.

[30.] Lee, B.I., and Kesler, M. G. "A Generalized Thermodynamic Correlation Based on Three-Parameter Corresponding States." AIChE Journal 21(3) (1975): 510-527.

[31.] Hankinson, R. W., and Thomson, G. W. "A New Correlation for Saturated Densities of Liquids and Their Mixtures." A.I.Ch.E. Journal 25.4 (1979): 653-663.

[32.] Thomson, G. H., Brobst, K. R., and Hankinson, R. W. "An improved correlation for densities of compressed liquids and liquid mixtures." AIChE Journal 28.4 (1982): 671-676.

[33.] Soave, G. "Equilibrium Constants from a Modified Redlich-Kwong Equation of State." Chemical Engineering Science 27 (1972): 1197-1203.

[34.] Redlich, O., and Kwong, J. N. S. "On the Thermodynamics of Solutions. V An Equation of State. Fugacities of Gaseous Solutions." Chemical Reviews 44 (1949): 233-244.

[35.] Pitzer, K. S. "The Volumetric and Thermodynamic Properties of Fluids I. Theoretical Basis and Virial Coefficients." Journal of the American Chemical Society 77.13 (1955): 3427-3440.

[36.] Pitzer, K. S., Lippmann, D. Z., Curl, Jr., R.F., Huggins, C. M., and Petersen, D. E. "The Volumetric and Thermodynamic Properties of Fluids. II. Compressibility Factor, Vapor Pressure and Entropy of Vaporization." Journal of the American Chemical Society 77.13 (1955): 3433-3440.

[37.] Benedict, M., Webb, G. B., and Rubin, L. C. "An Empirical Equation for Thermodynamic Properties of Light Hydrocarbons and Their Mixtures I. Methane, Ethane, Propane and n-Butane." Journal of Chemical Physics 8 (1940): 334-345.

[38.] Dymond, J. H., Robertson, J., and, Isdale, J. D. "(p, rho, T) of some Pure n-Alkanes and Binary Mixtures of n-Alkanes in the Range 298 to 373K and 0.1 to 500MPa." The Journal of Chemical Thermodynamics 14 (1982): 51-59.

[39.] Dymond, J. H., and Malhotra, R. "The Tait Equation: 100 Years On." International Journal of Thermophysics 9.6 (1988): 941-951.

[40.] Tegeler, Ch., Span, R., and Wagner, W. "A New Equation of State for Argon Covering the Fluid Region for Temperatures from the Melting Line to 700K at Pressures up to 1000MPa." Journal of Physical and Chemical Reference Data 28.3 (1999): 779-850.

[41.] Dymond, J. H., Young, K. J., and Isdale, J. D. "P, rho, T Behaviour for n-Hexane + n-Hexadecane in the Range 298 to 373K and 0.1 to 500MPa ." The Journal of Chemical Thermodynamics 11.9 (1979): 887-895.

[42.] Dymond, J. H., Isdale, J. D., and Glen, N. F. "Density Measurement at High Pressure." Fluid Phase Equilibria 20 (1985): 305-314.

[43.] Munoz, F., and Reich, R. "New Parameters for the Lee-Kesler Correlation Improve Liquid Density Prediction." Fluid Phase Equilibria 13 (1983): 171-178.

[44.] Smith, W. R., Lisal, M., and Missen, R. W. . "The Pitzer-Lee-Kesler-Teja (PLKT) Startegy and its Implementation by Meta-Computing Software." Chemical Engineering Education 35 (2001): 68-73.

[45.] Doolittle, A. K., Simon, I., Cornish, R. M., and Doolittle, D. B. "Compressions of Liquids." A.I.Ch.E. Journal 6.1 (1960): 150-162.

[46.] "PPDS2 for Windows v2.2." Software Package produced by NEL, East Kilbride, U.K.

[47.] Cibulka, I., and Takagi, T. "P-rho-T Data of Liquids: Summarization and Evaluation. 6. Nonaromatic Hydrocarbons (Cn, n>=5) except n-Alkanes C5 to C16." Journal of Chemical and Engineering Data 44 (1999): 1105-1128.

[48.] Cibulka, I., and Takagi, T. "P-rho-T Data of Liquids: Summarization and Evaluation. 5. Aromatic Hydrocarbons." Journal of Chemical and Engineering Data 44 (1999): 411-429.

[49.] Reid, R.C., Prausnitz, J. M., Poling, B. E. . "The Properties of Liquids and Gases." McGraw Hill, (1987)

[50.] Korsten, H. "Critical Properties of Hydrocarbon Systems." Chemical Engineering & Technology 21.3 (1998): 229-244.

[51.] Nelson, W. L. "Petroleum Refinery Engineering (Fourth Edition)." McGraw-Hill, 1958.

[52.] IP406/99 Boiling Range of Products - GC Method

[53.] ASTM D86-01e1 Standard Test Method for Distillation of Petroleum Products at Atmospheric Pressure

[54.] Twu, C. H. "An Internally Consistent Correaltion for Predicting the Critical Properties and Molecular Weights of Petroleum and Coal-Tar Liquids." Fluid Phase Equilibria 16.2 (1984): 137-150.

[55.] Assael, M. J., Dymond, J. H., and Exadaktilou, D. "An Improved Representation for n-Alkane Liquid Densities." International Journal of Thermophysics 15.1 (1994): 155-164.

[56.] Assael, M. J., Dymond, J. H., and Polimatidou, S. K. "Correlation and Prediction of Dense Fluid Transport Coefficients. VI. n-Alcohols." International Journal of Thermophysics 15.2 (1994): 189-201.

[57.] Aalto, M. M., and Keskinen, K. I. "Liquid Densities at High Pressures." Fluid Phase Equilibria 166 (1999): 183-205.

[58.] Rodriguez-Anton, L. M., Casanova-Kindelan, J., and Tardajos, G. "High Pressure Physical Properties of Fluids Used in Diesel Injection Systems." SAE Technical Paper Series 2000.

[59.] Glen, N. F. "Non-ambient Physical Property Measurement Techniques." DTI Reference WM 93/197 (1998)

[60.] Doolittle, A. K. "Specific Volume of n-Alkanes." Journal of Chemical and Engineering Data 9.2 (1964): 275-279.

[61.] Dymond, J.H., Glen, N., Robertson, J., and Isdale, J. D. "(p, rho, T) for (1-x)C6H6+xC6D6 and (1-x)C6H6+xC6F6 in the Range 298 to 373K and 0.1 to 400MPa." Journal of Chemical Thermodynamics 14 (1982): 1149-1158.

[62.] Dymond, J. H., Malhotra, R., Isdale, J. D., and Glen, N. F. "(p, rho, T) of n-Heptane, Toluene, and Oct-1-ene in the Range 298 to 373K and 0.1 to 400MPa and Representation by the Tait Equation." The Journal of Chemical Thermodynamics 20.5 (1988): 603-614.

[63.] Abbott, M. M., Kaufmann, T. G., and Domash, L. "A correlation for predicting liquid viscosities of petroleum fractions." The Canadian Journal of Chemical Engineering 49 (1971): 379-384.

[64.] Watson, K. M., Nelson, E. F., and Murphy, G. B. "Characterization of Petroleum Fractions." Industrial and Engineering Chemistry 27.12 (1935): 1460-1464.

[65.] Twu, C. H. "Generalized Method for Predicting Viscosities of Petroleum Fractions." A.I.Ch.E. Journal 32.12 (1986): 2091-2094.

[66.] Cameron, A. "The Determination of the Pressure-Viscosity Coefficient and Molecular Weight of Lubricating Oils by Means of the Temperature-Viscosity Equations of Vogel and Eyring." Journal of the Institute of Petroleum 31.262 (1945): 401-404.

[67.] Johnston, W. G. "A Method to Calculate the Pressure-Viscosity Coefficient from Bulk Properties of Lubricants." ASLE Transactions 24.2 (1981): 232-238.

[68.] Ozdogan, S., and Yucel, H. G. "Correlations Towards Prediction of Petroleum Fraction Viscosities: A Semi-Theoretical Approach." Fuel 79 (2000): 1209-1214.

[69.] Yucel, H. G. and Ozdogan, S. "A New Method for Predicting Viscosity of Pure Organic Liquids." The Canadian Journal of Chemical Engineering 76 (1998): 148-155.

[70.] Assael, M. J., Dymond, J. H., Papadaki, M., and Patterson, P. M. "Correlation and Prediction of Dense Fluid Transport Coefficients. I. n-alkanes." International Journal of Thermophysics 13.2 (1992): 269-281.

[71.] Assael, M. J., Dymond, J. H., and Patterson, P. M. "Correlation and Prediction of Dense Fluid Transport Coefficients. V. Aromatic Hydrocarbons." International Journal of Thermophysics 13.5 (1992): 895-905.

[72.] Eyring, H. "Viscosity, plasticity, and diffusion as examples of absolute reaction rates." Journal of Chemical Physics 4 (1936): 283-291.

[73.] Andrade, E. N. da C. "The Viscosity of Liquids." Nature 125 (1930): 309-310.

[74.] Andrade, E. N. da C. "The Viscosity of Liquids." Nature 125 (1930): 580-584.

[75.] Cohen, M. H., and Turnbull, D. "Molecular Transport in Liquids and Glasses." The Journal of Chemical Physics 31.5 (1959): 1164-1169.

[76.] Doolittle, A. K. "Studies in Newtonian Flow. II. The Dependence of the Viscosity of Liquids on Free-Space." Journal of Applied Physics 22.12 (1951): 1471-1475.

[77.] Doolittle, A. K. "Studies in Newtonian Flow. III. The Dependence of the Viscosity of Liquids on Molecular Weight and Free Space (in Homologous Series)." Journal of Applied Physics 23.2 (1952): 236-239.

[78.] Hildebrand, J. H. "Motions of Molecules in Liquids: Viscosity and Diffusivity." Science 174 (1971): 490-493.

[79.] Assael, M. J., Trusler, J. P. M., and Tsolakis, T. F. "Thermophysical Properties of Fluids - An Introduction to their Prediction." 1996.

[80.] Reed, T. M., and Gubbins, K. E. "Applied Statistical Mechanics." McGraw-Hill, 1973.

[81.] Dymond, J. H. "The Interpretation of Transport Coefficients on the Basis of the van der Waals Model. I. Dense Fluids." Physica 75 (1974): 100-114.

[82.] Carnahan, N. F., and Starling, K. E. "Equation of State for Non-Attracting Rigid Spheres." The Journal of Chemical Physics 51.2 (1969): 635-636.

[83.] Assael, M. J., Dymond, J. H., Papadaki, M., and Patterson, P. M. "Correlation and Prediction of Dense Fluid Transport Coefficients. II. Simple Molecular Fluids." Fluid Phase Equilibria 75 (1992): 245-255.

[84.] Dymond, J. H., and Awan, M. A. "Correlation of High-Pressure Diffusion and Viscosity Coefficients for n-Alkanes ." International Journal of Thermophysics 10.5 (1989): 941-951.

[85.] Assael, M. J., Dymond, J. H., Papadaki, M., and Patterson, P. M. "Correlation and Prediction of Dense Fluid Transport Coefficients. III. n-Alkane Mixtures." International Journal of Thermophysics 13.4 (1992): 659-669.

[86.] Dymond, J. H., Robertson, J., and Isdale, J. D. "Transport Properties of Nonelectrolyte Liquid Mixtures - III. Viscosity Coefficients for n-Octane, n-Dodecane, and Equimolar Mixtures of n-Octane + n-Dodecane from 25 to 100^{0}C at Pressures Up to the Freezing Pressure or 500 MPa ." International Journal of Thermophysics 2.2 (1981): 133-154.

[87.] Dymond, J. H., Glen, N. F., and Isdale, J. H. "Transport Properties of Nonelectrolyte Liquid Mixtures - VII. Viscosity Coefficients for Isooctane and for Equimolar Mixtures of Isooctane + n-Octane and Isooctane + n-Dodecane from 25 to 100C at Pressures up to 500 MPa or the Freezing Pressure." International Journal of Thermophysics 6.3 (1985): 233-250.

[88.] Neufeld, P. D., Janzen, A. R., and Aziz, R. A. "Empirical Equations to Calculate 16 of the Transport Collision Integrals for the Lennard-Jones (12-6) Potential." The Journal of Chemical Physics 57.3 (1972): 1100-1102.

[89.] Dymond, J. H., Awan, M. A., Glen, N. F., and Isdale, J. D. "Transport Properties of Nonelectrolyte Liquid Mixtures. VIII. Viscosity Coefficients for Toluene and for Three Mixtures of Toluene + Hexane from 25 to 100C at Pressures up to 500MPa." Interantional Journal of Thermophysics 12.2 (1991): 275-287.

[90.] Grunberg, L., Nissan, A. H. . "Mixture Law for Viscosity." Nature 1949: 799-800.

[91.] Hayward, A.T.J. "Compressibility equations for liquids: a comparative study." British Journal of Applied Physics 18 (1967): 965-977.

[92.] Hayward, A.T.J. "The Truth About Liquids Under Pressure." Engineering 198 (1964): 314-316.

[93.] ASTM D1250-80 Standard Guide for Petroleum Measurement Tables 2000 Annual Book of ASTM Standards 2000.

[94.] Whiting, W. B. "Effects of Uncertainties in Thermodynamic Data and Models on Process Calculations." Journal of Chemical and Engineering Data 41.5 (1996): 935-941.

Appendix A.

Viscometer Theory

Appendix A - Viscometer Theory

When a force is imposed on a liquid, the rate at which the liquid shears, $\frac{\partial \gamma}{\partial t}$, is related to the shear stress caused by the force. For the range of fluids of interest in this work, shear stress and shear rate are related by a proportionality constant as shown in the equation:

$$\tau = \eta \frac{\partial \gamma}{\partial t} \qquad (A.1)$$

This relationship was first proposed by Newton and hence the term Newtonian fluid is applied to the class of fluids which obey this rule. Shear rate is equivalent to the velocity gradient $\frac{\partial u_x}{\partial y}$ and when equation (A.1) is re-written in the form $\tau = \eta \frac{\partial u_x}{\partial y}$ it can be easily deduced that the term η is a resistance to the flow of fluid when a force is applied to the fluid. η, the internal resistance of the liquid is commonly called the liquid viscosity.

Knowing that the relationship (A.1) holds for the fluids to be studied. it is possible to devise a method for applying a constant force and measuring the resultant rate of shear caused by this. Viscosity measurement throughout this work is made by means of a falling cylinder type viscometer. With this method the liquid is sheared by the sinker which falls through the fluid under the influence of gravity. When the cylinder falls, it forces the liquid, which was previously at rest, through the annulus formed by the sinker and viscometer walls. For the liquid to flow, there must exist a pressure gradient along the length of the annulus. An analytical expression for the pressure gradient can be derived from an elemental force balance on the fluid in the

annulus. The force balance is as follows where the nomenclature corresponds to that given in Figure A.1.

Force due to pressure in the annulus is equal to the product of pressure drop per unit length, length and annulus area. Considering infinitesimal changes in length this force is given by;

$$F_P = \left(\frac{dP}{dl}\right) dl\pi\left(r^2 - r_1^2\right) \tag{A.2}$$

Resistance to flow due to the viscosity of the fluid causes a drag force on the tube wall and the sinker wall. Viscous force on the tube wall is equivalent to the shear stress due to viscosity multiplied by the area which the shear stress acts on. Hence:

$$F_v = \eta\left(\frac{du_x}{dr}\right) 2\pi r dl \tag{A.3}$$

where F_v is the force due to viscous drag at the tube wall. The force due to fluid viscosity acting on the wall of the sinker is given in terms of force per unit length and given the symbol λ. A force balance on a fluid element in the annulus can now be arranged in the form;

$$\left(\frac{dP}{dl}\right) dl\pi\left(r^2 - r_1^2\right) = \eta\left(\frac{du_x}{dr}\right) 2\pi r dl + \lambda dl \tag{A.4}$$

Rearrangement of the force balance yields;

$$du_x = \frac{1}{2\eta}\left(\frac{dP}{dl}\right)\left[\int r dr - \int \frac{r_1^2}{r} dr\right] - \frac{\lambda}{2\eta}\int \frac{1}{r} dr \tag{A.5}$$

The previous expression can then be integrated to give the velocity u_x as a function of radial distance r;

$$u_x = \frac{1}{2\eta}\left(\frac{dP}{dl}\right)\left[\frac{r^2}{2} - r_1^2 \ln r\right] - \frac{\lambda}{2\pi\eta}\ln r + c \tag{A.6}$$

where c is a constant. In order to find expressions for the pressure force per unit length of sinker, λ, and constant of integration, c, it is necessary to integrate equation (A.5) with known boundary conditions. Using the assumption of no slip then the velocity of the fluid at the tube wall will be zero and the fluid at the sinker wall will be equal to the velocity of the sinker. In terms of the nomenclature of Figure A.1, the boundary conditions are $u_x=0$ at $r=r_2$ and $u_x=u_{sinker}$ at $r=r_1$. Integrating equation (A.5) between r_2 and r_1 yields;

$$\lambda = \frac{2\pi\eta u_{\sin ker}}{\ln\frac{r_2}{r_1}} + \pi\left(\frac{dP}{dl}\right)\left[\frac{r_2^{\,2}-r_1^{\,2}}{2\ln\frac{r_2}{r_1}} - r_1^{\,2}\right] \qquad \text{(A.7)}$$

The expression for λ can then be substituted into equation (A.6) to give;

$$c = u_x - \frac{1}{2\eta}\left(\frac{dP}{dl}\right)\left[\frac{r^2}{2} - r_1^{\,2}\ln r\right] + \frac{u_{\sin ker}}{\ln\frac{r_2}{r_1}}\ln r + \frac{1}{2\eta}\left(\frac{dP}{dl}\right)\left[\frac{r_2^2-r_1^{\,2}}{2\ln\frac{r_2}{r_1}} - r_1^{\,2}\right]\ln r \qquad \text{(A.8)}$$

As this is a constant, its value will be the same at any value of r. Thus it is possible to simplify the expression by substituting for r at the boundary condition of $r=r_1$ to give;

$$c = -\frac{1}{2\eta}\left(\frac{dP}{dl}\right)\left[\frac{r_2^{\,2}}{2} - \frac{r_2^2-r_1^{\,2}}{2\ln\frac{r_2}{r_1}}\ln r_2\right] + \frac{u_{\sin ker}}{\ln\frac{r_2}{r_1}}\ln r_2 \qquad \text{(A.9)}$$

Having obtained expressions for λ and c, it is now possible to define u_x at any radial distance r by substitution of equations (A.7) and (A.9) into equation (A.6) to find;

$$u_x = \frac{1}{4\eta}\left(-\frac{dP}{dl}\right)\left[r_2^2 - r^2 - \frac{r_2^2 - r_1^2}{\ln\frac{r_2}{r_1}}\ln\frac{r_2}{r}\right] + \frac{u_{\sin ker}}{\ln\frac{r_2}{r_1}}\ln\frac{r_2}{r} \qquad (A.10)$$

Total flow rate through the annulus will be found from the summation of the individual products of velocity and area at every radial distance r. For a single elemental annulus the elemental flow rate dQ is;

$$dQ = u_x 2\pi r dr \qquad (A.11)$$

Total flow rate through all elemental annuli is found by substituting the equation for u_x as a function of r (A.10) into equation (A.11) and integrating between the boundary conditions of flow rate Q=Q at r=r_2 and Q=0 at r=r_1. The result of this process is;

$$Q = \frac{\pi}{8\eta}\left(-\frac{dP}{dl}\right)\left(r_2^2 - r_1^2\right)\left[r_2^2 + r_1^2 - \frac{r_2^2 - r_1^2}{\ln\frac{r_2}{r_1}}\right] - \pi u_{\sin ker}\left(r_1^2 - \frac{r_2^2 - r_1^2}{2\ln\frac{r_2}{r_1}}\right) \qquad (A.12)$$

The amount of fluid flowing through the annulus per unit time must be equal to the rate at which fluid is displaced from underneath the sinker. Assuming the sinker is a cylinder with flat ends, flow rate through the annulus will be;

$$Q = \pi r_1^2 u_{\sin ker} \qquad (A.13)$$

This can be equated with equation (A.12) to give pressure drop in the annulus per unit length of sinker in terms of viscosity, sinker velocity and tube and sinker radii;

$$-\frac{dP}{dl} = \frac{4\eta u_{\sin ker}}{\left(r_2^2 + r_1^2\right)\ln\frac{r_2}{r_1} - r_2^2 + r_1^2} \qquad (A.14)$$

With the expressions for pressure drop per unit length of sinker and viscous drag force at the sinker surface now evaluated it is possible to complete a force balance over the sinker;

$$\left(\rho_f - \rho_s\right) g \pi r_1^2 = -\frac{dP}{dl} \pi r_1^2 - \lambda \tag{A.15}$$

Substituting the expressions for pressure drop and viscous drag into the equation and re-arranging gives the expression for viscosity as a function of fall time;

$$\eta = \frac{\left(\rho_s - \rho_f\right) g t}{2L_t} \left[r_1^2 \ln \frac{r_2}{r_1} - r_1^2 \left(\frac{r_2^2 - r_1^2}{r_2^2 + r_1^2} \right) \right] \tag{A.16}$$

Substituting the definition of sinker density as mass / volume into the expression gives;

$$\eta = \frac{\left(1 - \frac{\rho_f}{\rho_s}\right) m_{\text{sinker}} g t}{2\pi L_s L_t} \left[\ln \frac{r_2}{r_1} - \left(\frac{r_2^2 - r_1^2}{r_2^2 + r_1^2} \right) \right] \tag{A.17}$$

The equation for viscosity derived thus is a function of fall time with corrections to be made for fluid and sinker density and tube and sinker length as temperature and pressure vary. Tube and sinker length will vary with temperature and pressure and this variation may be accounted for by use of a linear thermal expansion coefficient, α, and a linear compression coefficient, β;

$$L_s L_T = L_{s0} L_{T0} \left[1 + 2\alpha\left(T - T_0\right)\right]\left[1 - 2\beta\left(P - P_0\right)\right] \tag{A.18}$$

Both tube and sinker are made from the same block of titanium and will thus have the same expansion and contraction properties. For this reason no correction is necessary for radii of tube and sinker as the annular gap will remain constant. When expressing sinker density as a function of temperature and pressure, the difference in core material (1:1 nickel ferrite sinter) properties to those of the sinker body must be

accounted for. With individual thermal expansion coefficient, compression coefficient and ambient density values, the density at any temperature and pressure of either of the components may be found from the following expression;

$$\rho = \frac{\rho_0}{[1+3\alpha(T-T_0)][1-3\beta(P-P_0)]} \tag{A.19}$$

A combined sinker density at any condition may then be found by

$$\rho_{\text{sin ker}} = \frac{m_{Ti}+m_{NiFe}}{\frac{m_{Ti}}{\rho_{Ti}}+\frac{m_{NiFe}}{\rho_{NiFe}}} \tag{A.20}$$

Measurements of weight gave that the titanium sinker had a mass of 1.4506g and the nickel-ferrite core 0.7474g. An ambient density of 4.51g/cm^3 was used for titanium with α=7.6x10^{-6}K^{-1} and β=3.075x10^{-6}MPa^{-1}. Values for titanium were taken from Smithells' Metals Reference Book[A1.]. Nickel ferrite sinter properties were taken as being the same as those of a previous stainless steel sinker, α=1.4x10^{-5}K^{-1} and β=2x10^{-6}MPa^{-1}, with density estimated to be slightly higher at 8g/cm^3. Errors caused by this estimation in the final calculation may be assummed negligible; using a value of 8.5g/cm^3 leads to a change in bouyancy corrected fall time, $t^*=t(1-(\rho_f/\rho_s))$ of 0.2%.

[A1.] Smithells, C. J. "Smithells' Metals Reference Book (7th Edition)." Ed. Brandes, E. A., and Brook, G. Butterworth Heinemann, 1992.

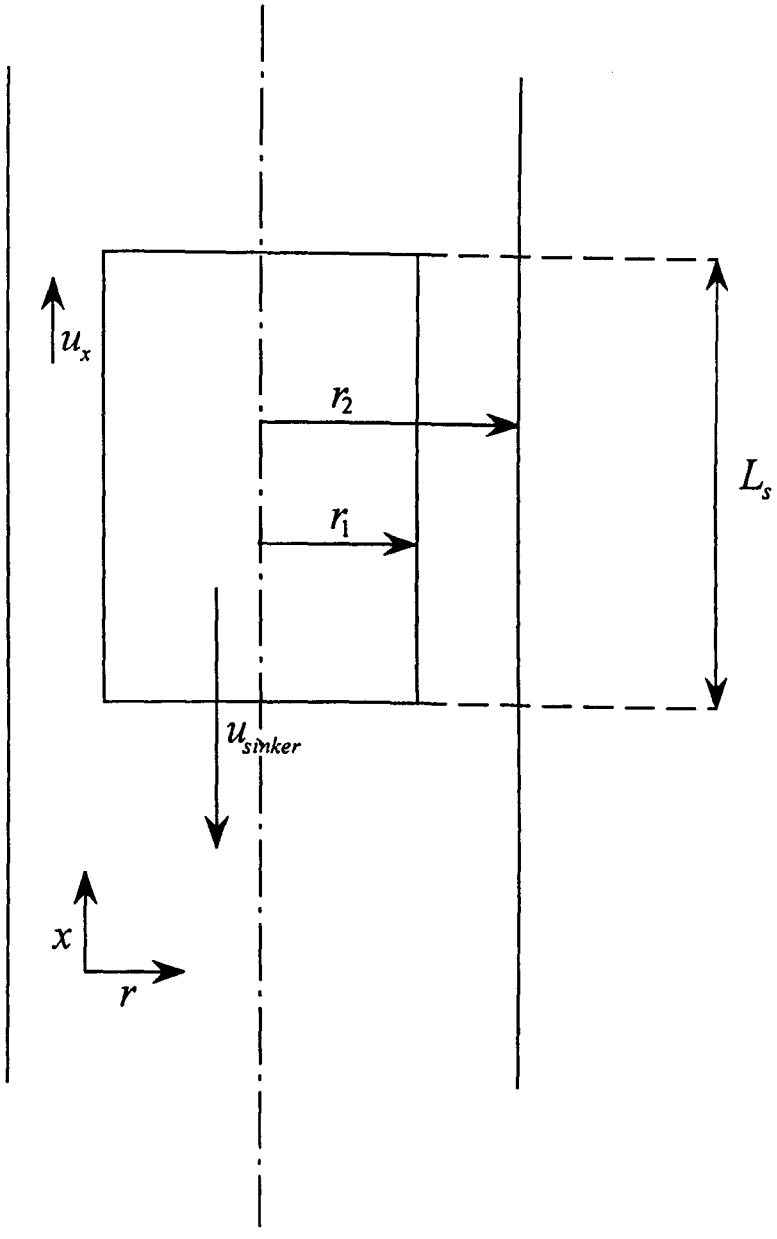

Figure A.1 Notation for falling cylinder viscometer force balance

Appendix B.

Corresponding States Program Code

Appendix B – Corresponding States Program Code

```
Public Const r As Single = 8.3145

'Coefficients for reference fluid 1 (i-octane)

'Fluid Properties
Public Const mwt1 As Single = 114.232
Public Const Tc1 As Single = 543.85
Public Const Pc1 As Single = 2563000
Public Const omega1 As Single = 0.3035

'Coefficients for calculation of reference fluid 1 Tait B as a function of temperature
Public Const bT01 As Single = 300.94
Public Const bT11 As Single = -1.1327
Public Const bT21 As Single = 0.0010926

Public Const c1 As Single = 0.207   'Reference fluid 1 Tait C coefficient

'Coefficients for calculation of reference fluid 1 atmospheric volume as a function of temperature
Public Const vT01 As Single = 0.0013549
Public Const vT11 As Single = -0.0000010667
Public Const vT21 As Single = 0.0000000046851

'Coefficients for reference fluid 2 (heptadecane)

'Fluid Properties

Public Const mwt2 As Single = 240.475
Public Const Tc2 As Single = 736.15
Public Const Pc2 As Single = 1358000
Public Const omega2 As Single = 0.7734

'Coefficients for calculation of reference fluid 2 Tait B as a function of temperature
Public Const bT02 As Single = 316.76
Public Const bT12 As Single = -0.93033
Public Const bT22 As Single = 0.00069114

Public Const c2 As Single = 0.203   'Reference fluid 2 Tait C coefficient

'Coefficients for calculation of reference fluid 2 atmospheric volume as a function of temperature
Public Const vT02 As Single = 0.0011382
Public Const vT12 As Single = -0.000000047394
Public Const vT22 As Single = 0.000000001878


'Function to calculate log to the base ten of a number

Private Function Log10(x)
  Log10 = Log(x) / Log(10#)
End Function

'Method of Kesler & Lee as described by Korsten is used to calculate critical properties from normal
'boiling point and specific gravity at 60F.  y is the normal boiling point.

Private Function CritProps(y, z)
```

```
Dim Tc As Double
Tc = 341.7 + (811 * z) + (y * (0.4244 + (0.1174 * z))) + ((1 / y) * (10 ^ 5) * (0.4669 - (3.2623 * z)))
Dim Pc1 As Double
Pc1 = 8.3634 - (0.0566 / z)
Dim Pc2 As Double
Pc2 = (0.24244 + (2.2898 / z) + (0.11857 / (z ^ 2))) * (10 ^ (-3)) * y
Dim Pc3 As Double
Pc3 = (1.4685 + (3.648 / z) + (0.47227 / (z ^ 2))) * (10 ^ (-7)) * (y ^ 2)
Dim Pc4 As Double
Pc4 = (0.42019 + (1.6977 / (z ^ 2))) * (10 ^ (-10)) * (y ^ 3)
Dim Pc As Double
Pc = Exp(Pc1 - Pc2 + Pc3 - Pc4)

CritProps = Array(Tc, Pc)

End Function

'Acentric factor calculated from correlation of Lee and Kesler (A.I.Ch.E. J. 1975)
'a is boiling point estimate and b and c are critical temperature and pressure calculated from this.

Private Function omega(A, b, C)

Dim Pbr As Double
Pbr = 101325 / (C * (100000 / 14.5))
Dim Tbr As Double
Tbr = A / b
Dim topline As Double
topline = Log(Pbr) - 5.92714 + (6.09648 / Tbr) + (1.28862 * (Log(Tbr))) - (0.169347 * (Tbr ^ 6))
Dim bottomline As Double
bottomline = 15.2518 - (15.6875 / Tbr) - (13.4721 * (Log(Tbr))) + (0.43577 * (Tbr ^ 6))

omega = topline / bottomline

End Function

'Calculation of compressibility of reference fluid 1 using estimated critical properties of fluid of
'interest to calculate equivalent reduced conditions.
'x and y are estimates of critical temperature and pressure respectively.

Private Function ref1z(x, y, T, P)

Dim eqP As Single
eqP = (P / (y * (100000 / 14.5))) * Pc1          'Equivalent pressure of reference fluid 1 in MPa.
Dim eqT As Single
eqT = (T / (x / 1.8)) * Tc1
Dim b As Single
b = (bT21 * (eqT ^ 2)) + (bT11 * eqT) + bT01
Dim eqPPa As Single
eqPPa = eqP * (10 ^ 6)                           'Equivalent reference fluid 1 pressure in Pa.
Dim Vo As Double
Vo = ((vT21 * (eqT ^ 2)) + (vT11 * eqT) + vT01) * (mwt1 / 1000)
Dim Tait As Double
Tait = c1 * (Log10((b + eqP) / (b + 0.1)))

ref1z = ((eqPPa * Vo) * (1 - Tait)) / (r * eqT)

End Function
```

```
'Calculation of compressibility of reference fluid 2 using estimated critical properties of fluid of
'interest to calculate equivalent reduced conditions.
'x and y are estimates of critical temperature and pressure respectively.

Private Function ref2z(x, y, T, P)

Dim eqP As Single
eqP = (P / (y * (100000 / 14.5))) * Pc2     'Equivalent pressure of reference fluid 2 in MPa.
Dim eqT As Single
eqT = (T / (x / 1.8)) * Tc2
Dim b As Single
b = (bT22 * (eqT ^ 2)) + (bT12 * eqT) + bT02
Dim eqPPa As Single
eqPPa = eqP * (10 ^ 6)                  'Equivalent reference fluid 2 pressure in Pa.
Dim Vo As Double
Vo = ((vT22 * (eqT ^ 2)) + (vT12 * eqT) + vT02) * (mwt2 / 1000)
Dim Tait As Double
Tait = c2 * (Log10((b + eqP) / (b + 0.1)))

ref2z = ((eqPPa * Vo) * (1 - Tait)) / (r * eqT)

End Function

'Calculation of compressibility factor of fluid of interest using compressibility factors of reference
'fluids 1 & 2 at equivalent pressures amd temperatures.  acf is the acentric factor of the fluid of
'interest.

Private Function fluidz(acf, z1, z2)

fluidz = z1 + ((acf - omega1) * ((z2 - z1) / (omega2 - omega1)))

End Function

'Routine to estimate critical properties and acentric factor from measured data.

Private Function diff(Tb, SG, Rho1, Rho2, P1, P2, T1, T2)

Dim v1 As Single
v1 = 1 / Rho1
Dim v2 As Single
v2 = 1 / Rho2
Dim meas As Single
meas = v1 / v2



'Estimation of critical properties from guess value of boiling point

Dim Tc As Single
Tc = CritProps(Tb, SG)(0)
Dim Pc As Single
Pc = CritProps(Tb, SG)(1)

'Calculation of fluid z at 60F and atmospheric pressure using estimates of critical properties.

Dim ref1z1 As Double
ref1z1 = ref1z(Tc, Pc, T1, P1)
Dim ref2z1 As Double
```

```
ref2z1 = ref2z(Tc, Pc, T1, P1)
Dim acf As Double
acf = omega(Tb, Tc, Pc)
Dim fluidz1 As Double
fluidz1 = fluidz(acf, ref1z1, ref2z1)

'Calculation of fluid z at measured temperature and pressure using estimates of critical properties.

Dim ref1z2 As Double
ref1z2 = ref1z(Tc, Pc, T2, P2)
Dim ref2z2 As Double
ref2z2 = ref2z(Tc, Pc, T2, P2)
Dim fluidz2 As Double
fluidz2 = fluidz(acf, ref1z2, ref2z2)

'Comparison of calculated values with measured.
Dim calc As Double
calc = (fluidz1 * T1 * P2) / (fluidz2 * T2 * P1)

diff = meas - calc

End Function



Private Function iteration(Tb, SG, Rho1, Rho2, P1, P2, T1, T2)

'Iterative procedure (method of false position) to find a calculated quantity (Z1*T1*P2)/(Z2*T2*P1)
'equal to the measured quantity v1/v2 by varying the normal boiling point hence adjusting the
'parmaters Tc, Pc and acentric factor.

Dim Tb0 As Single      'Determination of initial boundary conditions for iteration
Tb0 = Tb
Dim diff0 As Single
diff0 = diff(Tb0, SG, Rho1, Rho2, P1, P2, T1, T2)
Dim Tb1 As Single
Tb1 = Tb + 50
Dim diff1 As Single
diff1 = diff(Tb1, SG, Rho1, Rho2, P1, P2, T1, T2)

If diff0 * diff1 > 0 Then   'With this condition solution is outwith estimated boundaries of Tb0 and
Tb1
Dim i As Integer            'Variable i counts number of iterations performed
i = 0
Dim maxit As Integer        'MaxIt is maximum number of iterations to be performed before declaring
maxit = 50                  'an error.

Do While diff0 * diff1 > 0
Tb0 = Tb - 50
diff0 = diff(Tb0, SG, Rho1, Rho2, P1, P2, T1, T2)
Tb2 = Tb1 + 50
diff1 = diff(Tb2, SG, Rho1, Rho2, P1, P2, T1, T2)
Tb = Tb0
Tb1 = Tb2
i = i + 1
If i = maxit Then Exit Do
Loop
End If
```

```
Tb2 = ((Tb0 * diff1) - (Tb1 * diff0)) / (diff1 - diff0)
diff2 = diff(Tb2, SG, Rho1, Rho2, P1, P2, T1, T2)
Dim n As Integer

Do While Abs(diff2) > 0.0005

If diff0 * diff2 < 0 Then
Tb1 = Tb2
diff1 = diff(Tb1, SG, Rho1, Rho2, P1, P2, T1, T2)
Tb2 = ((Tb0 * diff1) - (Tb1 * diff0)) / (diff1 - diff0)
diff2 = diff(Tb2, SG, Rho1, Rho2, P1, P2, T1, T2)
n = n + 1
If n = maxit Then Exit Do

Else
Tb0 = Tb2
diff0 = diff(Tb0, SG, Rho1, Rho2, P1, P2, T1, T2)
Tb2 = ((Tb0 * diff1) - (Tb1 * diff0)) / (diff1 - diff0)
diff2 = diff(Tb2, SG, Rho1, Rho2, P1, P2, T1, T2)
n = n + 1
If n = maxit Then Exit Do

End If

Loop

iteration = Tb2

End Function

Function KLdensity(Tb, SG, den0, den2, Tden2, Pden2, T, P)

'Calculation of density at 60F from specific gravity using water density value of 999.02kg/m^3
'calculated at 15.56C using IAPS water property prediction program.

Dim SGRho As Single
SGRho = SG * 999.02

Dim atmTb0 As Single    'This line of code allows same initial boiling point guess to be used for
atmTb0 = Tb             'estimation of  atmospheric and elevated pressure critical properties
                        'and acentric factor.

'Calculation of Tc, Pc, and omega for correlation of atmospheric densities (SG and den0).

atmTbest = iteration(atmTb0, SG, SGRho, den0, 0.1, 0.1, 288.706, Tden2)

Dim atmTc As Single
atmTc = CritProps(atmTbest, SG)(0)
Dim atmPc As Single
atmPc = CritProps(atmTbest, SG)(1)
Dim atmacf As Double
atmacf = omega(atmTbest, atmTc, atmPc)


'Calculation of z at atmospheric pressure and reference temperature.
Dim atmTz1 As Double
atmTz1 = refIz(atmTc, atmPc, Tden2, 0.1)
```

```
Dim atmTz2 As Double
atmTz2 = ref2z(atmTc, atmPc, Tden2, 0.1)
Dim atmTz As Double
atmTz = fluidz(atmacf, atmTz1, atmTz2)

'Calculation of z at atmospheric pressure and temperature of interest.
Dim atmz1 As Double
atmz1 = ref1z(atmTc, atmPc, T, 0.1)
Dim atmz2 As Double
atmz2 = ref2z(atmTc, atmPc, T, 0.1)
Dim atmz As Double
atmz = fluidz(atmacf, atmz1, atmz2)

Dim atmdensity As Double
atmdensity = den0 * ((atmTz * Tden2) / (atmz * T))

'Calculation of Tc, Pc, and omega for correlation of density variation with pressure.
Dim pTb0 As Single
pTb0 = Tb

prTbest = iteration(pTb0, SG, den0, den2, 0.1, Pden2, Tden2, Tden2)

Dim prTc As Single
prTc = CritProps(prTbest, SG)(0)
Dim prPc As Single
prPc = CritProps(prTbest, SG)(1)
Dim pracf As Double
pracf = omega(prTbest, prTc, prPc)

'Calculation of z at reference pressure and reference temperature.
Dim patmTz1 As Double
patmTz1 = ref1z(prTc, prPc, T, 0.1)
Dim patmTz2 As Double
patmTz2 = ref2z(prTc, prPc, T, 0.1)
Dim patmTz As Double
patmTz = fluidz(pracf, patmTz1, patmTz2)

'Calculation of z at pressure and temperature of interest.
Dim prz1 As Double
prz1 = ref1z(prTc, prPc, T, P)
Dim prz2 As Double
prz2 = ref2z(prTc, prPc, T, P)
Dim prz As Double
prz = fluidz(pracf, prz1, prz2)

KLdensity = atmdensity * ((patmTz * P) / (prz * 0.1))

End Function
```

Appendix C.

Code for Estimation of Viscosity by Numerical Solution of Hard Sphere Theory

Appendix C – Code for Estimation of Viscosity by Numerical Solution of Hard Sphere Theory

```
Private Function rhs(x)

'Public function for calculation of experimental reduced viscosity.
'Input parameter x is reduced volume.

'rhs term represents a universal curve of reduced viscosity as a function of reduced volume.  This
'correlation was presented in Fluid Phase Equilibria, Vol. 75, p245-255 (1992) by Assael et al.

'Constants for calculation of 'universal reduced viscosity'.

Dim k0 As Single
k0 = 1.0945
Dim k1 As Single
k1 = -9.26324
Dim k2 As Single
k2 = 71.0385
Dim k3 As Single
k3 = -301.9012
Dim k4 As Single
k4 = 797.69
Dim k5 As Single
k5 = -1221.977
Dim k6 As Single
k6 = 987.5574
Dim k7 As Single
k7 = -319.4636

rhs = 10 ^ (k0 + (k1 * (1 / x)) + (k2 * ((1 / x) ^ 2)) + (k3 * ((1 / x) ^ 3)) + (k4 * ((1 / x) ^ 4)) + (k5 *
((1 / x) ^ 5)) + (k6 * ((1 / x) ^ 6)) + (k7 * ((1 / x) ^ 7)))

End Function

Private Function RetaDiff(y, den0, visc0, temp, mwt, viscP, denP)

'Function to calculate the difference between an initial guess value of Reta and the calculated value of
'Reta.  y represents guess value of Reta.

Dim vm As Double
vm = (1 / den0) * (mwt / 1000)

'lhs term is experimental reduced viscosity term.

Dim NAv As Double
NAv = 6.0221367 * (10 ^ 23)
Dim Pi As Single
Pi = 3.14159265359
Dim r As Single
r = 8.3145

Dim lhs As Double
lhs = (16 / 5) * ((2 * NAv) ^ (1 / 3)) * (Pi ^ (1 / 2)) * ((1000 / (mwt * r * temp)) ^ (1 / 2)) * (visc0 *
(vm ^ (2 / 3)) / y)

'Determination of initial boundary conditions for iteration.
```

```
'Note that rhs stands for "right hand side" (to be equated with lhs, the left hand side of the equation)
'and is not to be confused with rough hard sphere in this context.


Dim Vr0 As Single          'Reduced volume relative to Vo, the close packed volume.
Vr0 = 1.5
Dim rhs0 As Single
rhs0 = rhs(Vr0)
Dim Vr1 As Single
Vr1 = 1.6
Dim rhs1 As Single
rhs1 = rhs(Vr1)

Dim diff0 As Single
diff0 = rhs0 - lhs
Dim diff1 As Single
diff1 = rhs1 - lhs

If diff0 * diff1 > 0 Then  'With this condition solution is outwith estimated boundaries of Vr0 and
Vr1.
Vr = Vr0
Dim i As Integer           'Variable i counts number of loops performed.
i = 0
Dim maxit As Integer       'MaxIt is maximum number of iterations to be performed before declaring
maxit = 50                 'an error.


Do While diff0 * diff1 > 0
Vr0 = Vr - 0.05
rhs0 = rhs(Vr0)
diff0 = rhs0 - lhs
Vr2 = Vr1 + 0.05
rhs1 = rhs(Vr2)
diff1 = rhs1 - lhs
Vr = Vr0
Vr1 = Vr2
i = i + 1
If i = maxit Then Exit Do
Loop
End If

Vr2 = ((Vr0 * diff1) - (Vr1 * diff0)) / (diff1 - diff0)
rhs2 = rhs(Vr2)
diff2 = rhs2 - lhs

Dim n As Integer           'Variable n counts number of loops performed.
n = 0
Dim Maxn As Integer        'Maxn is maximum number of iterations to be performed before declaring
Maxn = 50                  'an error.

Do While Abs(diff2) > 0.05

If diff0 * diff2 < 0 Then  'With this condition solution is between boundaries of Vr0 and Vr2
Vr1 = Vr2
rhs1 = rhs(Vr1)
diff1 = rhs1 - lhs
Vr2 = ((Vr0 * diff1) - (Vr1 * diff0)) / (diff1 - diff0)
rhs2 = rhs(Vr2)
```

```
diff2 = rhs2 - lhs

Else
Vr0 = Vr2              'Otherwise solution is between boundaries of Vr2 and Vr1
rhs0 = rhs(Vr0)
diff0 = rhs0 - lhs
Vr2 = ((Vr0 * diff1) - (Vr1 * diff0)) / (diff1 - diff0)
rhs2 = rhs(Vr2)
diff2 = rhs2 - lhs

End If

n = n + 1
If n = Maxn Then Exit Do
Loop

Dim v0 As Single
v0 = vm / Vr2

'Calculation of Reta from estimated v0 value for comparison with original guess of Reta.

Dim vmP As Single
vmP = (1 / denP) * (mwt / 1000)
Dim vrP As Single
vrP = vmP / v0
Dim rhsP As Single
rhsP = rhs(vrP)
Dim RetaCalc As Single
RetaCalc = ((16 / 5) * ((2 * NAv) ^ (1 / 3)) * (Pi ^ (1 / 2)) * ((1000 / (mwt * r * temp)) ^ (1 / 2)) *
viscP * (vmP ^ (2 / 3))) / rhsP
RetaDiff = Array(y - RetaCalc, v0)

End Function


Function viscosity(den0, visc0, temp, mwt, viscP, denP, T, density, den1, visc1)

'den0 and visc0 are atmospheric pressure density and viscosity values necessary for the calculation of
'close packed volume, v0.  denP and viscP are elevated pressure values for the estimation of correction
'factor Reta.  Initial input Reta is a guess value at this point.

'Determination of initial boundary conditions for iteration

Reta0 = 1
RetaDiff0arr = RetaDiff(Reta0, den0, visc0, temp, mwt, viscP, denP)

'Initially an array containing Reta and v0 is returned.  0th element is Reta (called below) and 1st
'element is v0.

RetaDiff0 = RetaDiff0arr(0)
Reta1 = 2
RetaDiff1arr = RetaDiff(Reta1, den0, visc0, temp, mwt, viscP, denP)
RetaDiff1 = RetaDiff1arr(0)

If RetaDiff0 * RetaDiff1 > 0 Then        'With this condition solution is outwith estimated boundaries
Do While RetaDiff0 * RetaDiff1 > 0       'of Reta0 and Reta1
Reta = Reta0 - 0.1
  If Reta < 0 Then
```

```
    Reta = Reta0
  End If
Reta2 = Reta1 + 0.1
RetaDiff0arr = RetaDiff(Reta, den0, visc0, temp, mwt, viscP, denP)
RetaDiff0 = RetaDiff0arr(0)
RetaDiff1arr = RetaDiff(Reta2, den0, visc0, temp, mwt, viscP, denP)
RetaDiff1 = RetaDiff1arr(0)
Reta1 = Reta2
Reta0 = Reta
Loop
End If

Reta2 = ((Reta0 * RetaDiff1) - (Reta1 * RetaDiff0)) / (RetaDiff1 - RetaDiff0)
RetaDiff2arr = RetaDiff(Reta2, den0, visc0, temp, mwt, viscP, denP)
RetaDiff2 = RetaDiff2arr(0)

Do While RetaDiff2 > 0.0005
If RetaDiff0 * RetaDiff2 < 0 Then
Reta1 = Reta2
RetaDiff1arr = RetaDiff(Reta1, den0, visc0, temp, mwt, viscP, denP)
RetaDiff1 = RetaDiff1arr(0)
Reta2 = ((Reta0 * RetaDiff1) - (Reta1 * RetaDiff0)) / (RetaDiff1 - RetaDiff0)
RetaDiff2arr = RetaDiff(Reta2, den0, visc0, temp, mwt, viscP, denP)
RetaDiff2 = RetaDiff2arr(0)

Else
Reta0 = Reta2
RetaDiff0arr = RetaDiff(Reta0, den0, visc0, temp, mwt, viscP, denP)
RetaDiff0 = RetaDiff0arr(0)
Reta2 = ((Reta0 * RetaDiff1) - (Reta1 * RetaDiff0)) / (RetaDiff1 - RetaDiff0)
RetaDiff2arr = RetaDiff(Reta2, den0, visc0, temp, mwt, viscP, denP)
RetaDiff2 = RetaDiff2arr(0)

End If

Loop

'Calculation of viscosity at temperature and density of interest

Dim vm0 As Single      'Specific volume at temperature of interest and atmospheric pressure
vm0 = (1 / den1) * (mwt / 1000)

Dim NAv As Double
NAv = 6.0221367 * (10 ^ 23)
Dim Pi As Single
Pi = 3.14159265359
Dim r As Single
r = 8.3145

Dim lhs As Double
lhs = (16 / 5) * ((2 * NAv) ^ (1 / 3)) * (Pi ^ (1 / 2)) * ((1000 / (mwt * r * T)) ^ (1 / 2)) * (visc1 * (vm0
^ (2 / 3)) / Reta2)

'Determination of initial boundary conditions for iteration

Dim Vr0 As Single          'Reduced volume relative to Vo, the close packed volume.
Vr0 = 1.5
Dim rhs0 As Single
```

```
rhs0 = rhs(Vr0)
Dim Vr1 As Single
Vr1 = 1.6
Dim rhs1 As Single
rhs1 = rhs(Vr1)

Dim diff0 As Single
diff0 = rhs0 - lhs
Dim diff1 As Single
diff1 = rhs1 - lhs

Dim i As Integer          'Variable i counts number of loops performed.
i = 0
Dim maxit As Integer      'MaxIt is maximum number of iterations to be performed before declaring
maxit = 50                'an error.


If diff0 * diff1 > 0 Then 'With this condition solution is outwith estimated boundaries of Vr0 and Vr1
Vr = Vr0
Do While diff0 * diff1 > 0
Vr0 = Vr - 0.05
rhs0 = rhs(Vr0)
diff0 = rhs0 - lhs
Vr2 = Vr1 + 0.05
rhs1 = rhs(Vr2)
diff1 = rhs1 - lhs
Vr = Vr0
Vr1 = Vr2
i = i + 1
If i = maxit Then Exit Do
Loop
End If

Vr2 = ((Vr0 * diff1) - (Vr1 * diff0)) / (diff1 - diff0)
rhs2 = rhs(Vr2)
diff2 = rhs2 - lhs

Dim n As Integer          'Variable n counts number of loops performed.
n = 0
Dim Maxn As Integer       'Maxn is maximum number of iterations to be performed before declaring
Maxn = 50                 'an error.

Do While Abs(diff2) > 0.0005

If diff0 * diff2 < 0 Then 'With this condition solution is between boundaries of Vr0 and Vr2
Vr1 = Vr2
rhs1 = rhs(Vr1)
diff1 = rhs1 - lhs
Vr2 = ((Vr0 * diff1) - (Vr1 * diff0)) / (diff1 - diff0)
rhs2 = rhs(Vr2)
diff2 = rhs2 - lhs

Else
Vr0 = Vr2                 'Otherwise solution is between boundaries of Vr2 and Vr1
rhs0 = rhs(Vr0)
diff0 = rhs0 - lhs
Vr2 = ((Vr0 * diff1) - (Vr1 * diff0)) / (diff1 - diff0)
rhs2 = rhs(Vr2)
```

```
diff2 = rhs2 - lhs

End If
n = n + 1
If n = Maxn Then Exit Do
Loop

Dim v0 As Single
v0 = vm0 / Vr2

Dim vol As Single      'Specific volume at temperature of interest and elevated density.
vol = (1 / density) * (mwt / 1000)
Dim redV As Single
redV = vol / v0
Dim rhsvol As Double
rhsvol = rhs(redV)

viscosity = 1000 * rhsvol * (5 / 16) * ((2 * NAv) ^ (-1 / 3)) * (Pi ^ (-1 / 2)) * ((1000 / (mwt * r * T)) ^
(-1 / 2)) * Reta2 * (vol ^ (-2 / 3))

End Function
```

Appendix D.

Code for Estimation of Viscosity from Collision Integral Scheme

Appendix D – Code for Estimation of Viscosity from Collision Integral Scheme

```
Private Function rhs(vr) As Double

'rhs term represents a universal curve of reduced viscosity as a function of reduced volume. This
'correlation was presented in Fluid Phase Equilibria, Vol. 75, p245-255 (1992) by Assael et al.

'Constants for calculation of 'universal reduced viscosity'.

Dim k0 As Single
k0 = 1.0945
Dim k1 As Single
k1 = -9.26324
Dim k2 As Single
k2 = 71.0385
Dim k3 As Single
k3 = -301.9012
Dim k4 As Single
k4 = 797.69
Dim k5 As Single
k5 = -1221.977
Dim k6 As Single
k6 = 987.5574
Dim k7 As Single
k7 = -319.4636

rhs = 10 ^ (k0 + (k1 * (1 / vr)) + (k2 * ((1 / vr) ^ 2)) + (k3 * ((1 / vr) ^ 3)) + (k4 * ((1 / vr) ^ 4)) + (k5
* ((1 / vr) ^ 5)) + (k6 * ((1 / vr) ^ 6)) + (k7 * ((1 / vr) ^ 7)))

End Function

Private Function collint(T, koverep) As Double     'Calculation of collision integral

Dim CIA As Single     'Parameters for empirical collision integral correlation of Neufeld et al.
CIA=1.16145
Dim CIB As Single
CIB = 0.14874
Dim CIC As Single
CIC = 0.52487
Dim CID As Single
CID = 0.7732
Dim CIE As Single
CIE = 2.16178
Dim CIF As Single
CIF = 2.43787

Dim redT As Double
redT = koverep * T

collint = (CIA * (redT ^ (-CIB))) + (CIC * (Exp((-CID) * redT))) + (CIE * (Exp((-CIF) * redT)))

End Function


Private Function etastar(T, eta, mwt, vm) As Double
```

```
'Calculation of experimental reduced viscosity.

Dim NAv As Double
NAv = 6.0221367 * (10 ^ 23)
Dim Pi As Single
Pi = 3.14159265359
Dim r As Single
r = 8.3145

etastar = (16 / 5) * ((2 * NAv) ^ (1 / 3)) * (Pi ^ (1 / 2)) * ((1000 / (mwt * r * T)) ^ (1 / 2)) * (eta * (vm
^ (2 / 3)))

End Function
Private Function rhsdiff(v0, vm, lhs) As Double

Dim vr As Double
vr = vm / v0
Dim rhside As Double
rhside = rhs(vr)

rhsdiff = rhside - lhs

End Function


Private Function v0iteration(vm, lhs) As Double

Dim v00 As Single
v00 = 0.00019
Dim v01 As Single
v01 = 0.00021
diff0 = rhsdiff(v00, vm, lhs)
diff1 = rhsdiff(v01, vm, lhs)

Dim i As Integer
i = 0
Dim maxit As Integer
maxit = 50

If diff0 * diff1 > 0 Then      'Solution outwith initial guess values v00 and v01
   Do While diff0 * diff1 > 0
   v0 = v00 - 0.00001
      If v0 < 0 Then
      v0 = v00
      End If
   v02 = v01 + 0.00001
   diff0 = rhsdiff(v0, vm, lhs)
   diff1 = rhsdiff(v02, vm, lhs)
   v00 = v0
   v01 = v02
   i = i + 1
   If i >= maxit Then
   Exit Function
   End If
   Loop
End If

v02 = ((v00 * diff1) - (v01 * diff0)) / (diff1 - diff0)
```

```
diff2 = rhsdiff(v02, vm, lhs)

Dim n As Integer
n = 0
Dim maxn As Integer
maxn = 50

Do While Abs(diff2) > 0.01

If diff0 * diff2 < 0 Then      'Solution lies between v00 and v02
   v01 = v02
   diff1 = rhsdiff(v01, vm, lhs)
   v02 = ((v00 * diff1) - (v01 * diff0)) / (diff1 - diff0)
   diff2 = rhsdiff(v02, vm, lhs)
   v01 = v02

Else                           'Otherwise solution is between v02 and v01
   v00 = v02
   diff0 = rhsdiff(v00, vm, lhs)
   v02 = ((v00 * diff1) - (v01 * diff0)) / (diff1 - diff0)
   diff2 = rhsdiff(v02, vm, lhs)
   v00 = v02
End If
n = n + 1
If n >= maxn Then
Exit Function
End If
Loop

v0iteration = v02

End Function

Private Function cidiff(T, kep, eqterm) As Double

'Function to calculate difference between collision integral and ratio of universal to experimental
'reduced viscosity.

Dim clint As Double
clint = collint(T, kep)

cidiff = eqterm - clint

End Function



Private Function kepiteration(T, eqterm, guesskoverep) As Double

'Function to find value of k over epsillon such that the collision integral is equal to the ratio of
'universal to experimental reduced viscosity within specified tolerance.

kep0 = guesskoverep
kep1 = guesskoverep + 0.0001
cidiff0 = cidiff(T, kep0, eqterm)
cidiff1 = cidiff(T, kep1, eqterm)

Dim i As Integer
```

```
i = 0
Dim maxit As Integer
maxit = 50

If cidiff0 * cidiff1 > 0 Then      'Solution outwith initially guessed boundaries
Do While cidiff0 * cidiff1 > 0
kep = kep0 - 0.0001
   If kep < 0 Then
   kep = kep0
   End If
kep2 = kep1 + 0.0001
cidiff0 = cidiff(T, kep, eqterm)
cidiff1 = cidiff(T, kep2, eqterm)
kep0 = kep
kep1 = kep2
i = i + 1
   If i >= maxit Then
   Exit Function
   End If
Loop
End If

kep2 = ((kep0 * cidiff1) - (kep1 * cidiff0)) / (cidiff1 - cidiff0)
cidiff2 = cidiff(T, kep2, eqterm)

Dim n As Integer
n = 0
Dim maxn As Integer
maxn = 50

Do While Abs(cidiff2) > 0.00001

If cidiff0 * cidiff2 < 0 Then          'Solution is between kep0 and kep2
   kep1 = kep2
   cidiff1 = cidiff(T, kep1, eqterm)
   kep2 = ((kep0 * cidiff1) - (kep1 * cidiff0)) / (cidiff1 - cidiff0)
   cidiff2 = cidiff(T, kep2, eqterm)
   kep1 = kep2
Else
   kep0 = kep2
   cidiff0 = cidiff(T, kep0, eqterm)
   kep2 = ((kep0 * cidiff1) - (kep1 * cidiff0)) / (cidiff1 - cidiff0)
   cidiff2 = cidiff(T, kep2, eqterm)
   kep0 = kep2
End If
n = n + 1
   If n >= maxn Then
   Exit Function
   End If
Loop

kepiteration = kep2

End Function

Private Function kepdiff(den1, visc1, T1, den2, visc2, T2, mwt, guesskoverep)

Dim vm1 As Single
```

```
vm1 = (1 / den1) * (mwt / 1000)
Dim clint1 As Double
clint1 = collint(T1, guesskoverep)
Dim etastar1 As Double
etastar1 = etastar(T1, visc1, mwt, vm1)
Dim lhs1 As Double
lhs1 = clint1 * etastar1
Dim initialv0 As Double
initialv0 = v0iteration(vm1, lhs1)

Dim vm2 As Single
vm2 = (1 / den2) * (mwt / 1000)
Dim vr2 As Single
vr2 = vm2 / initialv0
Dim rhs2 As Double
rhs2 = rhs(vr2)
Dim etastar2 As Double
etastar2 = etastar(T2, visc2, mwt, vm2)
Dim eqterm As Double          'Collision integral will equal ratio of universal to experimental reduced
eqterm = rhs2 / etastar2.     'viscosity when appropriate value of k over epsillon is used
Dim calckep As Double
calckep = kepiteration(T2, eqterm, guesskoverep)
Dim diff As Double
diff = guesskoverep - calckep

kepdiff = Array(diff, initialv0)

End Function

Function viscosity(den1, visc1, T1, den2, visc2, T2, mwt, Ti, deni)

'den1 and visc1 are density and viscosity measured at atmospheric pressure and temperature T1.
'Similarly, den2 and visc2 are measured at atmospheric pressure and temperature T2. Ti and deni are
'temperature and density of interest.

Dim guesskep0 As Single
guesskep0 = 0.0029
Dim guesskep1 As Single
guesskep1 = 0.0031
Dim kepdiff0 As Double
kepdiff0 = kepdiff(den1, visc1, T1, den2, visc2, T2, mwt, guesskep0)(0)
Dim kepdiff1 As Double
kepdiff1 = kepdiff(den1, visc1, T1, den2, visc2, T2, mwt, guesskep1)(0)

Dim i As Integer
i = 0
Dim maxit As Integer
maxit = 50

If kepdiff0 * kepdiff1 > 0 Then
   Do While kepdiff0 * kepdiff1 > 0
   guesskep = guesskep0 - 0.0001
      If guesskep < 0 Then
      guesskep = guesskep0
      End If
   guesskep2 = guesskep1 + 0.0001
   kepdiff0 = kepdiff(den1, visc1, T1, den2, visc2, T2, mwt, guesskep)(0)
   kepdiff1 = kepdiff(den1, visc1, T1, den2, visc2, T2, mwt, guesskep2)(0)
```

```
  guesskep0 = guesskep
  guesskep1 = guesskep2
  i = i + 1
    If i >= maxit Then
    Exit Function
    End If
  Loop
End If

guesskep2 = ((guesskep0 * kepdiff1) - (guesskep1 * kepdiff0)) / (kepdiff1 - kepdiff0)
kepdiff2nd = kepdiff(den1, visc1, T1, den2, visc2, T2, mwt, guesskep2)
kepdiff2 = kepdiff2nd(0)   'kepdiff and v0 at guesskep2 are calculated at the same time to ensure
v0 = kepdiff2nd(1)         'consistency.

Dim n As Integer
n = 0
Dim maxn As Integer
maxn = 50

Do While Abs(kepdiff2) > 0.000001

If kepdiff0 * kepdiff2 < 0 Then    'Solution lies between guesskep0 and guesskep2
  guesskep1 = guesskep2
  kepdiff1 = kepdiff(den1, visc1, T1, den2, visc2, T2, mwt, guesskep1)(0)
  guesskep2 = ((guesskep0 * kepdiff1) - (guesskep1 * kepdiff0)) / (kepdiff1 - kepdiff0)
  kepdiff2nd = kepdiff(den1, visc1, T1, den2, visc2, T2, mwt, guesskep2)
  kepdiff2 = kepdiff2nd(0)   'kepdiff and v0 at guesskep2 are calculated at the same time to ensure
  v0 =  kepdiff2nd(1)        'consistency.
  guesskep1 = guesskep2
Else
  guesskep0 = guesskep2
  kepdiff0 = kepdiff(den1, visc1, T1, den2, visc2, T2, mwt, guesskep0)(0)
  guesskep2 = ((guesskep0 * kepdiff1) - (guesskep1 * kepdiff0)) / (kepdiff1 - kepdiff0)
  kepdiff2nd = kepdiff(den1, visc1, T1, den2, visc2, T2, mwt, guesskep2)
  kepdiff2 = kepdiff2nd(0)
  v0 = kepdiff2nd(1)
  guesskep0 = guesskep2
End If
n = n + 1
  If n >= maxn Then
  Exit Function
  End If
Loop

Dim koverep As Double
koverep = guesskep2

Dim NAv As Double
NAv = 6.0221367 * (10 ^ 23)
Dim Pi As Single
Pi = 3.14159265359
Dim r As Single
r = 8.3145

Dim clinti As Double
clinti = collint(Ti, koverep)
Dim vmi As Single
vmi = (1 / deni) * (mwt / 1000)
```

```
Dim vri As Double
vri = vmi / v0
Dim rhsi As Double
rhsi = rhs(vri)

viscosity = 1000 * (rhsi / clinti) * (5 / 16) * ((2 * NAv) ^ (-(1 / 3))) * (Pi ^ (-(1 / 2))) * ((1000 / (mwt *
r * Ti)) ^ (-(1 / 2))) * (vmi ^ (-(2 / 3)))

End Function
```